Moisture-induced static and cyclic properties of sisal fiber reinforced soil for resilient earthen construction

Submitted in fulfilment for the requirement

Of

Doctor of Philosophy

In

Civil Engineering Science

In the

FACULTY OF ENGINEERING AND BUILT ENVIRONMENT

UNIVERSITY OF JOHANNESBURG

By

Innocent Kafodya

(216063121)

Supervisor: Prof F.N Okonta

DECLARATION

I confirm that this thesis presented for the degree of Doctor of Philosophy in Civil Engineering has been composed solely by the author. It is a product of the original research work conducted by the author under supervision of Prof F.N Okonta in the Civil Engineering Science Department at the University of Johannesburg, South Africa.

The author declares that the thesis has not been submitted in part or in whole to any university or research institution. Except where states otherwise by reference or acknowledgment, the work presented is entirely the author's own.

ACKNOWLEDGEMENT

Honour and glory be unto God for giving me protection, good health, strength and intelligence to pursue this research study.

I am grateful to Prof FN Okonta for his guidance, support and recommendable supervision during this research work.

My sincere gratitude is extended to my family and my wife, Ellen for her encouragement during the course of the research.

I would like to thank University of Malawi for awarding me a scholarship to pursue my PhD studies at the University of Johannesburg, South Africa.

I would like to extend my sincere gratitude to the staff of Civil Engineering laboratory at the University of Johannesburg for their presence and support during my laboratory tests.

I also thank all friends, Malawians and South Africans who kept me company during my studies.

RESEARCH OUTPUT

Part of this research has been published and others under review in different peer reviewed journals. The following are publications and submission under review

1. I Kafodya, F Okonta, Effects of natural fiber inclusions and pre-compression on the strength properties of lime-fly ash stabilised soil. *Construction and Building Materials* 2018, (170), 737-746 https://doi.org/10.1016/j.conbuildmat.2018.02.194

2. Innocent Kafodya, Felix Okonta. Effect of fibre surface coating on the mechanical properties of natural fibre-reinforced soil. *International Journal of Geotechnical Engineering*. 2018, 1-11, https://doi.org/10.1080/19386362.2018.1542557

3. Innocent Kafodya, F Okonta. Density control method for compression test of compacted lime- fly ash stabilised fiber-soil mixtures, *MethodsX* 2018 (5), 848-856 https://doi.org/10.1016/j.mex.2018.04.010

4. Innocent Kafodya, F. Okonta. Cyclic and post cyclic shear behaviours of natural fiber reinforced soil. *International Journal of Geotechnical Engineering* http://dx.doi.org/10.1080/19386362.2019.1611720.

5. Innocent Kafodya, F Okonta. Desiccation characteristics and desiccation induced compressive strength of natural fiber-reinforced soil. *International Journal of geosynthetics and ground improvement* 2019 (5) 16 https://doi.org/10.1007/s40891-019-0169-7

6. Innocent Kafodya, F.Okonta. Role of fiber inclusion in adobe masonry construction *Journal of Building Engineering* 2019 (26) https://doi.org/10.1016/j.jobe.2019.100904

7. Innocent Kafodya, F Okonta. Compressive and tensile strength properties of pre-compressed and soaked natural fiber reinforced lime-fly ash stabilised soil *International Journal of Pavement research and Technology* https://doi.org/10.1007/s42947-020-0074-4

CONTRIBUTION TO LITERATURE

The major contributions of the research to existing literature include:

1. Advanced mechanics of fiber-soil matrix interaction.
2. Modelling of fiber-soil matrix interfacial strength mechanisms.
3. Improvement of soil-fiber composites for long term performance.
4. Effects of pre mature loading on the strength of stabilised fiber reinforced soil.
5. Durability of pre-loaded stabilised fiber reinforced soil composites.
6. Dynamic performance of fiber reinforced soil.
7. Modelling of dynamic behaviour of fiber reinforced soil.
8. Role of fibers in adobe earthen construction and design guildelines.

ABSTRACT

This study focused on investigating strength properties of the randomly distributed sisal fiber-reinforced soil subjected to applied static and dynamic loading conditions. Series of static laboratory tests were performed to determine compaction characteristics, compressive and interfacial shear strength properties of the composite. Dynamic properties were investigated by subjecting the composite to cyclic loading under undrained soil condition. The moisture induced properties were established by performing matric suction and desiccation cracking tests. The effects of soil matrix density, moisture content and fiber properties (content, length and surface coating with gum rosin) on the mechanical and macro structural properties were determined from the laboratory experiments.

Furthermore, unconfined compression and tensile tests were performed on the lime-fly ash stabilised soil composite to investigate the potential strength improvements. The synergic effects of pre-compression and moisture exposure on the mechanical performance of the stabilised composite were also investigated to establish the resilience of the material. The strength of sisal fiber-reinforced adobe masonry construction was eventually determined by performing series of laboratory tests on the reinforced masonry elements and structures. Finite-Element modelling of masonry construction was employed to validate results from the experiments.

The study revealed that fiber inclusions caused a decrease in the maximum dry density (MDD) and a marginal change in optimum moisture content (OMC) of the composite. The stiffness and ductility of the composite were enhanced by an increase in fiber content and length. However, high fiber content (1%) and long fiber length (50mm) indicated undesirable mechanical performance. The maximum compressive strength of fiber reinforced soil was shown with 25mm fibers. The post peak behaviour of fiber-reinforced composite was characterised as strain hardening while unreinforced soil was associated with softening.

The interfacial shear strength of coated fibers was lower than uncoated fibers at the matrix optimum moisture content. Increasing matrix density led to high interfacial shear strength of both coated and uncoated fibers due to enhanced interfacial frictional resistance. It was shown that matric suction reduced with high fiber content (1%) due to low free moisture in the pore spaces of the soil composite. Crack morphology of the desiccated fiber reinforced soil was characterised by the small cell areas of irregular shapes, short and thin cracks with non-orthogonal

intersections. Crack width and surface crack area ratio showed reduction of 74% and 35%, respectively with 1% fiber content. The crack growth rate and shrinkage strain significantly reduced with fiber inclusion. An increase in soil thickness led to large crack width and high evaporation.

It was revealed that fiber inclusions enhanced shear modulus to a limiting fiber content of 0.5% beyond which, the modulus reduced. Damping ratio was improved due to high deformation resistance of the composite. Both permanent and cumulative strains reduced with fiber inclusions. The fiber reinforced soil exhibited high resistance to liquefaction. Increasing fiber content improved post cyclic energy absorbing capacity, toughness and static energy ratio of the soil composite.

The lime-fly ash stabilised composite achieved maximum strength of 3.5MPa at 0.75% fiber content. Pre-compression with 10% unconfined compressive strength (UCS) showed maximum strength of 2.8MPa at 0.25% fiber content whereas 20% UCS indicated maximum strength of 3.04MPa at 0.25% fiber content. In comparison, pre-compressed composite exhibited lower strength values than un-precompressed composite. The capillary soaking in un-precompressed composite reduced compressive strength by 42%. Pre-compression of soaked composite reduced both tensile and compressive strength by 20% due to fiber slippage and debonding.

It was shown that fiber inclusion in the mortar of the masonry elements led to an increase in tensile bond strength of 31%, friction coefficient of 22%, and prism compressive strength of 25%. The reinforced wallets exhibited twofold increase in compressive strength while reinforced wall panels indicated threefold increase in shear strength. The stress state in the reinforced wall panels was not a pure shear state and could better be described by RILEM recommendation.

The study showed that sisal fiber inclusions can effectively be used for retrofitting earthen construction under gravity loads, earthquake and moisture exposure. Long term performance of sisal fiber-reinforced soil can be enhanced by fiber surface coating with gum rosin and lime-fly ash stabilisation.

TABLE OF CONTENTS

LIST OF FIGURES

LIST OF TABLES

LIST OF SYMBOLS

A area of the soil in shear zone

A_f area of the fiber in shear zone

A_s area of shear zone

A_g area parallel to mortar joint

A_{tc} total area of cracks

A_{ts} total surface area of desiccating specimen

C_u static undrained strength

D depth of shear zone

D_d damping ratio

D_{max} maximum damping ratio

D_s diameter of the specimen

D_r energy dissipation

d_f fiber diameter

E_s Young's modulus of soil

E_f Young's modulus of fiber

E_m Young's modulus of the matrix

F_h applied hoop force

G shear modulus

G_d dynamic shear modulus

G_f specific gravity of fibers

G_i initial tangential modulus

G_{max} maximum tangential modulus

K model constant

L length of specimen

l_c embedded fiber length

l_f fiber length

$l_{f\,x}$ arbitrary fiber length

l_{fd} fiber debonding length

M parameter constant

m_f fiber mass

m_s soil mass

m_c composite mass

N number of cyclic cycles

N_f number of fibers

N_r ultimate pull-out load

P applied load

P_{ult} ultimate applied load

P_{max} maximum pull-out load

P_a atmospheric pressure

p principal stress

p_c ' pre-consolidation pressure

R_r surface crack reduction ratio

R_{sc} surface crack ratio

R_{rw} surface crack width reduction ratio

R_o radius occupied by fibers

r_f radius of fibers

r_c cyclic stress ratio

r_{tv} threshold cyclic stress ratio

S shear strength of soil

S_{eq} equivalent shear strength of soil

T_{Rf} tension resistance of fibers

T_w water surface tension

t mobilised tension strength

t_m thickness of the matrix

U_{shr} radial deformations

u pore pressure

u_a air pore pressure

U_r radial deformations

v_f fiber volume fraction

V volume of soil composite

v_f fiber volume fraction

w_f moisture content of the filter

w soil moisture content

e soil void ratio

σ stress

σ_{ij} macroscopic stress

σ_o fiber yield stress

σ_n stress normal to fiber surface

$\overline{\sigma_n}$ average stress normal to fiber surface

σ_t fiber-soil induced tension

σ_{av} average tensile stress

σ_v vertical applied stress in the soil

σ_{xx} axial stress in the fiber

σ_c effective confining pressure

σ_p soil compaction pressure

σ_{shr} shrinkage stress

$\sigma_{sh\theta}$ circumferential shrinkage stress

σ_{tr} transition axial stress

σ_1 major principal stress

σ_3 minor principal stress

ε_θ strain rate

ε_1 minor principal strain

ε_3 minor principal stress

ε_{ij} average strain rate

τ_f tangential stress /interfacial resistance

τ_{max} maximum tangential stress

τ_{in} increase in shear stress

τ_{x} shear strength

τ_{ult} ultimate shear strength

γ_{w} unit weight of water

γ_{d} dry unit weight of soil

γ_{i} shear strain

γ_{u} hyperbolic strain

ρ_{f} fiber content/ concentration

ρ_{fv} fiber volumetric content

ρ_{d} soil dry density

ρ_{b} soil bulk density

ρ_{t} target density

ν_{m} soil matrix Poisons ratio

ν_{f} fiber Poisons ratio

η fiber aspect ratio

μ friction coefficient

φ soil angle of friction

LIST OF ABBREVATIONS

CV	coefficient of variation
IFSS	interfacial shear strength
IRSS	interfacial residual strength
MDD	maximum dry density
OMC	optimum moisture content
OCR	over consolidation ratio
UCS	unconfined compressive strength
XRF	X-ray fluorescence
XRD	X-ray diffraction

1 CHAPTER ONE-INTRODUCTION

1.1 Introduction

During the past three decades, there has been an increasing interest in the research and development of non-conventional materials such as local soil, natural fibers and vegetable fibers, as biodegradable and eco-effective materials in a wide range of civil engineering applications (Millogo et al., 2014). Soil is used in various civil engineering applications such as road, earthen buildings, dams, barrier systems, mine tailing construction, etc.

The earthen construction which has a long and successful history dates back a thousand years. The earthen construction techniques employed in most countries are rammed earth or adobe blocks, wattle and daub and cob (Varum et al., 2010). It is a common construction practice in almost all sub-Saharan African countries especially among rural communities. The earthen structures are the common dwelling units in the world especially among rural communities. The most notable world's ancient earthen construction are the Great Wall of China, the Horyuji Temple in Japan, city of Chanchán in Peru, village of Taos in New Mexico and city of Shibam in Yemen are notable (Pacheco-Torgal and Said Jalali, 2011; Wu et al., 2013a). The advantages of the earthen construction over conventional construction techniques include: cheap, easy, and fast production, good thermal-physical and hydric properties that provide for the regulation of thermal comfort, low life cycle costs, less energy consumption and environmental friendliness (Ciancio and Beckett, 2015; Reman, 2004; Tanaçan, 2008). The interest in earthen construction in the developed countries has been driven by the demands for more sustainable form of built environment. In this regard, earthen materials have been the attractive alternative to conventional high energy demand construction materials (Walker, 1999).

For the past decades majority of the research has focused on the chemical stabilised soil composite for earthen construction. Chemical stabilisation, i.e., by cement or lime has enjoyed a very good reception especially in the developed countries. Cement stabilised soil composites endow the soil with durability, improved mechanical and dynamic properties (Adam et al., 2016; Chen et al., 2011; Hamidi and Hooresfand, 2013; Kenai et al., 2006; Tang et al., 2007). However, cement production is energy intensive and is the main contributor of high carbon footprint.

The literature indicates that cement production accounts for 5% of CO_2 emissions (Allwood et al., 2010; Friedlingstein et al., 2010; UNSTATS, 2010). In response to the associated environmental unfriendliness and high production cost, most research works have been redirected towards green materials for construction industry. Some studies have focused on fiber reinforced polymer composite, the development that has contributed to the flourishing of polymer industry. Fiber reinforced polymers have been successfully applied in various industries such as automotive and civil engineering (Chand, 2000; Fu et al., 2000). This development has triggered an impetus to study the potential use of fiber reinforcement in natural soil (Hejazi et al., 2012). The positive results have so far been reported about glass, polypropylene and carbon fiber reinforced soil. These synthetic fibers exhibit good mechanical and hydrophilic properties and have been effectively applied in various geo structures such as embankments and retaining walls. However, the technology for their effective use and application is not well established in the developing countries such as sub-Saharan Africa; hence their application is limited especially in small scale construction works.

1.2 Problem statement

In all continents, soil is used for construction of low-cost shelters and the current world population statistics indicate that approximately 30% of the population still lives in earthen structures (United Nations, 2011). It is expected that the earthen structures in developing countries will continue to exist in the next decades due to prevalence of poor socio-economic conditions, especially among rural communities. The earthen construction possesses some shortcomings and its technical know-how has not been systematically established for the sustainable future applications. The demerits include poor mechanical properties such as low compressive and tensile strength, low resistance to water ingress, low resistance to swell and shrinkage. Hence issues pertaining to desiccating cracking arise.

Earthen construction is vulnerable to natural phenomena such as earthquakes and floods. Several reports have shown that unreinforced earthen structures suffer severe damage compared to reinforced structures (Morris et al., 2010). It can be hypothetically established that undesirable performance of the earthen construction during natural or manmade disasters is due to poor mechanical properties of the materials. This can be addressed by employing proper material improvement techniques such as fiber inclusions.

Therefore, it can be anticipated that improved material properties and good construction methods, could enhance performance of earthen structures during earthquakes or other loading conditions. Nevertheless, the design guidelines for low-cost earthen structures cannot be published unless thorough knowledge of material behaviour in different and extreme environments is acquired. Therefore, research focus on the potential application of low cost reinforcement of materials for earthen structures is fundamental to the establishment of the guidelines for earthen construction.

Earthen construction for dwelling units is currently at the verge of being abandoned especially in Africa due to lack of proper construction guidelines. Macroeconomics statistics have shown that most of rural communities in the sub Saharan Africa are living below poverty line and cannot afford cement or lime, the situation that has led to the development of non-resilient infrastructure. Therefore, it is imperative to investigate the mechanical properties of the potential low-cost and sustainable materials that enhance resilience and durability to low-cost earthen construction.

The biggest obstacle in earthen construction particularly in developed countries is lack of trust and confidence by the engineers, reluctance and apprehension of some clients and builders on the earthen construction methods. In Africa, engineers acknowledge the potential of earthen construction. The earthen construction industry can be promoted not only by introducing advanced techniques but also by the systematic establishment of its technical know-how. It is therefore imperative to establish well-documented design and construction guidelines for earthen structures that are supported by the scientific evidence on the performance and behaviour of the earthen materials in various environments.

Natural fiber inclusion is the best technique to achieve resilience of the low-cost earthen construction. Although natural fibers are more attractive in this regard, they have limitations such as moisture absorption which could cause dimensional changes and result in the composite with weak interfacial adhesion and low durability (Buitrago et al., 2015). Therefore, investigations are required to find possible ways of enhancing durability and fiber-matrix interfacial shear properties of natural fiber soil composites in order to achieve desired mechanical properties and long term mechanical performance.

The modification of the fiber surface through physical and chemical methods reduces the hydrophilic nature of the natural fibers and decreases the rate of biodegradation in natural settings (Ahmad et al., 2010a; Chand, 2000). Coating fibers with acrylic butadiene styrene (ABS) asphalt emulsion, rosin–alcohol mixture, paints, bituminous materials, a water soluble acrylic and polystyrene can improve composite long term performance (Prabakar and Sridhar, 2002). However, using synthetic materials is not cost effective and ecologically green approach to addressing shortcomings of natural fibers. In order to maintain the cost-effectiveness of using natural fibers for soil reinforcement, investigations that focus on application of natural based additives to improve fiber-matrix adhesion and ultimately the performance of natural fiber soil composites are paramount.

Besides fiber soil reinforcement, utilisation of industrial waste products in the developed countries can play a major role in achieving more resilient earthen construction. In most of the developed countries such as South Africa, the high production of industrial wastes poses challenges in waste management due to high quantities of waste disposal. Fly ash, a waste product from coal burning has shown positive effects on improving mechanical and durability properties of soil. The use of fly ash is more attractive as it is cheap and produced in abundance in the developed countries. Fly ash stabilised soils exhibit high stiffness and brittle behaviour (Abtahi et al., 2010a; Aqeel Al Adili et al., 2012a; Basha et al., 2005; Ghavami et al., 1999a; Tang et al., 2007). Therefore, incorporating fiber reinforcements within soil could be an effective and reliable technique to improve ductility of the soil. Natural fiber-fly ash soil stabilisation could be best techniques to ensure the balance of cost-effectiveness and environmental friendliness in construction. The level of strength improvements of fiber-lime fly ash stabilisation with construction uncertainties such as pre-loading is a problem worthy of investigations.

1.3 Research significance

The present study focuses on the assessment of the potential application of sisal fibers and pine resin coated fibers as soil reinforcing materials for low cost earthen construction. Sisal fibers are commonly grown in most of the developed and developing countries. Over the years, conventional materials such as cement or lime have been used in the construction of infrastructure and have been proven to be expensive to rural communities.

The use of natural fibers, in developing countries is more beneficial for the population as fibers are locally available in abundance and their production is cheap and requires low energy. The natural fiber inclusion in the soil makes the composite biodegradable, reproducible, eco-friendly and cost-effective besides having excellent physical and mechanical properties. Investigations have established the positive effects of vegetable fibers on the physical and mechanical properties of soil composites; however, no substantial reports have been established on the durability issues associated with natural fiber inclusions in the soil.

The use of locally available natural materials for infrastructure development offers three-fold benefits such as the improvement of rural house-hold income and socio-economic status of the countries, and control of climate change. In view of low-cost construction, using natural fibers such as sisal in soil reinforcement promotes agricultural sector through agribusiness. The downstream effect can be the improved income base of the rural communities at household level. The ultimate impact can be the improved economy of the developing countries through increased revenue from sisal exportation. The use of earth materials for construction offers economic benefits particularly in the developing countries where material costs overlap labour costs and where other conventional materials and technologies are not available.

The use of natural additives such as pine resin as pretreatment to natural fibers can positively impact on the forestry industry. The large scale application of natural fibers in construction can promote afforestation of pine trees to supply pine resin. Parallel to the aforementioned prospects, the lumbering industry can be improved as the downstream effect of pine afforestation. This can consequently create jobs for rural masses hence alleviating poverty among rural communities.

The anthropogenic changes, particularly increase in greenhouse gases (GHG), are responsible for the global climate change (Crowley et al., 2000). As reported in the previous section, 50% of greenhouse gas CO_2 emissions originate from cement industry. Using pine resin-treated natural fibers as an ingredient in earthen construction can significantly reduce greenhouse gas emissions since pine trees and sisal plants absorb carbon dioxide. This ultimately addresses effects of climate change.

This study attempts to revitalise the application of natural fibers for earthen construction in response to the need of sustainable and resilient infrastructure in the developing countries. Furthermore, it also shows the potential geo-remediation of fly ash as way of beneficiating the

waste industrial product in strength and durability improvements of fiber reinforced earthen construction in the developed countries.

1.4 Scope of the research

In this study, sisal fibers were used as reinforcing elements of soil matrix to investigate mechanical properties and durability of fiber-soil composites. The combined effects of fly ash stabilisation and sisal fiber inclusion were also investigated in order to establish the mechanics behind reinforcing mechanisms of chemically stabilised fiber soil composites. Natural based rosin was used to improve fiber-matrix interfacial and durability properties for long term performance of the fiber-soil composite. The resilience of the fiber-soil composite to seasonal moisture changes and associated suction stresses was also investigated by subjecting the composite to wet and dry cycles. The mechanical properties of the fiber-soil composite were tested statically and dynamically in order to establish static and dynamic behaviours with special interest in evaluating interfacial strength, macro structural deformation, fracture mechanisms, shrinkage and resilience to cyclic loading. The rationale behind dynamic testing was to mimic material behaviour during earthquake or vibrations while static testing was to evaluate material behaviour under sustained gravity loading. The constitutive model for dynamic behaviour of the fiber-soil composite with effects of material anisotropy and density was developed as tool for design of fiber reinforced earthen or geo systems. Investigation into the role of fiber inclusion in adobe masonry construction was conducted to establish design guidelines of low-cost earthen construction.

1.4.1 General objective

The aim of the research was to assess the potential use of sisal fiber reinforced soil and pine resin as construction materials for sustainable and resilient earthen construction as well as potential application of fly ash for the beneficiation of the waste product to improve durability and strength of earthen construction. The aim of the research was achieved by executing the following specific objectives;

a) Characterisation of macrostructural properties of sisal fiber soil composite.
b) The study of macro behaviour (strength and stiffness, failure modes) of sisal fiber reinforced soil

c) The investigations on the effects of sisal fiber surface coating with pine resin on the fiber-matrix interfacial shear behaviour.
d) The investigation on the moisture and suction induced properties of the sisal fiber-soil composite.
e) The investigation on the dynamic properties of sisal fiber reinforced soil composite
f) The formulation of the constitutive model for nonlinear behaviour of the fiber reinforced soil under dynamic loading: effects of material anisotropy and density.
g) The study on strength durability and strength properties of sisal fiber-fly ash stabilised soil under pre-loading conditions.
h) The study on the role of sisal fiber inclusion in the performance of adobe low-cost earthen masonry construction.

1.5 Research key questions

The key questions for the investigation included:

a) What is the macro structural behaviour of the compacted fiber reinforced soil composite?
b) What is the optimum fiber content and length for maximum soil composite strength mobilisation?
c) What are typical failure modes and reinforcing mechanisms of the fiber soil composite?
d) Does the fiber affect stiffness of the composite?
e) Can plant based repellant (Gum rosin) improve strength properties and durability of the fiber composite?
f) What is the behaviour of fiber reinforced soil composite under moisture variation?
g) How does fiber soil composite respond to the evolution of matric suction?
h) What are the effects of fiber inclusion on the dynamic properties of soil?
i) What is the post cyclic performance of fiber reinforced soil composite?
j) Do composite anisotropy and density affect prediction of dynamic response of soil?
k) What is the major contribution of fibers in fly ash stabilised soil composite?
l) What is the effect of pre-loading on the performance of fiber- fly ash stabilised soil?
m) Is pre-loaded fiber–fly ash soil composite under moisture exposure resilient to loading?
n) What is the role of fibers in low-cost adobe masonry construction and what is the structural performance of fiber reinforced adobe construction?

1.6 Flow chart of the research conducted in the dissertation

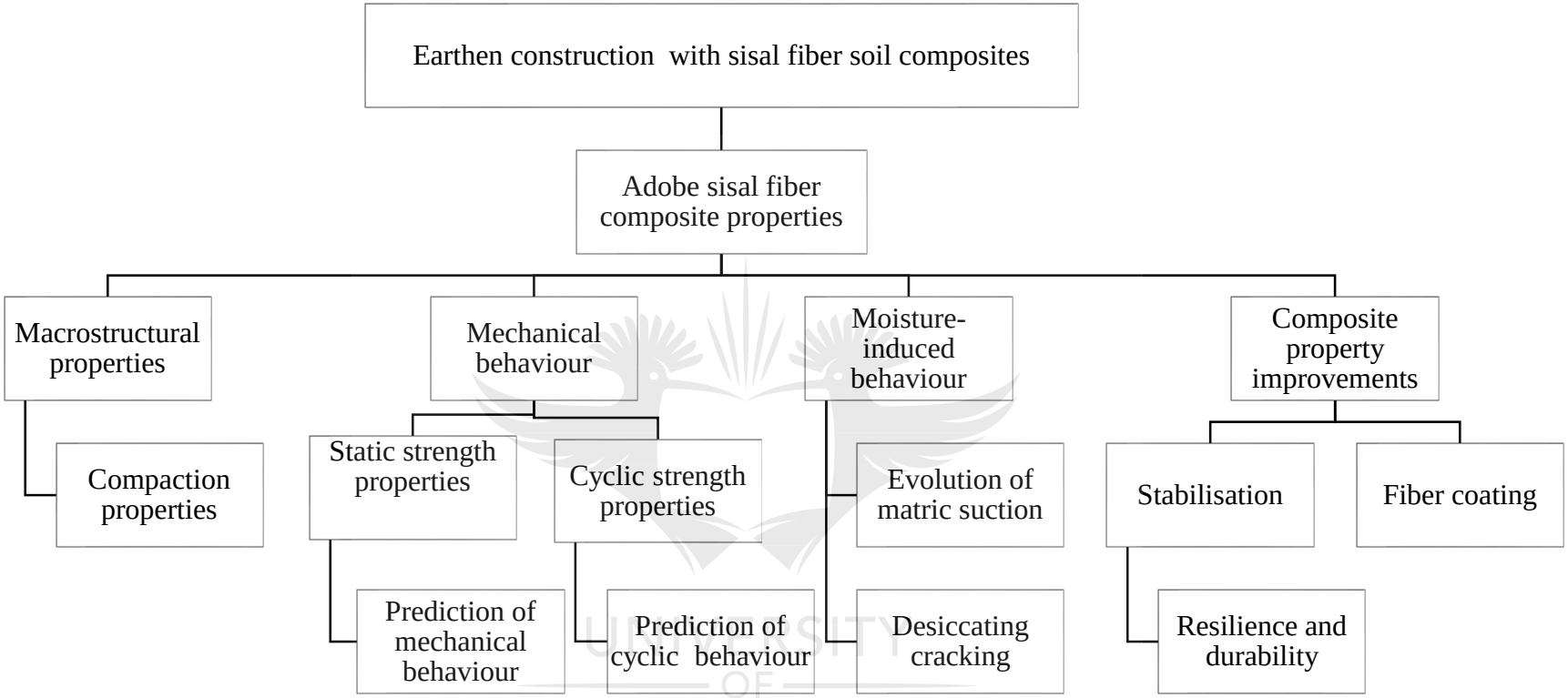

Figure 1.1: Illustration of scope of research

1.7 Thesis outline

The thesis is comprised of 13 chapters. The chronological arrangement of the chapters is as follows;

Chapter 1 presents firstly, the background and motivation for the research. Secondly, the problem to be addressed is highlighted. Thirdly, the significance of the research is elaborated and finally the main objective and scope of the study are outlined.

Chapter 2 presents relevant literature related to the study. It seeks to identify knowledge gap in the area of study. It also critiques the reports by previous researchers. It focuses on the review of the state-of-art of earthen construction, geotechnical perspective of earthen construction, elasticity and plasticity of soil, dynamic behaviour of soil, constitutive models for predicting dynamic behaviour of soil, soil reinforcement techniques such as chemical stabilisation and mechanical stabilisation by fibers, strength behaviour of fiber reinforced soil, prediction models for fiber reinforced soil, failure criteria of fiber reinforced soil, dynamic response of fiber reinforced soil, natural fibers-physical, mechanical and durability properties and studies on sisal fiber reinforced soil and their shortcomings

Chapter 3 deals with material characterisation, experimental design and programmes, and method customisation for quality assurance of specimens.

Chapter 4 presents investigation on the macro behaviour (compaction strength and stiffness) of sisal fiber reinforced soil.

Chapter 5 presents effects of sisal fiber surface coating with natural repellent on the interfacial strength and compressive strength of the sisal fiber soil composite.

Chapter 6 presents matric suction characteristics of the compacted sisal fiber reinforced soil.

Chapter 7 deals with desiccation characteristics and strength properties of the desiccated compacted sisal fibers reinforced soil.

Chapter 8 deals with cyclic and post cyclic shear behaviours of sisal fiber reinforced soil with special interest in dynamic and damping properties, accumulative and permanent strain, and post cyclic energy absorbing capacity of natural fiber reinforced soil.

Chapter 9 presents constitutive model to describe non-linear elastic behaviour of fiber reinforced soil under dynamic loading by incorporating effects of material anisotropy and change in density.

Chapter 10 deals with lime-fly ash stabilised sisal fiber reinforced soil and effects of pre-loading on the time dependent strength in of the stabilised soil.

Chapter 11 presents tensile and compressive strength properties of the lime-fly ash stabilised and pre-loaded sisal fiber reinforced soil subjected to capillary soaking.

Chapter 12 deals with role of sisal fiber inclusion in the performance of adobe masonry earthen construction.

Chapter 13 presents conclusions and recommendation for sisal fiber reinforced earthen construction.

Reference

Abtahi et al. (2010). *Improvement of soil strength by natural fibers.* Paper presented at the From res to des Europ prac, Bratislava, Slovak Republic.

Adam et al. (2016). Detailed Experimental Review of Flexural Behavior of Cement Stabilized Soil Block Masonry. *Journal of Materials in Civil Engineering, 28*(6).

Ahmad et al. (2010). Performance evaluation of silty sand reinforced with fibres. *Geotextiles and Geomembranes, 28*, 93–99.

Allwood et al. (2010). Options for Achieving a 50% Cut in industrial carbon emissions by 2050. *Environmental Science & Technology, 44*(6), 1888-1894.

Aqeel Al Adili et al. (2012). Strength of soil reinforced with fiber materials (papyrus). *Soil Mechanics and Foundation Engineering, 48*(6), 241-247.

Basha et al. (2005). Stabilization of residual soil with rice husk ash and cement. *Construction and Building Materials, 19*(6), 448-453.

Buitrago et al. (2015). Some Properties of Natural Fibers (Sisal, Pineapple, and Banana) in Comparison to Man-Made Technical Fibers (Aramide, Glass, Carbon). *Journal of Natural Fibers, 12*, 357-367.

Chand. S. (2000). Review Carbon fibers for composites. *Journal of Materials Science, 35*(6), 1303–1313.

Chen et al. (2011). Study on Strength Forming Process of Cement Stabilized Soil. *Advanced Materials Research, 250-253*, 1707-1710.

Ciancio.D and Beckett .C. (Ed.). (2015). *Rammed Earth ConstructionCutting-Edge Research on Traditional and Modern Rammed Earth*. Balkema Netherlands: CRS Press.

Crowley et al. (2000). Causes of Climate Change Over the Past 1000 Years. *Science, 289*(5477), 270-277.

Friedlingstein et al. (2010). Updates of Carbobdioxide emissions. *Nature Geoscience, 3*(12), 811-812.

Fu et al. (2000). Tensile properties of short-glass-fiber- and short-carbon-fiber-reinforced polypropylene composites. *Composites Part A: Applied Science and Manufacturing, 31*(10), 1117–1125.

Ghavami et al. (1999). Behaviour of composite soil reinforced with natural fibers. *Journal of cement concrete composite, 21*, 39-48.

Hamidi.A and Hooresfand. M. (2013). Effect of fiber reinforcement on triaxial shear behavior of cement treated sand. *Geotextiles and Geomembranes, 36*, 1-9.

Hejazi et al. (2012). A simple review of soil reinforcement by using natural and synthetic fibers. *Construction and Building Materials, 30*, 100-116.

Kenai et al. (2006). Experimental analysis of the effect of some compaction methods on mechanical properties and durability of cement stabilized soil. *Journal of Material Science (2006) 41:, 41*, 6956–6964.

Millogo et al. (2014). Experimental analysis of Pressed Adobe Blocks reinforced with Hibiscus cannabinus fibers. *Construction and Building Materials, 52*, 71-78.

Morris et al. (2010). Obsevations of the performance of earth buildings following the September 2010 Darfiled earthquake (Vol. 43): Bulletin of the New Zealand Society for Earthquake Engineering.

Pacheco-Torgal. F and Said Jalali. (2011). Earth construction: Lessons from the past for future eco-efficient construction. *Construction and Building Materials, 29*(1), 612-519.

Prabakar.J and Sridhar.R.S. (2002). Effect of random inclusion of sisal fibre on strength behaviour of soil. *Construction and Building Materials, 16*, 123-131.

Reman. O. (2004). Increasing the Strength of Soil for Adobe Construction. *Architectural Science Review,Taylor & Francis, 47*(4), 373-386.

Tanaçan.L.(2008).Adobe Construction: A Case Study in Turkey. *Architectural Science Review,Taylor & Francis, 51*(4), 349-359.

Tang et al. (2007). Strength and mechanical behavior of short polypropylene fiber reinforced and cement stabilized clayey soil. *Geotextiles and Geomembranes, 25*(5), 194-202.

United Nations. (2011). Compendium ofHumanSettlementsStatistics 2001. New York: United nation.

UNSTATS. (2010). Greenhouse Gas Emissions by Sector (Absolute Values). New York: United Nations Statistical Division.

Varum et al. (2010). Characterization of traditional tabique constructions in Douro North Valley region. *WSEAS - World Scientific and Engineering Academy and Society, 105-114*.

Walker. P. (1999). Bond Characteristics of earth block masonry. *Journal of Materials in Civil Engineering, 11*(3), 249-256.

Wu et al. (2013). Strength and stress–strain characteristics of traditional adobe block and masonry. *Materials and Structures, 46*(9), 1449–1457.

2 CHAPTER TWO-LITERATURE REVIEW

2.1 Earthen construction

Earthen construction is divided into three categories namely, adobe, cob and rammed earth structures. Adobe structures are built using unburnt sun-dried bricks shown in figure 2.1a. The soil used can be of a range of types. However, must have a high clay content to have a good consistency when wet, which is required to fill the brick moulds, but not considerably high to cause excessive shrinkage (Beckett, 2011). Cob structures are formed from a wet mixture of clayey subsoil which is placed onto stone foundations in courses prior to being trampled and left to dry. A range of soil types can be used but with similar clay content as adobe. Rammed earth (RE) structures (see figure 2.1b) are formed by compacting moist subsoil between formwork. Like cob, the material dries after it has been formed into the wall, rather than prior to construction as it does for adobe. Straw or other fibers can also be incorporated into the soil mix, depending on local practices (Beckett, 2011; Jaquin, 2008).

(a) (b)

Figure 2.1: (a) Adobe building (courtesy of Carmen Jiménez Delgado) (b) Rammed Earth Alhambra Palace in Spain (courtesy of Dobson)

2.2 State of art of earthen construction

There are 7.7 billion people in the world and about 48% of the population lives rural areas where typical dwelling units are earthen buildings such as mud brick, rammed earth and cob (United nations, 2018). Some major centers of earthen construction include sub Saharan Africa, Australia, regions of North and South America, China and Europe, including France, Germany and Spain. Earthen construction has been practiced in the UK for well over 200 years. Countries such as Australia, New Zealand, USA (New Mexico), and Zimbabwe developed national

standards and reference documents for earthen construction, and more specifically for rammed earth. Recently SADC harmonised standard code for rammed earth has been developed by the African Organization of standardisation. The SADC standard replaces Zimbabwe standard which is currently withdrawn (African Organisation of Standardization, 2014).

According to Houben & Guillaud (Houben and Guillaud, 1994) other countries that have produced codes include France, India, Tanzania, Mozambique, Morocco, Tunisia, Kenya, Ivory Coast, Mexico, Brazil, Peru, Turkey and Costa Rica. Many of these documents cover specific earthen construction techniques, whilst others have been withdrawn and are mostly inaccessible. Recently CRATerre has initiated development of regional standards for pressed earth block construction.

Europe leads the world in modern unstabilised earth structures. Australia leads the world in quality and volume of modern earthen structures specially rammed earth, all being cement stabilised and almost all load bearing and often unprotected from the elements and severe climatic zones, i.e., from the snowfields to the deserts (Dobson, 2015).

2.3 Suction in unsaturated soils

Since the earth materials are initially mixed with water and allowed to dry, they therefore become unsaturated where the soil particles are surrounded by air in addition to water. It is widely accepted that unsaturated soils achieve a component of strength through matric suction.

Suction is the chemical potential of the pore water in unsaturated soils and is so named due to it being invariably negative (i.e. the pore water has a lower potential than pure water under the same conditions). Suction in unsaturated soil is referred to total suction which is a combination of matric suction and osmotic suction (Beckett, 2011; Fredlund et al., 2012; Jaquin et al., 2009). Usually suction is referred to in units of pressure and is more appropriately thought of as a variable that expresses the degree of attachment" of the liquid to the solid phase, rather than as a physical negative pressure, as suctions can often be of considerable magnitude. Total suction ψ is linked to relative humidity (RH) through Kelvin equation which is expressed as equation 2.1

$$\psi = -\frac{\rho_w R_w T_w}{w_v} \ln(RH) \qquad (2.1)$$

where R_w is universal gas constant, T_w is absolute temperature, ρ_w is the density of water, and w_v is the molecular mass of water (Likos and Lu, 2002).

Suction is thought to be an apparent cohesion which increases when soil dries. Its mathematical expression is shown in equation 2.2.

$$. s = u_a - u_b \tag{2.2}$$

where u_a and u_b are pore air pressure and pore water pressure, respectively. Total suction is summation of matric and osmotic suctions that depends on the amount of salts dissolved in water.

The apparent cohesion is therefore expected to peak between the two limits of zero water content and saturation. It should however, be recognised that zero water content corresponds to an ideal limit condition as, even for an oven-dry soil, adsorbed water is still present on clay particles and is available to generate suction. The detailed components of suction are explained by Brackett (Beckett, 2011; Fredlund et al., 2012).

2.4 Desiccating cracking of the soil

Desiccation cracks are likely to occur if the shrinkage of soil is constrained and if tensile stresses are generated in the material beyond allowable tensile strength. These constraints may arise from a frictional or any other traction or displacement boundary conditions. Moreover, any eigen stress concentrations caused by a drying-induced water content heterogeneity, and intrinsic factors such as texture (existence of large particles, or a soil micro-structure (solid network), may form such constraints (Peron et al., 2013). The resulting cracks are critical in as far as the integrity of geotechnical structure is concerned. Drying affects permeability and may undermine the strength of the material. The compressibility of soil increases substantially while the rate of consolidation decreases with the evolution of desiccating cracks (Morris et al., 1992.). Cracks have been the possible precursor for the failure surfaces of most of earth structures. Currently, the analysis of such failures is difficult because the mechanisms and controlling variable in the process are not fully investigated (Peron et al., 2009). Moreover, the intensity differs from granular to fine soils.

It was reported that the unconstrained drying exhibits two stages: domain with large irrecoverable deformation and degree of saturation to 100% followed by the domain with lower deformation at decreasing degree of saturation (Peron et al., 2013). The homogeneous soil macroscopic cracking is possible only in the presence of boundary constraints or moisture gradients that induce generation of tensile stresses. It was suggested that the crack pattern is due to the energy redistribution. They further suggested that the cracks may be formed by sequential infilling or simultaneous growing (Peron et al., 2013).

(Tang et al., 2011) claimed that cracking occurs during the constant evaporation rate stage, when the soil is still fully saturated at a water content of 41%. A growing crack obeys certain laws, and it finally splits the soil surface into relatively regular patterns. Cracks intersect with one another at right angles, and the final crack pattern is dominated by square shapes. Most cracks develop before the air entry point at water content of 14.5% , and surface desiccation cracking tends to terminate after the shrinkage limit of 9.5% is reached (Tang et al., 2011).

2.5 Digital image analysis for desiccation crack measurement

Digital Image Analysis (DIA) has emerged as a powerful tool to investigate desiccation cracking of the soil and to measure the surface features of cracks and has been applied in several research studies. Digital image analysis is a transformation of an image to produce some information representing a description. Digital images that are used for analysis are composed of pixels that are small dots on the screen. The image size is described as m-by-n if it is composed of m pixels in the vertical direction and n pixels in the horizontal direction. The raw images are in RGB color system, consisting of three (red, green, and blue) individual component images (Chanda and Dutta Majumder, 2011). In the analysis, a colour image is converted to grayscale image. A grayscale image is a mixture of black and white colors. These colors are not composed of red, green or blue colors but contain various increments of colors between white and black. The grayscale image is segmented into binary black and white image. The goal of segmentation is to extract one or several regions of interest in an image. Depending on the context, a region of interest can be characterised based on a variety of attributes, such as grayscale level, contrast, texture, shape, size etc. The binary image is further converted to skeleton image in order to extract a region-based shape feature representing the general form of objects such as cracks (Tang et al 2012).

2.6 Behaviour of soil under dynamic loading

The behaviour of soil under cyclic or dynamic loading has been a subject research works for decades. The dynamic behaviour of soil is determined by different types of cyclic tests such as resonant column, cyclic simple shear, cyclic torsional simple shear and cyclic triaxial tests. Typical parameters such as shear modulus and damping ratio are used to evaluate cyclic behaviour of the soil. Amir Shajarati et al (Shajarati et al., 2012) reported that the behaviour of soil subjected to cyclic loading is dependent on; the relative density, mean effective stresses prior to cyclic loading, cyclic and average shear stresses and the drainage conditions. The accumulation of pore water pressure with repeated number of cycles may result in the reduced effective stress leading to liquefaction of soil which is associated with large shear strain. The opposite can also occur when the stress state is located above the cyclic limit state, thereby creating negative pore pressure, and a subsequent increase in effective stresses. Cyclic limit state describes the upper bound for non-failure conditions of cyclic loaded soils (Shajarati et al., 2012). Compared with sandy soils, clayey soils are generally more resistant to cyclic loading. In many cases however, the clay soil undergoes excess settlement if partially drained conditions prevail (Monideepa et al., 2014a; Ni et al., 2014; Pillai Robinson and Boominathan, 2007).Various researchers have shown that cyclic stress level, loading frequency, over consolidation ratio, confining pressure and static preshearing are factors that determine cyclic performance of soil (Ni et al., 2014).

The literature reports that soils under cyclic loading and with a finite number of load cycles do not necessarily reach the cyclic limit state. In some cases the soil reaches a state of equilibrium before failure thereby producing only an elastic response, i.e., no plastic strain or pore pressure accumulation with additional load cycles, a phenomenon called shakedown.

For an elastic-perfectly plastic material subjected to cyclic loading, the shakedown theorem states that the five response cases occur namely elastic response, ordinary collapse, incremental collapse, alternating plasticity and adaptation (Andersen, 2009; Shajarati et al., 2012).

Elastic response normally occurs at low cyclic amplitudes where no plastic deformations happen. Ordinary collapse is associated with high cyclic load amplitudes, the load carrying capacity of the structure becomes exhausted and failure occurs instantaneously as plastic, unconstrained deformations develop and the structure collapses (Głuchowsk, 2015; Shajarati et al., 2012).The typical response of soil under cyclic loading is depicted in figure 2.2.

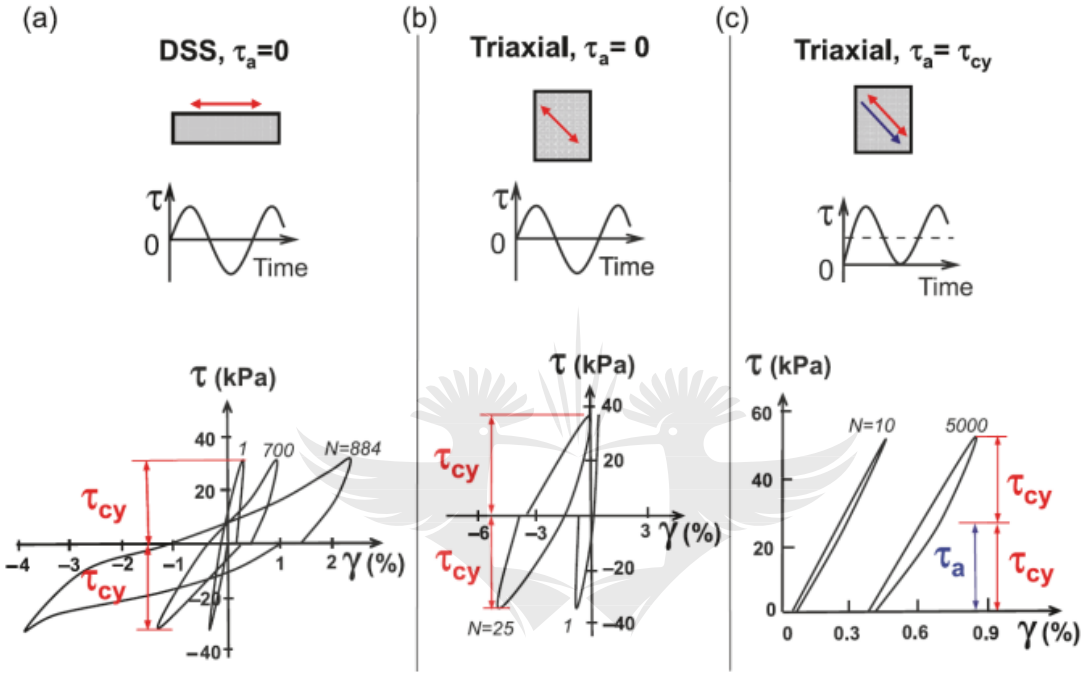

Figure 2.2: Stress-strain relation of soil under various cyclic loading conditions (Andersen, 2009; Shajarati et al., 2012).

The factors that influence the load bearing capacity of soil under cyclic loading include cyclic load ratio and average load ratio. The cyclic load ratio is defined as normalisation of cyclic shear stress with undrained shear strength for cohesive soil and with effective stress for granular soil. The average load ratio is the normalisation of average cyclic shear stress in the same manner as cyclic load ratio.

Saturated clay becomes softer when subjected to the cyclic loading a phenomenon called degradation. As the number of cycles increase, the excess pore water pressure builds up and causes reduction in effective stress, and consequently reduces friction resistance of clay grains. The bonding between clay particles is destroyed and the material becomes soft (Matsui, 1991; Zhou and Gong, 2001). The most important soil parameters under dynamic loading are shear

modulus and damping ratio. The shear modulus for clay is affected by strain amplitude, effective stress, density, void ratio and water content. The secant shear modulus decreases with increase in strain amplitude and void ratio. It should be noted that the effects of strain amplitude is more significant when the soil grains are separated or discrete from each other more substantially. Discreteness is the case when grains have no cohesion and when the effective stress is low. The high effective stress is associated with high shear modulus.

On the other hand damping ratio of clay is smaller than that of coarser materials. This is because clay is more continuous than sand and gravel. It may be concluded that the more discrete material has the greater energy damping capacity than more continuous soils (Towhata, 2008).

2.6.1 Constitutive models of soil under dynamic loading

Various studies have attempted to establish models for predicting behaviour of soil under various cyclic loading conditions. The shear modulus decreases with the increased level of shear strain. At a very low strain level, the magnitude of the shear modulus is maximum (that is, G = Gmax). (Hardin and Drnevich, 1972) proposed the shear stress-shear strain relationship to be approximated by equation 2.3.

$$\tau_x = \frac{\gamma}{1/G_{max} + \gamma/\tau_{max}} \tag{2.3}$$

where γ is the shear strain and τ_x is the shear stress.

(Hardin and Black, 1968) proposed shear modulus of soil for low amplitudes of vibration given by equations 2.4, 2.5 and 2.6 for clay and sand, respectively.

$$G_{max} = \frac{3230(2.17-e)^2}{1+e} OCR^K \sigma_x^{0.5} \quad \text{for clay soil} \tag{2.4}$$

$$G_{max} = \frac{6908(2.17-e)^2}{1+e} \sigma_x^{0.5} \quad \text{for rounded grained sand} \tag{2.5}$$

$$G_{max} = \frac{3230(2.17-e)^2}{1+e} \sigma_x^{0.5} \quad \text{for angular-grained sand} \tag{2.6}$$

where σ_x is the effective octahedral stress K is the constant related to plasticity index

Seed and Idriss, 1970 proposed that shear modulus of soil be expressed as equation 2.7.

$$G = 218.82K_2\sigma_x^{0.5} \tag{2.7}$$

For large strain, (Hardin and Drnevich 1972) suggested that shear modulus of the soil be described by equation 2.8.

$$G = \frac{G_{max}}{1+\gamma_h} \tag{2.8}$$

where γ_h is the hyperbolic strain given by $\left(\frac{\gamma}{\gamma_r}\right)\left[1+ae^{-b(\gamma/\gamma_r)}\right]$ a is the constant. They further proposed relationship between damping ratio and shear modulus given by equation 2.9.

$$D_d = D_{max}\left(1-\frac{G}{G_{max}}\right) \tag{2.9}$$

Some other modified expressions for dynamic parameters of soil were proposed by Kondner and Zelasko (Kondner and Zelasko, 1963) and Matasović and Vucetic (Matasović and Vucetic, 1993). Damping ratios for sands are affected by factors such as (a) grain-size characteristics, (b) degree of saturation, (c) void ratio, (d) earth pressure coefficient at rest (K_0), (e) angle of internal friction, (f) number of stress cycles (N), (g) level of strain, and (h) effective confining pressure. The last two factors however, have the major effect on the magnitude of the damping ratio (Hardin and Drnevich, 1972; Seed and Idriss, 1970).

(Sherrif et al., 1977) proposed the relationship for damping ratio of the dry sand given by equation 2.10.

$$D_d = \frac{50-0.087\sigma_c}{38}(73F-53)\gamma^{0.3}(1.01-0.0046\log N) \tag{2.10}$$

where F is the sphericity factor of the soil grains, N is the number of cycles of strain, σ_c is the effective confining pressure and others are as described in the previous equations.

The relationship between cyclic stress level, loading frequency, and number of cycles at failure was also modeled and concluded that the value of this limiting stress ratio is constant over the

frequency range between 0.0083 and 0.2 Hz and decreases for frequency of greater than 0.2 Hz. The fully weakened state can be achieved in any displacement controlled test provided strain rate is greater than 5% and number of cycles is at least 10, 000. However, the modelling did not account for development of pre pressure or axial strain during loading(David et al., 1984; Ni et al., 2014). Ansal and Erken (Ansal and Erken, 1989) developed regression expressions to estimate the cyclic yield strength given by equation 2.11 and excess pore pressure build-up based on the number of cycles and cyclic stress level is given by equation 2.12.

$$.\left(\frac{\tau}{\tau_f}\right)_y = a - b\log N_c \tag{2.11}$$

where N_c is the number of cycles, a and b are the material constants, representing properties of test material.

$$m = k + \log N_c \tag{2.12}$$

where m is the slope of pore pressure line, and k and p are material constants obtained from the regression analysis. Magnitude of the pore pressure build-up can be estimated using equation 2.12. If m and threshold cyclic stress ratio (S.R) are known, the pore pressure can be estimated by equation 2.13.

$$u_w = \left[\left(\frac{\tau}{\tau_f}\right) - (S.R)\right]m \tag{2.13}$$

The model did not account for the effect of the loading frequency. The model of axial strain and normalised excess pore pressure as a function of time-based power law was proposed. However, the predicted behaviour of the soils in this model is independent of the loading frequency (Hyde et al., 2007). An exponential relationship for pore pressure against time and corresponding stability criteria were developed using the critical state line. In this model, the effect of loading frequency was not taken into account (Hyodo et al., 1992). The mathematical model to quantify the influence of cyclic stress level, loading frequency, and over-consolidation ratio was proposed by (Zhou and Gong, 2001). Six parameters (see equations 2.14, 2.15, and 2.16) were introduced from the regression expression whose numerical values were not clearly determined.

$$\delta = [A + B]CInN + 1 \quad (2.14)$$

where δ is the degradation A is the effect of over consolidation ratio (OCR), B is the effect of cyclic stress ratio and is the influence of frequency and A, B and C are expressed as

$$A = \left(a_1 OCR^2 + a_2 OCR + a_3\right) In(OCR) \quad (2.15)$$

$$B = \left(b_1 (r_c - r_t) + b_2 \right. \quad (2.16)$$

$r_c = \left(\frac{\tau_d}{c_u}\right)$ where r_c is the cyclic stress ratio, c_u is the static undrained strength and τ_d is the vertical cyclic stress and $C = \left(\frac{1}{f}\right)^{c_1}$.

where, a_1, a_2, a_3, b_1, b_2 and c_1 are the test parameters and r_t is the threshold cyclic stress ratio below which no pore pressure is generated.

Having identified shortcomings of the proposed models for the behaviour of soil under cyclic loading, (Ni et al., 2014) developed a model based on Cam-clay theory with two additional parameters that characterise the cyclic behaviour are used together with the traditional parameters associated with the modified Cam-clay constitutive model. In this model, numerous factors that influence the cyclic performance of soft soils were considered, such as cyclic stress ratios, preshearing, and cyclic loading frequency. The critical cyclic stress ratio was also predictable using the proposed model in terms of excess pore pressures and axial strains. It was reported that permanent excess pore pressures and strains for normally consolidated soils, only occur in the first cycle if the Modified Cam-clay model is strictly used to simulate the cyclic performance as the yield surface remains unchanged after the first load cycle (Carter et al., 1982).

The behaviour of the soil is considered elastic and as such no further permanent excess pore pressures and strains develop. However, when saturated soft clays are unloaded and then reloaded repeatedly, the permanent excess pore pressures and strains often keep on increasing during the entire period of cyclic loading. One way of interpreting this real behaviour is to assume that the position and the shape of the yield surface are influenced by elastic unloading.

Therefore, the form of the yield surface can simply be assumed to remain unchanged, but with a reduced size in an isotropic manner by the elastic unloading. Therefore, a parameter θ is introduced (see equation 2.17) to indicate how much the yield surface contracts when the soil is elastically unloaded.

$$\frac{\partial p'_c}{p'_c} = \omega \frac{\partial p'_y}{p'_y} \tag{2.17}$$

where p'_c is a hardening parameter which can be considered as the pre-consolidation pressure, p'_y is a variable given by equation 2.18.

$$p'_y = p' + \left(\frac{q}{M}\right)^2 \frac{1}{p'} \tag{2.18}$$

where M is the slope of the critical state line in $p' - q$ space, where p' and q are the effective mean

stress and deviator stress defined by the major σ'_1 and minor, principal stress $p' = \frac{1}{3}\left(\sigma'_1 - 2\sigma'_3\right)$.

Parameter ω decreases with an increase in number of cycles and takes a form of the equation 2.19.

$$\theta = \frac{1}{N\xi_1 + \xi_2} \tag{2.19}$$

The determination of the effective stresses and strains is demonstrated against the stress path for normally and isotropically consolidated soils under cyclic loading shown in figure 2.3.

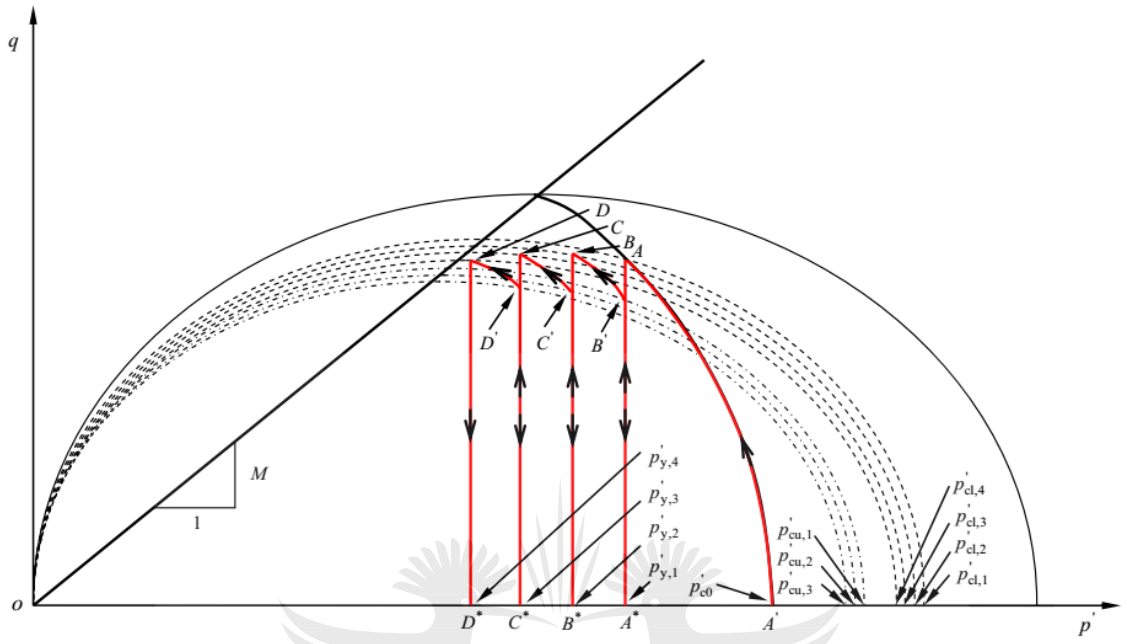

Figure 2.3: Stress path for cyclic loading (Ni et al., 2014).

where $p'_{cl,i}(i=1,2....,n)$ is the yield stress after loading part of the cycle, $p'_{cu,i}(i=1,2....,n)$ is yield stress after unloading part of each cycle and $p'_{y,i}(i=1,2....,n)$ is the loading parameter after each cycle. The shear strength parameter of soil under dynamic loading can be determined by laboratory tests such as; dynamic triaxial test, ring shear test, direct shear test, resonant column test among others.

The generalised hyperbolic model for prediction of undrained pore-water pressure as a function of cyclic stress ratio, frequency, and plasticity of soils using data reported by a number of researchers was developed by (Monideepa et al., 2014b) . The proposed model has been validated by a chi-square goodness-of-fit test.

2.7 Natural fibers

Natural fibers are classified based on their origins, whether they are derived from plants, animals, or minerals (see figure 2.4). Plant fibers include bast fibers, leaf or hard fibers, seed, fruit, wood, cereal straw, and other grass fibers.

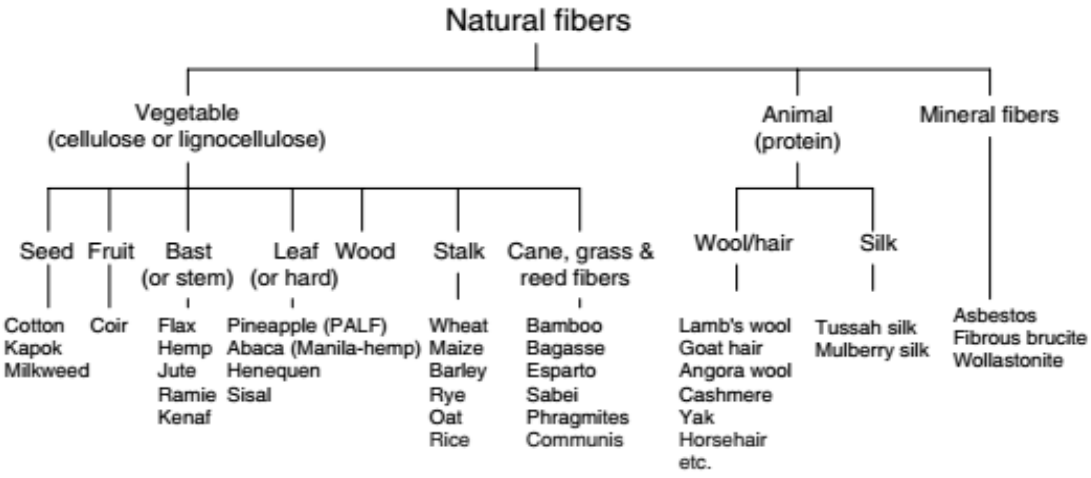

Figure 2.4: Classification of natural fibers (Amar et al., 2005).

2.7.1 Structural composition of natural fibers

Natural fibers are composite material by nature of their structural composition. The fibers are a rigid, crystalline cellulose microfibril reinforced amorphous lignin and/or hemicelluloses matrix (Amar et al., 2005). Most plant fibers, except for cotton, are composed of cellulose, hemicelluloses, lignin, waxes, and some water-soluble compounds, where cellulose, hemicelluloses, and lignin are the major constituents (Buitrago et al., 2015). The major component of most plant fibers is cellulose (α-cellulose). Cellulose is a linear macromolecule consisting of D-anhydroglucose ($C_6H_{11}O_5$) repeating units joined by β -1,4-glycosidic linkages with a degree of polymerisation of around 10,000 (Amar et al., 2005; Douglas et al., 2014). Each repeating unit contains three hydroxyl groups. These hydroxyl groups and their ability to form hydrogen bond play a major role in directing the crystalline packing and also govern the physical properties of cellulose materials. Solid cellulose has a semicrystalline structure, i.e., consists of highly crystalline and amorphous regions. Cellulose forms slender rod like crystalline microfibrils (Gurunathan et al., 2015; Komuraiah et al., 2014).

The crystal structure (monoclinic sphenodic) of naturally occurring cellulose is known as cellulose I. Cellulose is resistant to strong alkali (17.5 wt%) but is easily hydrolysed by acids to water-soluble sugars. Cellulose is relatively resistant to oxidising agents. Hemicelluloses are polysaccharides composed of a combination of 5- and 6-ring carbon ring sugars. The polymer chains are much shorter with degree of polymerisation around 50 to 300 and branched,

containing pendant side groups giving rise to its non-crystalline nature. Hemicelluloses form the supportive matrix for cellulose microfibrils. Hemicellulose is very hydrophilic and soluble in alkali and easily hydrolysed in acids (Amar et al., 2005; Gurunathan et al., 2015).

Lignin is the compound that gives rigidity to the plants. It is a complex with three dimensional copolymers of aliphatic and aromatic constituents of very high molecular weight. Its chemistry is not well understood, but most of its functional groups and building units of the macromolecule have been identified. It is characterised by high carbon but low hydrogen content. Lignin contains five hydroxyl and five methoxyl groups per building unit. It is believed that the structural units of a lignin molecule are derivatives of 4-hydroxy-3-methoxy phenylpropane (Nevell and Zeronian, 1985). Lignin is amorphous and hydrophobic in nature. It is a thermoplastic polymer, exhibiting a glass transition temperature of around 90°C and melting temperature at which the polymer starts to flow of around 170°C. It is not hydrolysed by acids, but soluble in hot alkali, readily oxidised, and easily condensable with phenol.

Natural fibers are bundles of elongated thick-walled dead plant cells. A single or elementary natural fiber is a single cell typically of a length from 1 to50 mm and a diameter of around 10-50 μm. Natural fibers are like microscopic tubes, i.e., cell walls surrounding the center lumen. The lumen contributes to the water uptake behavior of plant fibers. The fibers comprise of different hierarchical microstructures. The cell wall in a fiber is not a homogeneous membrane but is built up of several layers. The primary cell wall that is the first layer deposited during cell growth, and the secondary cell wall (S), which consists of three layers (S_1, S_2, and S_3). The cell walls are formed from oriented reinforcing semicrystalline cellulose microfibrils embedded in a hemicelluloses/lignin matrix of varying composition. Such microfibrils have typically a diameter of about 10-30nm and are made up of 30 to 100 cellulose molecules in extended chain conformation, and provide mechanical strength to the fiber (Mishra et al, 2004). The amorphous matrix phase in a cell wall is very complex and consists of hemicellulose, lignin, and in some cases pectin. The hemicellulose molecules are hydrogen bonded to cellulose and act as a cementing matrix between the cellulose microfibrils, forming the cellulose/hemicellulose network, which is the main structural component of the fiber cell. The hydrophobic lignin network acts as a coupling agent and increases the stiffness of the cellulose/hemicellulose composite. The cell walls differ in their composition, the ratio between cellulose and

lignin/hemicellulose, and in the orientation of the cellulose microfibrils. In most natural fibers, the cellulose microfibrils are oriented at an angle to the normal fiber axis called the microfibrillar angle. The summary of composition of various natural fibers is shown in Table 2.3.

Table 2.1: Chemical Composition, Moisture Content, and Microfibrillar Angle of Vegetable (Amar et al., 2005)

Fiber	Cellulose (wt%)	Hemicelluloses (wt%)	Lignin (wt%)	Pectin (wt%)	Moisture Content (wt%)	Waxes (wt%)	Microfibrillar Angle (deg)
Flax	71	18.6–20.6	2.2	2.3	8–12	1.7	5–10
Hemp	70–74	17.9–22.4	3.7–5.7	0.9	6.2–12	0.8	2–6.2
Jute	61–71.5	13.6–20.4	12–13	0.2	12.5–13.7	0.5	8
Kenaf	45–57	21.5	8–13	3–5			
Ramie	68.6–76.2	13.1–16.7	0.6–0.7	1.9	7.5–17	0.3	7.5
Nettle	86				11–17		
Sisal	66–78	10–14	10–14	10	10–22	2	10–22
Henequen	77.6	4–8	13.1				
PALF	70–82		5–12.7		11.8		14
Banana	63–64	10	5		10–12		
Abaca	56–63		12–13	1	5–10		
Oil palm EFB	65		19				42
Oil palm mesocarp	60		11				46
Cotton	85–90	5.7		0–1	7.85–8.5	0.6	—
Coir	32–43	0.15–0.25	40–45	3–4	8		30–49
Cereal straw	38–45	15–31	12–20	8			

2.7.2 Mechanical properties of natural fiber constituents

The structure, microfibrillar angle, cell dimensions and defects, and the chemical composition of the natural fibers are the most important variables that determine the overall properties of the fibers. In general, the tensile strength and Young's modulus of natural fibers increase with increasing cellulose content of the fibers. The orientation of the cellulose microfibrils with respect to the fiber axis governs stiffness of the fibers. Natural fibers are more ductile if the microfibrils have a spiral orientation to the fiber axis. Fibers are inflexible, rigid, and have a high tensile strength if the microfibrils are oriented parallel to the fiber axis.

Jochen et al have shown that the elastic modulus of the natural fiber decreases with increase in spiral angles and increases with increase in cellulose content. The shear modulus and degree of anisotropy increase linearly with increase in spiral angle (Gassan, 2001).

2.7.3 Hygroscopicity of natural fibers

Cellulose is the main component of natural fibers, and the elementary unit of a cellulose macromolecule is anhydro-D-glucose, which contains three hydroxyl (OH) groups. These

hydroxyl groups form hydrogen bonds inside the macromolecule itself (intramolecular) and between other cellulose macromolecules (intermolecular) (Amar et al., 2005). Because of its chemical structure, many hydroxyl groups are available for interaction with water molecules by hydrogen bonding. Cellulosic fibers interact with water not only at the surface, but also in the bulk. The quantity of absorbed water depends on the relative humidity of the confined atmosphere with which the fiber is exposed to (Douglas et al., 2014; Hamidi and Hooresfand, 2013; Martin et al., 2013). The sorption isotherm of cellulosic material is a function of the level of purity of cellulose. The raw cellulosic material such as non-washed sisal fibers absorbs at least twice as much water as washed fibers. This is due to the presence of 24% of pectic cements and the degree of crystallinity: all OH groups in the amorphous phase are accessible to water whereas only a small amount of water interacts with the surface OH groups of the crystalline phase. The water absorption characteristic of natural fibers causes variation in width of the fibers. All these characteristics of the cellulosic fiber play an important role when the fiber is to be incorporated in a matrix: Strong adherence is needed to take advantage of the high modulus of the fiber and this is achieved by fiber surface treatments.

2.8 Soil reinforcement

Soil reinforcement techniques have been applied for decades for ground improvement. The technique involves placing resisting inclusions in the soil. Depending on the type of the inclusion, there two extreme cases of inclusions namely: a uniform inclusion where the soil-reinforcement interaction develops in any point along the inclusion and a 'composite inclusion' which consists of an inclusion reinforced in some particular points where the soil-reinforcement interaction is concentrated. In the case of a uniform inclusion, a relatively high and uniform density of the reinforcements results in a reinforced soil composite (Schlosser et al., 1984). The objective of soil reinforcement is to improve mechanical properties of soil. The notable soil reinforcement techniques involve use of strips, sheets, geosynthetics and fibers and nailing. Soil reinforcement is applied in various areas of civil engineering including, bridge abutments, ladder wall dams, earth dam embankments, foundations, highway embankments, pipe works, housing, railways, etc (Jones, 1985).

The reinforcing mechanism is provided by the ability of the reinforcement to resist mobilised shear stress provided by the soil matrix by means of adhesion or friction interlock between the

soil and the reinforcement. The factors that affect soil reinforcement include soil type, reinforcement type and distribution, and soil state. The schematic presentation of soil reinforcement mechanism is shown in figure 2.5.

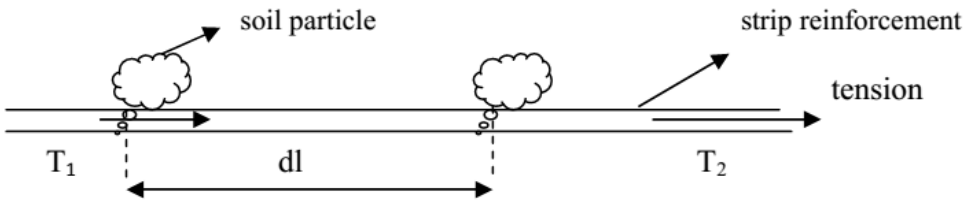

Figure 2.5: Development of adhesion in reinforcement strip(Jones, 1985).

For the circular strip of diameter D and length dl and with normal stress σ_v acting on the soil strip interface, bond between soil and reinforcement is given by equation 2.20.

$$T_{ad} = T_1 - T_2 \tag{2.20}$$

Normal force acting on the strip is $\pi D dl \sigma_v$ and tensile force generated in the reinforcement, assuming the coefficient of friction μ between soil and reinforcement is given by equation 2.21.

$$T_{ad} = \mu \pi D dl \sigma_v \tag{2.21}$$

In order to establish the logical area for the reinforcement, the potential failure mechanisms and planes have to be established together with the associated strain fields. For optimum effect, reinforcement should be positioned within the critical strain fields in the locations of greatest tensile strains. It is important that the reinforcement is placed along the principal tensile strain directions developed in the soil alone, under the same stress conditions. Altering the orientation of the reinforcement reduces its effectiveness, and if orientated in the direction of the principal compressive strains, the action of reinforcement changes from that of tensile strain reinforcement to compressive strain reinforcement (Jones, 1985). If the reinforcement is orientated along the zero extension directions, an overall reduction in the strength of the reinforced soil may occur. The reinforcement strength governs the capacity to withstand stress and stiffness dictates the deformability of the reinforcements. Rough reinforcement surface enhance friction between the soil and the reinforcement.

The soil used in a reinforced structure depends upon conditions and circumstances; in some instances the reinforcement may be used to improve a weak soil. The soil properties and the soil state have significant effects on the reinforced behaviour. The ideal particle size for reinforced soil is a well-drained, well-graded granular material that provides long-term durability, stability during construction and having good physio-chemical properties. In the normal stress range associated with reinforced soil structures, well-graded granular soils behave elastically, and post construction movements associated with internal yielding do not normally occur. Fine-grained soils are normally poorly drained and effective stress transfer between reinforcement and soil cannot be immediate, resulting in a slow construction rate. Fine-grained soils often exhibit elastoplastic or plastic behaviour, thereby increasing the chance of post-construction movements.

2.8.1 Fiber reinforced soil

The fiber-reinforced soil is defined as a soil mass that contains randomly distributed, discrete elements such as fibers, which provide an improvement in the mechanical behaviour of the soil composite (Li, 2005). Fiber reinforced soil behaves as a composite material in which fibers of relatively high tensile strength are embedded in a matrix of soil. The fibers can either be continuous-aligned or discontinuous and randomly oriented as shown in figure 2.6. Shear stresses in the soil mobilise tensile resistance in the fibers, which in response imparts greater strength to the soil. The laboratory and some in situ pilot test results (Estabragh et al., 2011; Gray and Ohash, 1983; Hejazi et al., 2008; Ibraim et al., 2006; Maher and Gray, 1990; Yetimoglu and Salbas, 2003) have reported encouraging conclusions proving the possible use of fibers for the reinforcement of soil mass providing an artificial replication of the effects of vegetation on soil mass (Ghiassian et al., 2008). The research has shown that fibers aligned in the direction of extension are more beneficial than other directions (Gray and Ohash, 1983; Neeraja et al., 2014).

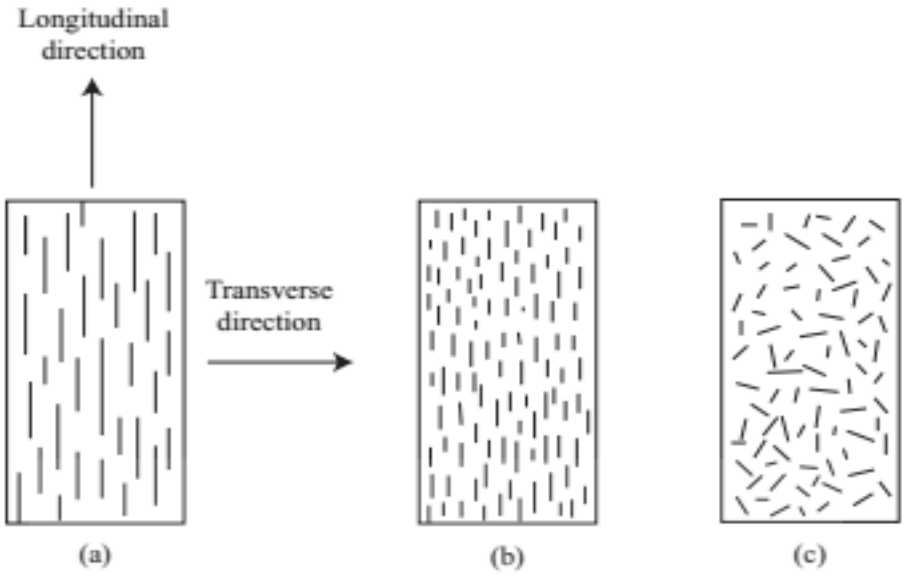

Figure 2.6: (a) Continuous aligned fibers (b) Discontinuous aligned fibers (c) Randomly distributed fibers (Douglas et al., 2014).

The reinforcing fibers can be natural, i.e., sisal, jute, flax, coconut, bamboo, ramie, pineapple, etc, or man-made (synthetic) such as glass, carbon, barmaid, etc. The industrial fibers have better mechanical properties (see Tables 2.1 and 2.2) than natural fibers. However, comparatively , natural fibers are locally available at a low cost (Karahan, 2015; Raju et al., 2008), biodegradable (Rozman et al., 2003), recyclable (Sreekala et al., 2004), flexible during processing, pose minimum health risks, have low density, desirable fiber aspect ratio, high specific strength (Park, 2009; Peponi et al., 2008; Yashwant et al., 2015), and relatively high resistance to tension and bending. The research has shown that soil shear strength, peaks stress, frictional angle and cohesion are significantly improved by fiber inclusion (Abtahi et al., 2010b; Ahmad et al., 2010b; Aqeel Al Adili et al., 2012b; Estabragh et al., 2013). Furthermore, fiber inclusions limit the post peak reductions in shear resistance and decrease the stiffness of the soil. Fiber reinforcements reduce soil brittleness providing smaller loss of post-peak strength (Tang et al., 2009 ; Yetimoglu and Salbas, 2003). Fibers reduce shrinkage cracks, swell behaviour and compressibility in expansive soils (Bhadriraju et al., 2005; Malekzadeh and Bilse, 2014; Malekzadeh and Bilsel, 2012; Malekzadeh and Bilse, 2012; Zhuang and Yu, 2015). The pre consolidation pressure decreases and the coefficient of swelling and compression generally increase with increasing fiber content for cohesive soil. By adding fiber to the soil (or increasing

the fiber content) some soil particles are replaced with fibers and they occupy the pores between the soil particles which results in increase in void ratio of the soil mass. As a result, the soil becomes more compressible (Estabragh et al., 2011). The most influencing fiber characteristics are aspect ratio, fiber concentration, surface characteristics and fiber orientation (Babu et al., 2008a; Harikumar et al., 2015; Michalowski and Cermak, 2003; Park, 2009; Tang et al, 2007b).

Table 2.2: Properties of inorganic (synthetic) fibers (Bunsell and Renard, 2005)

Fiber	Polymer	Diameter (µm)	Density (g/cm^3)	Young's modulus *E* (GPa)	Strength σ (GPa)	Strain to failure (%)	Specific modulus E/ρ (GPa/ g/cm^3)	Specific strength E/ρ (GPa/ g/cm^3)
Polyamide 66	PA66	20	1.2	<5	1	20	4	0.8
Polyester	PET	15	1.38	<18	1	15	13	0.6
Nomex	MPD-1	15	1.38	17	0.64	22	12	0.5
Technora	PPDT	12	1.39	70	3	4.4	50	2.2
Kevlar 49	PPTA	12	1.45	135	3	4.5	93	2.1
Zylon	PBO	12	1.56	280	5.8	2.5	180	3.7
M5	PIPD	12	1.7	330	4	1.2	194	2.4
Polyethylene	PE	38	0.96	117	3	3.5	120	3.1

Table 2.3: Characteristic Values for the Density, Diameter, and Mechanical Properties of Vegetable and Synthetic Fibers(Amar et al., 2005)

Fiber	Density (g cm^{-3})	Diameter (µm)	Tensile Strength (MPa)	Young's Modulus (GPa)	Elongation at Break (%)
Flax	1.5	40–600	345–1500	27.6	2.7–3.2
Hemp	1.47	25–500	690	70	1.6
Jute	1.3–1.49	25–200	393–800	13–26.5	1.16–1.5
Kenaf			930	53	1.6
Ramie	1.55	—	400–938	61.4–128	1.2–3.8
Nettle			650	38	1.7
Sisal	1.45	50–200	468–700	9.4–22	3–7
Henequen					
PALF		20–80	413–1627	34.5–82.5	1.6
Abaca			430–760		
Oil palm EFB	0.7–1.55	150–500	248	3.2	25
Oil palm mesocarp			80	0.5	17
Cotton	1.5–1.6	12–38	287–800	5.5–12.6	7–8
Coir	1.15–1.46	100–460	131–220	4–6	15–40
E-glass	2.55	<17	3400	73	2.5
Kevlar	1.44		3000	60	2.5–3.7
Carbon	1.78	5–7	3400[a]–4800[b]	240[b]–425[a]	1.4–1.8

[a] Ultra high modulus carbon fibers.

[b] Ultra high tenacity carbon fibers.

2.8.2 Prediction models for fiber reinforced soil

Soil reinforced with short fibers may be analysed as a composite material in which fibers of high tensile strength are embedded in a matrix of lower tensile strength. This analogy is the basis of the engineering technique of fiber reinforced soil in which true cohesion is imparted to the soil by linear reinforcing elements. Force is transmitted through the matrix by forces tangential to the fibers producing differing tensions along their length. These tangential forces are carried by friction and/or by bonding between fibers and surrounding matrix.

Sayyed Mahdi Hejazi et al developed a model to predict the interfacial shear strength based on the following assumptions;(1) composite shearing occurs in a horizontal zone of thickness D which is penetrated by vertical fibers; (2) D does not change during shear; (3) fibers are flexible with circular cross-section d_f, of uniform diameter and are linearly elastic with the elastic modulus of E_f (Hejazi et al., 2013). They utilised the theory of short fiber composite proposed by Cox whose model is schematically shown in figure 2.7.

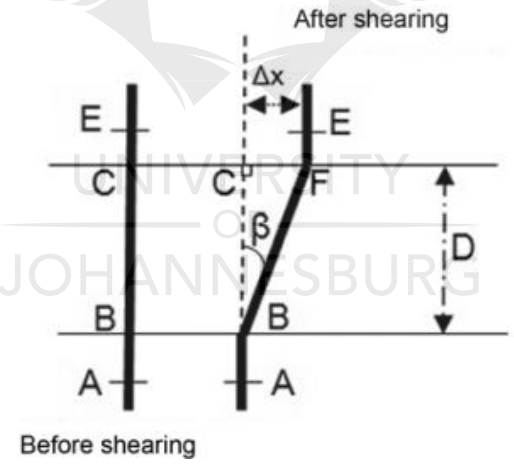

(a)

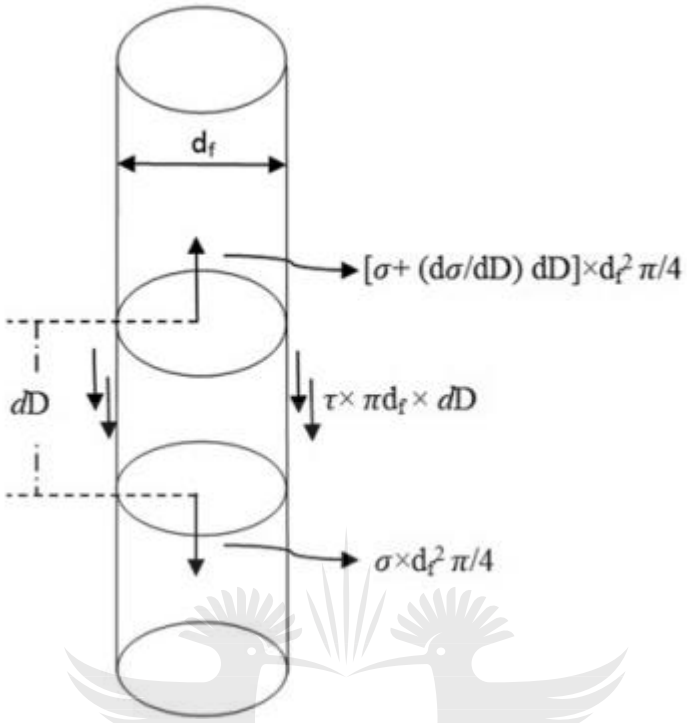

(b)

Figure 2.7: Schematic of the proposed model(Hejazi et al., 2013)

The soft matrix (soil) induces tension on the fibers through tangential stresses τ which has a maximum value at on-set of slippage of $\tau_{\max}$. When the upper mass of matrix (see figure 2.7a) has been displaced by a distance Δx, the fiber segment BC extends to new length BF (see figure 2.6a): after shearing. Consequently, the average tensile stress σ_{av} within the fiber depends on the elastic modulus E_f

Using force equilibrium of fiber element shown in figure 2.7b, the summation of forces results in the maximum tensile stress given by equation 2.22 and avarage stress given by equation 2.23.

$$\sigma_{\max} = 2\sqrt{\frac{\pi D E_f \left(\sec\beta - 1\right)}{d_f}} \tag{2.22}$$

$$\sigma_{av} = \frac{\sigma_{\max}}{2} = \sqrt{\frac{\pi D E_f (\sec\beta - 1)}{d_f}} \tag{2.23}$$

For N number of fibers within shear zone of area A_s and height of soil composite h_s and fiber volume fraction as v_f, the shear strength increase of the fiber reinforced soil composite is given by equation 2.24.

$$\tau_{inc} = (h_s v_f)\left(\frac{\pi D E_f}{d_f}\right)^{0.5} (\sec\beta - 1)^{0.5} \frac{(\sin\beta + \cos\beta \tan\varphi)}{L_f} \tag{2.24}$$

The tangential shear stress τ between the fiber and the soil matrix using coulomb law of friction is given by equation 2.25.

$$\tau = \mu\sigma_v \tag{2.25}$$

where μ and σ_v are the friction coefficient between fiber and soil and applied vertical stress in the soil, respectively. Therefore shear strength improvement in the soil is given by equation 2.26.

$$\tau_{inc} = (h_s v_f)\left(\frac{\mu\sigma_v D E_f}{d_f}\right)^{0.5} (\sec\beta - 1)^{0.5} \frac{(\sin\beta + \cos\beta \tan\varphi)}{L_f} \tag{2.26}$$

Gray and Ohashi proposed a force equilibrium model based on the results of a series of direct shear tests conducted on fiber-oriented reinforced sands. The model was developed on assumption that along the shear plane, the shearing of soil the causes fiber distortion, thereby mobilising its tensile resistance. The model assumes that fiber length, interface friction and confining pressure are large enough to avoid fiber pullout failure. Consequently, the fiber-induced tension σ_t can be expressed as a function of fiber modulus E_f, interfacial frictional resistance along fiber τ, fiber diameter d_f and thickness of the shear zone D, expressed as equation 2.27 (Gray and Ohash, 1983).

$$\sigma_t = \left(\frac{4E_f \tau D}{d_f}\right)(\sec\varphi - 1)^{0.5} \quad (2.27)$$

where φ is the friction angle of the soil, considering fiber area ratio, the mobilised tensile strength t is given by equation 2.28.

$$t = \frac{A_f}{A}\sigma_t \quad (2.28)$$

where A_f and A are area of fibers in shear and total area of soil in shear, respectively. Therefore, the shear increase in the soil τ_{inc}, due to the fiber reinforcement perpendicular to shear plane is determined by force equilibrium given by equation 2.29.

$$\tau_{inc} = t(\sin\beta + \cos\beta\tan\varphi) \quad (2.29)$$

where β is the angle of distortion.

Maher and Gray further expanded the model proposed by Gray and Ohashi to randomly-distributed fibers by using statistical approach. The average embedment length for randomly distributed fiber was adopted as quarter of the fiber length on either side of the failure plane (Maher and Gray, 1990). The average number of fibers N_f, intersecting the unit area of the shear plane can be obtained as in equation 2.30.

$$N_f = \frac{2v_f}{\pi d_f^2} \quad (2.30)$$

where v_f is the volume fraction of fibers .The tensile stress developed in fibers is can be obtained from equation 2.31.

$$\sigma_t = \frac{2(\sigma_n \tan\delta)L_f}{d_f} \quad (2.31)$$

where δ is the angle of skin resistance of the soil and σ_n is the confining stress acting on the fibers. The shear strength increase of the soil is given by equation 2.32.

$$\tau_{inc} = N_f \left(\frac{\pi d_f^2}{4} \right) \left[\frac{2(\sigma_n \tan\delta) L_f}{d_f} \right] (\sin\theta + \cos\theta \tan\varphi) \xi \qquad (2.32)$$

where ζ is the empirical coefficient depending on soil parameters.

The models above are valid only for extensible fiber with a frictional surface, and therefore can be used for predicting tensile strength of some natural fiber reinforced soil. The polymeric fibers have relatively high tensile strength and deformation modulus but relatively low interface friction. Certainly, these models may be inadequate when failure is governed by the pullout of fibers especially for soils reinforced by synthetic fibers. Furthermore, the models require determination of the thickness of the shear zone and fiber distortion as an input parameter, which is difficult to quantify (Hejazi et al., 2012). Most importantly, the effects of surface modifications by moisture and coating were not considered.

Sadi et al found that the energy-based model underestimate the measured friction coefficient on average by about 10%, and the discrete model overestimated the friction coefficient by 6%, with associated coefficients of variation on bias values of 0.20 and 0.17, respectively. With the introduction of minor modifications to these models, the average bias error was eliminated, and the coefficients of variation in the ratio of predicted to measured shear strength (bias) were reduced to 0.17 and 0.12, respectively, for the two models (Shadi et al., 2013).

Ranjan et al derived an expression for the shear strength of fiber reinforced soil using a regression analysis of test results from a series of triaxial compression tests. Fiber content, fiber aspect ratio, fiber–soil interface friction, and shear strength of unreinforced soil were identified as the main variables influencing the shear strength (Ranjan et al., 1996). The shortcoming of Ranjan's model is that it did not reflect the mechanisms of fiber-reinforcement and relied heavily on simple set of experimental results. The parameters that affect interfacial shear strength include soil dry density, water content, particle size, the confinement stress, displacement rate, embedded reinforcement length, reinforcement surface roughness and shape (Tang et al., 2010b).

Ding and Hargrove presented models based on a volumetric homogenisation technique but limited to the description of non-linear elastic behaviour of soil for monotonic loading condition (Ding and Hargrove, 2006). Li and Ding presented a model to describe a non-linear elastic behaviour of fiber reinforced soil under cyclic loading conditions (Ding, 2002). A complete

constitutive law for soils reinforced with continuous filament was presented by Villard et al (Villard et al., 1990) and Prisco and Novausing by utilising superposition of sand and fiber effects (Prisco and Nova, 1993). The model proposed by Villard et al was the only one that recognised the importance of fiber orientation as a parameter governing the effectiveness of fiber inclusion.

Two dimensional Distinct Element Method (DEM) has been developed for the micromechanical analysis of mixtures of granular materials and flexible fibers (Ibraim and Maeda, 2007; Ibraim et al., 2006). Babu et al successfully performed numerical analysis with finite difference code(Babu et al., 2008b). Abtahi et al extended the shear lag theory proposed by Cox (Cox, 1952) to explain the role of fiber length and fiber diameter in short fiber soil composites. It was found that by increasing the fiber length and decreasing fiber diameter, CBR value improves (Hejazi et al., 2008). Diambara et al presented a model based on the rule of mixtures of composite materials at conventional triaxial soil tests. The model considered that the fibers behave linear elastically and the unreinforced soil obeys the simple linear elastic perfectly plastic Mohr–Coulomb model (Diambra et al., 2010). Artificial neural network (ANN) was used by Abtahi et al and Shouling et al (He and Li, 2009) to predict the role of fiber parameters on the shear strength of short fiber soil composites (Abtahi et al., 2010b). Hejazi et al used fiber slippage theory and force equilibrium method in collaboration with artificial neural network (ANN) and least square error (LSE) to predict shear strength improvements of looped fiber reinforced soil. It was found that looped fiber reinforcement presented greater shear improvement than ordinary fiber reinforcement (Hejazi et al., 2014).

2.8.3 Failure criteria of fiber reinforced soil

Michalowski and Zhao proposed an energy-based homogenisation technique to define the average failure stress of the fiber–soil composites on the basis that fiber slippage occurs on the both ends of the fibers and tensile rupture takes place in the middle of the fibers. The model considered only energy dissipation due to fiber–soil slippage and to fiber tensile rupture (Michalowski and Zhao, 1994). In this homogenisation approach, an incipient deformation for a representative element as shown in figure 2.8 was assumed.

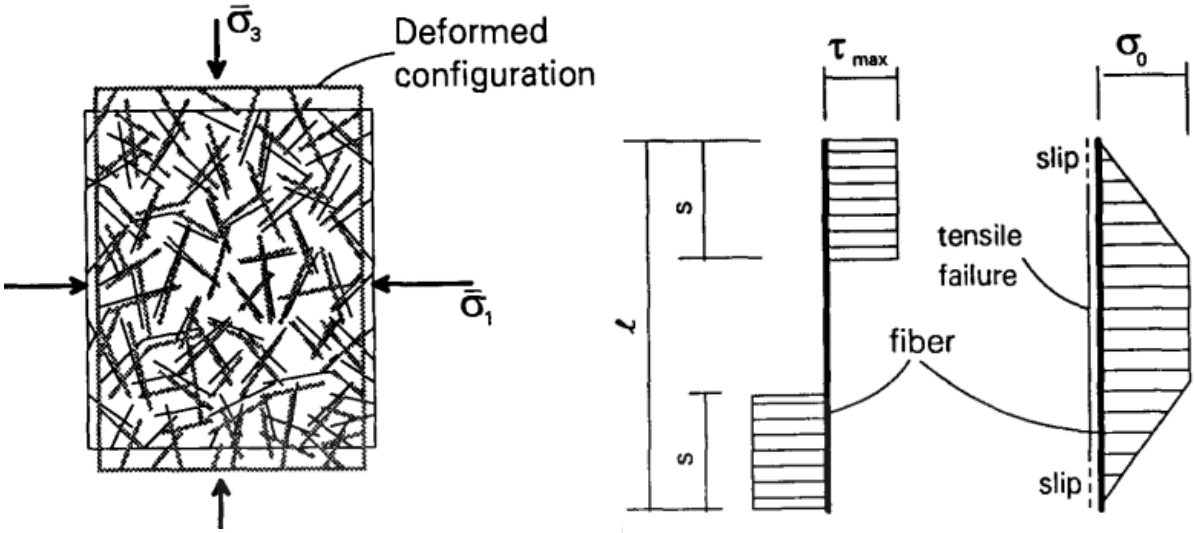

(a) (b)

Figure 2.8: (a) Plane-strain deformation of 3D specimen (b) Fiber-matrix shear stress and axial stress in rigid-perfectly plastic fiber (Michalowski and Zhao, 1994).

The energy dissipation rate, $D(\dot{\varepsilon}_{ij})$ in the soil and fibers was calculated during the incipient deformation process, and it was equated to the work rate of the macroscopic stress σ_{ij} given by equation 2.33.

$$\sigma_{ij}\varepsilon_{ij} = \frac{1}{V}\int_{v} D(\dot{\varepsilon}_{ij})dV \qquad (2.33)$$

where V is the volume of the element of soil composite and ε_{ij} is the average strain rate. The fibers were assumed to be cylindrical and uniformly distributed, both fibers and soil matrix were considered perfectly plastic and the influence of confining stress on fiber tensile strength was negligible. Failure of a single fiber in a deforming composite was assumed to occur due to fiber slippage or tensile rupture. However, even if a tensile rupture occurs, the ends of the fiber slips as the tensile strength of the fiber material cannot be mobilised throughout the entire fiber length. For a rigid-perfectly plastic behaviour of the granular soil, fibers, and interface, the expected distribution of the shear stress on the fiber surface and the axial stress in the fiber follow the pattern shown in figure 2. 8b. If fiber failure is the tensile rupture mode, the slippage occurs at

both fiber ends up to the distance *s* as shown in figure 2.8b. The energy dissipation rate during plastic deformation of soil conforming to the Mohr-Coulomb failure condition and associative flow rule is zero; therefore, only the fibers contribute to the dissipation in the composite.

The energy dissipation rate in a single fiber oriented in direction θ due to slippage along end sections *s* (see figure 2.8b) and plastic extension in the middle section of length is $l-2s$ is given by equation 2.34.

$$d = 2\pi r_f s^2 \sigma_n \tan\varphi_w \left(\dot{\varepsilon}_\theta\right) + \pi r_f{}^2 (l-2s)\sigma_o \left(\dot{\varepsilon}_\theta\right) \tag{2.34}$$

where σ_o is the yield stress of fiber material, σ_n is the stress normal to the fiber surface, φ_w is the friction angle of the fiber matrix interface, r_f is the fiber radius and $\left(\dot{\varepsilon}_\theta\right)$ is the strain rate in the direction of the fiber (zero for compressive stress). The volumetric energy dissipation is given by equation 2.35.

$$D_r = \frac{1}{V}\int_v \pi r_f{}^2 \sigma_o \left(l - \frac{r_f \sigma_o}{2\overline{\sigma_n}\tan\varphi_w}\right)\left(\frac{\rho_f}{\pi r_f{}^2 l}\right)\left(\dot{\varepsilon}_\theta\right) dV \tag{2.35}$$

where ρ_f is fiber concentration and $\overline{\sigma_n}$ is the average normal stress to the fibers in volume V.

The energy dissipation of the fiber reinforced soil composite is given by equation 2.36.

$$D_r = \frac{6}{\pi R_o{}^3}\int_v \left(1 - \frac{\sigma_o}{4\eta\overline{\sigma_n}\tan\varphi_w}\right)\rho_f \sigma_o \left(\dot{\varepsilon}_\theta\right) dV \tag{2.36}$$

where R_o is the radius of the volume that is occupied by the fibers, η is the fiber aspect ratio. The solution to preceding equation yields equation 2.37.

$$D_r = \frac{\rho_f \sigma_o}{3} M\left(1 - \frac{\sigma_o}{4\eta p_n \tan\varphi_w}\right)\dot{\varepsilon}_1 \tag{2.37}$$

where p_n is mean of maximum and minimum principal stresses, $\dot{\varepsilon}_1$ is the maximum principal strain and M can be obtained from equation 2.38.

$$M = \left(0.5 + \frac{\varphi}{\pi} + \frac{1}{\pi}\cos\varphi\right)\tan^2\left(\frac{\pi}{4} + \frac{\varphi}{2}\right) - \frac{1}{2} - \frac{\varphi}{\pi} + \frac{1}{\pi}\cos\varphi \tag{2.38}$$

If no fiber yielding occurs, expression for the energy dissipation rate per unit volume is independent of the fiber yield stress given by equation 2.39.

$$D_r = \frac{1}{3}\rho_f \eta M p_n \tan\varphi_w \dot{\varepsilon}_1 \tag{2.39}$$

The failure criterion for fiber reinforced soil for isotropic material under plane strain condition is given by equation 2.40.

$$\frac{R}{\rho\sigma_o} = \frac{p_n}{\rho_f \sigma_o}\sin\varphi + \frac{1}{3}N\left(1 - \frac{1}{4\eta}\left(\frac{\sigma_o \cot\varphi_w}{p_n}\right)\right) \tag{2.40}$$

where N, R and p are expressed as equation 2.41,2.42 and 2.43.

$$N = \frac{1}{\pi}\cos\varphi + \left(\frac{1}{2} + \frac{\varphi}{\pi}\right)\sin\varphi \tag{2.41}$$

$$R = \sqrt{\frac{\left(\overline{\sigma_x} - \overline{\sigma_y}\right)^2}{4} + \overline{\tau_{xy}}^2} \tag{2.42}$$

$$p_n = \frac{\overline{\sigma_1} + \overline{\sigma_3}}{2} \tag{2.43}$$

For the unreinforced soil, the failure criterion becomes Mohr-Coulomb criterion for granular soil given by equation 2.44.

$$R = p_n \sin\varphi \tag{2.44}$$

The aforementioned homogenisation method was further used to analyse the failure criteria of anisotropically oriented fibers and associated shear improvements. It was found that the random

distribution has lower shear strength improvements because some of the fiber are subjected to compression hence do not contribute to shear resistance. The convex conical failure criterion was therefore derived that could be used to solve stability problems for fiber-reinforced granular soil (Michalowskia and Cerma´ k, 2002). The kinematic hardening occurs due to the evolution of fiber orientation during deformation process. Fibers incline in the direction of extension offer greater shear strength improvements.

Diambra et al used the Severn-Trent sand model, which combines critical state theory, Mohr-Coulomb like strength criterion, bounding surface plasticity and kinematic hardening. In this formulation, fibers were considered as purely tensile elements following a linear elastic constitutive rule. It was indicated that only those fibers oriented within the tensile strain domain of the sample can mobilise tensile stress. The orientation of fibers was one of the key parameters to capture the anisotropic behaviour of fiber reinforced soil that was observed for triaxial compression and extension loading (Diambra et al, 2013). They derived a model to predict fiber orientation distribution based on moist tamping procedure which was applicable to various types of fiber reinforced soil (Diambra et al., 2007).

Zornberg proposed a 'discrete' framework to predict the equivalent shear strength of the fiber-soil composite by using parameters obtained from the independent characterisation of soil specimens and of fiber specimens. Under shearing, fiber reinforcement contributes to the increase of shear resistance by mobilising tensile stress within fibers (Zornberg, 2002a). The equivalent shear strength of fiber-reinforced specimens, S_{eq} , is expressed as equation 2.45.

$$S_{eq} = S + \alpha t = c + \sigma_n \tan\varphi + \alpha t \qquad (2.45)$$

where α is an empirical coefficient that accounts for the partial contribution of fibers (assumed α = 1 for randomly distributed fibers), *t* is the fiber-induced tension defined as the tensile force per unit area induced in a soil mass by randomly distributed fibers, S is the shear strength of the unreinforced soil, and c and φ are the shear strength parameters of unreinforced soil. The expression of *t* can be derived for different failure modes. At low confining stress when failure is governed by the pullout of the fibers, $S_{eq.p}$ can be estimated using equation 2.46.

$$S_{eq.p} = c_{eq.p} + \tan\varphi_{eq.p}\sigma_n \tag{2.46}$$

where parameters $c_{eq.p}$ and $\tan\varphi_{eq.p}$ are defined by equations 2.47 and 2.48.

$$C_{eq.p} = \left(1 + \alpha v_f \left(\frac{L_f}{d_f}\right) c_{ic}\right) c \tag{2.47}$$

$$(\tan\varphi)_{eq.p} = \left(1 + \alpha v_f \left(\frac{L_f}{d_f}\right) c_{i\varphi}\right) \tan\varphi \tag{2.48}$$

The shear strength envelop for the aforementioned model is shown in figure 2.9.

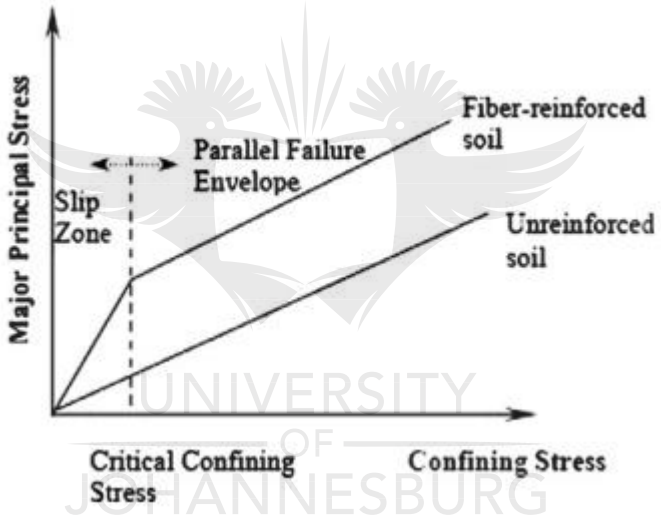

Figure 2.9:Shear strength envelope of fiber-reinforced soil: after Gray and Ohashi (Gray and Ohash, 1983).

2.8.4 Dynamic response of fiber reinforced soil

Existing knowledge on the behaviour of fiber-reinforced soil composites under dynamic loads is very limited. Recently, researchers have tried to investigate the dynamic response of fiber reinforced soil. The statistics show that most of research work were conducted on granular soils. However, results showed benefits of the fiber inclusion in improving dynamic properties of soil (Amir-Farya and Sherif Aggour, 2015; Bozyigit et al., 2016). Fiber inclusion tends to reduce the initial stiffness of soil composite at low strain level (Clariá and Vettorelo, 2015). Shear modulus of clay sand decreases with increasing deviator stress ratio at high confining pressure and the rate of loss of shear modulus is much lower for fiber reinforced clay sand. In addition, an increase in

shear modulus with loading repetition is more pronounced at higher deviator stress ratios (Sadeghi and Beig, 2014). Addition of basalt and glass fibers after freeze-thaw cycles increases the damping ratio and the shear modulus at constant confining pressure because of an increase in stiffness, but the shear modulus decreases with increasing shear strain (Orakoglua et al., 2017). Noorzad et al showed that inclusions significantly increase liquefaction resistance of sand. Upon increasing the fiber content and fiber length, the number of loading cycles leading to liquefaction increases. The reinforcement effect in medium dense samples is more significant than that of looser samples. Furthermore, the confining pressure has a considerable effect in reducing the liquefaction susceptibility. Shear modulus of unreinforced and reinforced samples was also evaluated and results revealed that the shear modulus increases with increasing fiber content (Noorzad and Fardad Amini, 2014).

Maher et al showed that the dynamic modulus increases with increasing fiber aspect ratio, modulus, and with increasing fiber content to a limiting amount. The presence of fibers reduces prestrain effect in unreinforced sands. The increase in dynamic modulus of fiber-reinforced sand is more pronounced at high shearing-strain amplitudes. The maximum percentage increase in modulus as a result of fiber inclusions occurs over a narrow range of confining stresses from 21 to 48 kPa.

Damping is less affected by the inclusion of fibers than shear modulus. The dynamic response of sands reinforced with vertically oriented fibers is very similar to that of randomly distributed fibers (Faryar and Behzad, 2012; Maher and Woods, 1990).

Krishnaswamy et al tested uniformly graded fine sand with geotextiles and coir fiber inclusions under cyclic triaxial tests. It was revealed that fiber inclusion has a significant effect on increasing the liquefaction resistance of sand deposits (Krishnaswamy and Isaac, 1994).

Ibraim et al tested sand reinforced with flexible polypropylene crimped fibers using static compression and extension undrained triaxial tests. It was shown that the presence of fibers reduces the potential for the occurrence of liquefaction in both compression and extension triaxial loadings (Ibraim et al., 2010).

Liu et al tested silica sand with polypropylene fibers using ring-shear tests. It was concluded that fiber reinforcement is useful for improving the static liquefaction resistance of sand (Liu et al., 2011).

Maheshwari et al tested sand reinforced with geogrid sheet, geosynthetic fiber, and natural coir fiber by shaking table (vibration table) tests. The reinforcements were very effective in increasing liquefaction resistance of sand under laboratory conditions (Maheshwari et al., 2012).

The reports on the behaviour of fiber reinforced soil under cyclic loading are very limited in the literature. Various methods, such as cyclic triaxial, resonant-column, torsional shear, bender elements and shake table are used to investigate dynamic properties of soil(Das and Ramana, 2011). The dynamic characteristics of fiber reinforced soil are greatly influenced by fiber content, fiber length, loading repetition, confining pressure, loading frequency and shear strain amplitude(Li and Senetakis, 2017; Sadeghi and Beig, 2014). Some recent studies have attempted to investigate the dynamic properties and liquefaction behaviour of fiber reinforced soil using various methods. It is conclusive that fiber inclusions increase both shear modulus and damping ratio (Amir-Farya and Sherif Aggour, 2015; Bozyigit et al., 2016). Shear modulus in low confining pressures (less than 100kPa) are negligible and in high confining pressures are considerable (Shahnazari et al., 2009).

Haiwen Li and Kostas Senetakis (Li and Senetakis, 2017) reported that the shear modulus of fiber reinforced sand at very small strains reduces with an increase in fiber content and the trend is more pronounced at fiber contents greater than 0.5%. Clariá and Vettorelo(Clariá and Vettorelo, 2015) found out that the inclusion of fibers tends to reduce the initial stiffness of fiber reinforced soils at low strain level. Sadeghi and Beigi (Sadeghi and Beig, 2014) found that shear modulus of clay sand decreases with increasing deviator stress ratio at high confining pressure and the rate of loss of shear modulus is much lower for fiber reinforced clay sand. In addition, an increase in shear modulus with loading repetition is more pronounced at higher deviator stress ratios. Orakoglu et al (Orakoglua et al., 2017) showed that addition of basalt and glass fibers after freeze-thaw cycles increases the damping ratio and the shear modulus at constant confining pressure because of an increase in stiffness, but the shear modulus decreases with increasing shear strain. Fiber inclusions in sand increase liquefaction resistance and number of cyclic cycles to reach liquefaction (Eskişar et al., 2016; Ibraim et al, 2010; Maheshwari et al., 2012; Mittal and

Chauhan, 2013). The aforementioned studies utilised synthetic fibers as reinforcing elements. These fibers are expensive and require a lot of energy in production. Natural fibers are more favourable than synthetic fibers due to their cost effectiveness and environmental friendliness (Hejazi et al, 2012; Kafodya and Okonta, 2018a). When the soil is subjected to the cyclic loading such as earthquake, strain accumulation may alter the post cyclic shear behaviour and energy absorbing capacity of soil.

2.8.5 Natural fiber reinforced soil

There is a pressing need for more environmentally friendly materials for the sustainable infrastructure development. In response to the need, there have been many experimental investigations related to sustainable materials. The great deal of interest has been created worldwide on potential applications of natural fibers for soil reinforcement. The concept of natural fiber reinforcement was recognised more than 5000 years ago. In the ancient civilizations straw and hay were used to reinforce mud blocks in order to create reinforced building blocks. Several earth structures were built with natural fiber inclusions like Great Wall of China (earliest example of reinforced earth using branches of trees as tensile elements)(Abtahi et al., 2009; Rao, 1996), Ziggurats of Babylon (woven mats of reed were used)(Rao, 1996)

2.8.6 Geotechnical properties of natural fiber reinforced soil

Some researchers have reported the effects of natural fiber inclusion on physical properties of granular and cohesive soils. Prabakar et al have shown that, for any particular percentage of fiber content, dry density decreases with longer fiber length. Therefore, it implies that the maximum dry density of the soil lowers with an increase in fiber length. For a particular fiber length, maximum dry density decreases at a high fiber content.

The increase in fiber length reduces optimum moisture content (OMC) and the presence of moisture in fibers undermines optimum moisture content at high fiber content (Prabakar and Sridhar, 2002). However, Soundara et al have reported some contradicting results on the effect of fiber content on OMC of clay soil using coir fiber (Soundara and Senthil kumar, 2015). The results showed that fiber content lowers OMC of the soil. Surprisingly, this trend was not properly analysed and explanation was not clearly articulated. F Ahmad et al have shown that natural fiber inclusion restrains the tendency of dilation in granular soil and effects are more significant in surface treated fibers. The surface treatment of fibers with polymers and

bituminous material raises the hydrophobicity of the composite and improves durability (Ghavami et al., 1999a; Santiago et al., 2013).

2.8.7 Shear strength of natural fiber reinforced soil

Many researchers have developed interest to investigate the effects of natural fiber inclusion on the shear strength and strength parameters of soil and the factors that affect shear strength mobilisation in both granular and cohesive soils. Fauziah et al have reported that fiber length, content of oil palm fiber and fiber coating affect the shear strength of sand. Inclusion of randomly distributed discrete fiber significantly improves the shear strength of silty sand. Coated fibers increase the shear strength of silty sand much more compared to uncoated fiber. Coating fiber increases interface friction between fiber and soil particles by increasing the surface area. In their study, reinforced silty sand containing 0.5% coated fibers of 30 mm length exhibited approximately 25% increase in friction angle and 35% in cohesion under undrained loading conditions compared to those of unreinforced silty sand. The results indicated that the shear strength parameters of the soil-fiber mixture, frictional angle and cohesion can be improved significantly with fiber inclusion (Ahmad et al., 2010a; Aqeel Al Adili et al., 2012a).

Prabakar et al and Chegenizadeh et al have also confirmed that random inclusion of natural fiber (sisal fiber) significantly improves soil shear strength. The frictional angle varies non-linearly with fiber concentration. However, their report does not include the microstructural deformations, shrinkage cracks and failures modes of the reinforced soil (Chegenizadeh and Nikraz, 2012; Prabakar and Sridhar, 2002).

Khosrow Ghavami et al have reported that optimum water to soil ratio is important in order to produce a high-strength soil matrix. Sisal or coconut fiber impart considerable ductility and also increase compression strength of the soil composite (Ghavami et al., 1999b).

Santiago et al have reported that the inclusion of natural fibers (curauá) increases the peak shear strength, the cohesion intercept and the internal friction angle values, and also the stiffness of the soil mixtures under triaxial compression(Santiago et al., 2013). However, they have not reported on the effects of fiber orientation on the strength of the soil composite. The evolution of interfacial shear strength was not elaborated for the polymer used.

Estabragh et al have shown that the random inclusion of natural fibers (palm) has a significant effect on the consolidation behaviour of randomly reinforced clay soil. The pre-consolidation pressure decreases and consolidation and swelling indices increase with increasing the fiber content in reinforced soil. Positive pore pressure is developed and is associated with the tendency of volumetric contraction. Ultimately, it was concluded that the fiber restrains the dilatancy of fiber reinforced soil (Estabragh et al., 2013). However, the researchers could not quantify the interaction mechanism of fiber and clay. They recommended that a comparison between shear strength envelops obtained from consolidated undrained (CU) and consolidated drained (CD) tests is fundamental as it may help in understanding the interaction mechanism between fiber and clay.

According to Jili Qu et al, inclusion of randomly distributed natural fiber (palm fibers) in cohesive soil increases peak and residual shear strength, unconfined compressive strength and CBR value of soil. The maximum strength could be achieved with optimum fiber length and content (Zhao and LI, 2015).

Bouhicha et al investigated effects of straw reinforcement at different reinforcement/soil ratios and fiber lengths on the behaviour of the soil. The results of the tests proved the positive effects of adding straw fibers in decreasing shrinkage both linear and volumetric (Bouhicha et al., 2005).

In their investigation, they observed increase in flexural, shear and compressive strengths of fiber reinforced soil and a more ductile failure mode was obtained with the reinforced specimens. The best water repellent treatment seemed to be that using a cement render with polymer addition. They recommended that further studies are necessary to elucidate the fracture mechanism, the effect of prior treatment of the fibers and the durability of the composite at long term and under more severe conditions.

2.8.8 Fiber surface treatments

In order to enhance adhesion between the matrix and fiber and durability of the fiber-matrix composite, fiber surface modification are done by physical or chemical methods. Physical methods involve surface fibrillation, electric discharge (Corona, cold plasma). Physical treatments change structural and surface properties of the fiber and thereby influence the mechanical bonding with the matrix (Amar et al., 2005). Surface modification by discharge treatment such as low-temperature plasma, sputtering, and corona discharge is of great interest in

relation to the improvement in functional properties of natural fibers. On the other hand, the chemical modification involves application of coupling agents to optimise stress transfer at the interface between fiber and matrix. Coupling agents are molecules possessing two functions (Amar et al., 2005; Douglas et al., 2014), the first is to react with OH groups of cellulose and the second is to react with functional groups of the matrix. The chemical composition of coupling agent allows them to react with the fiber surface, which forms a bridge of chemical bonds between the fiber and matrix.

The reports by Ghavami et al, Segetin et al and Subrahmanyam have indicated that treating fiber surfaces with water resistant coatings such as asphalt emulsion, rosin–alcohol mixture, paints, bituminous materials, a water soluble acrylic, a polystyrene coating and acrylonitrile butadiene styrene (ABS) can improve natural fiber hydrophilicity and durability (Ghavami et al., 1999a; Segetin et al., 2007; Subrahmanyam, 1984)

2.8.9 Interfacial shear strength improvement techniques

Interfacial bonding between fiber and matrix plays a vital role in determining the mechanical properties of fiber composites. As eluded in the preceding sections, stress is transferred between matrix and fiber across the interface. Therefore, good interfacial bonding is required to achieve optimum reinforcement, although, it is possible to have an interface that is too strong, enabling crack propagation which can reduce toughness and strength (Pickering et al., 2016). However, for plant based fiber composites, there is usually limited interaction between the hydrophilic fiber and matrices which are commonly hydrophobic, leading to poor interfacial bonding that limit long term mechanical performance of the composite.

For bonding to occur, fiber and matrix must be brought into intimate contact; wettability can be regarded as an essential precursor to bonding. Insufficient fiber wetting results in interfacial defects which can act as stress concentrators (Chen et al., 2006). Fiber wettability has been shown to affect the toughness, tensile and flexural strength of composites (Wu and Dzenis, 2006). Physical treatment and chemical treatment can improve the wettability of the fiber and thus improve the interfacial strength. Interfacial bonding can occur by mechanical interlocking, electrostatic bonding, chemical bonding and inter-diffusion bonding (Pickering et al., 2016).

Mechanical interlocking occurs to a greater extent when the fiber surface is rough and increases the interfacial shear strength, but has less influence on the transverse tensile strength. Chemical

bonding occurs when there are chemical groups on the fiber surface and in the matrix that can react to form bonds and as a consequence the resulting interfacial strength depends on the type and density of the bonds. Chemical bonding can be achieved through the use of a coupling agent that acts as a bridge between the fiber and matrix. Inter diffusion bonding occurs when atoms and molecules of the fiber and matrix interact at the interface (Liu et al., 2008; Sinha and Panigrahi, 2009). Physical approaches include corona, plasma, ultraviolet (UV), heat treatments electron radiation and fiber beating. Chemical approaches are more represented within the literature than physical with better improvements obtained to date. Chemical treatments include alkali, acetyl, silane, benzyl, acryl, permanganate, peroxide, isocyanate, titanate, zirconate and acrylonitrile treatments and use of maleated anhydride grafted coupling agent.

2.9 Effects of fiber inclusion on desiccating cracking of soil

Tang et al., (2016) have reported that addition of fibers to soil changes morphological properties of the composite. Increase in fiber content causes a decrease in crack width and surface area ratio. The crack networks become more irregular and crack segments become more jagged. Chaduvula et al (2017) in the similar soil desiccation study reported that longer fibers are not effective in restraining desiccation cracking effects of expansive soil. Xue Qiang et al (2014) observed that straw fiber inclusion could not exhibit insignificant effects on surface shrinkage of the soil.

2.10 Soil chemical stabilisation and fiber inclusions

Lime and cement stabilisation techniques have been applied for ages in construction of improved geo structures (Bell, 1996; Osinubi, 1998a). In practice, the techniques are effectively applied to expansive or clayey soils. Lime and cement stabilisation improve plasticity index, swelling, shrinkage, permeability and typical engineering properties such as shear strength and, compressibility of soil (Abdulrahman et al., 2014; Al-Mukhtar et al., 2010; Al-Swaidani et al., 2016; Bell, 1996; Di Sante et al., 2014; Jha and Sivapullaiah, 2016a; Tran et al., 2014). The combined addition of lime and fibers increases the efficiency to transfer load from matrix to fibers especially at extended curing time and also significantly affects the rate of unconfined compressive strength gain of the soil (Anggraini et al., 2014; Moghal et al., 2017). Literature has shown that compressibility of fly ash is highly affected by lime dosage and duration of load

increments. The addition of lime to fly ashes triggers hydration process that in turn causes formation of cementitious compounds that are responsible for enhanced cementation of soil particles. The lime-fly ash mixtures exhibit low compressibility and high equilibrium void ratio values. On the other hand, longer duration of load increments allows considerable curing time for the pozzolanic reaction between lime and fly ash. Ultimately, the improved stiffness and strength due to pozzolanic reaction offer resistance of fly ash to compression (Moghal and Sivapullaiah, 2011).

To allow pozzolanic reaction to occur in fly ash mixtures, an activator such as Portland cement or lime is added in ratio of 1: 2 to raise the pH up to 12.4. In some cases, the self-cementing fly ash possesses calcium oxide (CaO) in concentrations typically ranging from 20 to 30 percent which allow pozzolanic reaction to occur. Lime can also be added when concentration of calcium oxides is insufficient to facilitate pozzolanic reaction. However, high pH associated with the dissociation of hydrated lime $Ca(HO)_2$ reduces with the progression of pozzolanic reactions (Moghal and Sivapullaiah, 2011). The use of fly ash as a binder is more attractive because fly ash is an industrial by-product that is relatively inexpensive compared to cement and lime (Horpibulsuket al., 2012). Additionally, using fly ash for soil stabilisation, promotes sustainable construction through reduction of energy use and emissions of greenhouse gases (Tastan et al., 2011). Although field mechanised mixing and compression of lime-fly ash mixtures may promote carbon foot print emission, the application of natural fibers in construction ensures the balance between emitted and consumed carbon. Irrespective of benefits offered by soil chemical stabilisation, research has shown that the stabilised soils exhibit high stiffness and brittle behaviour (Abtahi et al., 2010a; Aqeel Al Adili et al., 2012a; Basha et al., 2005; Ghavami et al., 1999a; Tang et al., 2007). Incorporating fiber reinforcements within soil is an effective and reliable technique to improve the ductility of the soil (Park and Tan, 2005; Prabakar and Sridhar, 2002).

2.11 Critique of the previous research on sisal fiber reinforced soil

Very few studies have been done specifically dealing with sisal fiber reinforced soil. As far as the author is concerned few papers have been published dealing with sisal fiber reinforced soil. The scope of the works are summarised in Table 2.4.

Table 2.4: Previous research on sisal fiber reinforced soil: their shortcomings

Author	Test method	Variables	Conclusion	Shortcomings
(Abhijit and Aruna, 2015)	UCS ,Compaction with randomly mix fibers clay	Fiber content	UCS strength and CBR are improved MDD decreases with increase in fiber content 0.75% fiber content was optimum	Effects of fiber length, aspect ratio, orientation , fiber treatment and desiccation were not considered Methodology was not well explained Discussions were not articulated Deformation and failure mechanisms were not considered Interfacial shear strength mobilisation was not considered. Stiffness evolution was not explained Shrinkage and cracks were not investigated Data were not representative due to limited number of tests

Author	Test method	Variables	Conclusion	Shortcomings
(Raneesh, 2013)	UCS Compaction with randomly mix fibers clay soil	Fiber content and Fiber length	UCS strength and CBR are improved with increased in fiber content. MDD increases with increase in fiber content and OMC decrease with increases in fiber content. 0.9% fiber content was found to be optimum	Effects of fiber length, aspect ratio, orientation, fiber treatment and desiccation were not considered. Deformation and failure mechanisms were not considered. Interfacial shear strength mobilisation was not considered. Stiffness evolution not explained. Shrinkage and cracks were not investigated. Data were not representative due to limited number of tests
(Sayida, 2009)	UCS and Compaction with randomly mix fibers clay soil	Fiber content and Fiber length	MDD and OMC decrease with increase in fiber content. 0.5% fiber content and 25mm length were found to be optimum	Effects of fiber length, aspect ratio, orientation, fiber treatment and desiccation were not considered. Methodology was not well explained. Discussions were not articulated. Deformation and failure mechanisms were not considered. Interfacial shear strength mobilisation was not considered. Stiffness evolution not explained. Shrinkage and cracks were not investigated. Data were not representative due to limited number of tests.

Author	Test method	Variables	Conclusion	Shortcomings
(Ghavami et al., 1999b)	Compression Water to soil ratio. Moisture absorption and shrinkage with randomly mix fibers clay soil	Fiber content and Fiber length and	Peak deviator stress and cohesion are improved with increased in fiber content and fiber length. Failure deviator stress increase with increase in fiber content Crack, drum, end leaning and shear surface failure modes were the functions of independent variables Straining hardening was observed 1% fiber content and 10mm fiber length were optima	Fiber orientation, aspect ratio and pretreatment were not considered. Deformation and failure mechanisms were not characterised. Interfacial shear strength mobilisation was not considered. Stiffness evolution not explained. Shrinkage ,swell and cracks were not investigated

2.12 Research focus

Literature shows that fiber inclusions in the soil improve mechanical properties of the soil. However, some aspects of natural fiber (sisal) reinforcement are not fully addressed. Therefore, this study focused on the number of aspects including the investigation into the macro behaviour (strength and stiffness) of sisal fiber reinforced soil. This involved characterisation of macrostructural properties, deformations and failures of fiber soil composite. Secondly, the effects of fiber surface coating with pine resin on the fiber-matrix interfacial shear behaviour were investigated to assess potential improvement of sisal fiber reinforced soil using natural based additives. By virtue of natural fibers being sensitive to moisture exposure, strength resilience of the natural fiber-soil composite under moisture variation such as wet and dry cycles and desiccation was investigated. This aimed at bringing an understanding of the durability of natural fiber reinforced soil for life span prediction of the natural fiber reinforced earthen structures.

As far as the literature is concerned, no substantial publications are found on the dynamic behaviour of sisal fiber reinforced soil. Therefore, this study also focused on the investigation into the dynamic properties of natural fiber reinforced soil composite and also post cyclic behaviour of the sisal fiber reinforced soil composite. The main dynamic soil parameters investigated include shear modulus, damping ratio, liquefaction potential, toughness, energy absorbing capacity and static energy ratio. This aimed at bringing an understanding of the behaviour of natural fiber reinforced soil during earthquakes, tremors and after-shocks. Furthermore, an updated constitutive model for non-linear dynamic behaviour of fiber reinforced soil was proposed.

The strength development of fly ash stabilised soil when subjected to pre-loading has not been extensively investigated. Therefore, this study also focused on the natural fiber-reinforced lime fly ash stabilised soil. This aimed at investigating mechanical properties of stabilised soil when exposed to premature loading in order to simulate exposure of the material during construction. Furthermore, the ultimate tensile and compressive strengths of the stabilised natural fiber reinforced soil under moisture environment and pre-mature loading were investigated. This aimed at providing an insight into the durability of the pre-loaded and stabilised natural fiber soil composites for design and life span prediction of stabilised earthen construction.

In respect of earthen construction, the design specifications cannot be determined unless the material behaviours under all possible environments are fully understood. Limit state criteria of geostructures still remains uncertain with the current knowledge gap. The available design standards are not fully furnished with mechanical properties of earthen materials. Therefore, this study also focused on the role of natural fiber inclusion in the mechanical performance of adobe low-cost masonry construction. This aimed at providing information on the mechanical properties of fiber reinforced earthen structures as a basis for the design of low-cost earthen structures.

References

Abdulrahman et al. (2014). Soil–water characteristic curve of lime treated gypseous soil. *Journal of applied clay sciennce, 102* 128-138.

Abhijith.S and Aruna. T. (2015). Effect of Sisal Fibers and GGBS on Strength Properties of Black Cotton Soil. *International Journal of Innovative Research in Science, Engineering and Technology, 4* (7), 5409-5417. doi: DOI:10.15680/IJIRSET.2015.0407078

Abtahi et al. (2009). *Using textile fibers as soil stabilizers – new achievements.* Paper presented at the 1st International and 7th nationational conference in textile engineering, Rasht, Iran.

Abtahi et al. (2010a). *Improvement of soil strength by natural fibers.* Paper presented at the From res to des Europ prac, Bratislava, Slovak Republic.

Abtahi et al. (2010b). *Shear strength of composite soils reinforced with natural fibers*. Paper presented at the 5th national congregation of civil engineers, Mashad, Iran.

African Organisation of Standardization. (2014). Sadc harmonized standard for rammed earth structures –code of practice THC 03 (Vol. ADC ZW HS 983:2014): SADCSTAN.

Ahmad et al. (2010). Performance evaluation of silty sand reinforced with fibres. *Geotextiles*

Al-Mukhtar et al. (2010). Behaviour and mineralogy changes in lime-treated expansive soil at 20 °C. *Applied Clay Science, 50* 191–198.

Al-Swaidani et al. (2016). Effect of adding natural pozzolana on geotechnical properties of lime-stabilized clayey soil. *Journal of rock mechanics and geotechnical engineering, 8* 714-725.

Amar et al. (2005). *Natural fibers,Biopolymers and Biocomposites*. London: Taylor and Francis.

Amir-Farya .B and Sherif Aggour.M. (2015). Effect of fibre inclusion on dynamic properties of clay. *Geomechanics and Geoengineering*. doi: DOI:10.1080/17486025.2015.1029013

Andersen .K. H. (2009). Bearing capacity under cyclic loading - offshore, along the coast, and on land. *Canadian Geotechnical Journal, 46*(5), 513-535.

Anggraini et al. (2014). Effects of coir fibers on tensile and compressive strength of lime treated soft soil. *J Measurements*.

Ansal .A.M and Erken .A. (1989). Undrained behavior of clay under cyclic shear stresses. . *Journal of Geotechnical Engineering, 115*(7), 968–983.

.

Aqeel Al Adili et al. (2012). Strength of soil reinforced with fiber materials (papyrus). *Soil Mechanics and Foundation Engineering, 48*(6), 241-247.

Babu et al. (2008). Numerical simulation of fiber-reinforced sand behavior. *Geotextiles and Geomembranes, 26*, 181-188.

Basha et al. (2005). Stabilization of residual soil with rice husk ash and cement. *Construction and Building Materials, 19*(6), 448-453.

Beckett. C. (2011). *The Role of Material Structure in Compacted Earthen Building Materials: Implications for Design and Construction.* PhD, Durham University, Durham. (http://etheses.dur.ac.uk/3313)

Bell. F.G. (1996). Lime stabilization of clay minerals and soils. *Engineering Geology, 42* 223-237.

Bhadriraju et al. (2005). Digital Imaging Technique to Evaluate Shrinkage Strain Potentials of Fiber Reinforced Expansive Soils. *GSP 138 Site Characterization and Modeling, .*

Bouhicha et al. (2005). Performance of composite soil reinforced with barley straw. *Cement & Concrete Composites, 27*, 617–621.

Bozyigit et al. (2016). Dynamic Behavior of a Clayey Sand Reinforced with Polypropylene Fiber. *ACTA PHYSICA POLONICA, 132*, 674-678.

Buitrago et al. (2015). Some Properties of Natural Fibers (Sisal, Pineapple, and Banana) in Comparison to Man-Made Technical Fibers (Aramide, Glass, Carbon). *Journal of Natural Fibers, 12*, 357-367.

Bunsell .A.R and Renard. J. (2005). *Fundamentals of fiber reinforced composite material*. Bristol and Philadelphia: Institute of Physics Publishing.

Carter et al. (1982). A critical state soil model for cyclic loading. In G. N. Pande and 0. C. Zienkiewicz (Ed.), *Soil mechanics-transient and cyclic loads* (pp. 219-252). Chichester: John Wiley and sons.

Chegenizadeh .A and Nikraz. H. (2012). Performance of fiber reinforced clayey sand composite. *Frontiers of Structural and Civil engineering, 6*(2), 147–152.

Chen et al. (2006). Influence of fiber wettability on the interfacial adhesion of continuous fiber-reinforced PPESK composite. *Journal of Applied Polymer Science, 102*(3), 2544–2551.

Clariá.J.J and Vettorelo .P. (2015). *Modeling of the small strain shear modulus on a fiber reinforced sand.* Paper presented at the Proceedings of the conference of deformation characteristics of geomaterials, Buenos Aires, Argentina.

Cox .H.(1952). The elasticity and strength of paper and other fibrous materials. *British Journal of Applied Physics, 3*, 72-78.

Das.B.M and Ramana.G. V. (2011). *Principles of soil dynamics*. Stamford, USA: Cengage Learning.

David et al. (1984). Cyclic triaxial tests on remoulded clays. *Journal of geotechnical engineeirng, 110*(10), 1431-1445.

Di Sante et al. (2014). Time of reactions in a lime treated clayey soil and influence of curing conditions on its microstructure and behaviour. *Applied Clay Science, 99* 100–109.

Diambra et al. (2013). Fibre reinforced sands: from experiments to modelling and beyond. *International journal for numerical and analytical methods in geomechanics, 37:*, 2427–2455.

Diambra et al. (2007). Determination of fibre orientation distribution in reinforced sands. *Ge´otechnique, 57*(7), 623–628. doi: doi: 10.1680/geot.2007.57.7.623

Diambra et al. (2010). Fiber reinforced sands: experiments and modeling. *Geotextiles and Geomembranes, 28*, 238–250.

Ding.D and Hargrove.K. (2006). Nonlinear stress–strain relationship of soil reinforced with flexible geofibers. *Journal of Geotechnical and Geoenvironmental Engineering, 132*, 791-794.

Dobson.S. (2015). Rammed earth in the modern world. In Ciancio & Beckett (Ed.), *Rammed Earth construction*. London: Taylor and Francis.

Douglas et al. (2014). *Introduction to Wood and Natural Fiber Composites*. New Delhi India: John Wiley & Sons, Ltd.

Eskişar.T, Karakan. E and Altun.S. (2016). *Effects of Fiber-Reinforcement on Liquefaction Behavior and Pore Pressure Development of Sand*. Paper presented at the 12th International congress on advances in civil engineering, Bogazici University,Istabul Turkey.

Estabragh et al. (2011). Mechanical Behavior of a Clay Soil Reinforced with Nylon Fibers. *Geotechnical and Geological Engineering, 29*, 899–908.

Estabragh et al. (2013). A Study on the Mechanical Behavior of a Fiber-Clay Composite with Natural Fiber. *Geotechnical and Geological Engineering, 31*, 501–510.

Faryar.A and Behzad. (2012). *Improvement of dynamic properties and seismic response of clay using fiber reinforcement.* PhD, University of Maryland, University of Maryland.

Fredlund et al., (2012). *Unsaturated Soil Mechanics in Engineering Practice*. Hoboken, New Jersey: John Wiley & Sons, Inc

Gassan.J. (2001). Calculation of elastic properties of natural fibers. *Journal of material science, 36*, 3715-3720.

Ghavami et al. (1999). Behaviour of composite soil reinforced with natural fibers. *Journal of cement concrete composite, 21*, 39-48.

Ghiassian et al., (2008). *Dynamic performance of Toyoura sand reinforced with randomly distributed carpet waste strips*. Paper presented at the geology,earth engineeing and soil dynamics conference, California.

Głuchowsk.A. (2015). Repeated Loading of Cohesive Soil – Shakedown Theory in undrained conditions. *Studia Geotechnica et Mechanica, 37*(2), 11-16.

Gray.D.H and Ohash. (1983). Mechanics of fiber reinforcement in sand. *Journal of Geotechnical Engineering, 109*(3), 335–353.

Gurunathan et al. (2015). A review of the recent developments in biocomposites based on natural fibres and their application perspectives. *Composites: Part A 77, 77*, 1-25.

Hamidi.A and Hooresfand. M. (2013). Effect of fiber reinforcement on triaxial shear behavior of cement treated sand. *Geotextiles and Geomembranes, 36*, 1-9.

Hardin.B.O and Drnevich .V.P. (1972). Shear modulus and damping in soils: measurement and parameter effects. *Journal of Soil Mechanics and Foundations Division, 6*, 603-624.

Harikumar et al. (2015). Behaviour of Cohesionless Soil Reinforced with Three Dimensional Inclusions Under Plane Strain Conditions. *Journal of Institution of Engineers (India), 96*(3), 223–228.

He.S and Li.J. (2009). Modeling nonlinear elastic behavior of reinforced soil using artificial neural networks. *Applied Soft Computing, 9*, 954–961.

Hejazi et al. (2012). A simple review of soil reinforcement by using natural and synthetic fibers. *Construction and Building Materials, 30*, 100-116.

Hejazi et al. (2008). Introducing two simple models for predicting fiber reinforced asphalt concrete (FRAC) behavior during longitudinal loads. *International Journal of Applied Polymer Science, 109*, 2872–2881.

Hejazi et al. (2012). A simple review of soil reinforcement by using natural and synthetic fibers. *Construction and Building Materials, 30*, 100-116.

Hejazi et al. (2013). Shear Modeling of Fiber Reinforced Soil Composite on the Base of Fiber Pull-out Test. *Fibers and Polymers, 14*(2), 277-284.

Hejazi et al. (2014). Using slippage theory to analyze shear behavior of loop-formed fiber reinforced soil composites. *Journal of industrial textile, 43*(3), 415–439.

Horpibulsuket al. (2012). Soil Stabilization by Calcium Carbide Residue and Fly Ash. *Journal of Materials in Civil Engineering, 24*(2).

Houben and Guillaud. (1994). *Earth Construction: A Comprehensive Guide*. University of Michigan: Intermediate Technology Publications.

Hyde et al. (2007). Postcyclic recompression, stiffness, and consolidated cyclic strength of silt. *Journal of geotechnical and environmental engineering, 133*(4), 416–423.

Hyodo et al. (1992). Prediction of clay behaviour in undrained and partially drained cyclic triaxial tests. *Soils and Foundations, 32*(4), 117-127.

Ibraim et al. (2010). Static liquefaction of fibre reinforced sand under monotonic loading. *Geomechanics and Geoengineering, 28*, 374–385.

Ibraim et al. (2006). *Fiber-reinforced granular soils behavior*. Paper presented at the International symposium on geotechnical particle distinct element methods, Yamaguchi, Japan.

Ibraim.E and Maeda.K. (2007). *Numerical analysis of fiber-reinforced granular soils*. Paper presented at the 5th International symposium on earth reinforcement, Kyushu, Japan.

Jaquin et al. (2009). The strength of unstabilised rammed earth materials. *Ge´otechnique, 59*(5), 487–490.

Jaquin.P. A. (2008). Study of historic rammed earth structures in spain and india. *The Structural Engineer, 86*(2), 26-32.

Jha.A.K and Sivapullaiah. P.V.(2016).Volume change behavior of lime treated gypseous soil influence of mineralogy and microstructure. *Jourrnal of applied clay science, 119*, 202-212.

Jones.C.J. (1985). *Earth Reinforcement and Soil Structures*. London: Butterworth.

Kafodya.I and Okonta.F.N. (2018a). Effects of natural fiber inclusions and pre-compression on the strength properties of lime-fly ash stabilised soil. *Construction and Building Materials, 170*, 737-746.

Karahan.M and Karahan.N. (2015). Investigation of the tensile properties of natural and natural/synthetic hybrid fiber woven fabric composites. *Journal of Reinforced Plasticsand Composites, 0*(0), 1-12.

Komuraiah et al. (2014). Chemical Composition of Natural Fibers and its Influence on their Mechanical Properties. *2014, 50*(3), 359–376.

Kondner .R.L and Zelasko.J.S. (1963). *A hyperbolic stress–strain formulation of sands*

(1) 289-324; 1963. Paper presented at the 2nd Pan-American Conference on Soil Mechanics and foundation Engineering Sao Paulo, Brazil.

Krishnaswamy.N.R and Isaac.N.T. (1994). Liquefaction potential of reinforced sand. *Geotextiles and Geomembranes, 13*(1), 23-41.

Li.C. (2005). *Mechanical response of fiber-reinforced soil.* PhD, University of Texas, Austin.

Li.H and Senetakis .K. (2017). Dynamic properties of polypropylene fibre-reinforced silica quarry sand. *Soil Dynamics and Earthquake Engineering, 100*, 224-232.

Li.J and Ding. W. (2002). Nonlinear elastic behavior of fiber-reinforced soil under cyclic loading. *Soil Dynamics and Earthquake Engineering*(22), 977-983.

Likos.W. J. and Lu. N. (2002). Automated humidity system for measuring total suction characteristics of clay. *Geotechnical Test journal, 26*(2), 1-12.

Liu et al. (2008). Adjustable wettability of methyl methacrylate modified ramie fiber. *Journal of Applied Polymer Science, 109*(5), 2888–2894.

Liu et al. (2011). Static liquefaction behavior of saturated fiber-reinforced sand in undrained ring shear tests. *Canadian Geotechnical Journal, 29.*(5), 462–471.

Maher.H and Gray .H. (1990). Static response of sand reinforced with randomly distributed fiber. *Journal of Geotechnical Engineering, 116*, 1661–1677.

Maher.M.H and Woods .R.D. (1990). Dynamic response of sand reinforced with randomly distributed fibers. *Journal of Geotechnical Engineering 116*(7).

Maheshwari et al. (2012). Effects of reinforcement on liquefaction resistance of Solani sand. *Journal of Geotechnical and Geoenvironmental Engineering, 138*(7), 831–840.

Malekzadeh .M and Bilse. H. (2014). Hydro-mechanical Behavior of Polypropylene Fiber Reinforced Expansive Soils. *Journal of Civil Engineering, 18*(7), 2028-2033.

Malekzadeh. M and Bilse. H. (2012). Swell And Compressibility of Fiber Reinforced Expansive soils. *International Journal of Advanced Technology in Civil Engineering, 1*(2), 42-46.

Malekzadeh.M and Bilsel H. (2012). Effect of Polypropylene Fiber on Mechanical Behaviour of Expansive Soils. *EJGE, 17*(55-63).

Martin et al. (2013). Influence of the degree of retting of flax fibers on the tensile properties of single fibers and short fiber/polypropylene composites. *Industrial Crops and Products, 49* 755–767.

Matasović.N and Vucetic.M. (1993). Cyclic characterization of liquefiable sands. *J Geotech Eng, 119*(11), 1805–1822.

Mathew.A and Raneesh. K.Y. (2013). Effect on Strength Characteristics of Expansive Soil Using Sisal Fibre and Waste Materials. *International Journal of Science and Research, 5*(9), 17.12-1709.

Matsui T. (1991). *Degradation of Saturated Clays after Cyclic Loading.* Paper presented at the International Conference on Recent Advances in Geotechnical Earthquake Engineering and Soil Dynamics, St. Louis, Missouri.

Michalowski.R.L and Cermak .J. (2003). Triaxial compression of sand reinforced with fibers. *Journal of Geotechnical and Geoenvironmental Engineering, 129* ((2)), 125–136.

Michalowski.R.L and Zhao .A. (1994). Failure of fiber-reinforced granular soil. *Journal of Geotechnical Engineering, 122*(3).

Michalowskia.R.L and Cerma´ k .J. (2002). Strength anisotropy of fiber-reinforced sand. *Computers and Geotechnics, 29*, 279–299.

Mishra et al. (2004). A Review on Pineapple Leaf Fibers, Sisal Fibers and Their Biocomposites. *Macromolecular Material Engineering, 289*, 955–974.

Mittal.S and Chauhan. R. (2013). Liquefaction behavior of reinforced saturated sand under dynamic conditions. *International Journal ofGeotechnical Engineering, 7* (1), 109-114.

Moghal .A.A and Sivapullaiah.P. V. (2011). Effect of pozzolanic reactivity on compressibility characteristics of stabilised Low Lime Fly Ashes. *Geotechnical and Geological Engineering, 29*, 665-673.

Moghal et al. (2017). Target reliability approach to study the effect of fiber reinforcement on UCS behavior of Lime treated semiarid Soil. *Journal of Materials in Civil Engineering 29*(6), 04017014-04017011-04017015.

Monideepa et al. (2014a). Undrained Pore Pressure Prediction in Clayey. *International Journal of Geomechanics, 15*(5).

Monideepa et al. (2014b). Undrained Pore Pressure Prediction in Clayey Soil under Cyclic Loading. *International journal of Geomechanics*. doi: 10.1061/(ASCE)GM.1943-5622.000043

Morris et al. (1992.). Cracking in drying soils. *Canadian Geotechnical Journal, 29*, 263-277.

Neeraja et al. (2014). Numerical analysis of effect of orientation of fibers on stress–strain response of fiber reinforced soil. *International journal of geotechnical engineering, 8*(3), special issue on geosynthetics.

Nevell.T.P and Zeronian.S.H.(1985).*Cellulose Chemistry and its Applications*. New York: Wiley.

Ni et al. (2014). Model of Soft Soils under Cyclic Loading. *International Journal of Geomechanics, 15*(4).

Noorzad.R and Fardad Amini.P. (2014). Liquefaction resistance of Babolsar sand reinforced with randomly distributed fibers under cyclic loading. *Soil Dynamics and Earthquake Engineering, 66*, 281–292.

Orakoglua et al. (2017). Dynamic behavior of fiber-reinforced soil under freeze-thaw cycles. *Soil Dynamics and Earthquake Engineering, 101*, 269–284.

Osinubi.K.J. (1998). Influence of compactive efforts and compaction delays on lime-treated soil *Journal of Transportation Engineering, 124*(2), 149-155.

Park.S.S.(2009).Effect of fiber reinforcement and distribution on unconfined compressive strength of fiber-reinforced cemented sand. *Geotextiles and Geomembranes, 27*, 162-166.

Park.T and Tan.S.A. (2005). Enhanced performance of reinforced soil walls by the inclusion of short fiber. *Geotextiles and Geomembranes 23*(4), 348–361.

Peponi et al. (2008). Statistical Analysis of the Mechanical Properties of Natural Fibers and Their Composite Materials. *Polymer Composites DOI 10.1002/pc*.

Peron et al.(2009). Fundamentals of desiccating cracks of fined grained soils-experimental characterisation and mechanism identification. *Canadian Geotechnical Journal, 46*, 1177-1201.

Peron et al.(2013). Formation of drying crack patterns in soils: a deterministic approach. *Acta Mechanica, 8*, 215–221.

Pickering et al. (2016). A review of recent developments in natural fibre composites and their mechanical performance. *Composites: Part A 77, 83*, 98–112.

Pillai.R.J, Robinson.R.G and Boominathan. (2007). *Behavior of kaolinite clays under cyclic loading*. Paper presented at the Workshop on Earthquake Hazards and Mitigation, India.

Prabakar.J and Sridhar.R.S. (2002). Effect of random inclusion of sisal fibre on strength behaviour of soil. *Construction and Building Materials, 16*, 123-131.

Prisco.C and Nova.R. (1993). A constitutive model for soil reinforced by continuous threads. *Geotextiles and Geomembranes, 12*, 161-178.

Raju et al. (2008). Enhancement of PVC/ENR blend properties by poly(methyl acrylate) grafted oil palm empty fruit bunch fibe. *Journal of Applied Polymer Science, 110*, 368–375.

Ranjan et al. (1996). Probabilistic analysis of randomly distributed fiber-reinforced soil. *Journal of Geotechnical Engineering, 122*, 419–426.

Rao.J. (1996). *Jute geotextile for improving the performance of highway embankment on soft marine soil*. Paper presented at the Jute based geotextile, New Delhi India.

Rozman.H, Saad.M and Ishak Z. (2003). Flexural and impact properties of oil palm empty fruit bunch (EFB)–polypropylene composites—the effect of maleic anhydride chemical modification of EFB. *Journal of Polymer testing, 22*, 335–341.

Sadeghi.M.M and Beig.F.H. (2014). Dynamic behavior of reinforced clayey sand under cyclic loading. *Geotextiles and Geomembranes, 42*(5), 564-572.

Santiago et al. (2013). Mechanical Behavior of Curauá Treated Fiber-Reinforced Sand. *Materials Science Forum, 730-732*, 355-360.

Sayida.M.K.(2009). *Behaviour of Black Cotton Soil Reinforced with Sisal Fibre.* Paper presented at the 10th National Conference on Technological Trends (NCTT09) India.

Schlosser.F, Jacobsen .H. M. and Juran .I. (1984). *Soil reinforcement.* Paper presented at the European Conference on Soil Mechanics and Foundation Engineering

Seed.H.B and Idriss. I.M. (1970). Soil moduli and damping factors for dynamic response analysis. California: Earthquake Engineering Research Centre, University of California Berkeley.

Segetin et al. (2007). reinforcement of soil–cement building materials: manufacturability and propertie. *Build environment, 42*, 3066–3079.

Shadi et al. (2013). Quantification of Model Uncertainty in Shear Strength Predictions for Fiber-Reinforced Sand. *Journal of Geotechnical and Geoenvironmental Engineering, 139*(1).

Shahnazari et al. (2009). Shear Modulus of Silty Sand Reinforced by Carpet Waste Strips. *JSEE, 11*(3), 133-142.

Shajarati et al. (2012). Behaviour of Cohesionless Soils During Cyclic Loading. *DCE Technical Memorandum No.14 Aalborg University*.

Sherrif et al. (1977). Damping ratio for dry sand. *Journal Geotechnical and Geoenvironmental Engineering, 103,* 743-756.

Sinha. E and Panigrahi.S.(2009). Effect of plasma treatment on structure, wettability of jute fiber and flexural strength of its composite. *Journal of composite materials, 17*, 1791–1802.

Soundara.B and Senthil kumar.K. P. (2015). Effect of Fibers on Properties of Clay. *International Journal of Engineering and Applied Sciences (IJEAS), 2*(5), ISSN: 2394-2366.

Sreekala et al. (2004). Environmental effects in oil palm fiber reinforced phenol formaldehyde composites: studies on thermal, biological, moisture and high energy radiation effects. *Advanced Composite Materials, 13*(3), 171-197.

Subrahmanyam.(1984).*Bamboo reinforcement for cement matrices*. Uk: Surrey University Press.

Tang et al. (2007). Strength and mechanical behavior of short polypropylene fiber reinforced and cement stabilized clayey soil. *Geotextiles and Geomembranes, 25*(3), 194-202.

Tang et al. (2009). *Experimental study on the strength characteristics of expansive soil reinforced with synthetic fibers.* Paper presented at the 4th Asian Regional Conference on Geosynthetics, Shanghai, China.

Tang et al. (2010). Interfacial shear strength of fiber reinforced soil. *Geotextiles and Geomembranes, 28*, 54–62.

Tang et al. (2011). Experimental Investigation of the Desiccation Cracking Behavior of Soil Layers during Drying. *Journal of Materials in Civil Engineering, 23*(6), 873-877. doi: 10.1061/(ASCE)MT.1943-5533.0000242

Tastan et al. (2011). Stabilization of Organic Soils with Fly Ash. *Journal of Geotechnical and Geoenvironmental Engineering, 137*(9), 819-833.

Towhata.I. (2008). Laboratory Tests on Dynamic Properties of Soils *Geotechnical Earthquake Engineering* (pp. 180-216).

Tran et al. (2014). Effects of lime treatment on the microstructure and hydraulic conductivity of Héricourt clay. *Journal of rock mechanics and geotechnical engineering, 6*, 399-404.

United nations. (2018). World urbanisation prospects. New York: Department economic and social affairs.

Villard .P, Jouve.P and Riou .Y. (1990). Mode´ lisation du compertment me´ canique du Texsol. *Bulletin liaison Labo, 168*, 15-27.

Wu.X.F and Dzenis.Y.A. (2006). Droplet on a fiber: geometrical shape and contact angle. *Acta Mechanica, 185*(3-4), 215–225.

Yashwant et al. (2015). Theoretical modelling and Experimental verification of mechanical properties of natural fiber reinforced thermaplastics. *Procedia technology, 19*, 320-326.

Yetimoglu .T and Salbas. O. (2003). A study on shear strength of sands reinforced with randomly distributed discrete fibers. *Geotextiles and Geomembranes 21*(2), 103–110.

Zhao.J.Q.D and LI .B. (2015). Effect of Random Inclusion of Palm Fibers on Strength Characteristics of Shanghai Cohesive Soil. *Advanced Materials Research, 1096*, 572-581.

Zhou.J and Gong. X. (2001). Strain degradation of saturated clay under cyclic loading. *Canadian Geotechnical Journal, 38*(1), 208-2012.

Zhuang.X and Yu. X. (2015). Experimental Study on Strength Characteristics of Lime - basalt Fiber Reinforced Expansive Soil. *Applied Mechanics and Materials, 744-746* 495-498.

Zornberg.G. (2002). Discrete framework for limit equilibrium analysis of fiber reinforced soil. *Géotechnique, 52*, 593–604.

3 CHAPTER THREE-MATERIALS AND METHODOLOGY

3.1 Material characterisation

3.1.1 Soil properties

The soil batch used to investigate macrostructural properties, stiffness, deformations, failure mechanism, interfacial shear strength, dynamic properties and fly ash stabilisation of fiber reinforced soil was obtained by blending different particle sizes obtained from dry sieve analysis. The particle size blending was employed to minimise particle size variability that could affect test results. Batches of granular and fine soil were locally obtained from places within the vicinity of the University of Johannesburg. The granular and fine batches were mixed and air dried for 7 days. Dry sieving was conducted by firstly passing particles through 9.5mm sieve and subsequently sieved using 75μm, 4.75mm sieves to separate clay-silt, sand and gravel. The collected soil particle sizes were mixed in the ratio of 30:60:10 by mass for silt clay, sand and gravel, respectively. The soil particle mix ratio was adopted to obtain typical soil type for earthen construction. This mix ratio not only provides high strength and dry density but also makes handling of samples easy during testing (Smith and Augarde., 2013). Wet sieving for blended soil was eventually carried out in accordance with ASTM D1140-17 (ASTM D1140-17, 2017) and the grading curve of the soil is shown in figure 3.1.

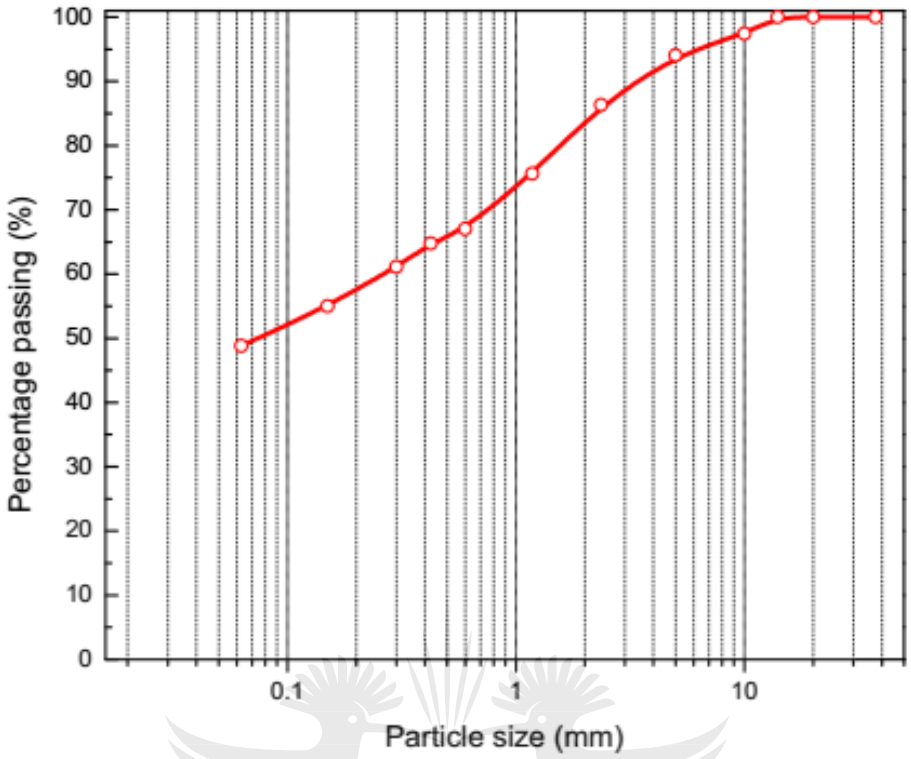

Figure 3.1: Gradation curve of soil batch 1.

The soil was classified as CL in accordance with Unified Soil Classification System (USCS).The average diameter of particles at D_{50} was less than 0.08mm.The soil properties are summarised in Table 3.1.

Table 3.1: Summary of soil properties used in the study.

Soil properties	Value
Specific gravity	2.7
Internal angle of friction	30.1
Consistency limits	
Liquid limit (%)	32
Plastic limit (%)	21
Plasticity Index	11
Linear shrinkage (%)	2.4
USCS	CL
Maximum dry density (kN/m^3)	19.61
Optimum moisture content (%)	10

Soil property	Value
Mineral composition (%)	
Al_2O_3	16.37
CaO	0.25
SiO_2	56
Fe_2O_3	17.34
MgO	0.42
K_2O	1.85

Another batch of soil was used to investigate effects of fiber inclusion on matric suction, desiccation characteristics, wet and dry cycles and fiber inclusion in adobe masonry construction. This soil was selected due to its higher shrinkage and clay content in order to clearly observe effects of fibers on matric suction. High shrinkage provided self-compacting characteristics to manufactured adobe brick and mortar. The soil was characterised by grading according to ASTM D1140-17 (ASTM D1140-17, 2017) and the grading curve of the soil is shown in figure 3.2.

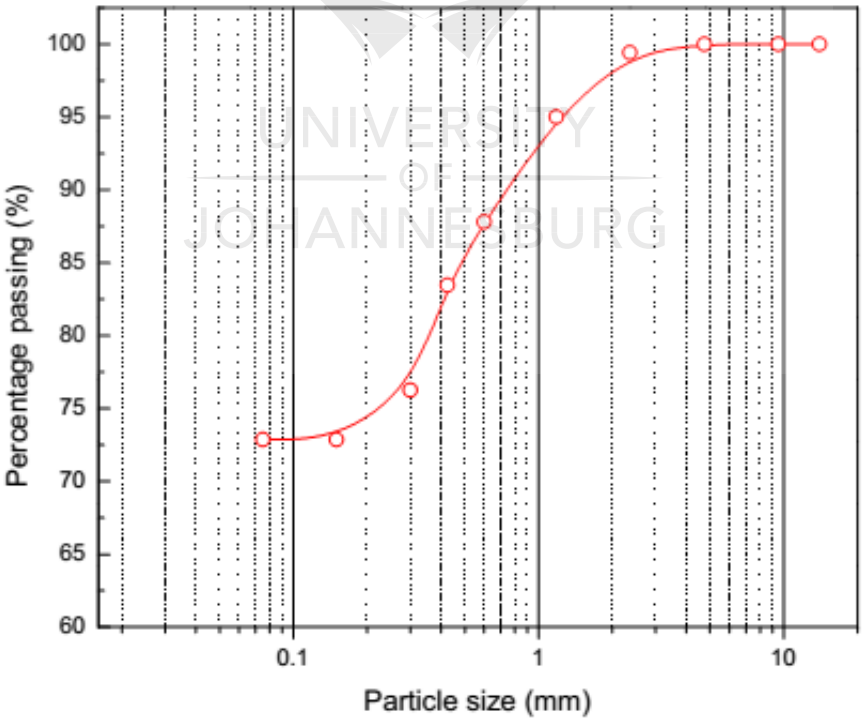

Figure 3.2: Gradation curve of soil batch 2.

The soil was classified as CL in accordance with Unified Soil Classification System (USCS). The average diameter of particles at D_{50} was less 0.075mm. The soil properties are summarised in Table 3.2.

Table 3.2: Soil properties of batch 2

Soil properties	Value
Specific gravity	2.7
Consistency limits	
Liquid limit (%)	40
Plastic limit (%)	21
Plasticity Index	19
Linear shrinkage (%)	12
USCS	CL
Compaction test	
Maximum dry density (kN/m^3)	17.61
Optimum moisture content (%)	17
Mineral composition (%)	
Al_2O_3	17.05
CaO	8.82
SiO_2	56.54
Fe_2O_3	7.48
MgO	0.78
K_2O	0.35

3.1.2 Sisal fiber conditioning and properties

Commercially available sisal fibers were supplied by a South African company in the form of ropes. The fibers were oven dried at 40^{o}C for 8h and subsequently cut into specified lengths using cutting blade prior to fabrication of fiber soil composite specimens. Single fiber tensile tests were conducted to determine fiber mechanical properties. The summary of the results is shown in Table 3.3.

Table 3.3: Properties of the sisal fiber used for the study.

Fiber property	Value
Breaking tensile strength (MPa)	500
Young's Modulus (GPa)	23
Elongation at break (%)	2.1
Average diameter (mm)	0.2

3.1.3 Properties of Gum rosin for fiber coating

The study of effects of fiber surface coating with natural water repellent was conducted using the commercially available Portuguese gum rosin (see figure 3.3) that was supplied by a South African company in crystalline form. The rosin crystals were ground into powder and sieved using 75µm sieve. The powder was dissolved at room temperature with turpentine to obtain a solution of 1.5g/ml concentration.

Figure 3.3: Portuguese Gum rosin.

The rosin composition was characterised by X-ray diffraction (XRD) analysis. The XRD results are shown in figure 3.4.

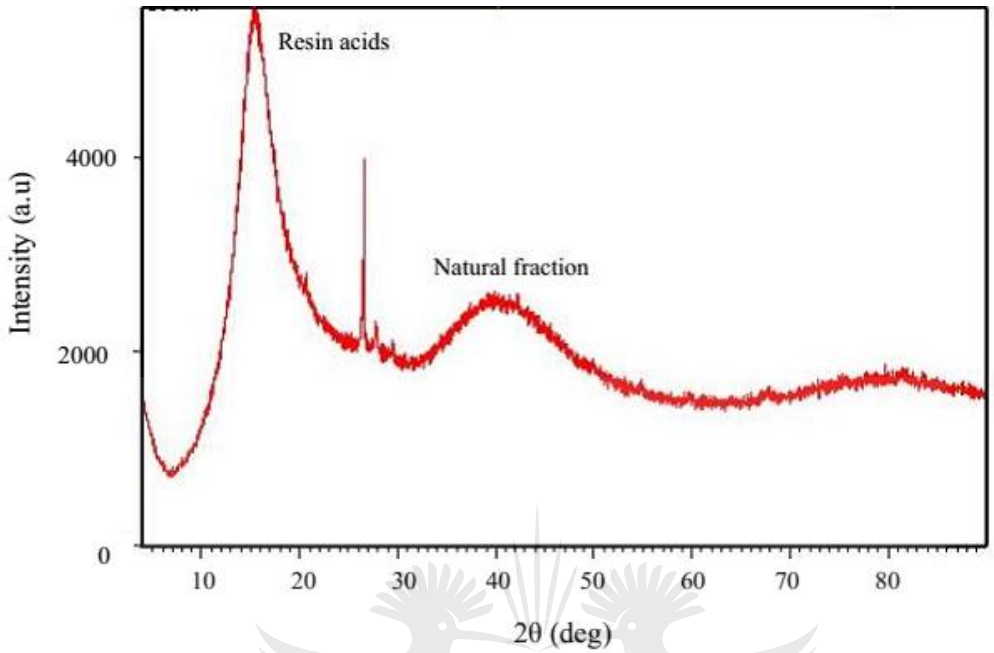

Figure 3.4: XRD analysis of Portuguese Gum rosin.

3.1.4 XRF analysis of fly ash and lime for soil stabilisation

A commercially available hydrated lime and fly ash (class F) for soil stabilisation were supplied by the South African companies. The chemical compositions of soil, lime and fly ash were characterised by X-ray Fluorescence (XRF) analysis and are summarised in Table 3.4.

Table 3.4: Chemical composition lime and fly ash.

Chemical composition (%)	Lime	Fly ash
Al_2O_3	0.55	31.31
CaO	65.29	4.50
SiO_2	1.61	55.50
Fe_2O_3	0.14	3.21
MgO	1.39	1.10
K_2O	-	0.77
SO_3	0.17	0.23
LOI	31.84	0.50

3.2 Method for quality control of fiber composite specimens for compression test

The triaxial test is the widely accepted protocol to investigate the strength properties of soil. As a quality control measure, specimens for triaxial compression test are prepared at a predetermined maximum dry density (MDD) using standard Proctor test. Replicating MDD in a small sized mould is difficult and subject to errors, which normally arise due to inconsistent compaction efforts. The conventional method for preparing specimens involves driving a core sampler into the compacted soil to extract the specimen. The approach proves to be laborious and is associated with high material usage, as such is not ideal for investigations of many variables. To address these challenges, an alternative protocol for specimen preparation at a controlled dry density was devised. In this attempt, a statistical analysis of the density values was used to validate the method. The regression analysis was employed to calibrate the compaction effort for a specified target density. The method was adopted to improve quality of specimens, reduce variability of test data, ensure efficiency in specimen preparation and reduce material usage. The fiber-soil composite was prepared by manually mixing soil with fibers at the optimum moisture content until homogeneous composite was formed. The fiber dosage was determined by equation 3.1.

$$\rho_f = \frac{m_f}{m_s} \tag{3.1}$$

where m_f is the total mass of fibers and m_s is the mass of the soil. The fiber-soil mixing protocol was adapted from (Tang et al., 2007; Zornberg, 2002b). The mixture of the soil composite was covered in a waterproof and airtight plastic bag for 24h prior to specimen fabrication to allow for moisture equilibration of the composite sample.

3.2.1 Specimen fabrication set-up

A special hydraulic jack system was devised for compacting soil composite sample shown in figure 3.5a.

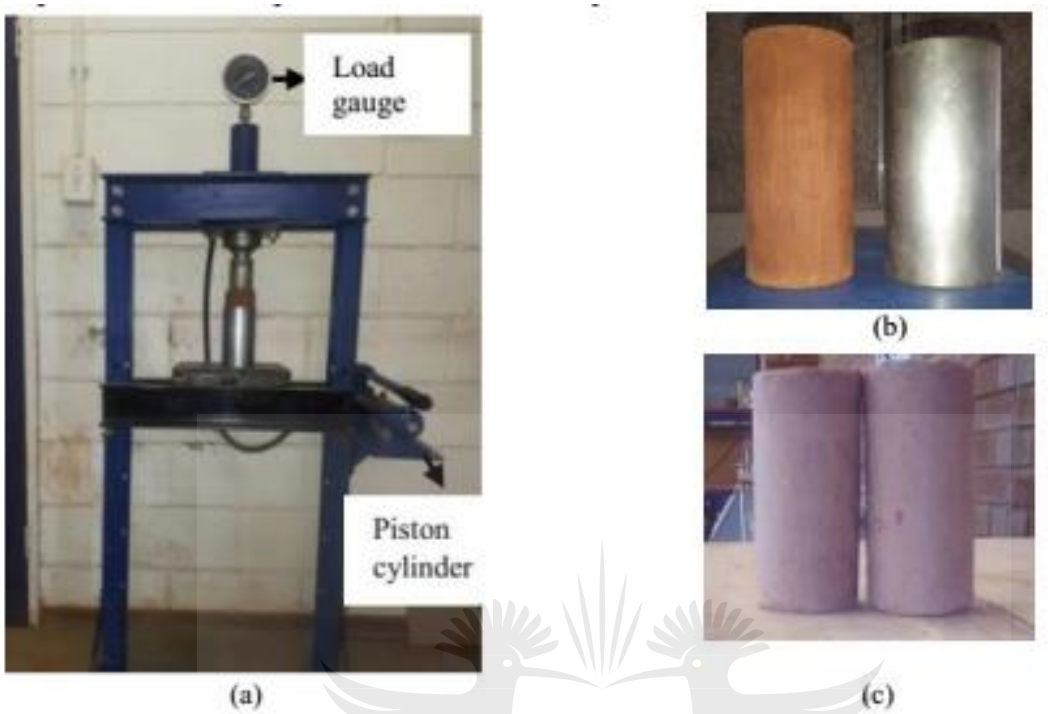

Figure 3.5: (a) Specimens compaction set-up (b) mould and kneading wood (c) fabricated specimens.

The applied load was monitored by a load gauge mounted on the frame. The jack components and specifications are summarised in Table 3.5.

Table 3.5: Specifications of hydraulic jack components

Component	Specification
Frame dimensions (bxh)	600mmx1500mm
Ram diameter	50mm
Load gauge capacity	20tons
Fluid cylinder diameter	60mm
Fluid pipe diameter	15mm

The mould size used herein was 70mm diameter and 140mm height (see figure 3.5b), and was selected to economise material usage while abiding by the recommendations in accordance with ASTM5102 (ASTM D5102, 2009) procedure A. Prior to compaction, the interior surface of the mould was smeared with oil to reduce friction effects. The specimens were prepared by static compaction of the soil composite into 3 layers. A wooden block of dimensions 50mm diameter

and 120mm height (see figure 3.5b) was used to exert pressure on the soil layer. The top surface of each layer was ripped and scarified before adding a succeeding layer in order to create a continuous mass of the composite. The top surface of the specimen was eventually leveled before extrusion. The specimen extrusion set-up is shown in figure 3.6.

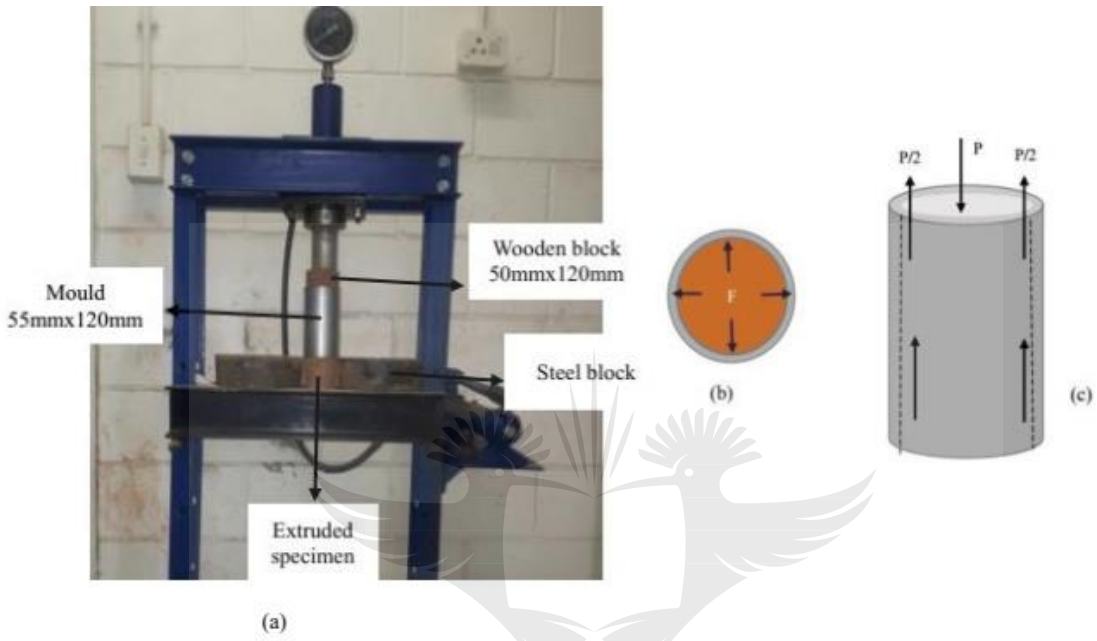

Figure 3.6: (a) Specimens extrusion set-up (b) hoop force after compaction (c) force system during extrusion.

The specimens were extruded by applying load onto the top surface of the moulded soil. The specimen was allowed to freely move out of the mould at a constant displacement of the ram. Great care was taken to ensure that the mould's support system could not interfere with the motion of specimen. During compaction, deformation of the soil exerted hoop force F perpendicular to the interior surface of the mould .The hoop force F=P for equilibrium state after plastic deformation of the soil. The reactive force of the mould balanced the hoop force at the end of the compaction. At the incipient of specimen movement (refer figure 3.6c), static frictional resistance of the specimen could be expressed by equation 3.2.

$$P = \mu F_h \qquad (3.2)$$

where P is maximum load to initiate rigid body motion at the first stroke, F_h is hoop force and μ is the coefficient of friction/adhesion. In this case, the subsequent strokes were subjected to lower static frictional resistance due to reduced coefficient of friction and adhesion between soil and the mould. Sliding resistance diminished with increase in number of strokes. Greasing the

interior surface facilitated sliding of the specimen. Hence, extrusion could not exert stress higher than compaction pressure that could affect soil stress state.

3.2.2 Method calibration for quality control

The quality control aspects ensure that the fabricated specimens possess homogeneous properties. In respect of fiber-soil composites, uniformly distributed macrostructure and mass continuity are the fundamental parameters that dictate mechanical performance of the tested specimens. The variation of test results can be significantly minimised if great care is taken when preparing the specimens. Albeit, ASTM5102 procedure B stipulates that specimens for unconfined compressive strength test be prepared by adapting ASTM D 698 (ASTM D698, 2012), extraction of specimens in the protocol is slow and labour intensive. Besides, material usage is high for experiments with several variables. In addition, human errors in counting number of blows (for 4.5kg/2.5kg rammers) lead to over compaction or under compaction of the sample. In particular, quite unlike standard compaction, this process cannot be automated.

The variation in compaction effort for soil layers was controlled by load gauge. However, it was imperative to determine required load level in order to achieve target dry density as obtained from the preliminary standard Proctor compaction test. To effectively estimate compaction load, regression analysis between dry density and compaction pressure was employed. The trial specimens were prepared with compaction pressures of 1.5MPa, 3MPa, 5MPa 7.5MPa and 10MPa at the constant OMC obtained from the preliminary standard Proctor test. The dry density of the specimens at specific compaction pressure was then computed. The compaction pressure and dry density were computed using equations 3.3 and 3.4, respectively.

$$\sigma_p = \frac{12.5x10^3 P}{A^2} \qquad (3.3)$$

where P is the load gauge reading in tons and A is the contact surface area in (mm^2) of the soil composite.

$$\rho_d = \frac{100\rho_b}{100 + w} \qquad (3.4)$$

where ρ_b is the bulk density and w is OMC. The relationship and corresponding regression equation are shown in figure 3.7.

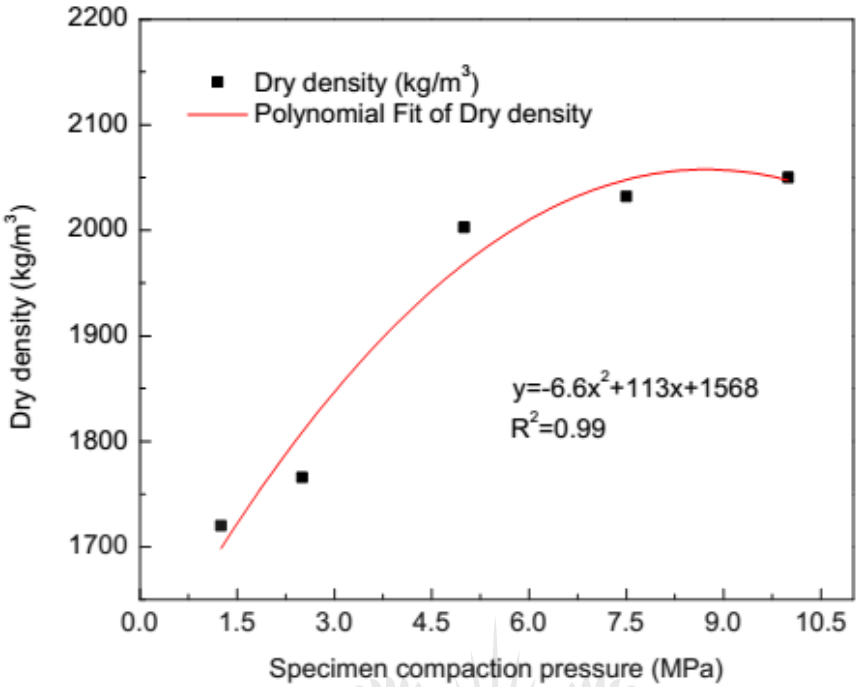

Figure 3.7: Dry density-compaction pressure relationship.

The required compaction pressure could be estimated by the model in figure 3.7 provided the target density was known. The coefficient of determination (R^2) showed that 99% of the data variability from 1700kg/m^3 to 2040kg/m^3 could be well explained by the model.

3.2.3 Method validation

The validation of the quality control method was carried out by utilising the regression model with known dry density obtained from standard Proctor test.The compaction test results of the soil composite are shown in figure 3.8.

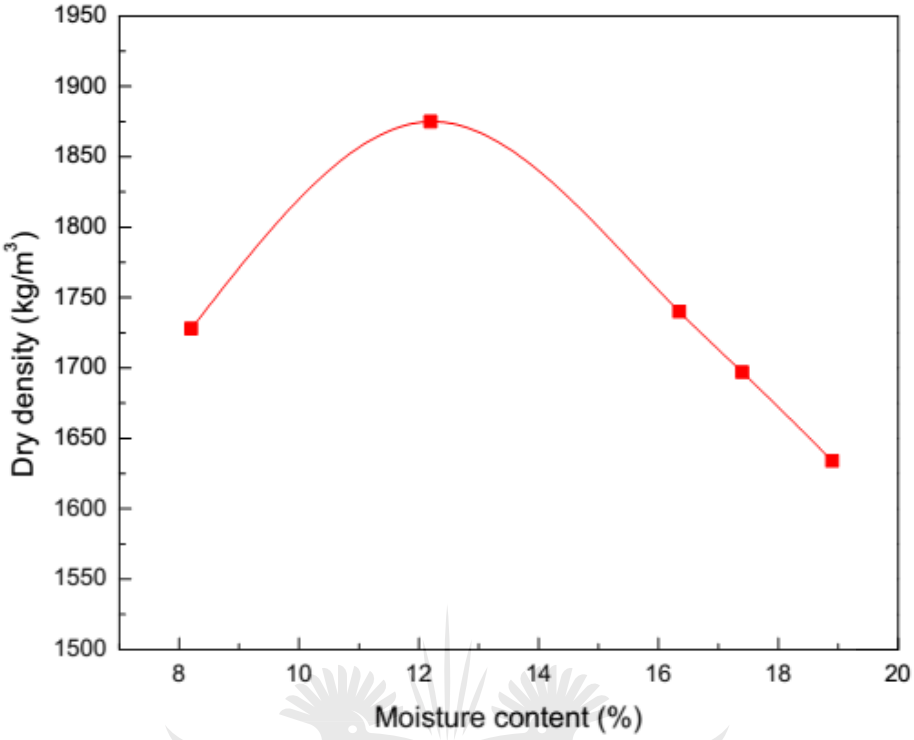

Figure 3.8: Target MDD for specimens according to ASTM D698 for batch 1.

The maximum dry density of the mixture was approximately 1890kg/m^3.To reproduce this density under static compaction, the compaction effort was determined. Therefore, regression model (see figure 3.7) was used to estimate compaction pressure required to achieve the target density. For the MDD of 1890kg/m^3, corresponding compaction pressure was estimated as 4MPa.The specimens were therefore prepared at 12% OMC (see figure 3.8) and every layer was compacted with 4MPa. Specimens were prepared randomly to assess variability of densities at 4MPa pressure. The dry density values for 70 specimens of soil-fiber composite were recorded and are shown in Appendix B. The statistical parameters and density values $\rho_{xi} \geq \rho_t$ and $\rho_{xi} < \rho_t$,where ρ_t is target density, are shown Table 3.6.

Table 3.6: Statistical parameters of density data

Parameter	Value
Mean density (kg/m^3)	1854.88
Coefficient of variation CV	0.029
Standard deviation	54.4
$\rho_{xi} \geq \rho_t$	30
$\rho_{xi} < \rho_t$	40
$\rho_t(1-CV) \leq \rho_i < \rho_t(CV+1)$	44

ρ_t is target dry density = 1870kg/m^3 ρ_{xi} is number of ith density values

To cater for variability in specific gravity of individual particles of fiber-composite, the probabilistic approach was employed by utilising coefficient of variation of recorded densities. The range of density values in equation 3.5 was considered as the most acceptable to address effects of varying particle specific gravity.

$$\rho_t(1-CV) \leq \rho_{xi} < \rho_t(CV+1) \tag{3.5}$$

where ρ_t is target dry density, ρ_{xi} is density of ith specimen, CV is coefficient of variation. Since density values are random variables and that for any specimen, density could fall either below or above target value, the binomial distribution was used to determine probability of success in obtaining density value within the specified range. Using recorded dry density data, the upper and lower limits of possible density values were 1924.5kg/m^{3}and 1815.5kg/m^3, respectively. Therefore, probability of success $P(x_i) = p$ was 0.62 and, the corresponding probability of failure was 0.38. The density range converged towards target density with the decrease in CV .Varying CV to 1.9% and 0.9% led to the probability of success equal to 0.37 and 0.13, respectively and corresponding probability of failure of 0.63 and 0.87, respectively. The binomial distribution model in equation 3.6 was used to plot the probability distribution graphs.

$$P(x,n,p) = \frac{n!\,p^x(1-p)^{n-x}}{x!(n-x)!} \tag{3.6}$$

where n is the number of fabricated specimens, x is the number of successes and *p* is probability of obtaining density within the range. The laboratory procedure recommends a minimum of 3 specimens for a set of UCS specimens. If 3 specimens are prepared, the binomial distribution graphs for the above highlighted probability scenarios are shown in figures 3.9a, b and c.

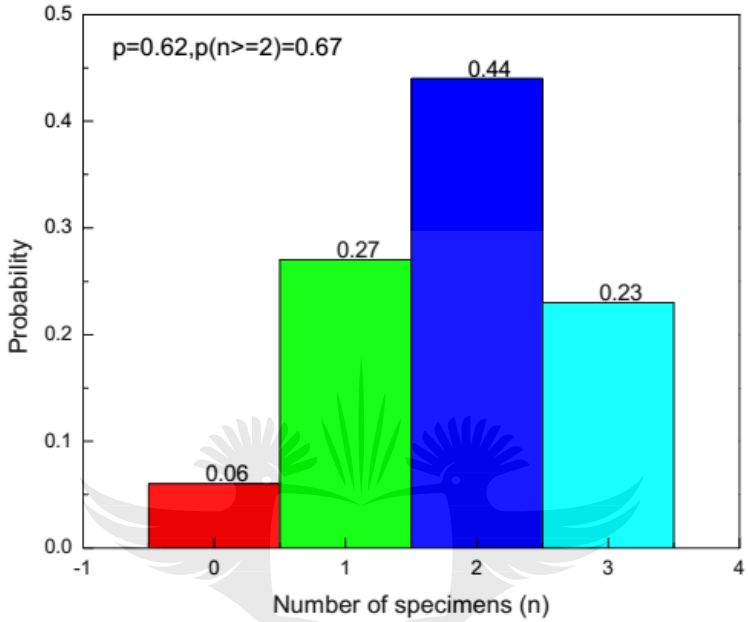

(a)

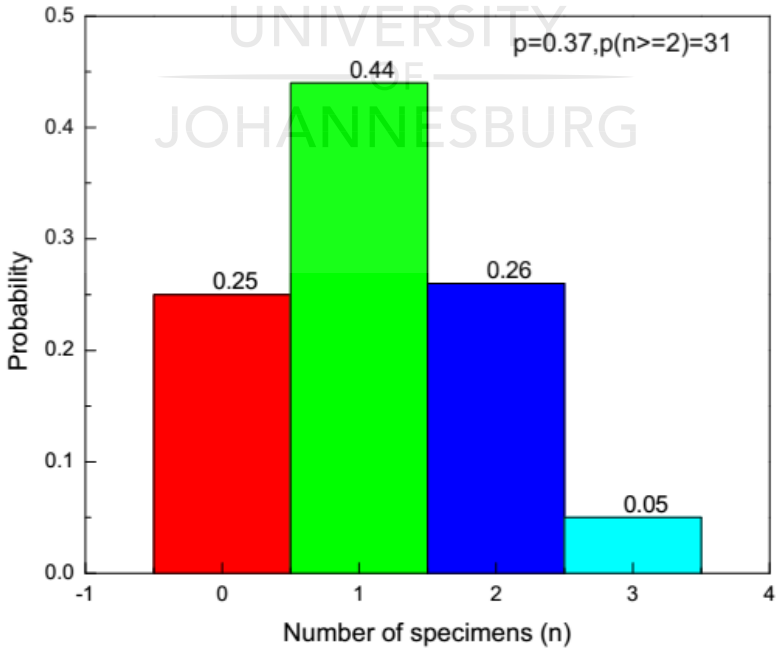

(b)

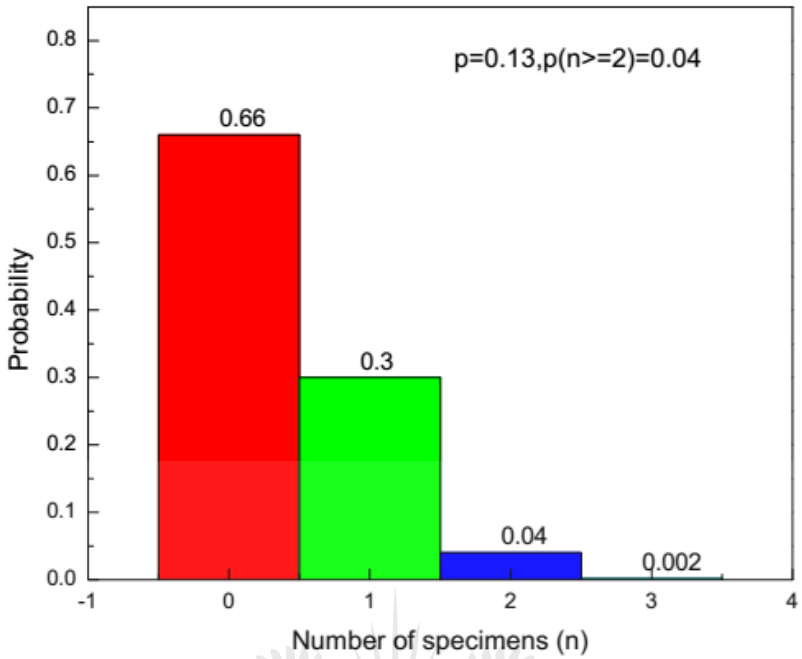

(c)

Figure 3.9: Binomial distribution graphs (a) ±3%deviation (b) ±2%deviation (c) ±1%deviation.

It is seen that for a minimum of 3 specimens, the acceptable density values of specimens should be within $\pm 3\%$ target density for at least 2 specimens to fall within the range.

3.2.4 Method optimisation

The forgone section has shown that for a given set of density data, values converge towards target density when the deviation reduces. Therefore, it is imperative to minimise the deviation of the data from the target value while utilising few specimens in order to save time and materials. Binomial probability distribution could be used to optimise the number of specimen and deviation. This could be achieved by formulating objective functions and associated constraints. In this case, two fundamental objective functions were formulated as shown in equations 3.7 and 3.8 subject to equation 3.9.

$$\text{Max: } P(x,n,p) = \frac{n!\, p^{x}(1-p)^{n-x}}{x!(n-x)!} \tag{3.7}$$

$$\text{Min: } \left(n, \rho_t(1-CV) \le \rho_{x_i} < \rho_t(CV+1)\right) \tag{3.8}$$

$$\text{Subject to constraints: } P(x,n,p) \ge 50\% \text{ and } 2 \le n \le 5 \tag{3.9}$$

If coefficient of variation is taken as maximum acceptable deviation, then conditions in equation 3.10, and denoting CV=β give;

$$\lim_{\beta \to 0} \rho_t (1 - \beta) \leq \rho_{xi} < (1 + \beta)\rho_t \qquad (3.10)$$

For β=2.9%,1.9% ,0.9% and 0%,the 4x5 matrix could be generated with elements representing likelihood and probability of success of a given number of specimens (n,P(x,n,p)). Figure 3.10a, b and c show matrices of the most likely number of specimens for a given deviation and the corresponding probability of falling within acceptable range.

Number of specimens (n)

Deviation β %

	0	1	2	3	4	5
2.9	0	1	1	2	3	3
1.9	0	0	1	1	1	2
0.9	0	0	0	0	0	0
0	0	0	0	0	0	0

(a)

Number of specimens (n)

Deviation β %

	0	1	2	3	4	5
2.9	0	0	38	67	84	93
1.9	0	0	14	31	47	61
0.9	0	0	2	5	8	12
0	N	0	0	0	0	0

(b)

Number of specimens (n)

Deviation β %

	0	1	2	3	4	5
2.9	0,0	1,0	1,38	2,67	3,84	3,93
1.9	0,0	0,0	1,14	1,31	1,47	2,61
0.9	0,0	0,0	0,2	0,5	0,8	0,12
0	0,N	0,0	0,0	0,0	0,0	0,0

(c)

Figure 3.10: Probability matrices (a) possible number of specimens to fall within acceptable range (b) at least 2 specimens fall within acceptable range (c) combination of a and b matrices.

The above matrices imply that if 3 specimens were prepared, it was likely to get 2 or more density values within approximately ±3% deviation from the target density. When the acceptable deviation range was reduced to approximately ±2%, the minimum number of specimens should be 5. On the basis of material usage and time, 3 was the optimal number of specimens and was adopted to compute average strength properties of the specimens. From the foregone analysis, the compaction pressure of any given soil was well calibrated in order to achieve desired density. For every 3 specimens, at least 2 would fall within±3% of the target density.

3.3 Matric suction test

The filter paper method for matric suction measurement was employed according to ASTM D 5298-94 (ASTM D5298 - 94, 1994). Filter paper method for matric suction is cheap and easy to use. In order to determine suction, a calibrated wetting and drying curve is used to estimate total and matric suctions. Although a single calibration curve is used, the wetting and drying curves of the soil do not match and this renders the method more conservative (Bulut et al., 2001). Schleicher & Schuell filter papers of 45mm diameter were used. Two halves of soil sample were moulded at OMC by static compaction. The smaller filter paper (45mm) was inserted in between two large protective filters of 70 mm diameter. The three filter papers were subsequently sandwiched between two halves of soil samples that were taped together by electrical insulting tape as shown in figure 3.11.

Figure 3.11: Matric suction test apparatus.

The surfaces of the moulded soil samples were made smooth and flat to ensure intimate contact between soil and the filters for moisture equilibration. The specimen size was 55mm diameter and 40mm thickness. The specimens were sealed in the glass jars and eventually inserted into a well-insulated container for moisture equilibration. Insulation ensures that no moisture exchange occurs between the sealed specimens and the environment. Moisture exchange may lead to loss of the moisture from the jar and temperature fluctuations and may affect moisture equilibration and moisture measurements. During moisture equilibration, temperature was kept almost constant at 25^{o}C.The moisture content of filters was determined after 7 days of equilibration. Analytical balance of 0.0001g precision was used to measure moisture contents of the filters (see figure 3.11). The matric suction was computed using (Bulut et al., 2001) calibration curve shown in equation 3.11. This curve is specifically for wetting curve of initially dry cohesive soil .The ASTM soil- moisture characteristic curve is derived from the combination of two separate curves (for wetting and drying processes) which sometimes do not match. Therefore, ASTM calibration curve was considered not suitable for this measurement of matric suction.

$$h = -8.2414 w_f + 5.4246 \qquad (3.11)$$

where w_f is the moisture content of the filter.

The effects of fibers on the matric suction were investigated at constant moisture content (10%).The evolution of matric suction was investigated by varying composite moisture content. Moisture content variation was determined by gravimetric measurement of composite moisture at different drying periods namely, 8h,24h,72h and 168h.The drying was conducted at laboratory temperature of between 25-30^{o}C.

3.4 Specimen preparation for desiccation test

The soil was initially pulverised and sieved using 2.36 mm sieve to obtain soil powder. The slurry specimens were prepared by mixing dry soil powder with distilled water. The water content of the slurry was 60 %, representing 1.5 times the liquid limit state. Figure 3.12 shows the slurry that was produced after mixing.

Figure 3.12: Slurry of the soil for desiccation test.

Fibers were manually added to the slurry in small increments. The fibers were thoroughly mixed with the slurry to achieve a uniform mixture with no visible clumping. A desired quantity of slurry mixture was poured onto circular stainless steel desiccators with diameter of 100mm. The entrapped air bubbles in the mixture were removed by tamping the desiccator for about 10min until all bubbles disappeared. The mixture was then sealed in plastic bag and kept for at least 24h so that the composite slurry could settle down. Two sets of specimens were prepared for investigating effects of fiber content and slurry thickness. The fiber contents were determined by percentage dry mass of the soil. Fiber contents of 0.5% and 1% were prepared to study effects of fiber content on desiccation characteristics. The constant fiber length of 25mm was used for all soil-fiber mixtures. Specimens with fiber content of 0.75% were prepared with varying slurry thicknesses of 6mm, 12mm and 24mm. The average fiber content (0.75%) was selected to allow easy mixing of soil with fibers and also to achieve uniform distribution of fibers. The final deposited slurry for both reinforced and unreinforced soil were exposed to controlled room temperature, and relative humidity of 45% ± 2% for drying until the mass of the specimen was stabilised. During drying, a digital camera was mounted above the specimen to take surface images of the crack pattern over time. The images were consequently used to quantify geometrical and morphological parameters of the cracks by employing image processing technique. The test set-up for desiccation test is shown in figure 3.13.

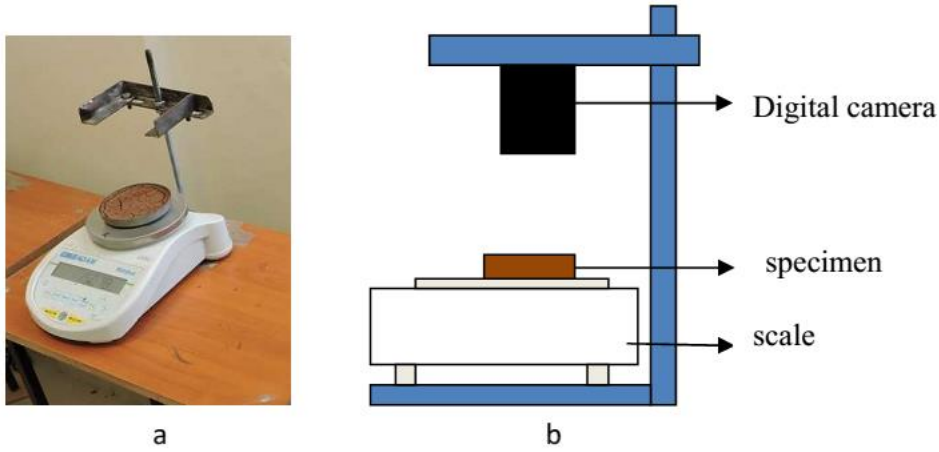

Figure 3.13: Test set-up for desiccation test.

3.4.1 Image processing technique for crack measurement

Digital image processing technique was adopted to analyse crack features of the desiccated soil composite. Image analysis is an easy and cost effective method and has been effectively used by several researchers. The image analysis process in this study was carried out in stages. The sequence of the process includes image acquisition, image processing, and measurements of crack features. The images with good resolution were uploaded in an image analysis program, ImageJ. The scale of the images was first converted from pixels to millimeters by measuring the diameter of the desiccators in pixels against the known diameter in millimeters. The images were then converted from gray scale to binary scale using colour split channels. The binary image was converted to a skeleton image by adjusting threshold. Crack analysis was performed by using particle analysis and measurement commands of the programme. The sequential process of digital image analysis is outlined in figure 3.14.

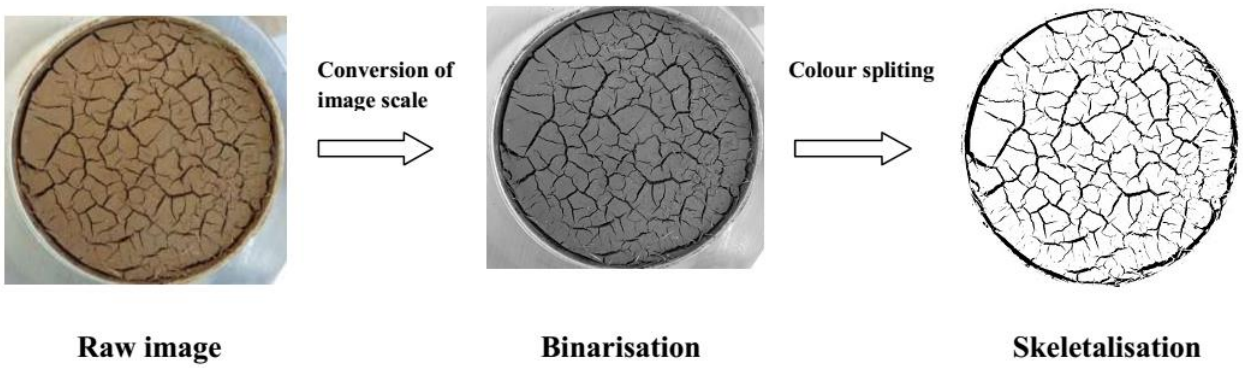

Figure 3.14: Digital image processing.

The raw image is composed of a system of composed red, green or blue colors. In binarisation the raw image in converted to grayscale image and eventually the grayscale image is segmented into binary black and white image. In skeletalisation, the binary image is further converted to skeleton image in order to extract a region-based shape feature representing the general form of objects such as cracks.

3.4.2 Crack feature measurement

The quantitative characterisation of the geometrical properties of the crack pattern was performed using image-processing software. Crack features such as surface crack area ratio/ crack intensity factor and crack width were determined from the processed images. The surface crack area ratio was determined as ratio of total area of cracks to total area of the specimen given by equation 3.12. The average crack width was determined by dividing area of the cracks by the total length of the cracks. The total length of cracks was computed by the software.

$$R_{scf} = \frac{A_{tc}}{A_{ts}} \times 100 \qquad (3.12)$$

where A_{tc} is the total area of cracks and A_{ts} is the total surface area of the specimen.

3.5 Cyclic test for fiber reinforced soil

To investigate the dynamic behaviour of unreinforced and reinforced soil, series of strain-controlled cyclic triaxial tests were conducted according to ASTM 3999-11(ASTM D3999, 2011). The tests were performed by using Dynatrax cyclic triaxial set. The experimental device is shown in figure 3.15.

Figure 3.15: Cyclic triaxial test device used for testing.

The pneumatic loading system of the device was provided by a 10 bar air compressor. The vertical load, deformation and volume changes were measured by electronic transducers. Compact Dynamic Controller (CDC) unit was used to control and monitor changes during testing. The CDC unit transmitted transducer data back to the computer via a high-speed communication network. Soil specimens were saturated using water back pressure up to B value (Skempton coefficient) of at least 0.98, indicating sufficient water saturation for undrained test. The cyclic loading at the constant strain of 0.1 and frequency of 1 Hz was applied with confining pressures of 50kPa, 100kPa and 200kPa. The cyclic loading was applied in 100 cycles and the test data (hysteresis loops, shear modulus, damping ratio and pore pressure ratio) were collected and processed through a data acquisition system. This number of cycles was selected in order to simulate and obtain material behaviour during short earthquake tremors. Permanent strain was determined as average strain of first cycle according to recommendations by (Vucetic and Mortezaie, 2015). Cumulative strain was determined as sum of permanent strain after 100cycles.

3.5.1 Post cyclic monotonic shear test

Post cyclic tests involved standard monotonic loading that was applied to specimens after completion of the cyclic loading. The specimens were tested under conventional triaxial compression tests after subjecting them to 100 cycles of cyclic load. The post-cyclic tests were

conducted at confining pressure of 50kPa. The post cyclic stress-strain relationship of the soil specimens was obtained and used to determine post cyclic toughness, energy absorbing capacity and static energy ratio. The energy absorbing capacity at any fiber content was calculated as the area under the stress-strain curve from 0 to failure strain. The post cyclic toughness was calculated as the energy absorbing capacity divided by area under stress-strain curve from 0 to yield strain of the same specimen. The mathematical expression for the computation of the post cyclic toughness is shown in equation 3.13.

$$T(\sigma) = \frac{\int_0^{\varepsilon_f} \sigma(\varepsilon) d\varepsilon}{\int_0^{\varepsilon_y} \sigma(\varepsilon) d\varepsilon} \tag{3.13}$$

where ε_f and ε_y are failure strain and yield strain, respectively. The static energy ratio was determined as the energy absorbing capacity at a given fiber content (0.5% and 1% fiber contents) divided by energy absorbing capacity of unreinforced soil. The mathematical expression that was used to compute post cyclic static energy ratio is shown in equation 3.14.

$$E(\sigma) = \frac{\int_0^{\varepsilon_f} \sigma(\varepsilon)_R d\varepsilon}{\int_0^{\varepsilon_f} \sigma(\varepsilon)_U d\varepsilon} \tag{3.14}$$

where subscripts R and U represent reinforced and unreinforced soil, respectively.

3.6 Lime fixation for stabilisation of fiber-soil composite

The minimum lime demand for the soil was approximated by conducting Eades-Grim pH test according to ASTMD 6276 (ASTM D6276, 2019) and was found to be 7% of lime as shown in figure 3.16.

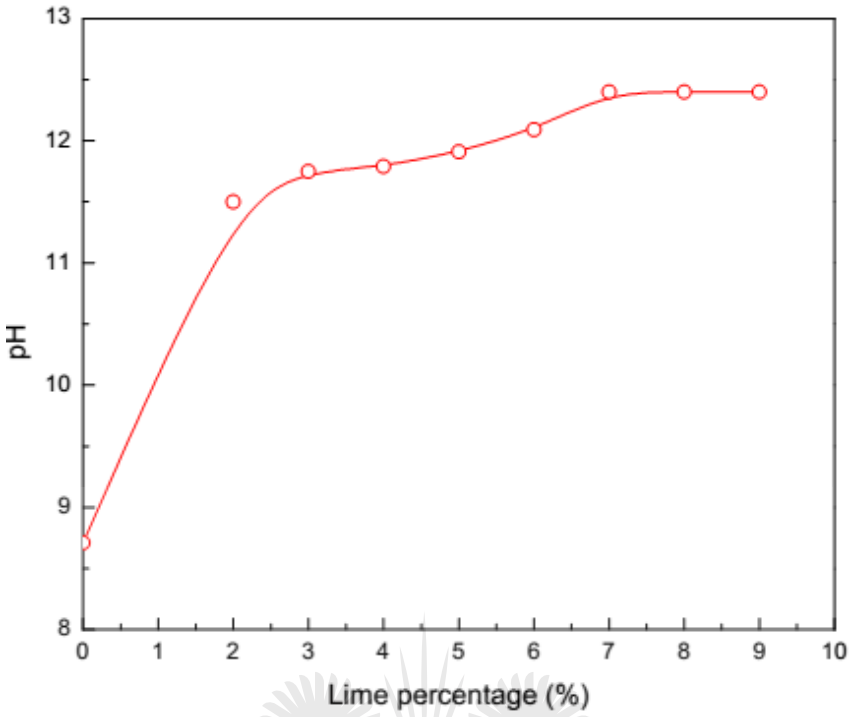

Figure 3.16: Lime demand of the soil used for study.

The mix design for stabilising agents was 1:2 of lime and fly ash respectively according to (Kumar et al., 2007).

3.7 Test procedures for fiber reinforced adobe masonry

3.7.1 Preparations and characterisation of masonry constituents

The constituents of masonry elements comprised of reinforced and unreinforced mud mortar and adobe bricks. In the manufacture of adobe bricks, dry soil was weighed in the gauge box of dimensions 300x300x300mm. The prescribed fiber content (0.75%) for the adobe composite mix was subsequently determined by the percentage dry mass of soil

The soil was mixed with water at the moisture content of +2% plastic limit and fibers were gradually added to wet soil until a homogeneous composite paste was formed. The soil paste was cast into a mould of dimensions 215x102x65mm according to BIS recommendation and was immediately demoulded to produce adobe brick. The adobe bricks produced (see figure 3.17) were covered with grass and sun dried for 28days.The grass cover was used to limit evaporation in order to prevent premature shrinkage and cracking of the bricks. The average outdoor humidity for the curing period was 40%. After drying, the average dimensions of the adobe bricks were reduced to 200x100x60mm due to shrinkage of the material. The local methods for

moulding and curing of adobe bricks were adopted to emulate common practice in rural areas of Eastern and Southern regions of Africa. The unreinforced adobe bricks were also manufactured following the same moulding and curing procedures.

Figure 3.17: (a) Soil sample (b) mould (c) manufactured adobe bricks (d) sisal fibers used.

The fiber reinforced and unreinforced mud mortar were also prepared and cast into cubes of 50x50x50mm. The mud mortar specimens were prepared in the same manner as the bricks. A total of 6 specimens per mortar type were prepared and cured for 28days under uncontrolled laboratory temperature. This number of specimens was selected in order to obtain good statistical data of the test results. The compression tests were performed on mortar and adobe bricks in order to characterise their strength properties. The irregularities of manufactured adobe brick specimens were smoothened by abrasion before testing to avoid pre-mature failure. The typical strength properties for mortar and adobe bricks used for masonry specimens are shown in figure 3.18.

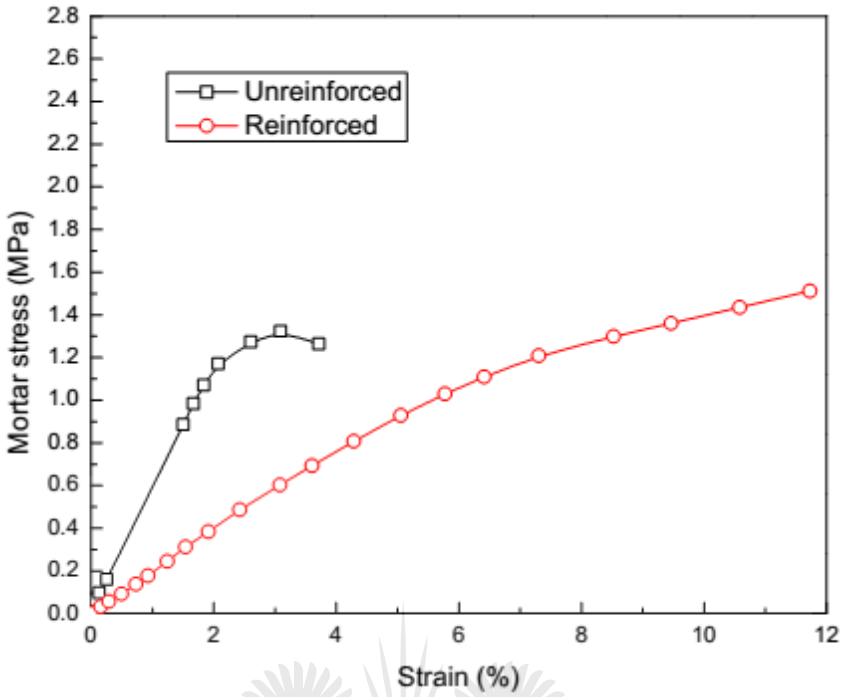

(a)

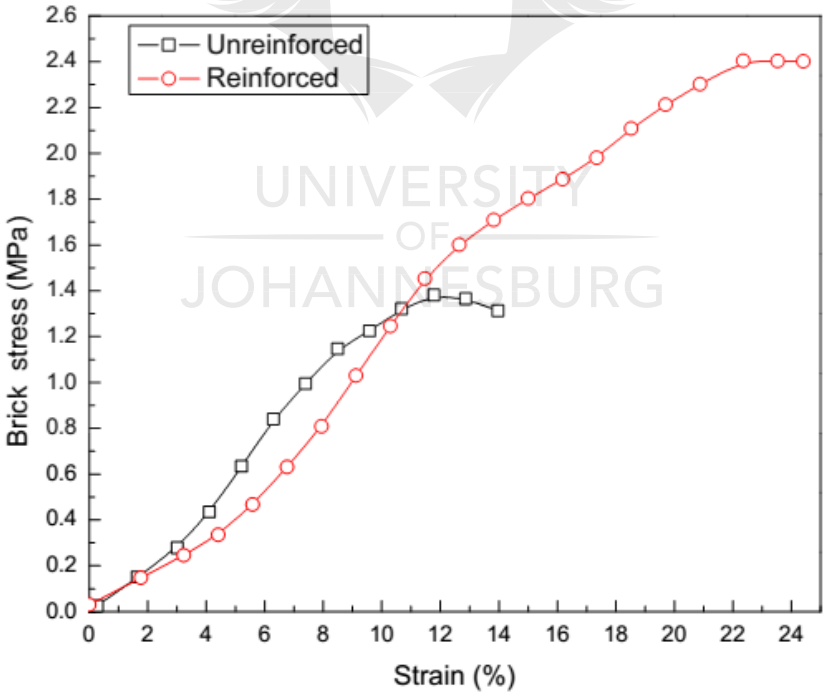

(b)

Figure 3.18: (a) Typical properties of mortar (b) Typical properties of adobe bricks.

3.7.2 Specimen preparation for adobe masonry testing

Masonry elements, namely prisms, triplets and couplets were prepared using the manufactured adobe bricks and the aforementioned mortar types (reinforced and unreinforced). Different reinforcement patterns for the prism specimens were adopted. The specimens' reinforcement patterns were as follows; (a) reinforced brick and mortar (coded as RBRM), (b) unreinforced brick and reinforced mortar (coded as UBRM), (c) reinforced brick and unreinforced mortar (coded as RBUM) and, (d) unreinforced mortar and bricks (coded as UBUM). The variations in the reinforcement patterns of masonry prism components aimed at determining the optimum fiber reinforcement design for masonry construction. The masonry elements were cured for 28days under uncontrolled laboratory temperature of between 20^{o}C and 30^{o}C at relative humidity between 30% and 40%. These are prevailing in situ conditions when the adobe materials possess considerable strength.

Two sets of wallets of average dimensions of 500x480x200mm were prepared, one with both reinforced mortar and bricks that was labeled as (RMRB) and the other with both unreinforced mortar and bricks that was labeled as (URUB). The wall panels of average dimensions of 1080x1100x100mm were prepared. Since failure of the wall panels in diagonal shear is governed by strength of the mortar (Alecci et al., 2013), the panel reinforcement was applied to mortar only. The unreinforced adobe bricks were used to prepare panel specimens according to RILEM (RILEM LUMB6, 1994) recommendation. The panel specimens were labeled as UBUM and UBRM to stand for the unreinforced and reinforced panels, respectively. The local procedure used in the Eastern and Southern Africa for masonry construction was adopted. A total of 3 specimens were prepared for both wallet and panel testing.

References

Alecci et al. (2013). Shear strength of brick masonry walls assembled with different types of mortar. *Construction and Building Materials, 40*, 1038–1045.

ASTM D698. (2012). Standard Test Methods for Laboratory Compaction Characteristics of Soil Using Standard Effort. West Conshohocken, PA.

ASTM D1140-17. (2017). Standard Test Methods for Determining the Amount of Material Finer than 75-μm (No. 200) Sieve in Soils by Washing. West Conshohocken PA: ASTM International.

ASTM D3999. (2011). Standard Test Methods for the Determination of the Modulus and Damping Properties of Soils Using the Cyclic Triaxial Apparatus. West Conshohocken, PA: ASTM International.

ASTM D5102. (2009). Standard Test Method for Unconfined Compressive Strength of Compacted Soil-Lime Mixtures. West Conshohocken, PA.

ASTM D5298 - 94. (1994). Standard Test Method for Measurement of Soil Potential (Suction) Using Filter Paper (Withdrawn 2003),, . West Conshohocken, PA: ASTM International.

ASTM D6276. (2019). Standard Test Method for Using pH to Estimate the Soil-Lime Proportion Requirement for Soil Stabilization. West Conshohocken, PA: ASTM International.

Bulut et al. (2001). Suction Measurements by Filter Paper," Expansive Clay Soils and Vegetative Influence on Shallow Foundations. In M. B. A. C.Vipulanandan, and M. Hasen (Ed.), (pp. 243-261). Reston, Virginia: ASCE.

Kumar et al. (2007). Influence of fly Ash, lime, and polyester Fibers on compaction and strength properties of expansive Soil. *Journal of Materials in Civil Engineering, 19*, 242-248.

RILEM LUMB6. (1994). Diagonal tensile strength tests of small wall specimens 1991 *Rilem recommendations for the testing and use of constructions materials.* (pp. 488–489). London: RILEM.

Tang et al. (2007). Strength and mechanical behavior of short polypropylene fiber reinforced and cement stabilized clayey soil. *Geotextiles and Geomembranes, 25*(5), 194-202.

Vucetic.M and Mortezaie. A. C. (2015). Cyclic secant shear modulus versus pore water pressure in sands at small cyclic strains. *Soil Dynamics and Earthquake Engineering., 70*, 60- 72.

Zornberg J. G. (2002). Discrete framework for limit equilibrium analysis of fibre-reinforced soil. *Géotechnique, 52*(8), 593-604.

4 CHAPTER FOUR-MACROSTRUCTURAL PROPERTIES AND MECHANICAL PERFORMANCE OF COMPACTED SISAL FIBER REINFORCED SOIL

4.1 Introduction

The objective of this study was to bring an understanding of macro structural properties and mechanical performance of compacted natural fiber reinforced soil with varying fiber content and length in order to establish the optimum fiber properties for maximum strength mobilisation. This was achieved by investigating the effects of randomly distributed sisal fibers on the macrostructural properties related to compaction. The performance of compacted soil composites was investigated by series of unconfined compression tests at various fiber contents and lengths. The study was carried out in three steps. Firstly, the effects of 10mm, 25mm and 50mm fibers at fiber contents of (0.5%, 0.75% and 1% by mass) on maximum dry density (MDD) and optimum moisture content (OMC) were established. Secondly, optimum compressive strength of the soil composite with varying fiber content and length were established. The energy-based homogenisation model was used to predict the strength and validate the hypotheses developed from the experimental results.

4.2 Materials and experimental programme

4.2.1 Materials

The soil sample used in this study was prepared and characterised as in section 3.1.1 according to ASTM D1140-17.The properties are summarised in Table 3.1. The fibers were oven dried at 40^{o}C for 8h and were subsequently cut into lengths of 10mm,25mm and 50mm. The summary of the fiber properties is shown in Table 3.3

4.2.2 Compaction test

The fiber contents were determined by percentage dry mass of the soil. The fiber dosages used herein were 0.5%, 0.75% and 1%. The specified fiber content was manually mixed with soil using hands. Great care was taken to distribute fibers evenly in order to prevent formation of air pockets during wet mixing. The specimen preparation was in accordance with ASTM D698-00 for standard Proctor compaction test. The compaction was performed in 5 layers using an automatic compaction machine at 55 blows per layer. The maximum dry density (MDD) and optimum moisture content (OMC) of the composite for each fiber content and length were determined.

4.2.3 Unconfined compression test

Initially, fibers were incrementally added into the soil and manually mixed in dry state. Water of equivalent optimum moisture content (10%) was subsequently added to the soil-fiber composite. The wet mixing was carried out until a homogeneous soil composite was formed. After wet mixing, the soil composite was covered with plastic sheet to prevent loss of moisture. The moisture content of +1% (OMC) was used to provide for marginal loss of moisture during specimen fabrication. The specimens were prepared in the mould of diameter 70mm and height of 140mm, by static compaction using gauge-mounted hydraulic jack. By following the customised method in section 3.2, the soil composite specimens were compacted into 3 layers. The static compaction pressure of 4MPa was used to compact all specimens. The specimens were extruded by the jack at a constant displacement of 1mm/stroke as highlighted in section 3.2.

The compression test was immediately carried out to determine strength and stress-strain relationship of soil-fiber composite. The specimens were tested in accordance with ASTM D2166 using Dynamic Triaxial machine (DYNATRIX), at the displacement rate of 1mm/min. A minimum of three specimens for each fiber dosage was used to determine the average unconfined compressive strength of the composite.

4.3 Results and discussions

4.3.1 Compaction test

The results of compaction test are shown in figures 4.1 a-c.

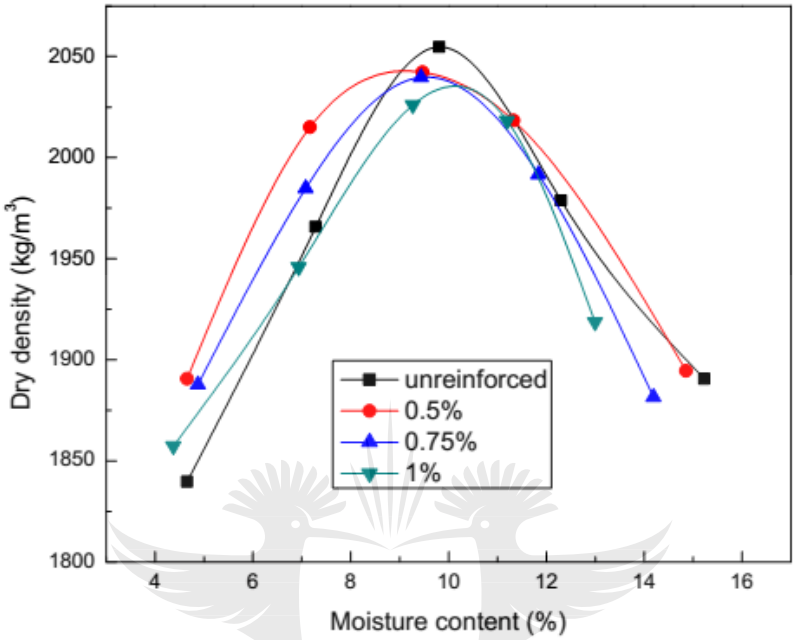

(a)

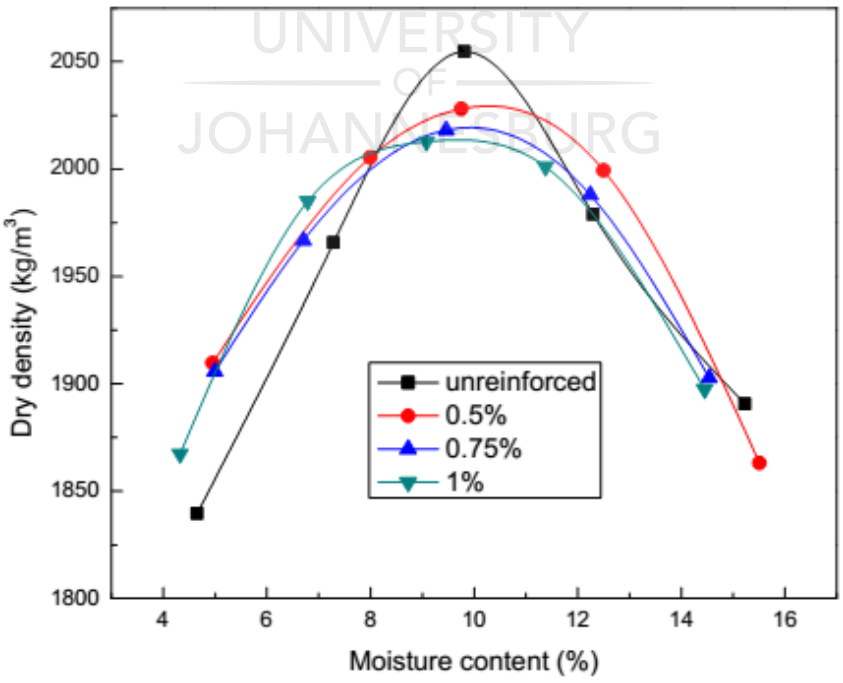

(b)

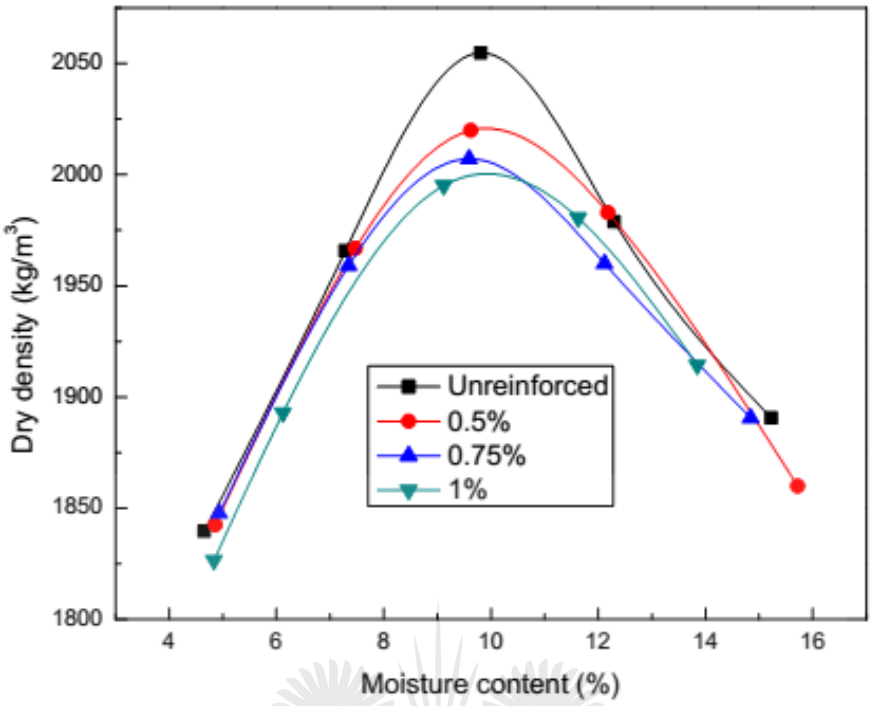

(c)

Figure 4.1: Dry density and moisture content curves (a) L=10mm (b) L=25mm (c) L=50mm.

It can be noted that increasing fiber contents and lengths causes decrease in maximum dry density and no significant change in optimum moisture content. The effects of fiber inclusions and lengths are relatively high at higher fiber content (1%) and longer fiber length (50mm). The MDD reductions of 1.1%, 1.2% and 1.4% for 10mm, 25mm and 50mm fiber lengths respectively, are registered. The effect of sisal fiber inclusions on density could be explained in two perspectives with respect to the physical properties of the fibers and fiber-solids macro-mechanical interactions during compaction. Sisal fibers possess low density (1.24g/cm^3). The sisal inclusions in the present study reduced overall weight of the composite and ultimately decreased density of the soil composite (Aqeel Al Adili et al., 2012b; Prabakar and Sridhar, 2002; Sayida, 2009). Fundamentally, increasing volume of fibers caused changes in the volume of solids and voids within a given constant volume of the composite. The addition of fibers essentially provided resistance to the compaction and prevented dense packing of grains while creating voids along the peripheral of the fibers. This phenomenon was pronounced with longer fiber lengths. The fiber reinforced soil could be considered to possess both macro voids as a result of packing of a smaller number of solids within a given total volume and micro voids

emanating from the inability of fibers to form perfect bonds with particles (Ajayi, 2016; Ibraim and Fourmont, 2006). The aforementioned phenomena caused the apparent reduction of maximum dry density of the fiber reinforced soil. The material property difference caused small gravimetric changes of the composite to guarantee noticeable change in moisture content.

4.3.2 Unconfined compressive strength

The results of unconfined compressive strength with fiber dosages and lengths at (OMC) are shown in figure 4.2a and b.

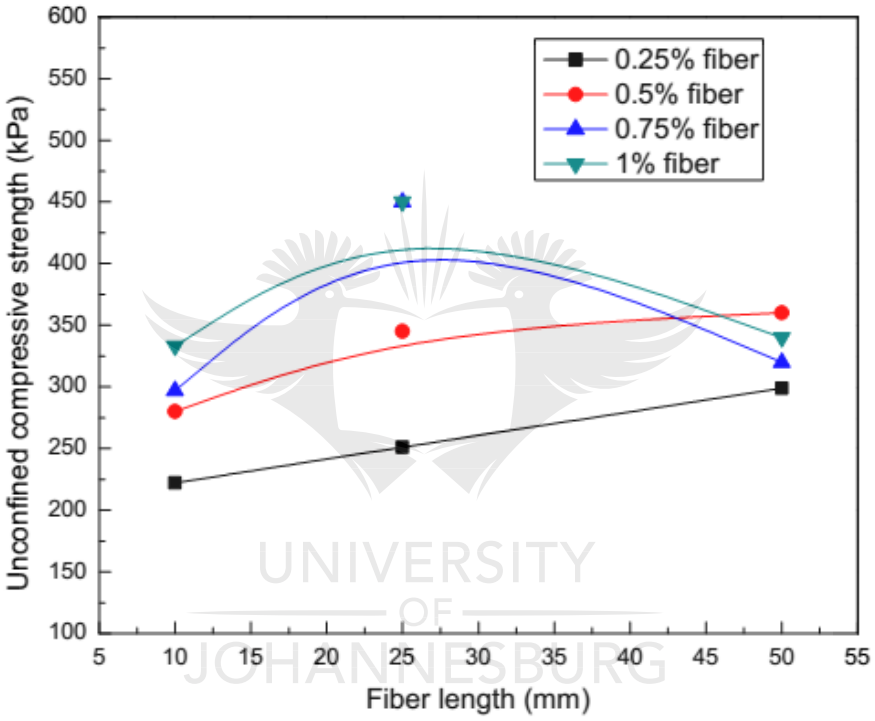

(a)

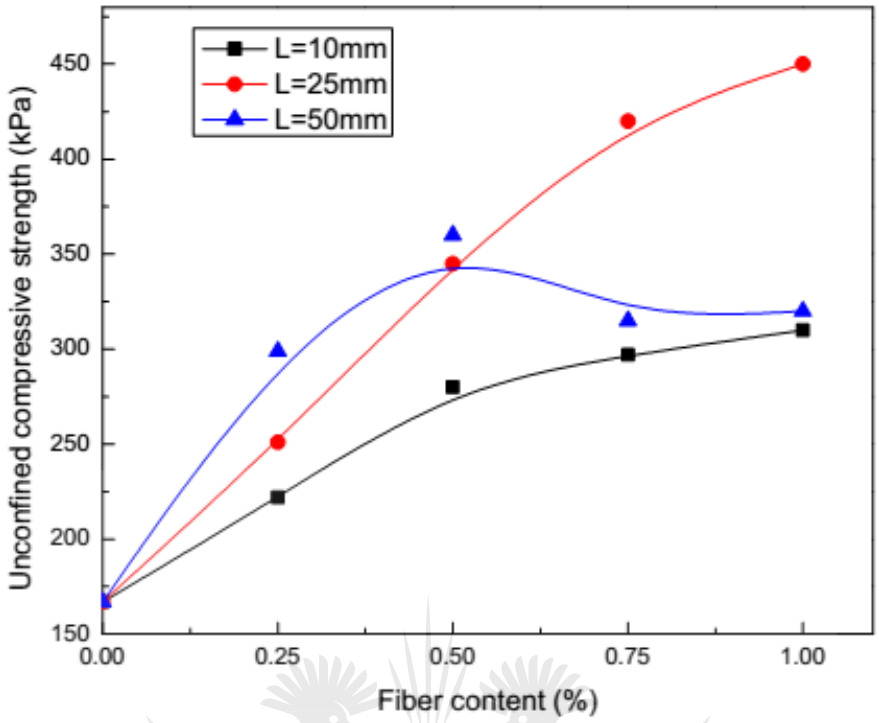

(b)

Figure 4.2: Variation of UCS at optimum moisture content (a) with fiber length (b) with fiber content.

It is noted that increasing fiber content causes an increase in compressive strength. Strength gain is high for 25mm fibers, from the fiber dosage greater than 0.5%. The optimum strength is shown at 0.75% fiber content. The strength gain of 50mm fiber length is high at fiber contents less than 0.5% and reduces at high fiber contents (0.75% and 1%). Fiber composites with 10mm fibers show steady increase in strength up to 1% fiber content. The maximum strength gains with respect to unreinforced soil for 10mm, 25mm and 50mm are 99%, 167% and 115 %, respectively. The similar study by (Yixian et al., 2016) indicated maximum shear strength of 240kPa at 0.6% fiber content and 400kPa cell pressure and about 190kPa at low cell pressure of 100kPa. In comparison these values are slightly higher than what was obtained from the experiment due to the variation of soil and fiber properties and applied confinement.

Strength evolution of fiber reinforced soil depends of the mechanical properties of the fibers and fiber-soil mechanical interaction (Shukla et al., 2009; Tang et al., 2010b). Shear stresses in the soil mobilise tensile resistance in the fibers that imparts greater strength to the soil (see figure 4.3) (Hejazi et al, 2012; Hejazi et al., 2013; Wu et al., 2014a).

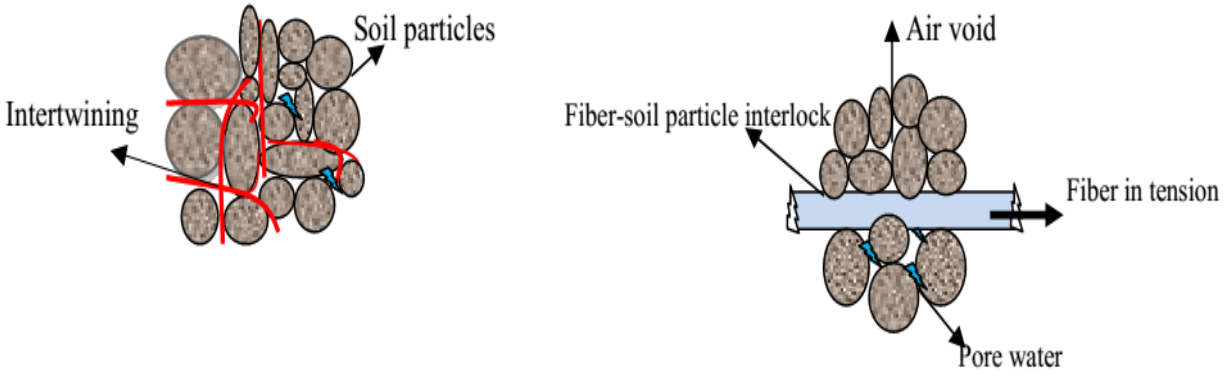

Figure 4.3: Schematic diagram of fiber-soil reinforcement mechanisms.

The matric suction increases cohesion and effective stress acting on the fiber surface and enhances fiber-matrix interfacial shear strength. Strong bond between fiber and soil particles gives rise to high fiber tensile strength mobilisation (Fredlund et al., 2012). Therefore, the strength gain exhibited by the specimens in this study could be due to combined mechanisms namely, fiber-matrix mechanical interlocking and fiber interweaving. The subsequent decrease in strength gain was attributed to the reduced fiber-soil interlocking mechanism. The non-uniform distribution of fibers and an increase in the amount of fiber particles placed horizontally in the specimen as a result of (1) longer fiber lengths, (2) thin layer of soil interphase between adjacent fibers also caused strength reduction (Ahmad et al., 2010a; Diambra et al., 2013). The strength gain exhibited by 10mm and 25mm fibers at high fiber content was due to the high efficiency of fiber-matrix mechanical interaction. The contribution by matric suction was assumed negligible due to the presence of moisture in the composite.

4.3.3 Stress-strain relationship of fiber reinforced soil

The stress-strain relationships of soil composites with various fiber contents (0.5%, 0.75% and 1%) at optimum moisture content are shown in figures 4.4a-c.

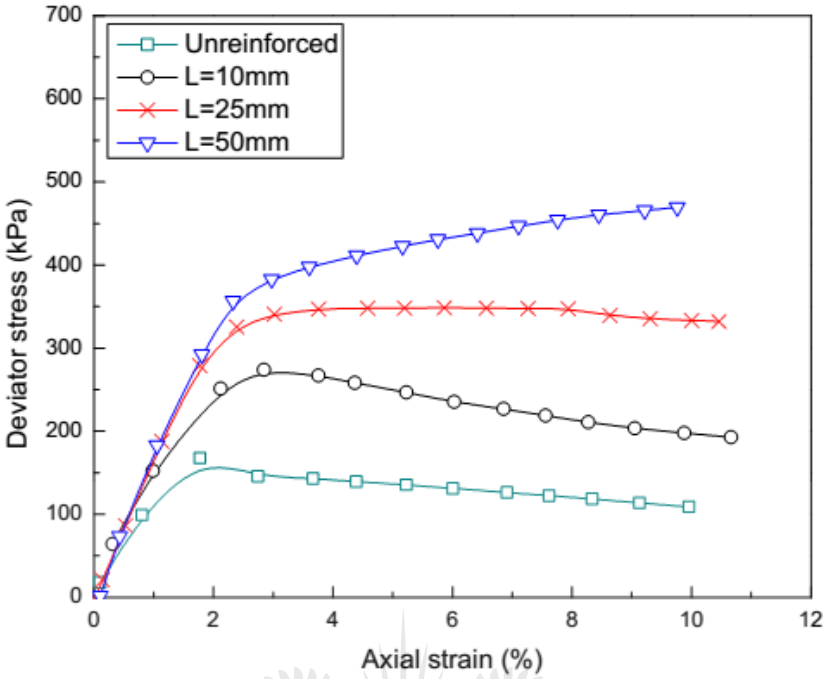

(a)

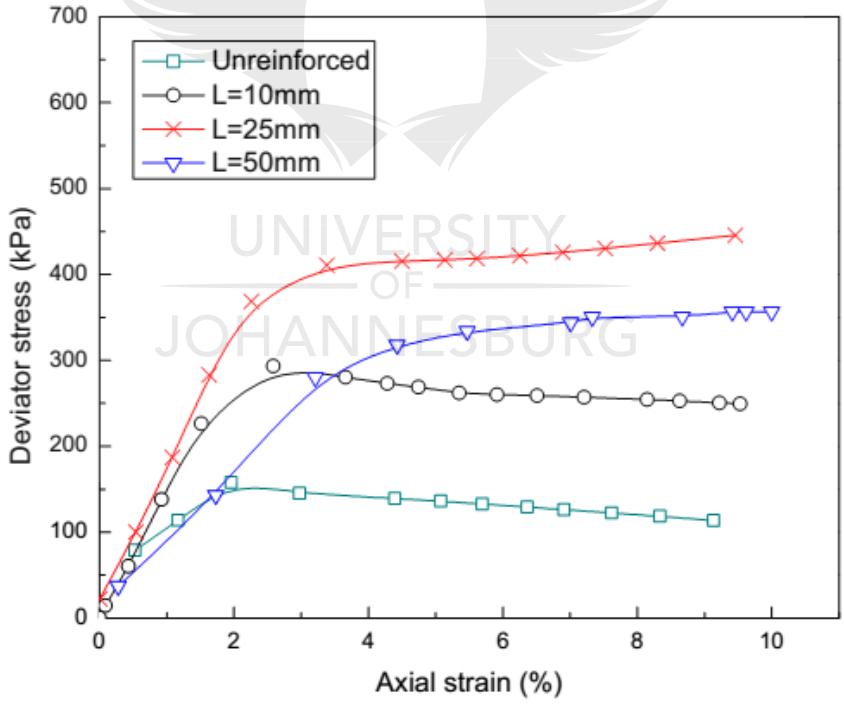

(b)

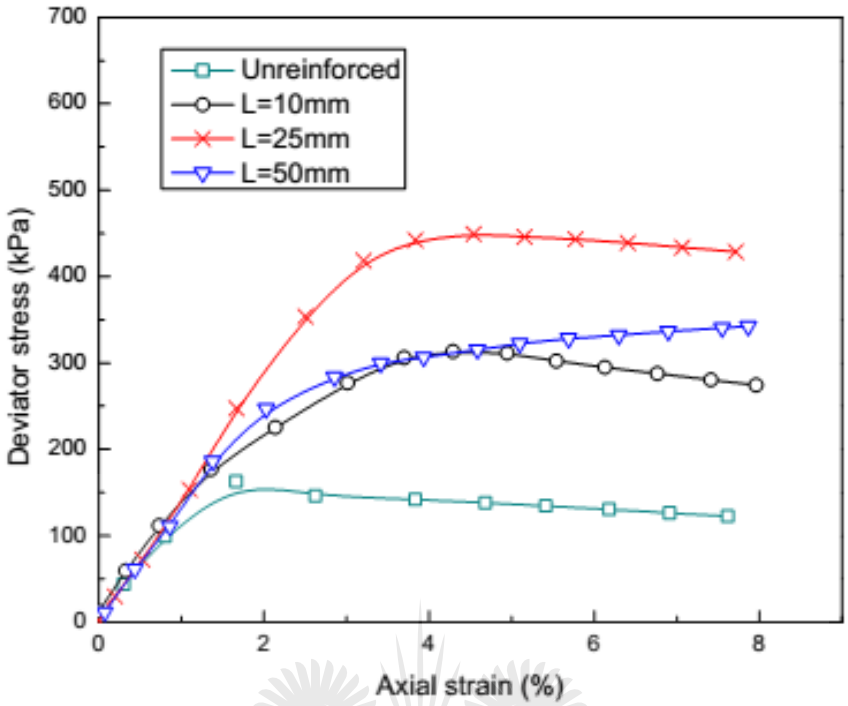

(c)

Figure 4.4: Stress-strain relationships of soil composites at OMC (a) 0.5%, (b) 0.75% (c) 1%.

It can be seen that the strain softening behaviour is exhibited by unreinforced and short fiber reinforced composites. The typical post peak behaviour is strain hardening at high fiber contents (1%). Composites with 25mm and 50mm fibers show strain hardening behaviour with apparent increase in strength in plastic phase. The unreinforced specimens show brittle behaviour while fiber reinforced soil composites show ductile behaviour. The ductility is more pronouncedly with 50mm fiber length. In comparison, 25mm fiber composites show significant stiffness. The fiber-controlled strength properties caused strain hardening behaviour exhibited by reinforced soil composites at high fiber content. As shown in figure 4.4, the composite stiffness increases with fiber length. This could be due to macro structural properties of the composite endowed by fibers. Figures 4.5a and b show the digital image analysis of failure modes of specimens with low and high fiber contents.

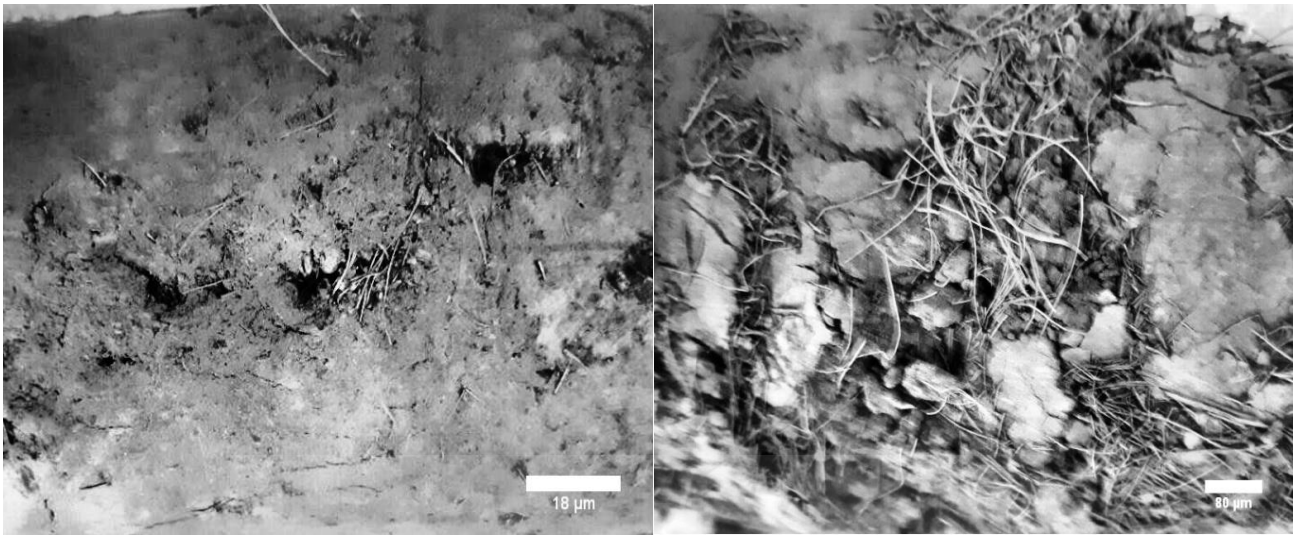

(a) (b)

Figure 4.5: Effects of fiber content on failure modes (a) 25mm fibers at 0.5% fiber content (b) 25mm fibers at 1% fiber content.

It can be seen that a failure plane is shown for low fiber content. This is an indicative of brittle failure characterised by strain softening. Multiple planes of failure coupled with fiber interweaving are shown for high fiber content. This is an indicative of kinematic strain hardening. It is evident that fiber pull out was the typical failure mode of the composite.

4.3.4 The analytical estimation of composite strength and failure criteria

An attempt to estimate strength evolution and associated failure criteria for natural fiber reinforced soil was undertaken by utilising energy–based homogenisation technique according to (Michalowski and Zhao, 1994). The model was applied on the unconfined compression test of specimens with varying fiber contents and lengths. In applying the homogenisation model, plane-strain deformation of an element of fiber reinforced soil was considered. The rate of work due to the external forces on an element was assumed equal to the energy dissipation rate. The energy–based homogenisation model is given by equation 4.1.

$$R = p\left(\sin\varphi + \frac{1}{3}N\rho\eta\varphi_w\right) \qquad (4.1)$$

where φ_w is the interaction coefficient between fiber and soil matrix, φ is the angle of friction of the soil matrix, p is the mean principal stress of the composite, R is maximum shear stress

defined by equation 4.2 for UCS, N is the parameter defined by equation 4.3, ρ is the fiber volume ratio given by equation 4.4, η is the fiber aspect ratio given by equation 4.5.

$$p_n = \sigma_1 \text{ and } R = \tau_{\max} = \frac{\sigma_1}{2} \tag{4.2}$$

$$N = \frac{1}{\pi}\cos\varphi + \left(\frac{1}{2} + \frac{\varphi}{\pi}\right)\sin\varphi \tag{4.3}$$

$$\rho_f = \frac{V_f}{V_c} \tag{4.4}$$

$$\eta = \frac{l_f}{d_f} \tag{4.5}$$

where l_f is the fiber length, d_f is the fiber diameter, V_f is the volume of fibers in the specimen, V_c is the volume of the composite specimen.

In this study, a series of undrained unconfined compression tests was performed on 45 specimens. The fiber content was determined by percentage by mass of dry soil $\ell_f = \frac{m_f}{m_s}$. Therefore, the equivalent volume fraction of fibers v_f was computed using the volume and average mass of the tested specimens. After preparing specimens at 10% water content, measured as percentage dry mass of fiber and soil, the average mass was found to be 1150g which was composed of mass of fibers, soil and moisture. Therefore specimen mass in this respect was expressed as equation 4.6.

$$m_c = m_f + m_s + m_m \tag{4.6}$$

where m_f is total mass of fibers and m_s is mass of soil and m_m is mass of water given by equation 4.7.

$$m_m = 0.1(m_f + m_s) \tag{4.7}$$

Therefore, mass of the specimens was expressed in terms of mass of fibers and soil as equation 4.8.

$$m_c = 1.1(m_f + m_s) \tag{4.8}$$

The fiber volume fraction in the specimen was approximated as $\rho_{fv} \approx 0.4\%$ using average mass of specimen (1150g), diameter of 70mm and height of 140mm, fiber content of 0.25% and density of sisal fibers of $1.4\, g/cm^3$ (Pickering et al., 2016). Therefore, fiber volume fractions for 0.25%, 0.75% and 1% were in the order of 0.4%, 0.8%, 1.2% and 1.6%, respectively. The fiber aspect ratios were computed using equation 4.5 for fiber diameter of 0.2mm. The aspect ratios for 10mm, 25mm and 50mm fibers were determined as 50,125 and 250, respectively. The interaction coefficient was taken as 0.5 (Li and Zonberg, 2005). The matrix friction angle was determined as $\varphi = 30.1^o$. The summary of principal stresses at failure for the unconfined compressive strength of the specimens is shown in Table 4.1.

Table 4.1: Experimental principal stresses at failure for various fiber lengths and volume fractions

Fiber volume fraction (%)	Average principal stress *p* (kPa)		
	Aspect ratios (η)		
	50	125	250
0.4	222	251	299
0.8	280	345	360
1.2	298	420	315
1.6	310	450	320

The simplified failure criterion for unconfined compression test can be written as equation 4.9 and was used to compute estimated failure shear strength of the specimens. Take note that the model does not account for effects of matric suction.

$$\tau_{max} = p_n\left(sin\varphi + \frac{1}{3}N\rho_f \eta \varphi_w\right) \tag{4.9}$$

The estimated composite shear strength for $\varphi = 30.1^o$, p_n, η and ρ_f (see Table 4.1), are summarised in Table 4.2.

Table 4.2: Predicted and experimental shear stresses of the composite at failure

Fiber Volume fraction %	Shear strength $\tau_{\max}$ (kPa) Aspect ratios(η)								
	50			125			250		
	τ_{EXP}	τ_{PRE}	Deviation (%)	τ_{EXP}	τ_{PRE}	Deviation (%)	τ_{EXP}	τ_{PRE}	Deviation (%)
0.4	111	113	1.8	126	130	3	149	159	6.7
0.8	140	144	2.8	178	184	3.3	180	204	13
1.2	149	155	4	210	232	10.5	158	190	23
1.6	155	163	5	225	256	14	160	184	15

* τ_{EXP} Is the shear strength from experiment τ_{PRE} is the predicted shear strength

It is noted that the prediction model is more accurate for short fibers in the composite of low fiber content. The percentage of accuracy diminishes with an increase in fiber content. It is seen that aspect ratio of 50 corresponding to 10mm fibers shows the more accurate values with about 5% deviation at high fiber content, whereas fibers of aspect ratio 125 and 250 hereto 25mm and 50mm fibers register large deviation of 13% and 23%, respectively at high fiber content. The percentage of deviation increases with an increase in the fiber content and length. The more reasonable accuracy for short fibers is due to uniform fiber distribution in the composite. Fiber distribution and orientations become increasingly non-uniform with increase in fiber content and length (Diambra et al., 2007; Michalowski and Cermak, 2002). The normalised estimated failure criteria, using yield stress of fibers (in Table 4.1) and fiber content are shown in figure 4.6.

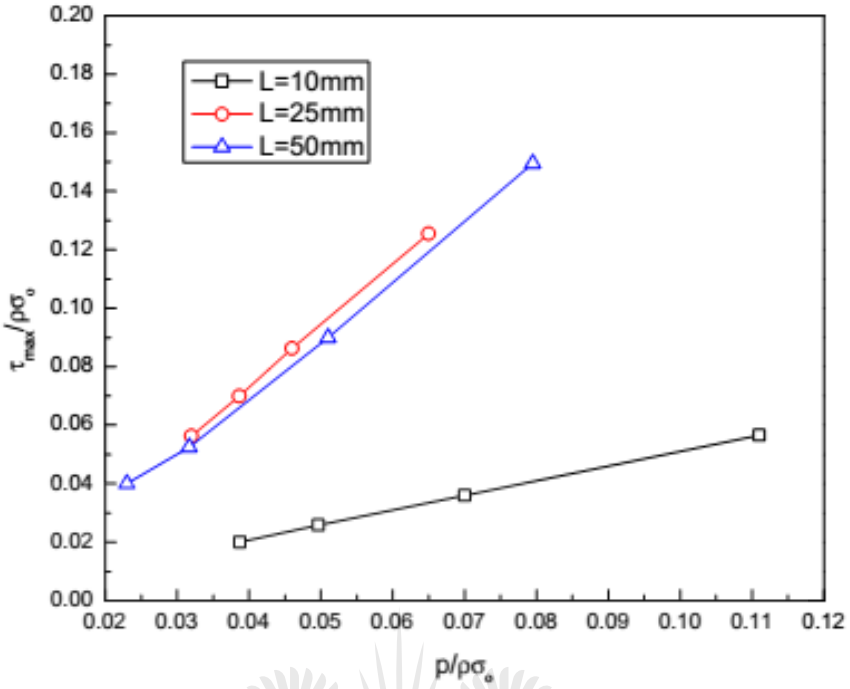

Figure 4.6: Normalised estimated failure criteria of soil composites with various fiber lengths and contents.

It is obvious that composite with 25mm fiber benefit more from the fiber strength mobilisation and, 10mm fibers indicate lower capacity. This validates the hypothesis earlier established that increasing fiber lengths reduces strength due to non-uniform fiber distribution.

Conclusions

Based on the foregone experimental and analytical results, the following conclusions are drawn;

1. Increasing fiber content at designated fiber length and content causes decrease in maximum dry density and marginal change in optimum moisture content. This is attributed to the low unit weight of fibers.
2. Fiber inclusion improves unconfined compressive strength of the composite.
3. Increasing fiber length beyond 25mm and corresponding fiber content beyond 0.75% may reduce unconfined compressive strength. This is due to non-uniform distribution of fibers and the reduced fiber–soil interlocking mechanism.
4. The kinematic strain hardening behaviour and the improved ductility are associated with an increase in fiber length and content.

5. Energy based homogenisation can estimate failure shear strength of short fiber and reasonable accuracy is achieved with low fiber content.
6. In practice, incorporating fibers in earthen construction can endow the foundation structure and walls with significant ductility and strength. Ductility is beneficial for the resilience of the structure to seismic loading. Enhanced strength increases structure performance under sustained gravity loads and may prolong service life of the structure.

References

Ahmad et al. (2010). Performance evaluation of silty sand reinforced with fibres. *Geotextiles and Geomembranes* 28:93–99.

Ajayi O. (2016). Feasibility Study of Random Fibre Reinforced Railway Ballast. University of Southampton: University of Southampton.

Aqeel Al Adili et al. (2012). Strength of soil reinforced with fiber materials (papyrus). *Soil Mechanics and Foundation Engineering, 48* (6), 241-247

ASTM D2166. (2016). Standard Test Method for Unconfined Compressive Strength of Cohesive Soil. West Conshohocken, PA: , ASTM International.

Diambra et al. (2007). Determination of fibre orientation distribution in reinforced sands. *Ge´otechnique* 57 (7):623–628.

Diambra et al. (2013).Fibre reinforced sands: from experiments to modelling and beyond. *International journal for numerical and analytical methods in geomechanics* 37:2427–2455.

Fredlund.D.G, Rahardjo.H and Fredlund.M.D. (2012). *Unsaturated Soil Mechanics in Engineering Practice.* Hoboken, New Jersey: John Wiley & Sons, Inc

Hejazi et al. (2012). A simple review of soil reinforcement by using natural and synthetic fibers. *Construction and Building Materials* 30: 100-116.

Hejazi et al. (2013). Shear Modeling of Fiber Reinforced Soil Composite on the Base of Fiber Pull-out Test. *Fibers and Polymers* 14 (2): 277-284.

Ibraim.E and Fourmont. S. (2006). Behaviour of sand reinforced with fibers. In Soil Stress-Strain Behavior: Measurement, *Modeling and Analysis Geotechnical Symposium*. Roma, Italy.

Li.C and Zonberg .J.G. (2005). Interface shear strength in fiber reinforced soil. Paper read at 16th *International conference of soil mechanics and geotechnical engineering*, at Osaka Japan.

Michalowski. R.L and Cermak. J. (2002). Strength anisotropy of fiber reinforced sand. *Computers and Geotechnics* 29:279-299.

Michalowski. R.L and Zhao.A. (1994). Failure of fiber-reinforced granular soil. *Journal of Geotechnical Engineering* 122 (3):226-234.

Pickering et al. (2016). A review of recent developments in natural fibre composites and their mechanical performance. *Composites: Part A* 77 83:98–112.

Prabakar. J and Sridhar.R.S. (2002). Effect of random inclusion of sisal fibre on strength behaviour of soil. *Construction and Building Materials* 16:123-131.

Sayida. M.K. (2009). Behaviour of Black Cotton Soil Reinforced with Sisal Fibre. Paper read at *10th National Conference on Technological Trends (NCTT09)* at India.

Shukla et al. (2009). Fundamental concept of soil reinforcement-an overview. *International journal of geotechnical engineering* 3 (3):329-342.

Tang et al. (2010). Interfacial shear strength of fiber reinforced soil. *Geotextiles and Geomembranes* 28:54–62.

Wu et al. (2014). Investigation of mechanical properties of randomly distributed sisal fiber reinforced soil. *Materials research innovation* 18:953-959.

Yixian et al. (2016). Study on strength influence mechanism of fiber-reinforced expansive soil using jute. *Geological and geotechnical Engineering* 34:1079–1088.

5 CHAPTER FIVE-EFFECT OF FIBER SURFACE COATING ON THE MECHANICAL PROPERTIES OF SISAL FIBER REINFORCED SOIL

5.1 Introduction

Natural fibers exhibit dimensional instability when exposed to moisture. Their hydrophilic characteristics undermine adhesion between fibers and soil matrix. The hygrothermal performance of natural fiber reinforced composites is reduced with exposure to moisture (Pickering et al., 2016). Investigations have shown that durability and mechanical properties of natural fiber composites are improved when fibers are coated with water repelling agents (Ahmad et al., 2010a; Sarbaz et al., 2014). The commonly used water repelling agents are bitumen and acrylic butadiene styrene. The aforementioned agents are expensive and energy intensive in production. Furthermore, bitumen is the toxic by-product of petroleum refinery. Its production is associated with emissions of hydrofluorocarbons that are environmentally unfriendly (Philibert et al., 2016). It is therefore imperative to find alternative water repelling agents that offer multifaceted economic and environmental benefits. The effective use of natural water repellent in soil fiber reinforcement is a milestone towards achieving sustainable built environment, especially in earthen construction. Meanwhile, investigations on the potential use of natural-based water repellents have received little attention.

Rosin shows high potential of water repellency and adhesion. It is a solid form of natural resin obtained from pine trees. The three types of rosins are gum, wood, and tall oil. They are defined by the part of the pine tree from which they are obtained. About 90% of rosin composition is resin acid of similar molecular structure. The composition depends on the origin, type and geographical location of the tree. The abietic resin acid constitutes the highest percentage of the composition and provides rosin with hydrophobic properties (Jin et al., 2000; Kruge, 2002; Miyono et al., 2006; Wang et al., 2011; Zheng et al., 2010).

The objective of this study was to investigate the potential use of gum rosin in improving durability and mechanical properties of natural fiber reinforced soil for long term geo-structure application.

5.2 Materials and experimental programme

5.2.1 Materials

The soil sample used in this study was prepared and characterised as in section 3.1.1 according to ASTM D1140-17. The grading curve of the soil is shown in figure 3.1, and the properties are summarised in Table 3.1. The sisal fibers used herein were sourced and prepared as in section 3.1.2. Fiber threads were obtained for surface coating. The mechanical properties of the sisal fiber used in this study are summarised in Table 3.3. The gum rosin used in this study was sourced and prepared as highlighted in section 3.1.3.

5.2.2 Specimen preparation and experimental programme

The specimens for compression tests were prepared in the same manner as in section 4.2.3. Specimens for fiber pull out test were prepared by mixing the soil matrix with water of equivalent optimum moisture content. The interfacial shear strength and compressive strength properties of coated and uncoated sisal fiber reinforced soil were investigated in the following steps. Firstly, single fiber pull-out tests were performed at optimum moisture content of soil matrix. The interfacial shear strength was also determined at soil densities of 1.3g/cm^3, 1.5g/cm^3, and 1.9g/cm^3. Secondly, the interfacial shear strength was determined at a constant soil density with varying water contents. Lastly, unconfined compression tests were performed on the randomly distributed soil composites at varying water contents, (1%, 3%, 5%, and 9%). For all tests, a comparative analysis of mechanical properties between coated and uncoated fibers was conducted to determine potential benefits of rosin coating.

In preparing the specimen for pull-out test, the fiber was embedded in the soil matrix encased by a perforated rigid PVC ring. The ring dimensions were 25mm in diameter and 15mm thickness as shown in figure 5.1.

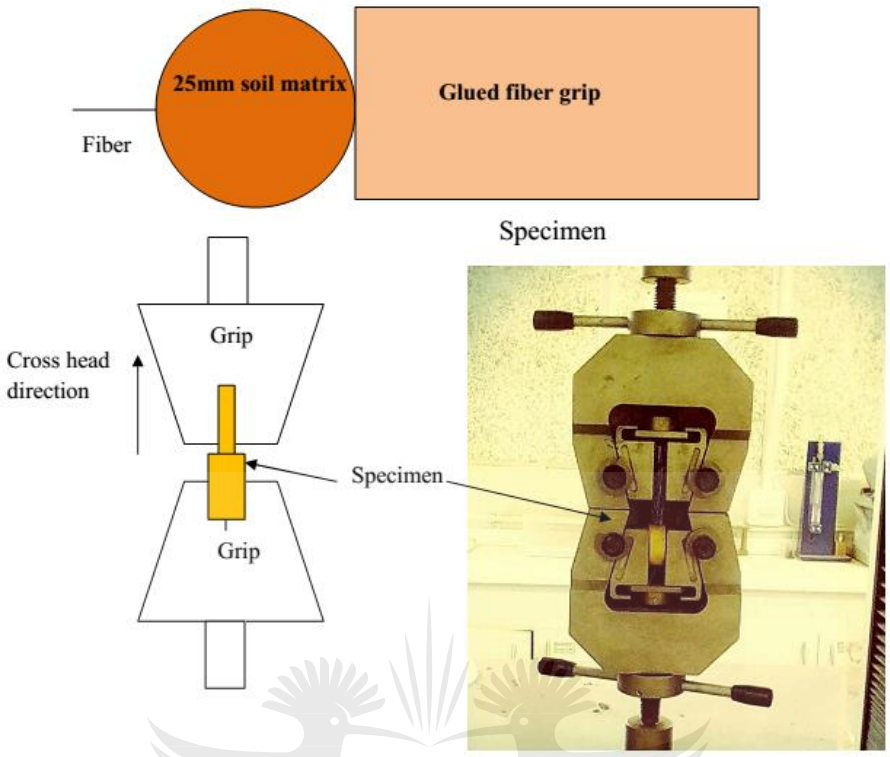

Figure 5.1: Single fiber pull-out specimen and test set-up.

The soil matrix was statically compacted using hydraulic jack at compaction pressures of 5MPa, 10MPa and 20MPa. The compaction levels achieved soil densities of 1.3g/cm^3, 1.5g/cm^3 and 1.9g/cm^3, respectively. The fiber was glued to the thick and tough paper pieces. The gripping pieces were made to touch the encasement to ensure fiber pulled-out during testing.

Immediately after preparing specimens at designated densities, interfacial shear strength (IFSS) and interfacial residual shear strength (IRSS) were determined by fiber pull-out tests according to the set-up in figure 5.1. The interfacial shear strength and interfacial residual shear strength were computed using equation 5.1 and 5.2, respectively.

$$IFSS = \frac{P_{max}}{\pi d_f l_c} \tag{5.1}$$

$$IRSS = \frac{N_r}{\pi d_f l_c} \tag{5.2}$$

where P_{max} is the maximum pull-out load, N_r is the ultimate pull-out load after considerable displacement (3mm), d_f is fiber diameter and l_c is embedded fiber length.

5.2.3 Testing programmes

Single fiber tensile test was conducted on the coated and uncoated fibers to investigate the effects of coating on the fiber mechanical properties. Fiber pull out test was performed to determine fiber-matrix interfacial shear strength and residual shear strength. Both fiber tensile and pull out tests were carried out using Quasar 10 universal tensile machine at a displacement rate of 0.5mm/min. A minimum of five specimens for each test was used to determine average strength value. The moisture related interfacial shear strength was investigated by using specimens that were compacted to dry density of 1.5g/cm^3 by the static compaction pressure of 10MPa. This compaction effort was selected in order to prevent premature fiber slippage and rupture. The synergic effects of matrix moisture content and fiber coating on interfacial shear strength were investigated after 4h, 8h, 24h and 72h of air drying. The corresponding soil matrix moisture content was determined for each drying period.

The compression test was carried out to determine strength and stress-strain relationship of soil-fiber composites. The specimens were tested in accordance with ASTM D2166 (ASTM D2166, 2016b) using Dynamic Triaxial machine (DYNATRIX), at a displacement rate of 1mm/min. A minimum of three specimens was used to determine the average unconfined compressive strength value. The synergic effects of fiber coating and matrix moisture content on the compressive strength were investigated after 8h, 1d, 3d, 7d and 14d. The air drying was conducted at uncontrolled laboratory temperature of 25^o-30^{o}C. The corresponding composite moisture contents were determined for each drying period.

5.3 Results and discussions

5.3.1 Effects of coating on the fiber tensile properties

The effect of coating on the tensile strength properties of fibers is shown in figure 5.2.

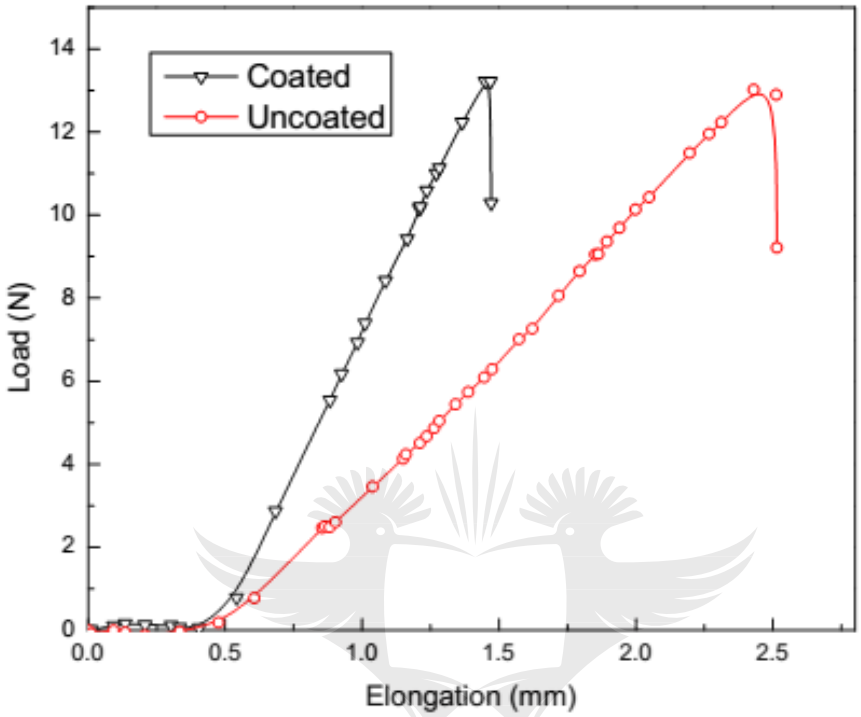

Figure 5.2: Tensile properties of coated and uncoated fibers.

It is noted that fiber coating enhanced stiffness of the fibers. The ultimate tensile strength was not significantly affected by rosin coating. The coated fibers indicated lower failure elongation than uncoated fibers. The brittle failure was exhibited by both fiber types. The crystalline nature of rosin endowed the fibers with enhanced stiffness.

5.3.2 Interfacial shear strength at matrix optimum moisture content

The interfacial shear strength and interfacial residual shear strength at various matrix densities are shown in figures 5.3a and b

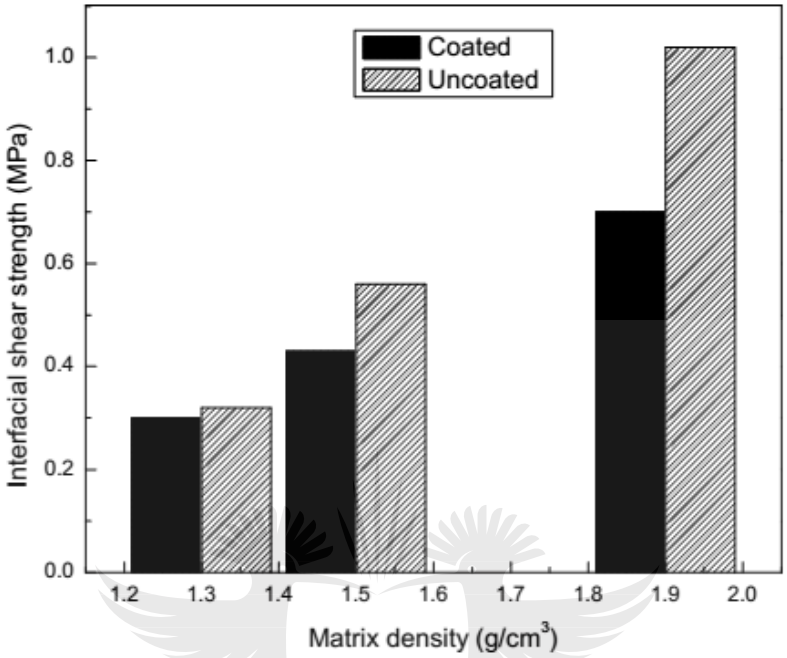

(a)

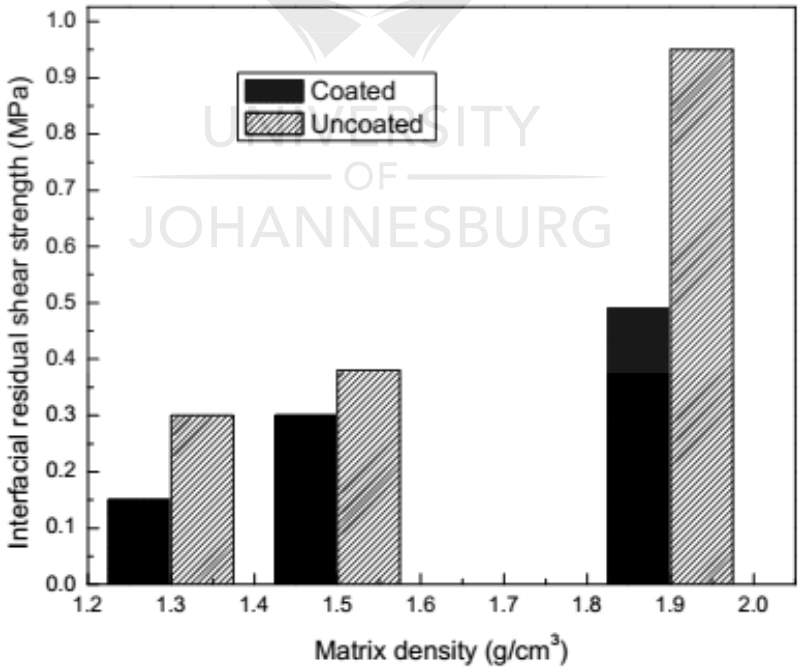

(b)

Figure 5.3: (a) Interfacial shear strength (b) Interfacial residual strength of coated and uncoated fibers at OMC of the matrix.

It is worth noting that uncoated fibers exhibited higher strengths (IFSS and IRSS) than coated ones. The interfacial shear strength and interfacial residual shear strength increased with matrix density. The IRSS indicated lower values than IFSS. The coated fibers showed low interfacial shear strength at all soil matrix densities. The increase in the interfacial shear strength of the composites due to an increase in matrix density was also reported elsewhere (Tang et al., 2010b). Rosin consists primarily of abietic and pimaric-type resin acids with characteristic hydrophenanthrene ring structures. The hydrophenanthrene rings are considered to have cycloaliphatic and aromatic structures. The molecular structures of rosin increase contact angle of the liquid and provide rosin with hydrophobic characteristics (Gandini, 2008; Wang et al., 2011). Therefore, lower interfacial shear strength and residual shear strength exhibited by coated fibers (at OMC) was due to the presence of thin film of moisture emanating from the water repelling mechanism of rosin. The film of moisture consequently reduced adhesion between fibers and soil particles. Furthermore, moisture acted as lubricant at the fiber surface. The moisture undermined mechanical inter-lock between soil particles and fiber surface. The decrease in the fiber pull-out resistance due to moisture was also reported by (Tang et al., 2010b). High matrix density enhanced frictional resistance on the fiber surface and improved mechanical inter-lock between soil particles and fibers. The typical load displacement curves for fiber pull-out test at various matrix densities are shown in figure 5.4a and b for coated and uncoated fibers, respectively.

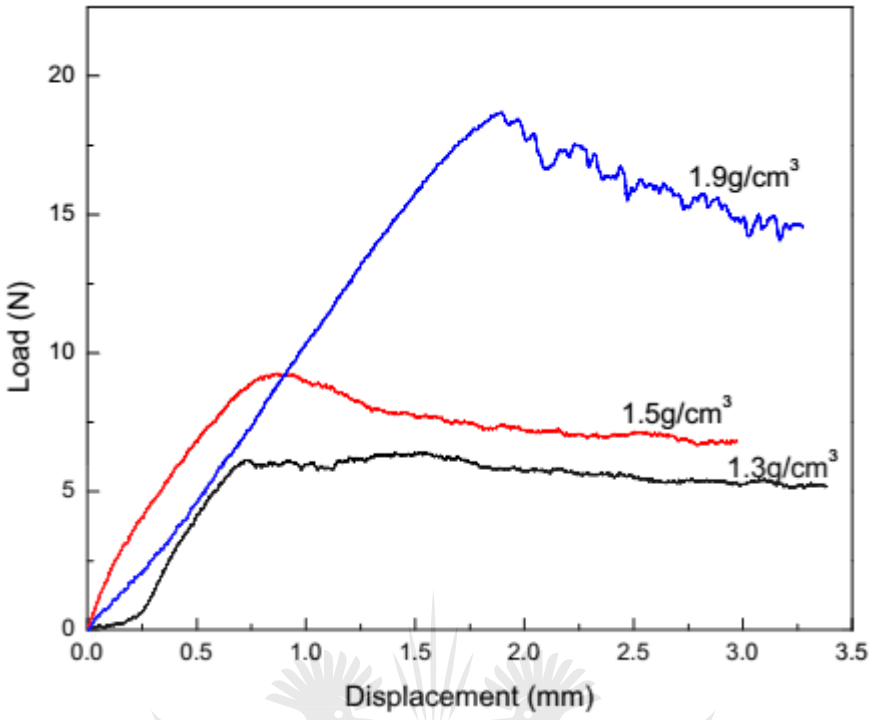

(a)

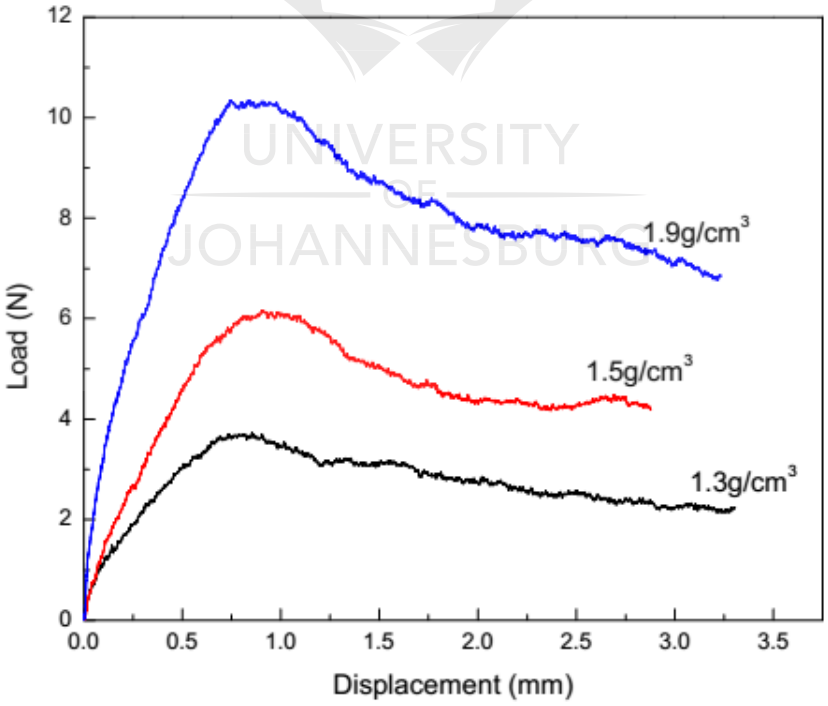

(b)

Figure 5.4: Load-displacement curves for single fiber pull-out test (a) Uncoated fibers (b) Coated fibers.

It is noted that the rising portion of the load–displacement curve was typically linear without any apparent stick-slip. There was no significant load-drop after complete interfacial debonding at low matrix density. The load-drop was pronounced at high matrix density. Stick-slips were observed for uncoated fibers at high matrix density. This was an indicative of high mechanical inter-lock between fibers and soil. Figures 5.5a and b show SEM images of fiber surface morphology for sheared coated and uncoated fibers, respectively.

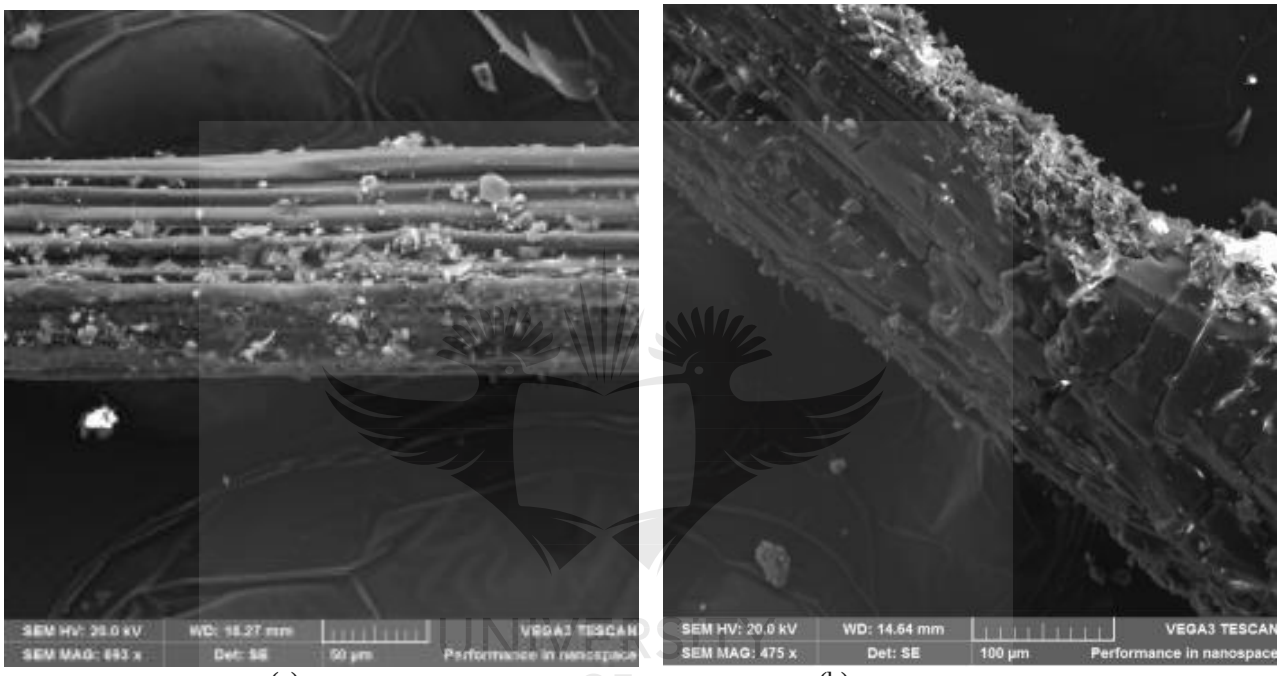

(a) (b)

Figure 5.5: SEM images for sheared fibers (a) Uncoated (b) Coated.

It is evident from SEM micrographs that the surface of the uncoated fiber was rough with patches of soil particles sticking to the fiber. On the other hand, coated fiber was smoother with significant amount of particles sticking to the surface. In a previous experimental study (Liu et al., 2018) revealed that the interfacial strength behaviour of fiber composite is significantly influenced by fiber surface roughness. The rough surface of uncoated fibers signified high mechanical inter-lock between the fiber and soil particles. The mechanical inter-lock was therefore responsible for the high interfacial shear strength mobilised by uncoated fibers. Albeit, the soil particles were bonded to coated fiber surface, the synergy of smooth surface and lubricating effect of moisture undermined fiber-soil mechanical interlocking (Tang et al., 2010b). Shear lag analysis could be utilised to predict load transfer at fiber-matrix interface with linear,

isotropic and elastic material behaviours. In this case, the soil matrix and embedded fiber were assumed to be linked by a frictional interface with slippage and zero axial stress at the ends of the fiber. The shear lag formulation for axial stress in the fiber according to (Abramento and Whittle, 1993) is given by equation 5.3.

$$\sigma_{xx}^{f} = \left(\sigma_{tr} - \frac{K_2\sigma}{K_1}\right)\left[\frac{cosh\sqrt{K_1}\left(\frac{l_f}{2} - l_{fx}\right)}{cosh\sqrt{K_1}\left(\frac{l_f}{2} - l_{fd}\right)}\right] + \frac{K_2\sigma}{K_1} \tag{5.3}$$

where l_f is the length of the fiber, l_{fx} and l_{fd} are arbitrary length along the fiber and debonding length, respectively. Assuming that the maximum axial stress in the fiber during pull out was mobilised at the middle of the fiber length, therefore $l_{fx\,max} = \frac{l_f}{2}$, σ_{tr} is the transition axial stress at $l_{fx} = l_{fd}$, K_1 and $K_2\sigma$ are constants defined by material properties and geometry. The transition stress for $l_{fx} = l_{fd}$ is given by equation 5.4.

$$\sigma_{tr} = \frac{K_2\sigma}{K_1} - \frac{\sigma_1}{\left(\frac{mfK_1}{8} + \left(\frac{f\sqrt{K_1}}{2\mu}\right)tanh\sqrt{K_1}\left(\frac{l_f}{2} - l_{fd}\right)\right)} \tag{5.4}$$

where σ_1 is the major applied principal stress, μ is the coefficient of friction at fiber-matrix interface. For the negligible applied minor principal stress, $K_2\sigma$ is given by equation 5.5.

$$K_2\sigma = Z_1\sigma_1 \tag{5.5}$$

where σ_1 is the major applied principal stress and Z_1 is the constant defined by material properties and geometry. The constants K_1 and Z_1 are expressed by equations 5.6 and 5.7, respectively.

$$K_1 = \left(\frac{6}{mf}\right)\left(\frac{(1-\nu_m)a + 2\left(\frac{E_m}{E_f}\right)\left(1-\nu_f{}^2\right)}{1+\frac{\nu_m}{4}-\left(\frac{3E_m}{2E_f}\right)\left(1+\nu_f\right)\nu_f}\right) \tag{5.6}$$

$$Z_1 = \left(\frac{6}{t_m f}\right)\left(\frac{(1-2\left(\frac{E_m}{E_f}\right)\left(1+\nu_f\right)\nu_f}{1+\frac{\nu_m}{4}-\left(\frac{3E_m}{2E_f}\right)\left(1+\nu_f\right)\nu_f}\right) \tag{5.7}$$

where m and f arebthe thicknesses of matrix and fiber, respectively, $a = \frac{f}{m}$, E_f and E_m are the elastic moduli of fiber and matrix, respectively, ν_f and ν_m are Poison's ratios of fiber and matrix, respectively. With respect to the pull-out test performed on the specimens, the load transfer at the fiber-soil matrix interface could therefore be predicted using equations 5.4-5.7. The fiber axial force in this scenario was assumed to be in equilibrium with the surface tangential shear force at the incipient of slippage (Hejazi et al., 2013). In this case, the hoop/confinement pressure emanating from static compaction in the rigid matrix encasement was assumed to exert vertical pressure on the fiber surface. The minor principal stress parallel to fiber direction was negligible owing to the shape of the specimen. Therefore, equations 5.4 to 5.7 could be utilised using material and specimen properties shown in Table 5.1. The predicted values of maximum axial load transfer in the fiber are summarised in Table 5.2. It is seen that shear lag analysis can predict load transfer of fiber pull-out to some acceptable values. With respect to the fiber coating, the predicted load values are almost 85% of pull-out load of coated and uncoated specimens. The model accuracy depends on the material properties, geometry and the nature of fiber-matrix interface. The model does not include precise effects of moisture on the debonding. The quantification of debonding length requires rigorous machine computation.

Table 5.1: Parameters for prediction

Parameter	Value	Reference/Remark
Matrix depth (mm)	24.8	calculated
Fiber thickness (mm)	0.2	Table 2
Fiber Poison's ratio(ν_f)	0.2	(Sun et al., 2014)
Matrix Poison's ratio (ν_m)	0.3	(Muni Budhu, 2011)
Coefficient of friction (μ)	0.2	(Tsubakihara et al., 1993)
Fiber Elastic modulus E_f (GPa)	22	Exp
Matrix Elastic modulus E_m (MPa)	20	Exp
Maximum debonding length (mm)	3*	
Fiber inclusion ratio (a)	0.008	
		calculated

Exp- experimental value *- assumed value

Table 5.2: Prediction of maximum fiber axial load transfer by shear–lag model

Applied pressure (MPa)	Predicted fiber axial load (N)	Experimental pull-out load (N)	
		Uncoated	Coated
5	3.3	4.7	3.5
10	6.8	8.1	6.7
20	13.4	16.1	10

5.3.3 Effects of moisture on interfacial shear strength

The effect of moisture variation on the interfacial shear strength at constant matrix density (1.5g/cm^3) is shown in figure 5.6.

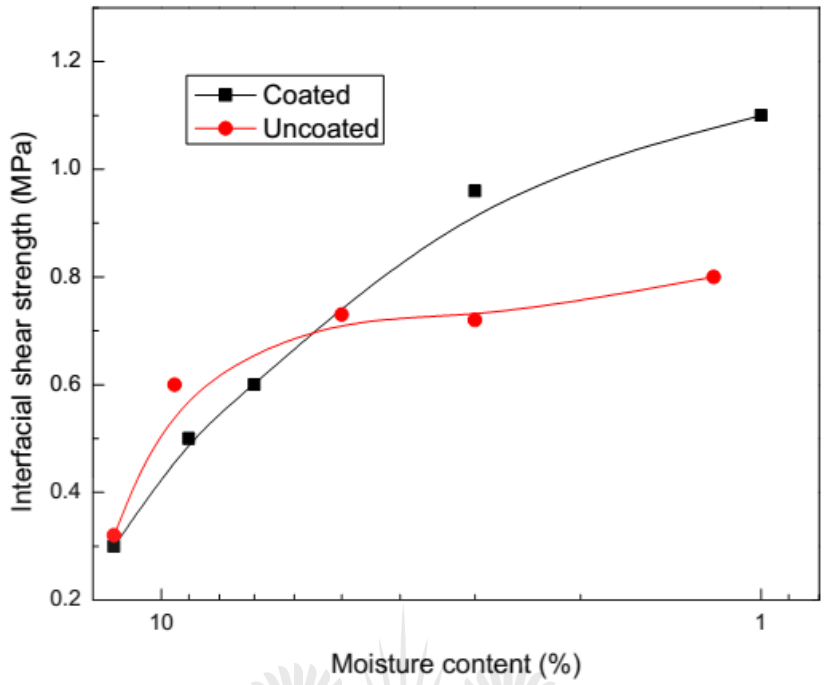

Figure 5.6: Moisture related interfacial shear strength of coated and uncoated fibers.

It is apparent that interfacial shear strength for both fiber conditions improved with the reduction in moisture content until strength equilibrium was reached. In comparison, uncoated fibers mobilised higher interfacial shear strength at high moisture content than coated fibers. With further reduction in moisture content, coated fibers indicated higher strength than uncoated fibers. When the matrix completely dried, coated fibers exhibited strength of about 27% higher than uncoated fibers. The bonding force at the contact area of soil particles–fiber contributed to the interfacial shear resistance. In addition, matrix suction that developed during drying caused an increase in effective stress on the fiber/soil interface. High effective stress improved resultant interfacial shear strength (Portelinha et al., 2018). Furthermore, the thin film of moisture on the surface of coated fibers due to hydrophobic characteristics of rosin caused low strength mobilisation at high moisture content. The bonding of soil particles to coated fiber was enhanced by the reduced lubrication at low matrix moisture content.

5.3.4 Moisture related mechanical properties of fiber reinforced soil.

5.3.4.1 Unconfined compressive strength

The evolution of compressive strength of fiber reinforced soil composite with rosin at varying moisture content is shown in figure 5.7.

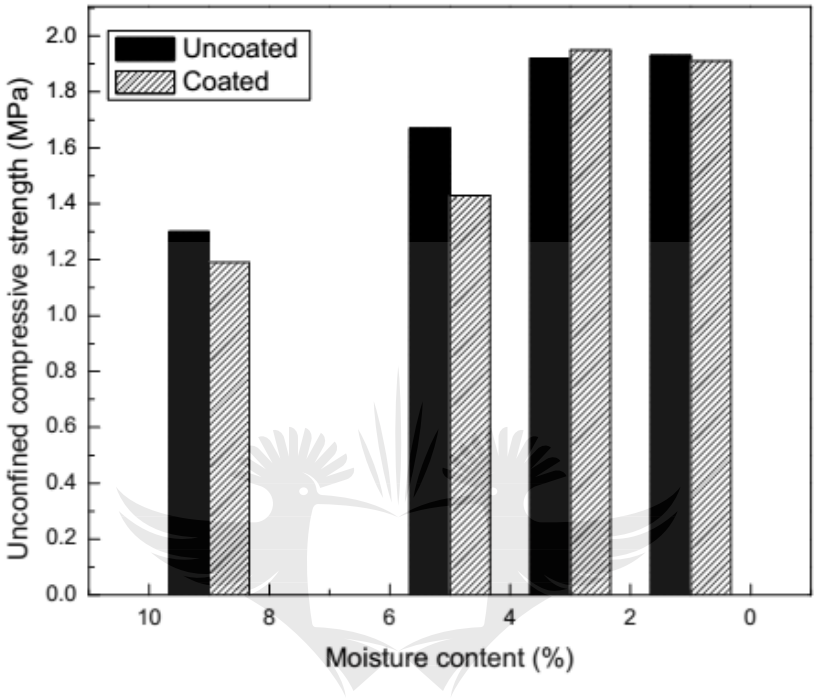

Figure 5.7: Moisture related UCS of fiber reinforced soil with coated and uncoated fibers.

It is noted that compressive strength improved with the reduction in moisture content. In comparison, marginal difference in strength was exhibited by both composite specimens at low moisture content. The specimens with coated fiber showed enhanced strength gain at low moisture content. The strength behaviour exhibited in figure 5.7 was in agreement with the interfacial shear strength behaviour reported in the foregone section. It is well established that strength of fiber reinforced soil is controlled by the tensile resistance of the fibers to shear stresses at the fiber-matrix interface. The adhesion between fiber and composite matrix is a major factor in determining the response of the interface and its integrity under stress (Jacob et al., 2005; Tang et al., 2010b). It can be deduced that lower strength exhibited by specimens with coated fibers was due to the weak bond at the fiber matrix interface in the presence of moisture. Fiber-soil adhesion improved with drying due to the evolution of matric suction.

5.3.5 Stress-strain relationship and stiffness

The stress-strain behaviour of fiber reinforced soil composite with coated and uncoated fibers at various moisture contents is shown in figure 5.8.

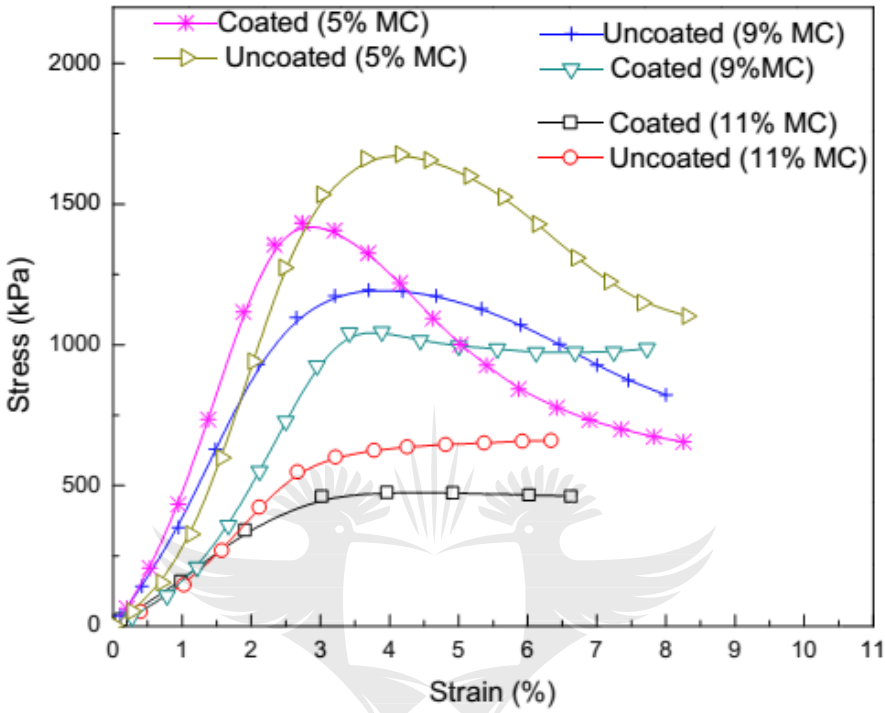

Figure 5.8: Stress-strain behaviour of soil composite with varying moisture content.

It is noted that at high moisture content, both composites exhibited strain hardening behaviour. As moisture content reduced, specimens with coated fiber exhibited strain softening at 9% moisture content, whereas specimens with uncoated fiber still indicated strain hardening behaviour. Both specimens showed strain softening at 5% moisture content. It is vivid in figure 5.8 that presence of moisture governed the stress-strain behaviour of the specimens. The change in behaviour of specimens with coated fiber signified loss of moisture by the composite. Since fibers used herein were natural (sisal), the considerable amount of moisture was absorbed by the uncoated fibers during specimen preparation. This was due to the hydrophilic characteristics of fibers (Azwa et al., 2013 ; Mohanty et al., 2005). It can be anticipated that the low amount of free moisture in the composite of uncoated fibers caused the reduced rate of moisture loss. The presence of moisture endowed the composite with strain softening behaviour. The effects of water repellency by rosin led to high amount of free moisture in the matrix that promoted

composite drying. The rapid loss of moisture is beneficial for the durability of composite as reported in the literature (Hejazi et al, 2012).

Figure 5.8 indicates that elastic modulus (stiffness) of both specimen types increased with the reduction in moisture content. In comparison, fiber coating had negligible effects on the composite stiffness. It can be concluded that large volume fraction of soil matrix dictated the stiffness behaviour of the composite. This was due to the evolution of matrix suction during drying.

Conclusions

Based on the acquired results, the following conclusions are drawn.

1. Interfacial shear strength and interfacial residual shear strength of rosin coated fibers reduced in the presence of moisture. This was attributed to the lubrication at the fiber-matrix interface by the film of moisture.
2. Interfacial shear strength of both coated and uncoated fibers improved with reduced moisture content of the matrix. The coated fibers mobilised higher strength than uncoated at low moisture content. The increased adhesion and mechanical interlock of the coated fibers caused an increase in the interfacial shear strength.
3. High matrix density increased interfacial shear strength and interfacial residual shear strength of both coated and uncoated fibers. This was as a result of high frictional resistance on the fiber surface that enhanced mechanical interlock of the fiber and soil matrix.
4. Unconfined compressive strength of the natural fiber reinforced soil with coated fibers might be lower than of uncoated fiber at high moisture content and strength was also noted to be significantly enhanced with drying.
5. Shear-lag analysis could predict fiber axial load transfer with some acceptable value for both coated and uncoated fibers.
6. In practice, Gum rosin could therefore effectively be used to enhance strength properties and potentially durability of fiber reinforced earthen walls

References

Abramento .M and Whittle.A.J. (1993). Shear- lag analysis of planar soil reinforced in plane - strain compression. *Journal of Engineering Mechanics, 119*(2), 270-291.

Ahmad et al. (2010). Performance evaluation of silty sand reinforced with fibres. *Geotextiles and Geomembranes, 28*, 93–99.

ASTM D2166. (2016). Standard Test Method for Unconfined Compressive Strength of Cohesive Soil. *ASTM International, West Conshohocken, PA*.

Azwa et al. (2013). A review on the degradability of polymeric composites based on natural fibres. *Materials & Design, 47*, 424-442.

Gandini. (2008). Polymers from renewable resources: A Challenge for the future of macromolecular materials. *Macromolecules, 41*(24), 9491-9504. .

Hejazi et al. (2012). A simple review of soil reinforcement by using natural and synthetic fibers. *Construction and Building Materials, 30*, 100-116.

Hejazi et al. (2013). Shear Modeling of Fiber Reinforced Soil Composite on the Base of Fiber Pull-out Test. *Fibers and Polymers, 14*(2), 277-284.

Jacob et al. (2005). A study of advances in characterization of interfaces and fiber surfaces in lingocellulosic fiber-reinforced composites. *Composite Interfaces, 12*(1-2), 95–124. .

Jin et al. (2000). Separation of rosin acids by molecular recognition: crystal structure of the complex of neoabietic acid with 2-amino-6-methyl-pyridine. *Journal of Chemical Crystallography, 30*(3), 195-198

Kruge. C. (2002). Generally Recognised as safe(GRAS) notification for Glycerol Ester of Gum rosin. Clint, TX: T&R Chemicals Inc.

Liu et al. (2018). Improved wettability and interfacial adhesion in carbon fibre/epoxy composites via an aqueous epoxy sizing agent. *Composites Part A: Applied Science and Manufacturing, 112*, 337-345.

Miyono et al. (2006). Chemical compositions of pine resins,rosin and turpentine oil from west Java. *Journal of Forestry research, 3*(1), 7-17.

Mohanty et al. (2005). *Natural fibers,Biopolymers and Biocomposites*. London: Taylor and Francis.

Muni Budhu (Ed.). (2011). *Soil mechanics and foundations* (3rd ed.). Arizona United states: Jonh Wiley and sons.

Philibert et al. (2016). Comparison of diluted bitumen (Dilbit) and conventional crude oil toxicity to developing zebrafish. *Environ. Sci. Technol, 50*(11), 6091–6098.

Pickering et al. (2016). A review of recent developments in natural fibre composites and their mechanical performance. *Composites: Part A, 7*(83), 98–112.

Portelinha et al. (2018). Small-scale pullout Test of a geogrid-reinforced unsaturated soil with suction monitoring. *Geotechnical Testing Journal, 41*(4).

Sarbaz et al.(2014).CBR strength of reinforced soil with natural fibres and considering environmental conditions. *International Journal of Pavement Engineering, 15*(7),577-583.

Sun et al. (2014). Predicting the elastic properties of sisal fiber reinforced polypropylene composites by a new method based on generalized method of cells and laminate analogy approach. . *Composites Science and Technology, 91*, 45–49.

Tang et al. (2010). Interfacial shear strength of fiber reinforced soil. *Geotextiles and Geomembranes, 28*, 54–62.

Tsubakihara et al. (1993). Friction between cohesive soils and steel. Soils and Foundations:Japanese society of soil *Mechanics and Foundation Engineering, 33* (2), 145-156.

Wang et al. (2011). Combining renewable Gum rosin and lignin: Towards hydrophobic polymer composites by controlled polymerization. *Journal of Polymer Science Part A :Polymer Chemistry, 49*, 3728–3738.

Zheng et al. (2010). Well-Defined Renewable Polymers Derived from Gum Rosin. *Macromolecules, 43*, 5922–5924.

6 CHAPTER SIX-MATRIC SUCTION CHARACTERISTICS OF COMPACTED SISAL FIBER REINFORCED SOIL COMPOSITE

6.1 Introduction

The geo structures such as embankments and foundations are subjected to varying climatic conditions that produce changes in the soil pore-water pressure distribution. Due to seasonal climate changes, soil undergoes wet and dry cycles and significant depth of soil exists in unsaturated state. Reductions in the bearing capacity, shear strength and resilient modulus of soils are related to an increase in the positive pore water pressures during wetting. On the other hand, an increase in shear strength and stiffness is associated with negative pore pressures during drying. The loss of strength of soil during wetting indicates the important role that negative pore-water pressure (matric suction) plays in controlling the mechanical behaviour of unsaturated soils. Fibers improve cracking resistance of cohesive soil during evolution of matric suction (Jingyu et al., 2018; Rasool and Kuwano, 2018). It is therefore important to establish the matric suction characteristics of the natural fiber reinforced soil since natural fibers are sensitive to moisture regimes. The soil moisture regimes dictate variation matric suction and ultimately performance of the geo system. Studies on the matric suction characteristics of natural fiber reinforced soil have received little attention in the recent times. The objective of this study is to highlight the geomechanical importance of the matric suction characteristics of compacted natural fiber reinforced soil with varying moisture content in relation to the fiber-matrix stability.

This study investigated the effects of fiber length and content on the macrostructural properties related to the evolution of matric suction in the soil with varying moisture content

6.2 Materials and experimental programme

6.2.1 Materials

The properties of the soil used herein are summarised in Table 3.1. Fiber lengths used for the study were 10mm, 25mm and 50mm. The fiber mechanical properties are summarised in Table 3.3. The test was performed in accordance with procedure in section 3.3 on chapter 3.

6.2.2 Validation of matric suction characteristics

The validation of the results was conducted by varying contact pressure of the filter paper and composite surface. Two compaction methods according to BS1377 (BSI - BS 137-4, 1990) and

ASTM698 (ASTM D698, 2012), were employed to investigate effect of compaction effort on the matric suction characteristics. The moisture equilibration was performed as in section 3.3. The filter papers were kept airtight through the entire equilibration period and subjected to the self-weight of the compacted soil composite as shown in figure 6.1. The self-weight was kept constant by adding required extra weight onto the moulds depending on the initial measured weight of the mould. The self weights were 100N and 50N for BS1377 mould and ASTM 698D moulds, respectively. Three matric suction measurements were taken from each mould. Since the effectiveness of the filter paper method for matric suction depends on the contact pressure between the soil and the filter, it is expected that high contact pressure expedites the moisture equilibration and also reduces possible loss of moisture.

(a) (b)

(c)

Figure 6.1 : (a) Specimen preparation for matric suction measurement (a) BS 1377 (b) ASTMD698 (c) moisture equilibration.

6.2.3 Specimen preparation for matric suction related compression test

The preparations of specimens for compression test were done in accordance with the protocol in section 4.2.3. The specimens were prepared in a 70mm diameter mould height 140mm by static compaction. The specimen quality control measures were applied according to the protocol highlighted in section 3.2 on chapter 3. The suction related compression test was performed by varying moisture content of the composite. The unconfined compressive strength of the composite was determined after 8h, 24h, 72h and 168h of air drying. The composite drying was done at varying laboratory temperature between 25^{o}C and 30^{o}C. The specimens were thereafter tested in accordance with ASTM D2166 (ASTM D2166, 2016a) using Dynamic Triaxial machine (DYNATRIX), at a displacement rate of 1mm/min. A minimum of three specimens for each fiber dosage was used to determine the average unconfined compressive strength of the composite.

6.3 Results and discussions

6.3.1 Variation of matric suction with fiber content and length

The variation of matric suction with fiber contents and lengths is shown in Table 6.1 and the fitted curves are shown in figure 6.2.

Table 6.1: Varitation of matric suction with fiber contents and lengths

Fiber content (%)	Matric suction (kPa)		
	Fiber length (mm)		
	10	25	50
0	1862.81	1862.82	1862.82
0.25	820.63	1526.52	967.931
0.5	1179.19	915.01	897.97
0.75	2517.55	3535.93	1510.16
1	1851.39	2716.63	1802.43

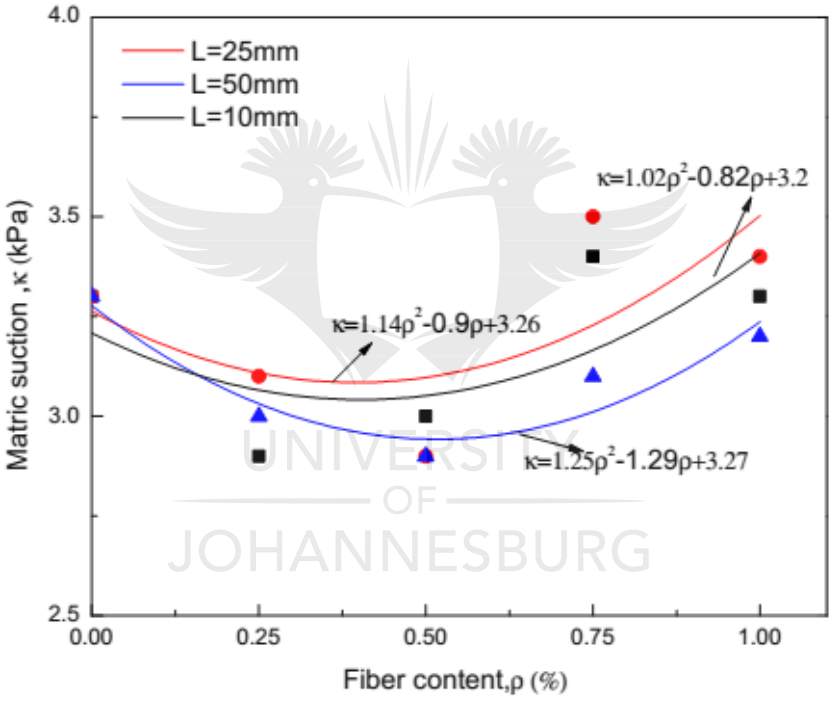

Figure 6.2 : Fitted curves of matric suction against fiber contents at various fiber lengths.

It is evident that increase in fiber content causes decrease in matric suction to minimum value and subsequently increase. The minimum values are shown at 0.25% for 10mm fiber length and 0.5% for both 25mm and 50mm lengths. This represents matric suction reductions of about 55%, 51% and 52% for 10mm, 25mm and 50mm, respectively. On the other hand, increasing fiber length causes an increase in matric suction to optimum fiber length. The optimum length is shown to be 25mm with matric suction increase of 41% relative to 10mm fiber length. The

specimens for matric suction measurements in this study were prepared by static compaction. This implies that the addition of fibers essentially provided resistance to compaction and prevented dense packing of solids while creating voids along the peripheral of the fibers (Ajayi, 2016; Ibraim and Fourmont, 2006).The magnitude of matric suction depends on the pore size of the soil and the amount of free moisture. The bigger the pore size the lower the matric suction (Fredlund et al., 2012).The increase in the soil pore sizes due to the inability of the soil to compact with fibers caused reduction in matric suction. Since the fibers used herein were natural and hydrophilic in nature, a portion of the moisture was absorbed and held by the lignocellulosic polymer structures of the fibers. This consequently, caused total amount of free moisture to reduce. Therefore, at high fiber content (1%), the amount of free moisture was significantly reduced and in turn caused increase in matric suction. The intertwining of fibers in the soil is more pronounced with longer fibers (Wu et al., 2014b)It can be anticipated that this phenomenon affected distribution of pore sizes for compacted soil and influenced composite macrostructural properties. The longer fiber length caused non-uniform pore size distribution with predominant larger pore sizes due to fiber interweaving. This was dominant with 50mm fiber length. The initial increase in the matric suction with fiber length was due to reduced pore sizes as a result of compaction. The proposed mechanism of matric suction evolution with fiber inclusion is schematically presented in figure 6.3.

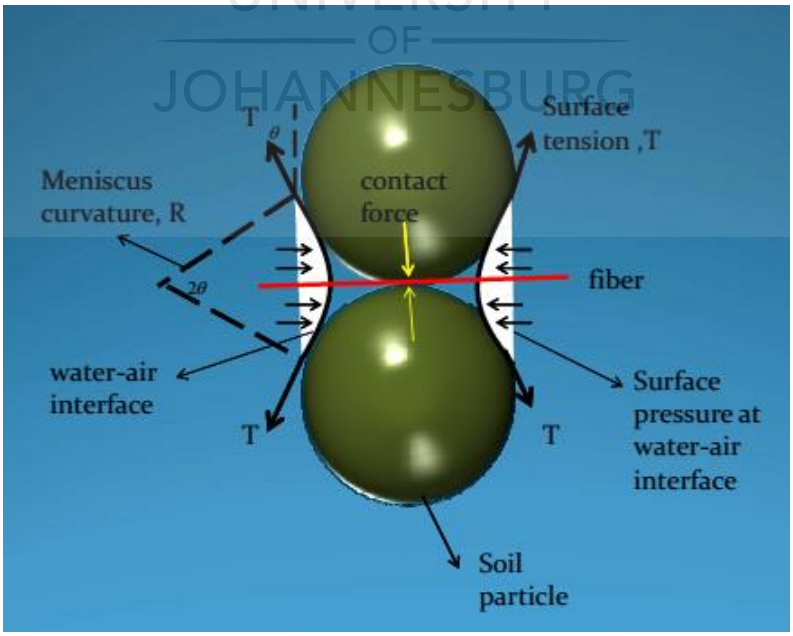

Figure 6.3: Proposed mechanism of matric suction evolution in fiber reinforced soil.

Using force equilibrium of the matric suction and resistance of fiber to suction stresses, force equilibrium is given by equation 6.1.

$$2T\ sin\theta_c = \pi dl_{fe}\tau_f + 2\Delta uR sin\theta_c \quad (6.1)$$

where dl_{fe} and τ_f are fiber diameter, effective fiber length and shear resistance mobilised by the fiber, θ_c is the contact angle of water molecules with air and $\Delta u = u_a - u_w$ is the pressure difference at air-water interface, where u_a is the air pressure, and u_w is the pore water pressure. Shear resistance of fibers is given by equation 6.2.

$$\tau_f = C_a + \sigma_n tan\delta \quad (6.2)$$

where σ_n is the contact vertical pressure at fiber- soil contact surface and $\tan\delta$ is the fiber-soil friction coefficient and C_a is the cohesion of soil. The matric suction of fiber reinforced soil can therefore be expressed by equation 6.3.

$$u_a - u_w = \frac{T}{R} - \frac{\pi dl_{fe}\tau_f}{2R sin\theta} \quad (6.3)$$

where $\frac{T}{R}$ is the matric suction of unreinforced soil. For N_f number of fibers crossing the air-water interface line (contractile line) and v_f being volume fraction of the fibers in the soil composite, total effective area of fibers that resist matric suction according to (Rifai et al., 2009) is given by equation 6.4.

$$A_f = \frac{\rho_f \gamma_d l_f}{2d_f G_f \gamma_w} \quad (6.4)$$

where ρ_f, γ_d, G_f and γ_w are fiber content, dry unit weight of soil, specific gravity of fibers and unit weight of water, respectively.

For θ_c=90°, matric suction of the fiber reinforced soil can therefore be expressed as equation 6.5.

$$u_a - u_w = \frac{T}{R} - \delta\frac{\rho_f \gamma_d l_f \tau_f}{4Rd_f G_f \gamma_w} \quad (6.5)$$

where δ is the gradient of the matric suction change with variation in fiber geometrical properties.

It can be seen that with an increase in fiber content at constant fiber length, specific gravity, diameter and shear resistance of fiber, the net matric suction decreases. On the other hand, increase in fiber diameter and specific gravity at constant fiber content, length and shear resistance results in an increase in the net matric suction. Increase in the fiber specific gravity and diameter (fiber dilation) may be caused by fiber moisture absorption through diffusion. The moisture diffusion gradient reduces with an increase in the amount of absorbed moisture (Célino et al., 2013). Therefore, the rate of increase in the specific gravity of fibers and fiber dilation reduces with time as more moisture is absorbed by the fibers. Therefore, the change in the matric suction would follow the rate of change of fiber properties. From the proposed model of matric suction behaviour in the fiber reinforced soil, the normalised relationship between fiber properties and matric suction is expressed in figures 6.4a and b.

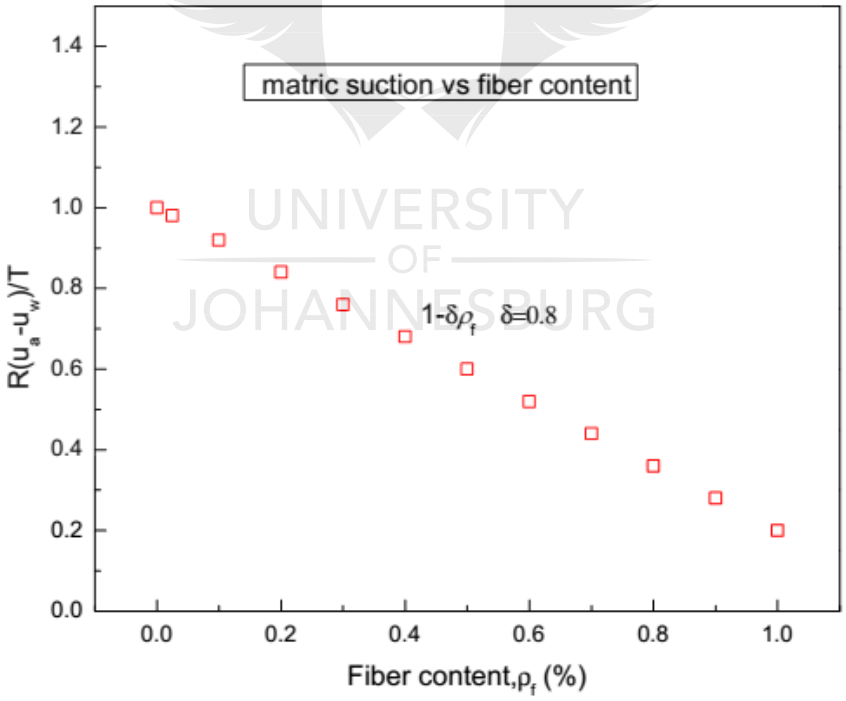

(a)

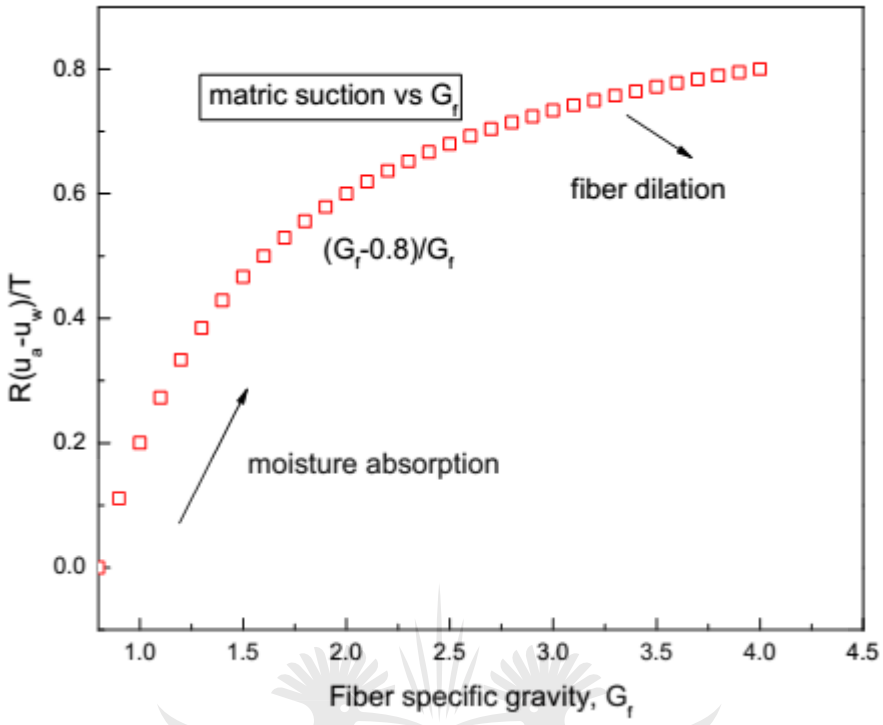

(b)

Figure 6.4: The relationship of matric suction with fiber properties (a) effects of fiber content (b) effect of fiber specific gravity.

The trend in figure 6.4b substantiates an idea that matric suction at high fiber content is associated with low free moisture.

The soil-moisture characteristic curves of composites with 10mm, 25mm and 50mm fiber lengths were developed to support the matric suction behaviour exhibited by the soil-fiber composites. The moisture variations of the designated composites were recorded from OMC (10%) to almost dry state shown in figure 6.5.

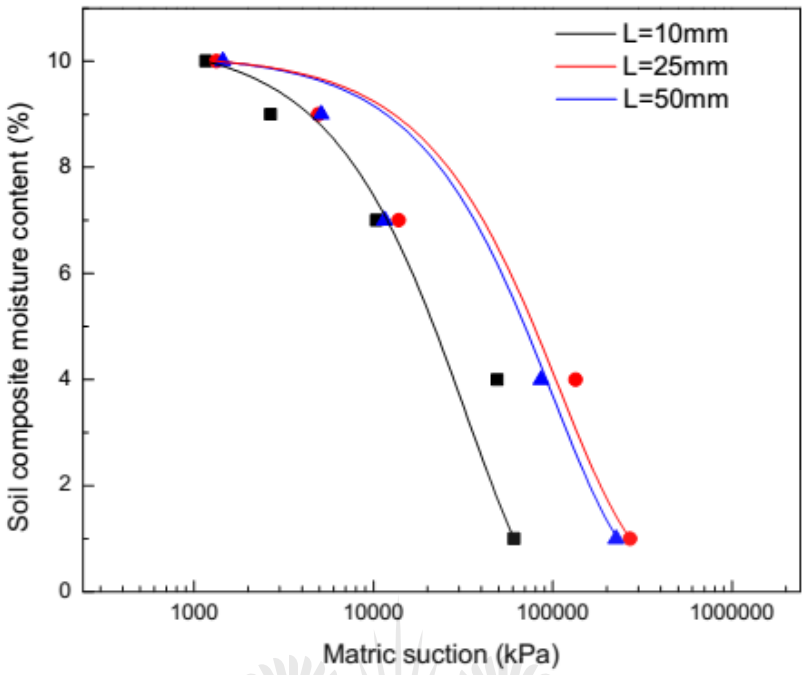

Figure 6.5: Soil-moisture curves.

It can be seen that the composite soil characteristic curves are in the order similar to the variation of matric suction with fiber length. The validation of the matric suction characteristics is shown in figure 6.6.

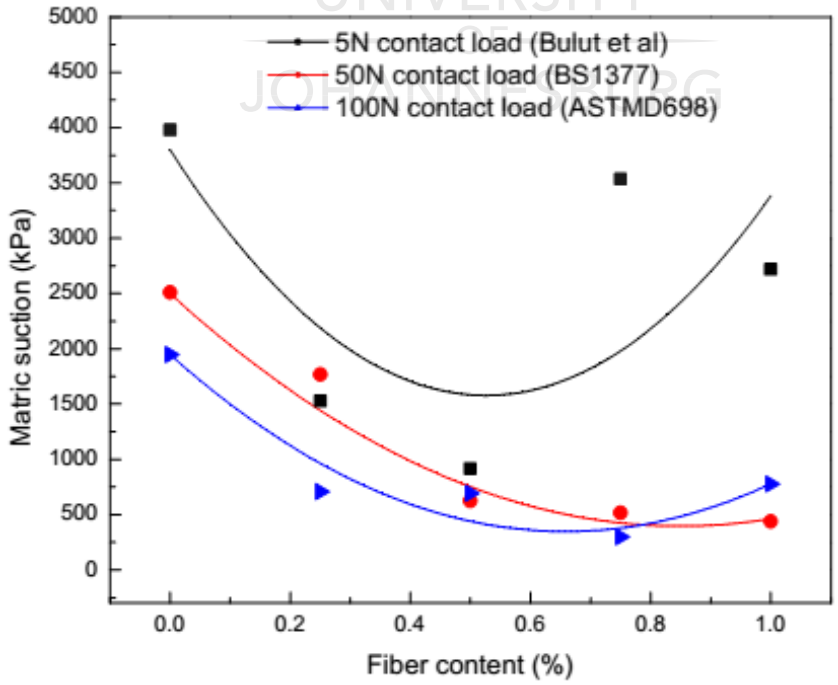

Figure 6.6:.Matric suction characteristics with varying compaction methods and filter contact loads.

It is noted that matric suction behaviour assumes similar trends. The magnitude of matric suction reduces with an increase in filter contact pressure. However, the effect is not significant with high fiber content. The compaction effort has negligible effects on the results. It is anticipated that utilising standard Proctor compaction mould according to ASTMD698 may provide more representative moisture measurement data as long as good filter insulation is ensured.

6.3.2 Matric suction related compression test

The evolution of unconfined compression with various moisture contents at constant fiber content (0.5%) is shown in figure 6.7.

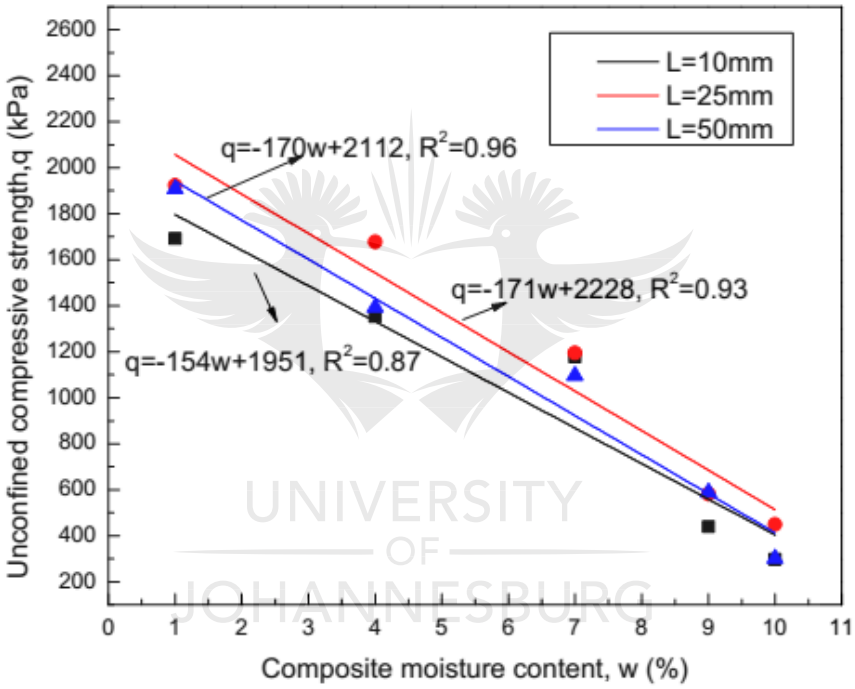

Figure 6.7: Variation of UCS with composite moisture content.

It is noted that decrease in moisture content causes an increase in compression strength. It is evident that 25mm fiber length exhibited higher strength with reduction in moisture content. It is anticipated that an increase in strength was due to the enhanced adhesion between fiber and soil due to matric suction. Composite with 25mm fibers benefited the more from the matric suction due to its compacted macrostructural properties. The stress-strain behaviour of the composite with moisture reduction is shown in figure 6.8.

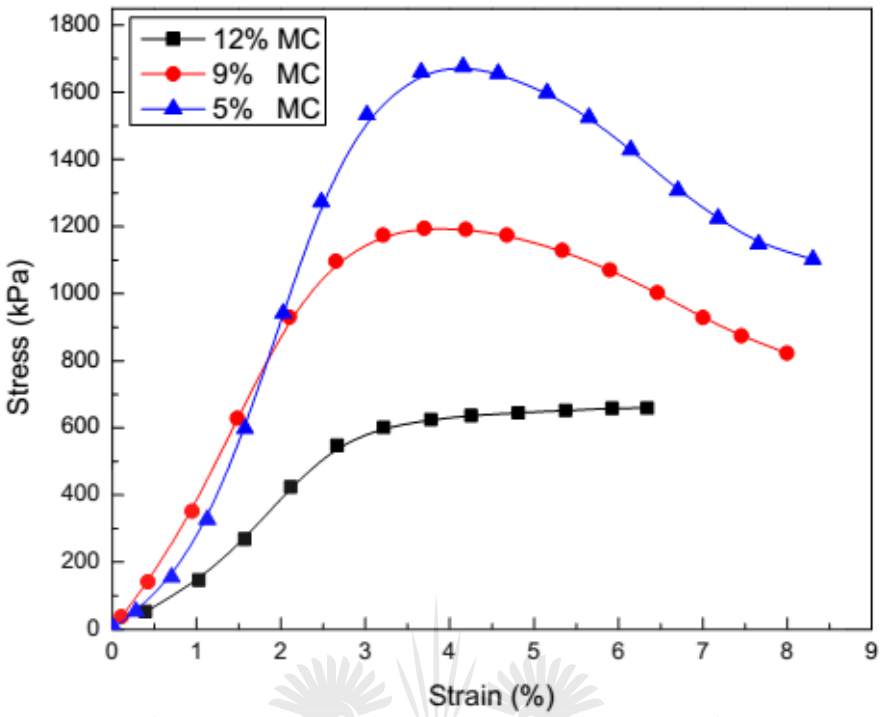

Figure 6.8: Stress-strain relation of soil composites at various moisture contents.

It is seen that the presence of moisture governed the stress-strain behaviour of the specimens. It is noted that at high moisture content, composite exhibited strain hardening behaviour. As moisture content reduced, strain softening behaviour occurred. Figure 6.8 indicates that elastic modulus (stiffness) increases with the reduction in moisture content. It can be concluded that large volume fraction of soil matrix dictated the stiffness behaviour of the composite. This was due to the evolution of matric suction during drying. In respect of earthen structures, the moisture content of structural material dictates the post peak strength of the earthen structure.

Evolution of matric suction (low moisture content) during dry conditions would endow the unreinforced earthen structures with stiffness. The heavy loading onto unreinforced earthen structure when dry may result into excessive deformation of the structural elements such as walls due to the softening of the material. Fiber inclusion may enhance the suction induced strength and substantial structural resilience may be achieved. Furthermore, unreinforced earthen structures may assume some strain hardening in presence moisture, presumably close to maximum dry density. The imposed loading in this condition may cause densification of the structural material and consequently enhance load resistance of the earthen structural elements. On the other hand, presence of the moisture may suppress reinforcing mechanism of the fibers

with soil particles in the fiber reinforced earthen structures. However, moisture absorbing properties of natural fibers (sisal fibers) may expedite evolution of matric suction and in turn enhance resilience of the structural elements.

Conclusions

An experimental investigation into the effects of macrostructural properties on the matric suction evolution and matric suction induced strength properties of natural fiber reinforced soil was undertaken. Based on the experimental results, the following conclusions are drawn;

1. Increasing fiber content of the compacted soil composite reduces matric suction due to an increase in pore size as a result of resistance of soil composite to compaction. Moisture absorption of natural fibers at high fiber content increases matric suction due to low free moisture.
2. The mechanical properties of soil composites are enhanced by reduction in moisture due to evolution of matric suction.
3. Evolution of matric suction is associated with softening post-peak behaviour of the soil composite.
4. In practice, the evolution of matric suction in the soil-fiber composite during dry spells would enhance strength and resilience of the earthen walls and foundation. The moisture absorption by fibers would expedite matric suction induced strength of the earthen structure which is beneficial to maintain integrity of the structure. In application, fiber length should not be excessively long (preferably 25mm) to avoid creating large soil void volume that would suppress suction induced strength in earthen structure.

References

Ajayi .O. (2016). Feasibility Study of Random Fibre Reinforced Railway Ballast. *University of Southampton:* University of Southampton.

ASTM D698. (2012). Standard Test Methods for Laboratory Compaction Characteristics of Soil Using Standard Effort. *West Conshohocken,* PA.

ASTM D1140-17. (2017). Standard Test Methods for Determining the Amount of Material Finer than 75-μm (No. 200) Sieve in Soils by Washing. West Conshohocken PA: *ASTM International.*

ASTM D2166. (2016). Standard Test Method for Unconfined Compressive Strength of Cohesive Soil. West Conshohocken, PA: , *ASTM International*.

ASTM D5298 - 94. (1994). Standard Test Method for Measurement of Soil Potential (Suction) Using Filter Paper (Withdrawn 2003),,. West Conshohocken, PA: *ASTM International.*

BSI - BS 1377-4. (1990). Methods of test for Soils for civil engineering purposes - Part 4: Compaction-related tests. *BSI.*

Célino et al. (2013). The hygroscopic behavior of plant fibers: a review. *Frontiers in Chemistry* 1 (43):1-12.

Fredlund et al. (2012). *Unsaturated Soil Mechanics in Engineering Practice*. Hoboken, New Jersey: John Wiley & Sons, Inc

Ibraim.E and Fourmont.S. (2006). Behaviour of sand reinforced with fibers. In *Soil Stress-Strain Behavior: Measurement, Modeling and Analysis Geotechnical Symposium*. Roma, Italy.

Jingyu et al. (2018). Influence of matric suction on the long term behaviour of fouled road base materials under traffic loading. *Paper read at China-Europe conference on geotechnical engineering*, at Vienna.

Rasool .A.M and Kuwano. J. (2018). Role of matric suction on shear strength of unsaturated compacted soil at low confining stress. *Paper read at Geo Shanghai Innternational conference at Shanghai China.*

Rifai et al. (2009). Theoretical Assessment of Increased Tensile Strength of Fibrous Soil Undergoing Desiccation. *Journal of Geotechnical and Geoenvironmental Engineering, 135*(12), 1857-1862.

7 CHAPTER SEVEN-DESICCATION CHARACTERISTICS AND DESICCATION INDUCED COMPRESSIVE STRENGTH OF SISAL FIBER REINFORCED SOIL

7.1 Introduction

Soil undergoes seasonal variations in water content at considerable depth due to seasonal changes in precipitation and evapotranspiration. Evaporation usually results in soil volumetric shrinkage that is accompanied by desiccation cracks. Desiccation cracks are more pronounced in clay-rich soils due to evolution of matric suction in the pore structure of the soils (Nahlawi and Kodikara, 2006). The presence of cracks significantly affects mechanical, hydrological, physicochemical and thermal properties of soil and ultimately the integrity of earthen structure. (Albrecht et al., 2001; Morris et al., 1992; Rayhani et al., 2007; Tang et al., 2010a). Water conductivity is drastically increased by cracking, leading to malfunction of the geo structures (Miller et al., 1998). In other instances of exposed terrain, instability of natural slopes and vertical cuttings may occur when cracking causes groundwater recharge to be quicker than drawdown (Baker, 1981). The bearing capacity of foundations is decreased with evolution of cracks (Silvestri et al., 1992). The desiccation induced cracks create zones of weakness in the soil mass with reduced mechanical properties and bearing capacity, and increased compressibility. The adverse impacts of desiccation cracks prompted researchers to pay attention to the mechanisms behind desiccation cracking of soil (Costa et al., 2013; Lakshmikantha et al., 2006; Nahlawi and Kodikara, 2006; Péron et al., 2009; Prat et al., 2006; Rodríguez et al., 2007).

The tensile strength of soil is the fundamental parameter that dictates the initiation and propagation characteristics of cracks. It is therefore necessary to establish methods that can effectively improve tensile strength and cracking resistance of soil in order to achieve resilient and sustainable construction. Efforts have been made to address problems of soil desiccation cracking. Chemical stabilisation of soil by lime, cement, or fly ash improves soil tensile strength however, chemical additives decrease yield strain, plasticity index, and ductility of soil, leading to undesired brittle behaviour (Consoli et al., 2011; Jain, 2008). The behaviour of chemically stabilised soil is not ideal for the long term stability of the earthen structures. Moreover, chemical additives lead to permanent macro-structural modification of soil properties (Tang et al., 2016).

Alternatively, reinforcing soil with randomly distributed fibers both synthetic and natural has the advantages of easy mixing procedure, strength isotropy, and ecological prospects. The merits of fiber soil reinforcement have attracted attention in various engineering application. Several studies (Baldovino et al., 2018; Diambra et al., 2013; Ibraim and Consoli, 2018; Kafodya and Okonta, 2018; Moghal et al., 2018; Tang et al., 2010b, 2016) have been conducted to assess the potential application of fibers in terms of the mechanical properties of soil fiber composites. Soil reinforcement with synthetic fibers exhibits better engineering properties than natural or vegetable fibers. However, cost-benefit analysis favours the use of natural fibers due to their low energy demand and cost effectiveness in production (Hejazi et al., 2013) . The aforementioned economic merits and the benefits offered by randomly distributed fibers have attracted wide applications of natural fibers in civil engineering.

The application of fiber reinforcement has been extended to address problems of desiccation in clay soils. Several studies (Abdi et al., 2008; Chaduvula et al., 2017; Harianto et al., 2008; Qiang et al., 2014; Rifai et al., 2009) have reported that soil cracking is reduced with the fiber inclusion. The mechanical properties of fiber reinforced soil have been extensively reported compared to desiccation cracking behaviour. Moreover, few studies focused on the application of natural fibers in desiccation crack control. Natural fibers are hydrophilic in nature and possess high swelling potential with water ingress. It is not established whether hydrophilic characteristics of natural fibers have a bearing on the ability of the fibers to control desiccation cracking of the soil. The compressive strength changes of natural fiber reinforced soil exposed to wet-dry cycles have not been thoroughly investigated. The overall performance of the geo structures depends on the desiccation characteristics of the soil. It is anticipated that globe performance of the earthen structures under seasonal moisture variations may be enhanced with adequate reinforcement. It is against this background that this study was conducted to evaluate desiccation crack control of the natural fiber reinforced soil for resilient earthen construction.

This study aimed at investigating the effects of the fiber inclusions on the desiccation characteristics and associated strength properties of the desiccated cohesive soil that is commonly used for construction of earthen dwelling units.

7.2 Materials and experimental programme

7.2.1 Materials

The soil used in this study was locally collected and air dried for 48h. The soil was manually sieved to remove any organic particles. Wet sieving for the soil was eventually carried out in accordance with STM D1140-17 (ASTM D1140-17, 2017) and the grading curve of the soil is shown in figure 3.2. The soil properties are summarised in Table 3.2. Randomly distributed sisal fiber with length of 25mm was used. The summaries of soil and fiber properties are shown in Table 3.2 and 3.4, respectively.

7.2.2 Specimen preparation for compression test after wet and dry cycles

The preparations of specimens for compression test were done by adding fibers incrementally to the soil. The fiber dosage of 0.75% based on the results in chapter 4 was used to assess effect of fiber inclusion on compressive strength with varying number of wet and dry cycles. Water of equivalent optimum moisture content (17%) was added to the soil composite. The wet mixing was performed until a homogeneous soil composite was formed. After mixing, the soil composite was covered with plastic sheet to prevent loss of moisture. The moisture content of +1% (OMC) was used to provide for the marginal loss of moisture during specimen fabrication. The specimens were prepared in the split moulds of diameter 50mm and height of 100mm. The moulds were clamped in place by adjustable cable ties. The soil composite was compacted by tamping into 3 layers. The target density (MDD of the soil) was used to control quality of the specimens. The specimen was deemed ready for testing if its density was at least ± 3% of the target density. The specimens were then subjected to wet and dry cycles. The specimens' conditioning was performed by immersing them in water until saturation. The saturation of specimens was performed in the moulds to prevent loss of fine particles. The bottom of the moulds was covered with permeable cloth to prevent erosion and allow capillary flow of water through the specimen. During saturation, the specimens were separated from the wall of the mould by loosening cable ties to facilitate capillary action. A completed cycle comprised of 24h of water immersion followed by 24h of drying at the controlled temperature of 40^{o}C. The compression test of specimens was performed after 5, 10 and 15 cycles. The compression test was conducted in accordance with ASTM D2166 (ASTM D2166, 2016a) using Cooper compression machine at a displacement rate of 1mm/min. A minimum of three specimens for

each number of cycles was used to determine the average unconfined compressive strength of both unreinforced and reinforced soil composite.

7.3 Results and discussions

7.3.1 Crack morphology for reinforced and unreinforced soil

The crack patterns for reinforced (0.75% fiber content and 6mm thick) and unreinforced specimens are shown in. figure 7.1.

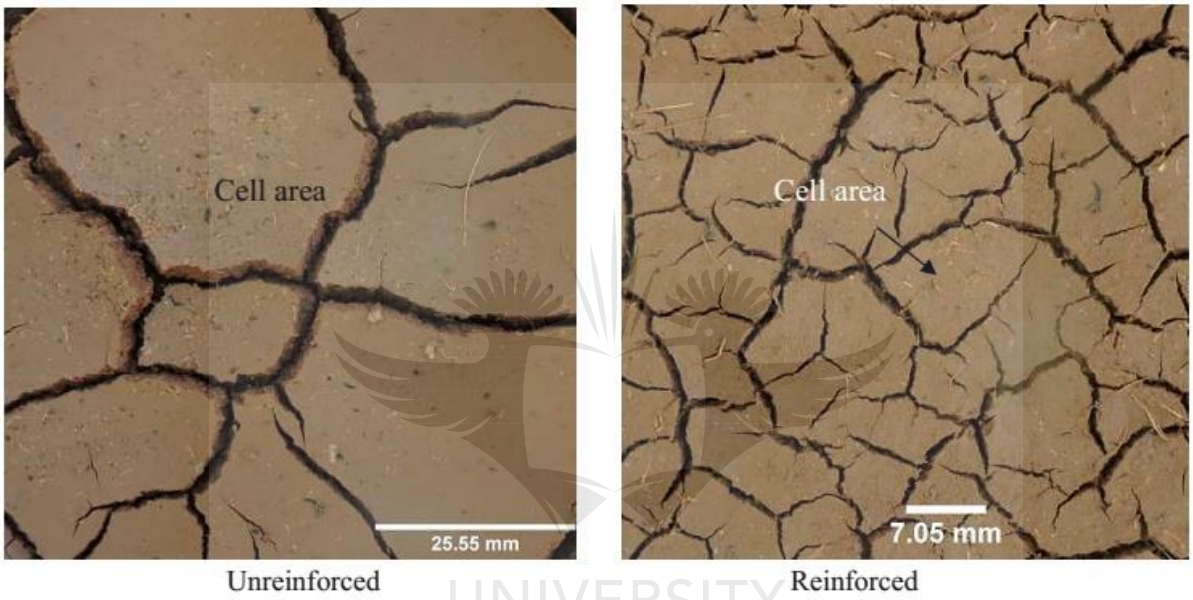

Figure 7.1: Crack morphology of reinforced and unreinforced soil

It is noted that crack pattern for unreinforced soil is comprised of large cells of about 750mm^2. The cells are non uniform and irregular in shape. Long and wide cracks are indicated. On the other hand, fiber reinforced specimen shows small cells of about 80mm^2. The intersections of the cracks for both specimens are shown to be non orthogonal. The non-orthogonality of cracking pattern occurs due to non-uniform drying and thin soil layer that lead to high concentration of strain energy in comparison to fracture energy required for crack propagation (Costa et al., 2013; Kodikara et al., 2002). The presence of fibers changes the intrinsic propagation and release of the developed tensile stress through the thickness of the soil. The intersection angle is a function of the orientation and distribution of fibers in the soil during crack initiation (Chaduvula et al., 2017). In respect of the observed pattern, the presence of fibers might cause bifurcation or diversion of single propagating crack hence the crack intersection angles varied from greater

than 90^{o} to less. The thin size of the unreinforced specimens increased non-orthogonality of the crack intersections. The effect of fiber inclusion on the crack pattern is shown in figure 7.2.

Figure 7.2 : Effect of fiber inclusion of crack surface morphology

It is noted that the morphology of the crack patterns is significantly affected by the fiber inclusion. With fiber content increase, the number of wide cracks decreases and the number of fine cracks significantly increases. The crack networks become more irregular and a large amount of dead-end cracks or single cracks that do not intersect other cracks are indicated. The relatively straight and smooth crack segments at lower fiber content tend to be more jagged and tortuous at higher fiber content. This observation is in agreement with report by (Tang et al., 2012) on synthetic fiber inclusion. The irregular crack pattern was attributed to the material heterogeneity. It is anticipated that the observed decrease in crack width reflects strength improvement of the soil endowed by fibers. The fibers enhanced tensile resistance of the soil to suction stresses. In addition, change in the soil macro structure due to fiber inclusion weakened evolution of suction stresses. This was attributed to the increase in the soil pore spaces.

7.3.2 Variation of moisture content with time

The variation of moisture content for reinforced and unreinforced soil is shown in figure 7.3.

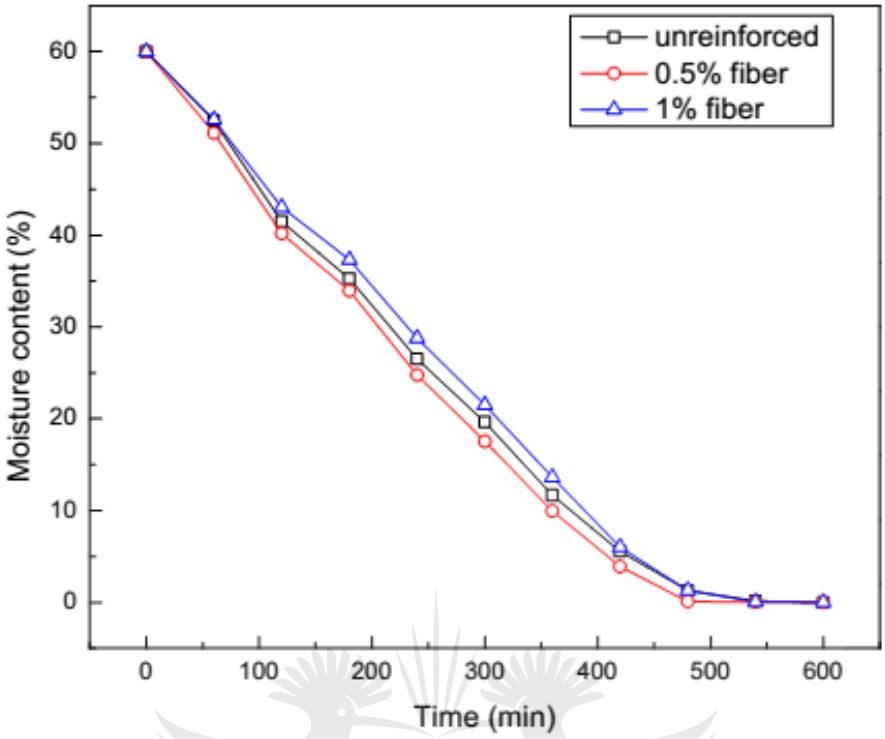

Figure 7.3: Variation of moisture content with drying time

As expected, rapid reduction of moisture content is shown during early period of drying and gradually reduces to a constant value. The marginal difference in moisture content between reinforced and unreinforced specimens is indicated at high moisture content. It is noted that at low fiber content (0.5%), the rate of evaporation is higher than unreinforced soil. At high fiber content (1%), the rate of evaporation is lower than the unreinforced soil. Both reinforced and unreinforced soils exhibit the same behaviour at low moisture content. The change in suction to small changes in moisture content was significant at low moisture content, i.e., less than 6% due to coexistence of matric and osmotic suction.

Since the specimens were tested at constant prevailing atmospheric conditions, the difference in evaporation rates at high moisture content was due to the macrostructure of the specimens and the characteristics of the fibers. The fiber used herein was hydrophilic in nature, it is anticipated that at 0.5% fiber content, moisture was absorbed and held by the fibers, resulting in less free moisture for evaporation. The presence of large amount of fibers (1% fiber content) created large volume of water pathways and improved water flow during capillary action and this in turn increased rate of moisture loss.

7.3.3 Variation of crack surface fraction and width with moisture

The variation of surface crack area ratio with moisture content for unreinforced and a fiber-reinforced soil is shown in figure 7.4.

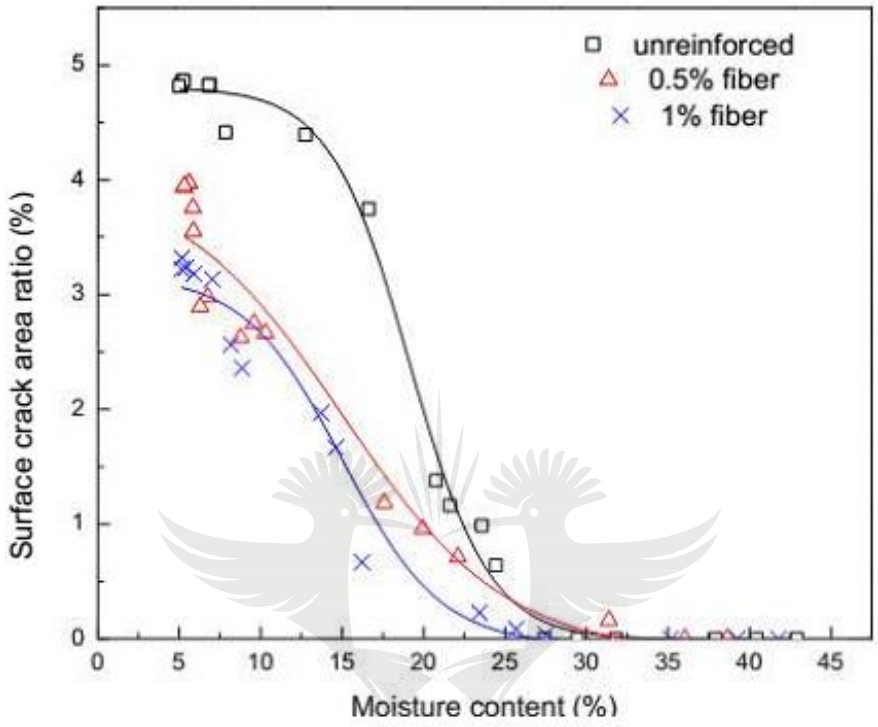

Figure 7.4: Variation of surface crack area ratio with moisture content

It is indicated that surface crack area ratio for unreinforced soil is higher (15.5%) than the values of the fiber reinforced soil, 12.8% and 10.5% for 0.5% and 1% fiber contents, respectively. The shorter and irregular cracks in the fiber reinforced soil give rise to lower surface crack area ratio. In this study, fiber inclusion reduced width and the surficial area of cracks and in turn, reduced the crack intensity. Similar observations were reported elsewhere (Chaduvula et al., 2017; Harianto et al., 2008; Qiang et al., 2014). The variation of surface crack area ratio with moisture content is substantiated by variation of the crack width with moisture content shown in figure 7.6.

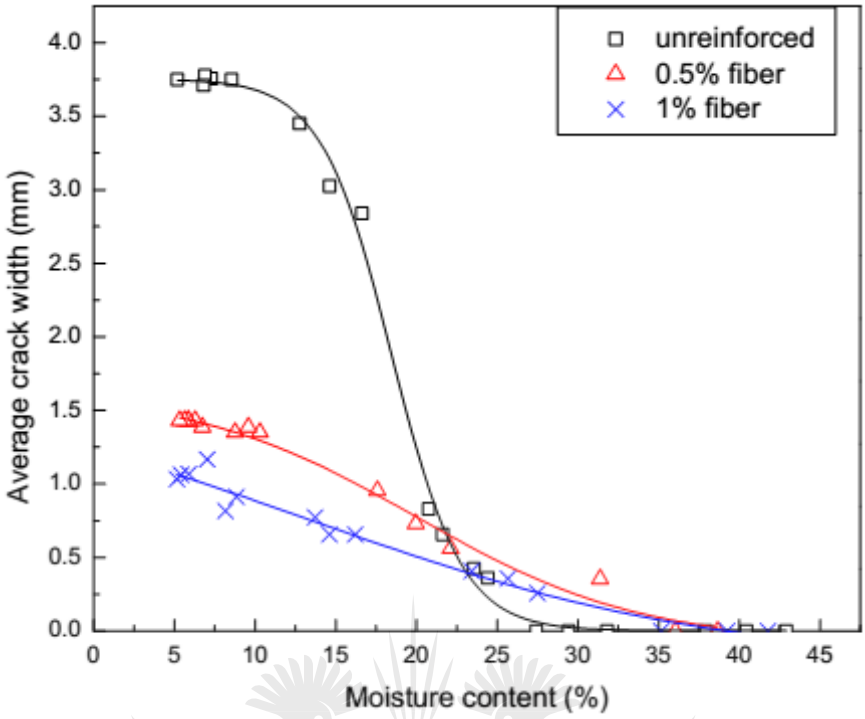

Figure 7.5: Variation of crack width with moisture content

It is noted that the trend is similar to the surface crack area ratio. As expected, crack width increases with decrease in moisture content for both reinforced and unreinforced soil. Fiber inclusion causes decrease in crack width. With 1% fiber content, average crack width reduction of about 73% is indicated. The reduced crack width is beneficial for the improved mechanical and hydraulic performances of the soil in landfill applications, barrier systems and foundations.

7.3.4 Crack resistance of reinforced and unreinforced soil

The results in figure 7.2 show that fiber inclusion effectively reduces desiccation cracks and enhance resistance to crack growth. The ability of fiber inclusion to control crack growth was quantitatively determined by using surface crack reduction ratio computed by equation 7.1 and crack width reduction ratio calculated by equation 7.2 at various fiber contents.

$$R_r = \left(\frac{R_{ru} - R_{rf}}{R_{ru}} \right) \times 100 \qquad (7.1)$$

where R_{ru} is the surface crack area ratio of unreinforced soil and R_{rf} is the surface crack area ratio of fiber reinforced soil.

$$R_{wr} = \left(\frac{R_{rwu} - R_{rwf}}{R_{rwu}} \right) \times 100 \qquad (7.2)$$

where R_{rwu} is the surface crack width of unreinforced soil and R_{rwf} is the surface crack width of fiber reinforced soil. The variation of surface crack reduction ratio alongside corresponding surface crack area ratio with fiber content is shown in figure 7.6.

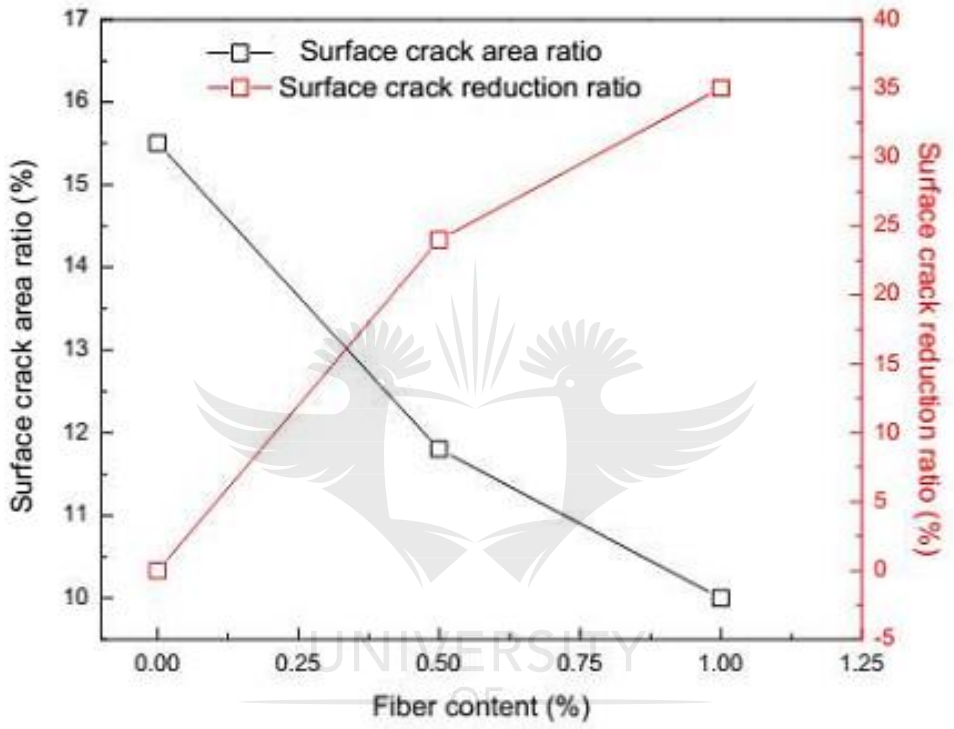

Figure 7.6: Variation of surface crack area ratio and reduction ratio with fiber content

It is noted that surface crack reduction ratio increases by 35% with 1% fiber content. The variation of crack width reduction ratio alongside the average crack width with fiber content is shown in figure 7.7. It is noted that crack width reduction ratio increases by 73% at 1% fiber content. The improved cracking resistance of fiber reinforced soil was attributed to the fact that fibers enhanced soil tensile strength (Tang et al., 2016). The adhesion and friction between sisal fibers and soil matrix restricted relative movement of the fibers with soil matrix (Kafodya and Okonta, 2018b; Tang et al., 2010b).The tensile stresses were effectively transferred to the fibers and thereby increased tensile strength of the soil composite. The increased tensile strength endowed the soil composite with resistance to crack initiation during drying. When the cracks

were formed in the soil, bridging effect of fibers inhibited the growth of the cracks hence decreased crack width (Tang et al., 2010b).

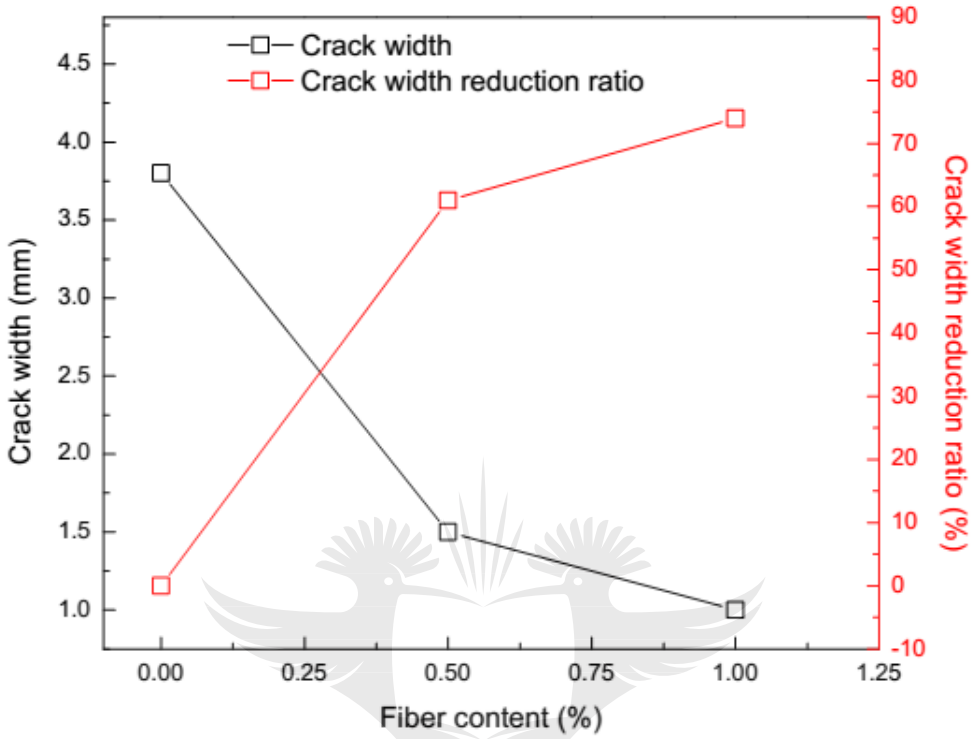

Figure 7.7: Variation of surface crack width and reduction ratio with fiber content

The crack growth and final shrinkage strain were quantified by using the image processing technique. The primary crack that developed during drying was used to assess growth rate. The shrinkage was estimated by measuring average width of the edge crack. Shrinkage strain was computed as average width of edge crack divide by original diameter of the specimen. Tracing growth of the primary cracks was difficult when crack surface density increased. Therefore, shrinkage measurements were conducted during the initial drying period before wide evolution of surface cracks. The variation of primary crack growth rate and shrinkage strain with fiber content is shown in figure 7.8.

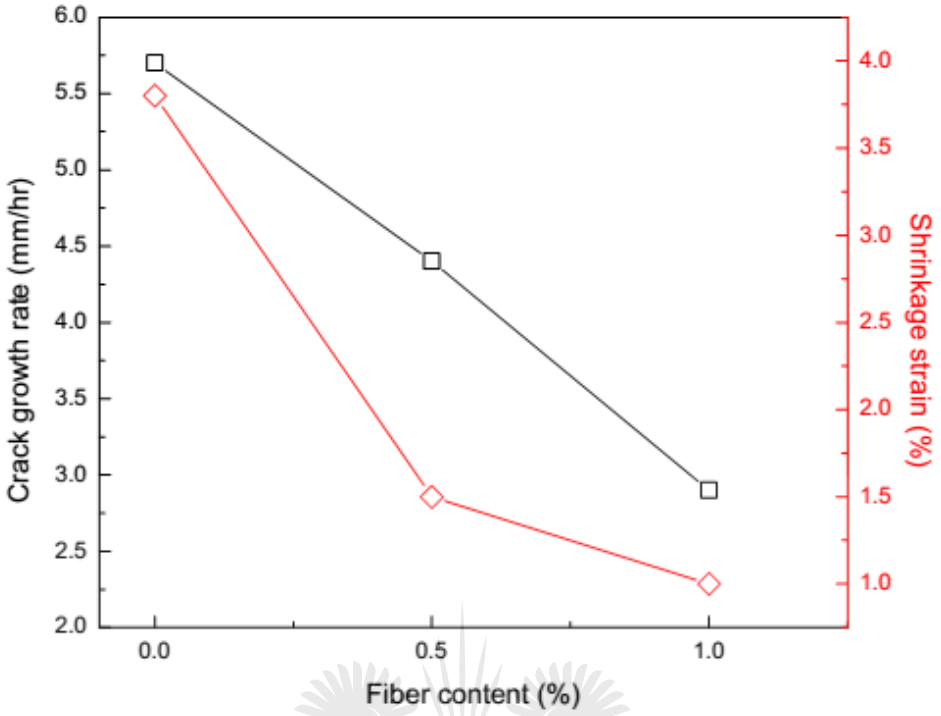

Figure 7.8: Variation of primary crack growth rate and shrinkage strain with fiber content

It is indicated that fiber inclusion significantly reduced both crack growth rate and shrinkage strain. The efficiency of the fibers to control shrinkage strain was evidenced by the arrest of shrinkage shown in figure 7.9.

Shrinkage of unreinforced soil

Shrinkage of reinforced soil

Figure 7.9: Shrinkage of the reinforced and unreinforced soil

It is shown that suction stresses in unreinforced soil resulted in the development of curved layer of soil. The maximum curvature was shown towards the center of the soil layer. This curvature implied that the soil was subjected to tension at the bottom of the layer and compression at the surface. The fiber inclusion reduced lateral shrinkage however moisture gradient and associated suction stresses caused cracking at the surface of the reinforced soil layer. It is clear that fibers sustained tensile stresses induced by matric suction. This substantiates the fact that adhesion and friction between fibers and soil particles inhibited the growth of cracks and shrinkage. The results indicated the potential application of natural fibers in controlling the growth of tension cracks and shrinkage that is commonly encountered in geotechnical and geoenvironmental engineering applications. The stress state of the soil shrinkage behaviour in figure 7.9 can further be analysed by considering the following assumptions (1) the edges were free such that specimens generated separation at the edges prior to generation of internal cracks (see figure 7.5). Development of these edge cracks changed the boundary conditions by setting the edge free, (2) a uniform tensile stress field was developed all over the specimen at the beginning of the drying process under ideal conditions, (3) the bond between the soil and the desiccator was negligible compared to bonding within the soil matrix. Therefore, radial and circumferential stress distributions and displacement profile in the dessicator may be given by equations 7.3, 7.4 and 7.5, respectively according to (Costa et al., 2013).

$$\sigma_{shr} = \frac{\tau(2+\nu_m)}{3h_t}(r_o - r) \tag{7.3}$$

$$\sigma_{\theta sh} = \frac{\tau_b}{3h_t}\left[(2+\nu_m)r_o - (1+\nu_m)r\right] \tag{7.4}$$

$$U_{shr} = \frac{\tau_b(1-\nu_m)r}{3Eh_t}\left[(2+\nu_m)r_o - (1+\nu_m)r\right] - r\varepsilon_s \tag{7.5}$$

where σ_{shr} is the shrinkage stress in the radial direction $\sigma_{\theta sh}$ is the shrinkage stress in the circumferential direction, τ is the shear at the interface between base of the desiccator and the soil, r is the distance along the radius of the specimen, r_o is the center of the specimen, ν_m is the Poison's ratio of the soil matrix, h_t is the thickness of the soil layer and U_{shr} is the radial deformation of the soil. The shrinkage stresses vary linearly with distance along the radius and

inversely with thickness. The stresses at the center of the specimen can be estimated as equations 7.6, 7.7 and 7.8 for radial, circumferential and deformation, respectively.

$$\lim_{r\to 0}\sigma_{shr} = \frac{\tau(2+\nu_m)}{3h_t} r_o \tag{7.6}$$

$$\lim_{r\to 0}\sigma_{\theta sh} = \frac{\tau_b(2+\nu_m)}{3h_t} r_o \tag{7.7}$$

$$\lim_{r\to 0} U_{shr} = 0 \tag{7.8}$$

The above expressions imply that, both radial and circumferential shrinkage stresses approach maximum towards the center of the specimens and deformation approaches zero. It is clearly shown in figure 7.9 that high tensile stresses were exerted at the center of the unreinforced specimen and the deformation at the center was almost zero at the end of drying (see figure 7.9). For the force equilibrium condition, the bottom of the soil was subjected to tensile stress equivalent to $+\frac{\tau_b(2+\nu_m)}{3h_t}$ and the surface was subjected to compressive shrinkage stress of -$\frac{\tau_b(2+\nu_m)}{3h_t}$. The increased tensile strength of the fiber reinforced soil that was responsible for the arrest of lateral shrinkage during desiccation is given by equation 7.9 according to (Rifai et al., 2009).

$$T_f = \frac{\rho_f \gamma_d l_f}{2 d_f G_f \gamma_w}\left\{C_a + \left[(\sigma_v - u_a)K_e + (u_a - u_w)\psi^K\right]\tan\delta\right\} \tag{7.9}$$

where ρ_f is the fiber content, γ_d is the dry unit weight of soil, l_f is the fiber length, d_f is fiber diameter, G_f is the specific gravity of fibers, C_a is the soil cohesion, $(u_a - u_w)$ is the product of matric suction, ψ^K is the dimensionless number as function of normalised volumetric moisture content. $(\sigma_v - u_a)K_e$ is the average effective normal stress acting on the soil which is zero for this thin layer of the soil. Then equation 7.9 is reduced to equation 7.10.

$$T_f = \frac{\rho_f \gamma_d l_f}{2 d_f G_f \gamma_w}\left\{C_a + (u_a - u_w)\psi^K \tan\delta\right\} \tag{7.10}$$

For equilibrium condition, the fibers sustained suction stress equivalent to the maximum stress at center of the soil specimen and may presented by equation 7.11. The opposing effects of fibers resulted in zero deformation at the center as evidenced by figure 7.9.

$$\frac{\rho_f \gamma_d l_f}{2d_f G_f \gamma_w E_f}\left\{C_a + (u_a - u_w)\psi^K \tan\delta\right\} = -\frac{\tau_b(2+\nu_m)}{3h_t E_m} \tag{7.11}$$

where E_f and E_m are the elastic moduli of fibers and soil matrix, respectively. The relationship of product of matric suction and fiber content is presented in equation 7.12.

$$u_a - u_w = -\frac{1}{\psi^K \tan\delta}\left(\frac{2d_f G_f \gamma_w E_f \tau_b(2+\nu_m)}{3h_t E_m \rho_f \gamma_d l_f} + C_a\right) \tag{7.12}$$

Equation 7.12 shows inverse relationship between product of matric suction and fiber content. This implies that with constant material properties, the impact of matric suction reduces with increasing fiber content. This therefore, supports the strain behaviour exhibited by fiber reinforced soil in figure 7.9.

7.3.5 Crack morphology at various soil thicknesses

The crack patterns for reinforced and unreinforced specimens with slurry thicknesses of 6mm, 12mm and 24mm are shown in figure 7.10. For unreinforced soil, it is noted that thin layer (6mm) of soil has crack connections that are non-orthogonal. With thicker layer (24mm), both orthogonal and non-orthogonal crack connections are shown. The trend in cell areas with increasing thickness is not obvious. Both regular and irregular cell shapes are shown with thicker layer of soil and some of cells are almost quadrangles. For reinforced soil, cell area increases with an increase in thickness and crack widths become wider with the mixture of orthogonal and non-orthogonal intersections.

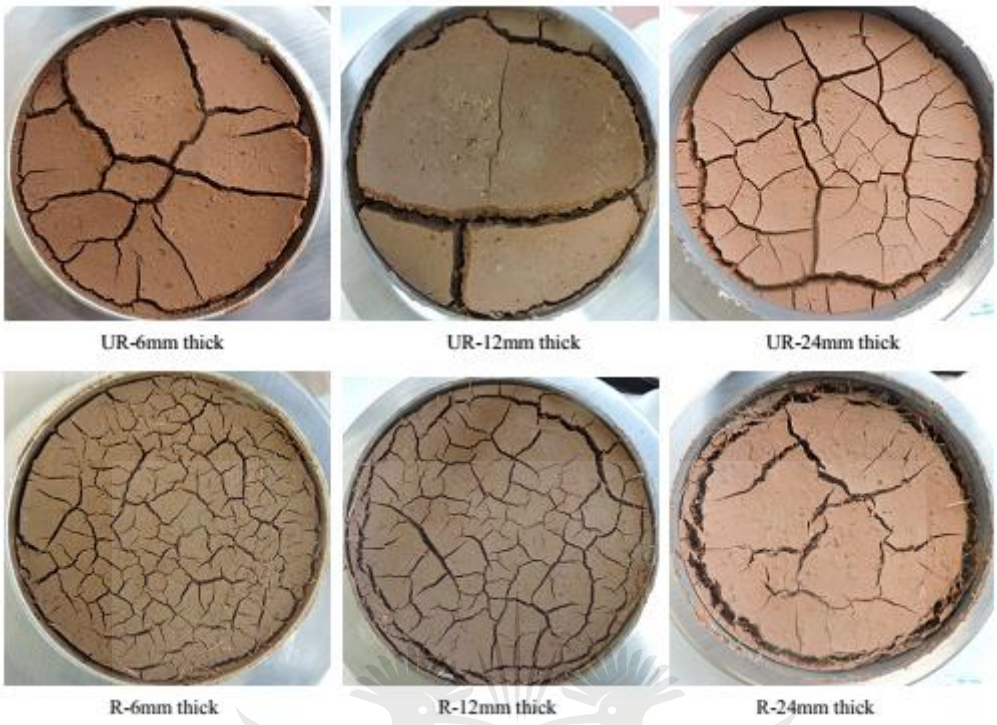

*UR stands for unreinforced soil *R stands for reinforced soil

Figure 7.10: Crack morphology of reinforced and unreinforced soil at various thicknesses

There are two major controls in crack initiation during soil desiccation. First is the control that arises due to generated tensile stress distribution as a result of restraining of free shrinkage strain in the soil. According to this control, the cracks initiate at the midpoint of the drying soil mass (with free edges), where the stresses are likely to be maximum (Kodikara and Costa, 2013; Nahlawi and Kodikara, 2006).The second is the influence of flaws which are either imperfections such as micro-cracks, inclusions such as air bubbles or large stiff particles and large pores that desaturate quickly. The crack initiation is activated by tensile stresses at the location of the flaw. It is possible for cracks to occur at locations away from the points where the tensile stress is maximum, if flaws at those locations are sufficiently large to get activated by the prevailing tensile stress.

The evolution and propagation of shrinkage cracks can be either pure orthogonal or pure non-orthogonal patterns. Non-orthogonal patterns occur when the nominal thickness of the drying soil is small, which leads to high concentration of strain energy in comparison to fracture energy

required for crack propagation (Costa et al., 2013). In drying soil, the soil thickness that holds suction scales with the ratio of moisture diffusion coefficient to rate of evaporation from the surface. The thickness can become small with decrease in moisture diffusion coefficient or when the evaporation rate is high. Ultimately, final state of the crack pattern can be a mixture of orthogonal, non-orthogonal, simultaneous and sequential crack as shown by thicker specimens for both reinforced and unreinforced soil in figure 7.10.

7.3.6 Variation of crack surface crack area ratio and width with soil thickness

The variation of surface crack area ratio and width with soil layer thickness for reinforced soil is shown in Table 7.1.

Table 7.1: Variation of surface crack area ratio and width of reinforced soil

Layer thickness (mm)	Surface crack features	
	Surface crack area ratio (%)	Average crack width (mm)
6	14.9	1.88
12	16.8	3.44
24	17.7	4.75

It is shown that increase in thickness results in an increase in both surface crack area ratio and width. The primary requirement for formation of desiccation cracks is restrained shrinkage, leading to tensile stress development exceeding the tensile strength of soil. The restraints against free shrinkage can be internal, external or a combination of the two. Internal constraints are usually due to soil structure such as differing soil fabric units and moisture gradient. Displacement boundary conditions and interface friction are external constraints (Kodikara and Costa, 2013). It is anticipated that increasing thickness of the desiccating soil increases volume of restraints against free shrinkage due to the increased heterogeneity of the soil. In this investigation, moisture content of specimens was in relation to mass of the soil. Increasing mass of the soil required high water content to produce slurry. Therefore, the difference between moisture content inside the soil layer and the surface (moisture gradient) was high in

thicker specimens. Moisture gradient would cause differential shrinkage and eigenstresses which could reduce the tensile strength of the soil, hence increase values of crack parameters

Table 7.2 presents variation of surface crack area ratio and width with soil layer thickness of unreinforced soil.

Table 7.2: Variation of surface crack area ratio and width of unreinforced soil

Layer thickness (mm)	Surface crack features	
	Surface crack area ratio (%)	Average crack width (mm)
6	16.6	3.41
12	14.7	3.99
24	18.6	3.78

It is noted that surface crack area ratio drops with 12mm thick layer and increases with 24mm thick layer. The crack width initially increases and drops with thicker layer. The erratic trend of the crack parameters is exhibited. The drop in surface crack area ratio was attributed to the increased modification in the effects of external and internal constraints, leading to the erratic trend in crack parameters. In addition, localised increase in tensile strength in the presence of flaws and non-uniform distribution of soil macro structure also contributed to the trend. The same effects applied to the drop of crack width.

7.3.7 Comparative analysis of desiccation characteristics between reinforced and unreinforced

7.3.7.1 Surface crack area ratio

The comparison of the effects of soil layer thickness on the desiccation surface crack area ratio of reinforced and unreinforced soil is presented in Table 7.3. It is indicated that overall crack area ratio of fiber reinforced soil is smaller than unreinforced soil with an average percentage reduction of 7.5%. This indicates potential benefit of natural fiber inclusion in controlling desiccation cracking of soil irrespective of the thickness of the soil layer.

Table 7.3: Effect of soil layer thickness on surface crack area ratio

Soil layer thickness (mm)	Surface crack area ratio (%)		
	Reinforced	Unreinforced	Variance (%)
6	14.9	16.6	-10.2
12	16.8	14.7	+14.3
24	17.7	18.6	-4.8

*Variance is the difference in fraction between unreinforced and reinforced

+ is increase and – is decrease

In practice, sisal fibers can be applied in improving hydraulic and mechanical properties of the clay liners, pavements, foundations and system barriers. However, long term performance can be enhanced by fiber surface treatment to improve it hydrophilic properties.

7.3.7.2 Average crack width

The comparison of the effects of soil layer thickness on the desiccation surface crack width on reinforced and unreinforced soil is presented in Table 7.4. It is indicated that average crack width of fiber reinforced soil is smaller than unreinforced soil with an average percentage reduction of 21%. This also indicates potential benefit of natural fiber inclusion in controlling desiccation cracking width of soil irrespective of the thickness of the soil layer. This behaviour is advantageous in preventing loss of shear strength of soil after undergoing desiccation. From the soil-structure interaction point of view, it is critical for the soil to maintain its integrity in order to sustain overburden pressure from the supported structures.

Table 7.4: Effect of soil layer thickness on surface crack width

Soil layer thickness (mm)	Surface crack width (mm)		
	Reinforced	Unreinforced	Variance (%)
6	1.88	3.41	-44.9
12	3.44	3.99	-13.8
24	4.75	4.98	-4.6

*Variance is the difference in fraction between unreinforced and reinforced, - is decrease

7.3.8 Rate of water loss from the soil

The rate of soil water content loss was investigated within the first 24h of drying for both reinforced and unreinforced soil specimens. The comparison of soil water content reduction between reinforced and unreinforced soil with various soil thicknesses is shown in figure 7.11.

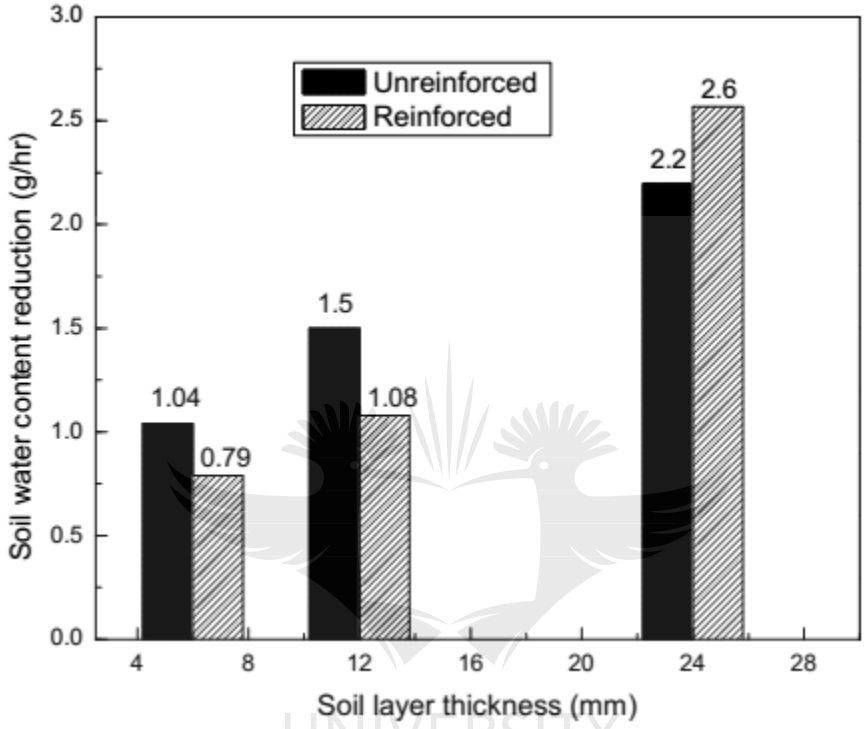

Figure7.11: Moisture loss of reinforced and unreinforced soil

It is indicated that higher rate of water loss occurs in unreinforced soil with thicknesses of 6mm and 12mm than reinforced specimens. The vice versa occurs in thicker layer (24mm). The rate of soil water loss increases with increasing soil layer thickness. The desiccation behaviour of reinforced thin layers can be explained in respect of the hydrophilic characteristics of sisal fibers. Sisal fibers being natural, absorb moisture when exposed to humid or moisture environment (Pickering et al, 2016). Therefore, when the soil was in slurry form, moisture diffusion gradient between soil and fibers was so high that some moisture was absorbed by fibers through osmosis and in turn impeded capillary flow of water to the surface. These two competing processes gave rise to the low rate of moisture loss of reinforced soil compared to unreinforced soil. With thick soil layers, the amount of fibers in the specimen was relatively high since the fiber content was determined by dry weight of the soil. The larger volume of soil would require high fiber content

for a given fiber dosage. In this case, high amount of fibers in the soil created large surface area of water pathways. Since moisture diffusion coefficient of sisal fibers is low, the high rate of capillary flow in the presence of large volume of pathways caused significant amount of moisture to evaporate from the reinforced soil at the prevailing atmospheric conditions. The increase in loss of moisture with thickness was attributed to the high amount of initial moisture content of the soil. The initial moisture content was determined as 1.5 times of the liquid limit state. Therefore, larger amount of soil would require large amount of water to form slurry.

7.3.9 Effects of wet-dry cycles on compressive strength

The effect of saturation and desaturation on the compressive strength of compacted fiber reinforced and unreinforced soil is shown in figure 7.12.

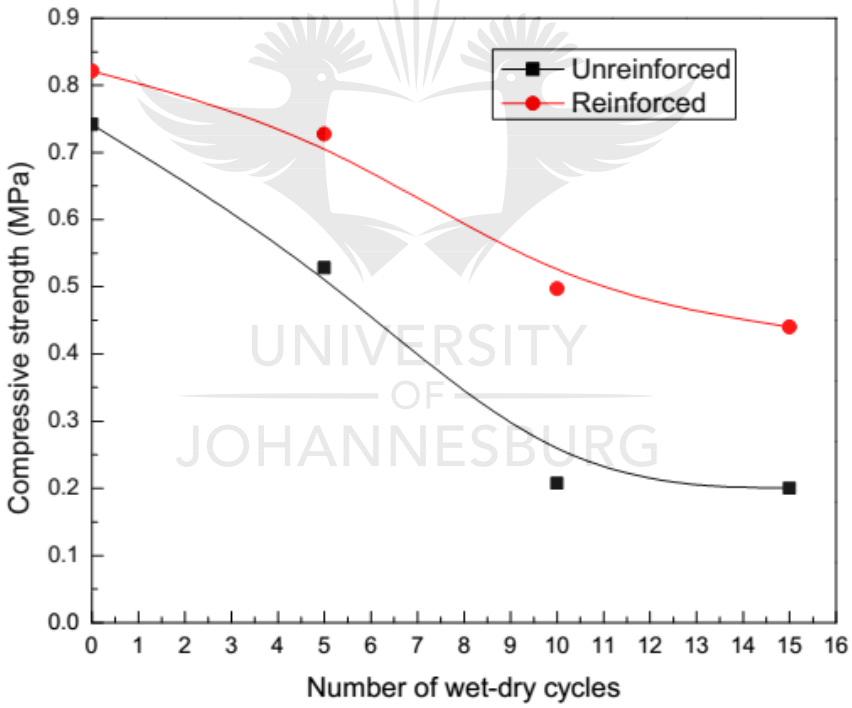

Figure 7.12: Effect of wet-dry cycles on the compressive strength of the compacted soil

It is shown that increase in number of wet-dry cycles results in the decrease in compressive strength. The strength reductions of about 41% and 66% for reinforced and unreinforced soil respectively are indicated. Fiber reinforced soil specimens show some resilience to strength degradation compared to unreinforced soil. It is noted that 10 cycles show the onset of residual

strength for both reinforced and unreinforced soil. The change in macrostructure of the compacted specimens with number of wet-dry cycles (5 and 15 cycles) is shown in figure 7.13.

Figure 7.13: Morphology of soil macro structure after wet and dry cycles

It is shown that the soil gets eroded with increasing wet and dry cycles for both reinforced and unreinforced specimens. The unreinforced specimen shows significant cracking after 15cycles.It is evident that the strength degradation was due to loss of integrity of the soil as a result of erosion of fine particles. The resilience of the reinforced soil to cracking enhanced the strength of the soil. In practice, the behaviour of reinforced soil exhibited in this study is beneficial to the resilience of pavement, liners, barriers and foundation during seasonal moisture fluctuation of the soil. It is anticipated that reinforced soil has high potential to sustain considerable loading as compared to unreinforced soil in the case of prolonged saturation and desaturation of the soil.

Conclusions

Based on the acquired results, the following conclusions are drawn;

1. The crack morphology of reinforced soil is characterised by small cell area with irregular shapes, short and thin cracks and non-orthogonal crack intersections while unreinforced soil shows large cell area with irregular shapes, large cracks and non-orthogonal crack intersections.
2. The fiber content dictates rate of moisture loss from the soil. With 0.5% fiber content the rate of moisture loss may be lower than unreinforced soil. This is attributed to the low

free moisture in the composite caused by the absorption of moisture by the fibers. With 1% fiber content rate of moisture loss may be greater than unreinforced soil due to increased volume of water pathways created by the fibers.

3. Crack width and surface area ratio reduce with increase in fiber content. Crack width reduction of 74% and surface crack reduction of 35% may be achieved at 1% fiber content.
4. Crack growth and shrinkage strain are significantly reduced with fiber inclusion. The growth rate may reduce from 5.8mm/hr for unreinforced soil to 1.2mm/hr at 1% fiber content. The shrinkage may reduce from 5.5% for unreinforced soil to 1% for reinforced soil with 1% fiber content.
5. Increasing thickness of the soil layer increases crack width and rate of moisture loss for both reinforced and unreinforced soil.
6. Increasing number of wet and dry cycles causes strength degradation of both reinforced and unreinforced soil due to loss of binding fine particles of the soil. However, reinforced soil indicates considerable resilience to strength degradation compared to unreinforced soil.
7. In practice, natural fiber inclusion can effectively be applied to control desiccation cracking of soil which is beneficial in maintaining integrity of earthen structures. It is anticipated that fiber reinforced earthen walls would exhibit resilience to cracking during moisture evaporation and this in turn maintains strength and renders the structure with good serviceability during its service life.

References

Abdi et al. (2008). Effects of Random Fiber Inclusion on Consolidation, Hydraulic Conductivity, Swelling, Shrinkage Limit and Desiccation Cracking of Clays. *International Journal of Civil Engineering,, 6*, 284-292.

Albrecht et al. (2001). Effects of desiccation on the compacted narural clays. *Journal of Geotechnical and Geoenvironmental Engineering, 127*(1), 67-75.

ASTM D1140-17. (2017). Standard Test Methods for Determining the Amount of Material Finer than 75-µm (No. 200) Sieve in Soils by Washing. West Conshohocken PA: *ASTM International.*

ASTM D2166. (2016). Standard Test Method for Unconfined Compressive Strength of Cohesive Soil. West Conshohocken, PA: , *ASTM International*.

Baker. (1981). Tensile strength, tension cracks, and stability of slopes. *Soils and Foundations, 21*, 1-17.

Baldovino et al. (2018). Effects of lime addition on geotechnical properties of sedimentary soil in Curitiba, Brazil. *Journal of rock mechanics and geotechnical engineering, 10*(1),188-194.

Chaduvula et al. (2017). A study on desiccation cracking behavior of polyester fiber-reinforced expansive clay. *Applied Clay Science, 142*, 163-172.

Consoli et al. (2011). Voids/cement ratio controlling tensile strength of cement-treated soils. *Journal of Geotechnical and Geoenvironmental Engineering*, 1126–1131. doi: 10.1061/(ASCE)GT.1943-5606.0000524,

Costa et al. (2013). Salient factors controlling desiccation cracking of clay in laboratory experiments. *Ge ´otechnique, 63*, 18–29.

Diambra et al.(2013).Fibre reinforced sands: from experiments to modelling and beyond. *International journal for numerical and analytical methods in geomechanics, 37*,2427–2455.

Harianto et al. (2008). Effects of Fiber Additives on the Desiccation Crack Behavior of the Compacted Akaboku Soil as A Material for Landfill Cover Barrier. *Journal of Water Air Soil Pollution, 194*, 141–149.

Hejazi et al. (2013). Shear Modeling of Fiber Reinforced Soil Composite on the Base of Fiber Pull-out Test. *Fibers and Polymers, 14*(2), 277-284.

Ibraim .E and Consoli.N.C. (2018). Energy efficiency of fibre reinforced soil formation at small element scale.Laboratory and numerical investigation. *Geotextile Geomembranes, 46*(4), 497-510.

Jain, S. a. (2008). *Effect of freezing-thawing and wettingdrying on tensile strength of lime-fly ash stabilized black cotton soil*. Paper presented at the 12th Int. Conf. Int. Association for Computer Methods and Advances in Geomechanics (IACMAG), Goa, India.

Kafodya.I and Okonta.F.N. (2018b). Effect of fibre surface coating on the mechanical properties of natural fibre-reinforced soil,. *International Journal of Geotechnical Engineering*. doi: DOI: 10.1080/19386362.2018.1542557

Kafodya.I and Okonta.F.N. (2018). Effects of natural fiber inclusions and pre-compression on the strength properties of lime-fly ash stabilised soil. *Construction and Building Materials, 170*, 737-746.

Kodikara. J and Costa. S. (2013). Desiccation Cracking in Clayey Soils: Mechanisms and Modelling. In F. A. Laloui L. (Ed.), *Multiphysical Testing of Soils and Shales:Springer Series in Geomechanics and Geoengineering*. Berlin Heidelberg: Springer.

Kodikara et al. (2002). Structure development in surficial heavy clay soils: a synthesis of mechanisms. . *Aust. Geomech, 37* (3), 25–40.

Lakshmikantha et al. (2006). *An experimental study of cracking mechanisms in drying soils.* . Paper presented at the The 5th ICEG Environmental Geotechnics, London.

Miller et al. (1998). Experimental analysis of desiccation crack propagation in clay liners. *Journal of the American Water Resources Association, 34*(3), 677-686.

Moghal et al. (2018). Effect of polypropylene fibre reinforcement on the consolidation, swell and shrinkage behaviour of lime-blended expansive soil. *International journal of geotechnical engineering, 12* (5), 462-471.

Morris et al. (1992). Cracking in drying soils. *Canadian Geotechnical Journal, 29*, 263-277.

Nahlawi.H and Kodikara.J.K. (2006). Laboratory experiments on desiccation cracking of thin soil layers. *Geotechnical and Geological Engineering, 24*, 1641–1664.

Péron et al. (2009). Fundamentals of desiccation cracking of finegrained soils: experimental characterisation and mechanisms identification. *Canadian Geotechnical Journal, 46*, 1177–1201.

Pickering et al. (2016). A review of recent developments in natural fibre composites and their mechanical performance. *Composites: Part A 77, 83*, 98–112.

Prat et al. (2006). *Size effect in the cracking of drying soil.* Paper presented at the 16th European Conference of Fracture

Qiang et al. (2014). Cracking, water permeability and deformation of compacted clay liners improved by straw fiber. *Engineering Geology, 178*, 82-90.

Rayhani et al. (2007). Desiccation-induced cracking and its effect on the hydraulic conductivity of clayey soils from Iran. *Canadian Geotechnical Journal, 44*, 276–283.

Rifai et al. (2009). Theoretical Assessment of Increased Tensile Strength of Fibrous Soil Undergoing Desiccation. *Journal of Geotechnical and Geoenvironmental Engineering, 135*(12), 1857-1862.

Rodríguez et al. (2007). Experimental and numerical analysis of desiccation of a mining waste. *Canadian Geotechnical Journal, 44*, 644-658.

Silvestri et al. (1992). *Evapotranspiration, trees and damage to foundations in sensitive clays.* . Paper presented at the Canadian Geotechnical Conf

Tang et al. (2010a). Experiment evidence on the temperature dependence of desiccation cracking behavior of clayey soils. *Engineering Geology, 141*, 261-266.

Tang et al. (2010b). Interfacial shear strength of fiber reinforced soil. *Geotextiles and Geomembranes*, *28*, 54–62.

Tang et al. (2012). Desiccation cracking behavior of polypropylene fiber–reinforced clayey soil. *Canadian Geotechnical Journal, 49*, 1088–1101.

Tang et al. (2016). Tensile Strength of Fiber-Reinforced Soil. *Journal of Materials in Civil Engineering*, *28*(7), 04016031-04016031-04016013.

8 CHAPTER EIGHT-CYCLIC AND POST CYCLIC SHEAR BEHAVIOURS OF SISAL FIBER REINFORCED SOIL

8.1 Introduction

Various methods, such as cyclic triaxial, resonant-column, torsional shear, bender elements and shake table are used to investigate dynamic properties of soil (Das and Ramana, 2011). Shear modulus and damping ratio are the fundamental soil parameters in evaluating dynamic response of soil.

Cyclic loading leads to an accumulation of strain and/or excess pore water pressures in the soil because the generated stress or strain loops are not perfectly closed. The strain accumulation results in the decrease in the effective confining stresses of the soil. For a given applied cyclic shear stress, the magnitude of the shear strains depends on the soil stiffness, which in turn depends on the level of shear strain and excess pore pressure (El Mohtar et al., 2013). Liquefaction occurs when the cyclic strains are high enough to generate excessive pore pressure leading to a complete loss of the effective stresses. Clay soil is more resistant to liquefaction than sand (Indraratna et al., 2016). Moreover, the cumulative phenomena in the soil during cyclic loading are of importance in many practical cases. In the earthquake prone areas such as Great rift valley, a limited number of load cycles with large strain amplitudes greater than 0.001 during an earthquake may lead to an accumulation of high pore water pressures and consequently to a dramatic loss of the bearing capacity of structures. Under drained conditions if the strain amplitude is less than 0.001 and the number of cycles is high, the accumulation of settlements becomes problematic in structures Furthermore, non-engineered structures (earthen) are extremely sensitive to differential settlements especially when material resilience to deformation is low (Wichtmann et al., 2005). The past earthquake events at the tip of East Africa rift valley (Malawi earthquake) severely affected the rural community housing infrastructure, especially earthen houses. The damage was attributed to the poor material properties and improper construction methods. However, the post- earthquake assessment indicated that other more traditional building types, such as bamboo reinforced wattle structures, performed better than low-quality adobe unreinforced masonry structures (Goda et al., 2018; Kloukinas et al., 2019). Therefore, reinforcing earthen structures with natural fibers may as well endow the adobe earthen structures with considerable resistance to collapse at relatively low cost.

The post-earthquake rehabilitation of earthen structures depends on the level of damage and overall structural integrity. Post cyclic load resistance of the structures is achieved by adequate reinforcement. Resilience of the earthen structures to aftershocks is of fundamental importance as it reduces cost of reconstruction and retrofitting. It also ensures safe evacuation since total collapse of the dwellings is effectively controlled(Blondet et al., 2004).

The post cyclic shear strength, energy absorbing properties, ductility and toughness of natural fiber reinforced soil is not well documented in the literature. The cyclic and post cyclic soil properties dictate the design of earthen structures (AI Wahab and Heckel, 1995). It is imperative therefore to investigate cyclic behaviour of natural fiber reinforced soil in order to establish proper guideline for the applicability of the natural fiber composites for earthen construction.

In this study, sisal fibers were used to reinforce reconstituted soil. The objective was to evaluate effects of fiber contents on the shear modulus, damping ratio, permanent strain, cumulative permanent strain and liquefaction potential and post cyclic shear strength.

8.2 Materials and experimental programme

8.2.1 Materials

The soil sample used in this study was prepared and characterised as in section 3.1.1 according to ASTM D1140-17. The grading curve of the soil is shown in figure 3.1 and the properties are summarised in Table 3.1. Dry fibers with length of 25mm were used to prepare specimens. The summary of the fiber properties is shown in Table 3.3.

8.2.2 Sample preparation

The prescribed fiber contents for the specimens were determined by the percentage dry mass of soil. The fiber dosages used herein were 0.25%, 0.5%, and 1%. In preparing the specimen, water of equivalent optimum moisture content of 11% was added to the soil. The fibers were added gradually to wet soil and mixed thoroughly until a homogeneous soil composite was formed. The mixture of the soil composite was then covered in an airtight plastic bag for 4h prior to specimen fabrication to ensure uniform distribution of moisture. The moisture content of ± 1% (OMC) was applied to provide for marginal loss of moisture during specimen preparation.

8.2.3 Specimen preparation experimental programme

After moisture equilibration, specimens were prepared in the mould of diameter 50mm and height of 100 mm by static compaction. By following method in section 3.2, the compaction pressure for each fiber dosage was determined and each specimen was deemed suitable for testing when the density after preparation was at least 95% of the maximum dry density obtained from the preliminary compaction test.

Shear modulus, damping ratio, permanent strain, cumulative permanent strain and liquefaction potential were determined by performing series of cyclic triaxial tests at various confining pressures (50kPa, 100kPa and 200kPa) to represent low and high in-situ confining stress scenarios, for light weight overburden pressure.

The post cyclic monotonic shear strength, energy absorbing capacity, static energy ratio and toughness were investigated at the fiber contents of 0.5% and 1% and with constant confining pressure of 50kPa. The low confining pressure was used to assess post cyclic behaviour with a view that the high confining pressures are not usually exerted by low-cost earthen construction.

8.3 Results and discussions

8.3.1 Effects of fiber inclusion on shear modulus

The variation of shear modulus with fiber inclusions at various confining pressures is shown in figure 8.1.

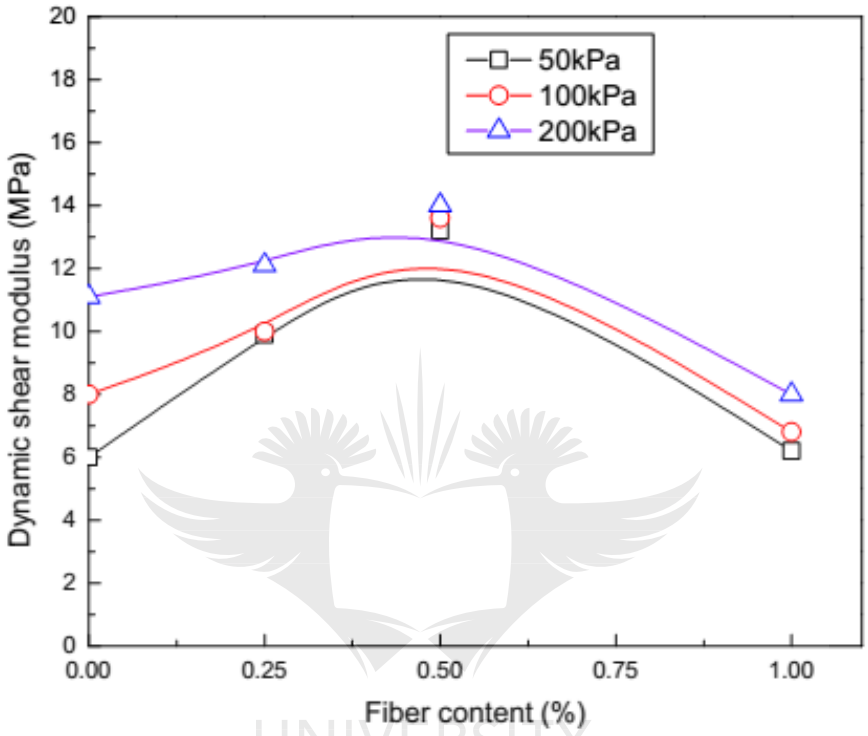

Figure 8.1: Variation of shear modulus with fiber content

It is noted that increase in fiber content causes an increase in shear modulus to limiting fiber content (0.5%). It is evident that increase in confining pressure causes an increase in shear modulus. For unreinforced specimens, shear modulus is enhanced by 83% at confining pressure of 200kPa as compared to 50kPa. The fiber reinforced specimens with 0.5% content indicate strength improvement of 40% at confining stress of 200kPa relative to 50kPa. The results imply that both fibers and confining pressure enhanced stiffness of the soil however, beyond 0.5% fiber content, the stiffness was not significantly improved. The sisal fiber inclusions reduced average unit weight of solids in the soil composite since sisal fibers possess low unit weight of about 1.4g/cm^3 (Aqeel Al Adili et al., 2012b; Prabakar and Sridhar, 2002; Sayida, 2009). Fundamentally, increasing volume of fibers caused changes in the volume of solids and voids within the composite. Since specimens used herein were prepared by compaction, addition of

fibers provided resistance to compaction and prevented dense packing of grains while creating voids along the peripheral of the fibers (Ibraim and Fourmont, 2006). This phenomenon was pronounced at high fiber content (1%) and consequently reduced stiffness of the soil composite.

The variations of shear modulus with strain for unreinforced and reinforced soil with 1% fiber content at various confining pressure are shown in figures 8.2a and b, respectively.

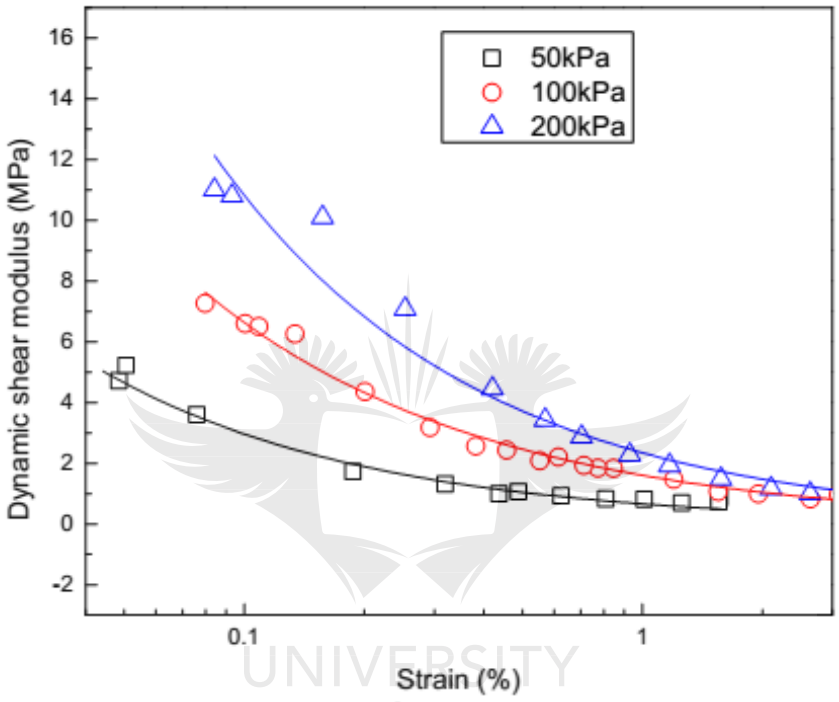

(a)

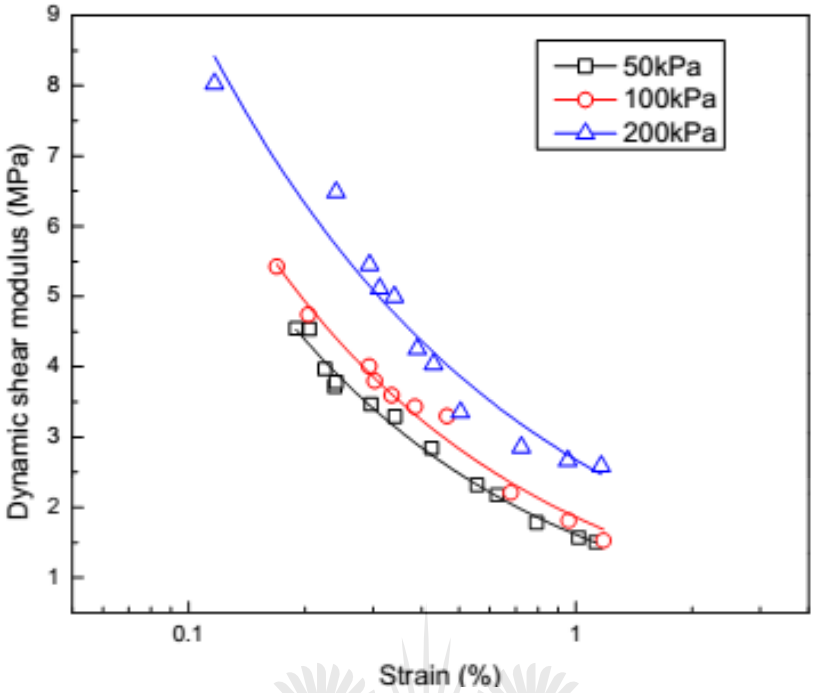

(b)

Figure 8.2: Variation of shear modulus with shear strain (a) unreinforced soil (b) reinforced soil (1% fiber content)

The results show that unreinforced specimens exhibit lower rate of shear modulus degradation than reinforced specimens. The change in shear modulus for unreinforced soil is highly influenced by the confining pressure. On the other hand, the effects of confining pressure on the degradation of shear modulus for reinforced soil composite are not significant. This might be attributed to the anisotropic properties of the soil composite due to the non uniform distribution of fibers. A modulus reduction curve is used to represent the degradation of shear modulus with shear strain in terms of normalised shear modulus (G/G_{max}) (Kramer, 1996). G_{max} is the maximum shear modulus of the soil that is generally defined at a very low shear strain ($\gamma \leq 5\times10$-6) (Kumar et al., 2017). Due to low accuracy of cyclic triaxial systems in the small-strain ranges, the maximum shear modulus is rarely calculated. However, a resonant column device or bender element system can be used to determine G_{max} (Ghayoomi et al., 2017). In the absence of experimental data at low strain, empirical correlations proposed by Hardin and Drnevich (Hardin and Drnevich, 1972) shown in equation 8.1, was used in this study to evaluate G_{max}.

$$G_{max} = 102132648\frac{(2.973-e)^2}{1+e}(OCR)^k(\sigma_c)^{0.5} \quad (8.1)$$

where e is the void ratio, OCR is the over consolidation ratio, σ_c is confining pressure and k is an index parameter. In this study, k was taken as 0 since the soil matrix was remoulded and void ratio was calculated using equation 8.2 for dry densities of 1.9g/ cm^3 and 1.8 g/ cm^3 for unreinforced and reinforced soil, respectively that were obtained from the preliminary test.

$$e = \frac{G_s \gamma_w}{\gamma_d} - 1 \qquad (8.2)$$

where G_s is the specific gravity of soil which is 2.67 and 2.66 for unreinforced and reinforced soil, respectively), γ_w is unit weight of water and γ_d is the dry unit weight of soil. The normalised shear moduli for unreinforced and reinforced soil are shown in figures 8.3a and b, respectively. It is noted that the trend is similar to what has been reported in the classical reports (Kokusho, 1980; Seed and Idriss, 1970; Vucetic and Dobry, 1991) however, the rate of cyclic degradation for both reinforced and unreinforced soil is not highly affected by the confining pressure but fiber inclusion. Fiber inclusion causes higher rate of modulus degradation. This might be due to the debonding of the fibers from the soil matrix with an increase in strain level.

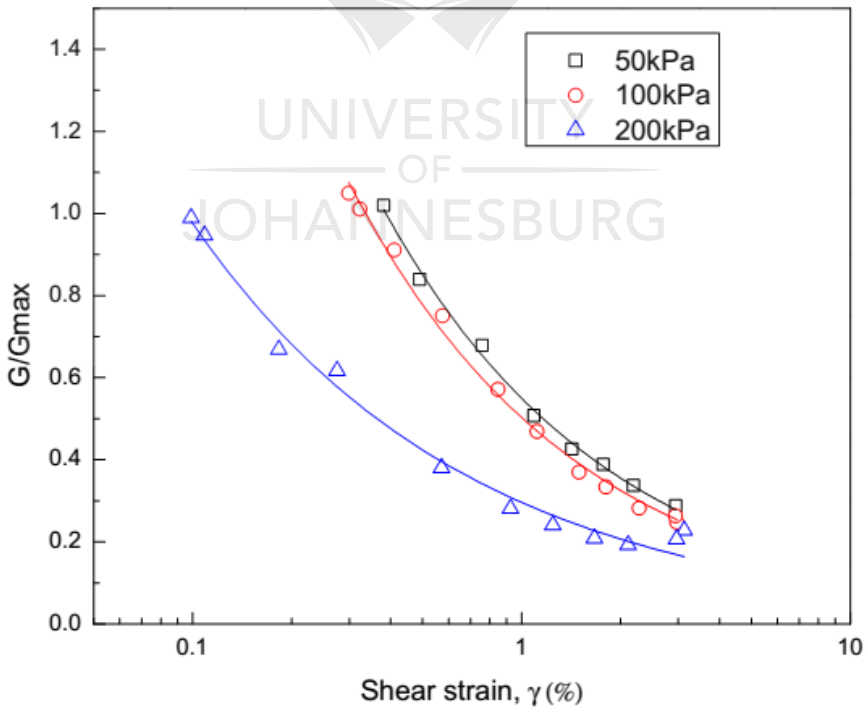

(a)

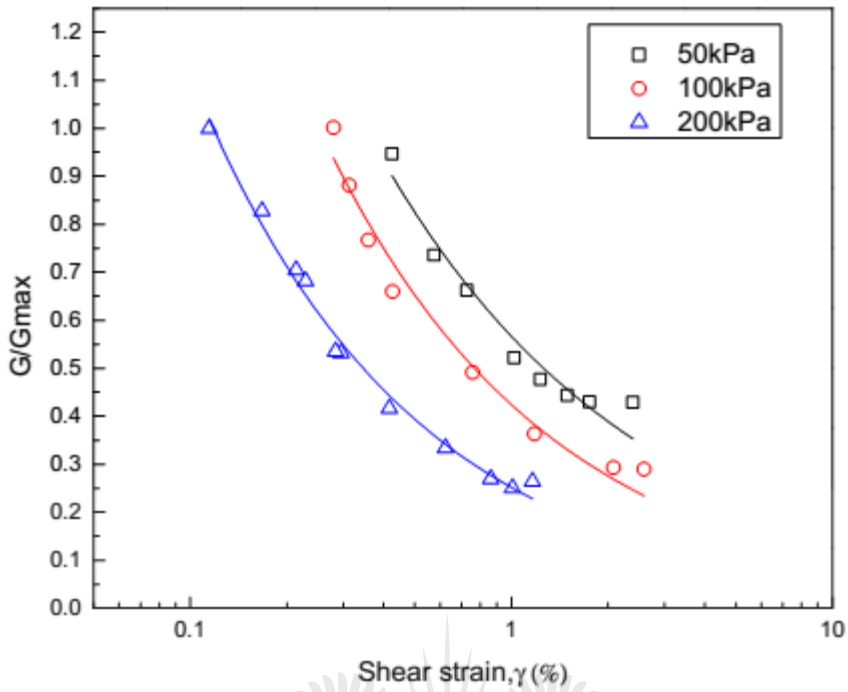

(b)

Figure 8.3 :Variation of normalised shear modulus with shear strain (a) unreinforced soil (b) reinforced soil (1% fiber content)

8.3.2 Effects of fiber inclusion on damping ratio

The variation of damping ratio with fiber content is shown in figure 8.4. It is indicated that increasing fiber content causes an increase in damping ratio. With 1% fiber content, damping ratio improvements of about 36%, 70% and 90% for 50kPa, 100kPa and 200kPa, respectively are displayed. The indicated behaviour of the fiber reinforced soil is in agreement with the findings reported elsewhere (Amir-Farya and Sherif Aggour, 2015; Orakoglua et al., 2017; Sadeghi and Beig, 2014). The damping properties are dependent on the confining pressure. This behaviour was also reported elsewhere (Kumar et al., 2017). The confining pressure enhanced stiffness of the soil composite and hence improved damping properties. The enhanced shear resistance of the soil composite by the mechanical inter-lock of the fibers improved damping properties of the composite.

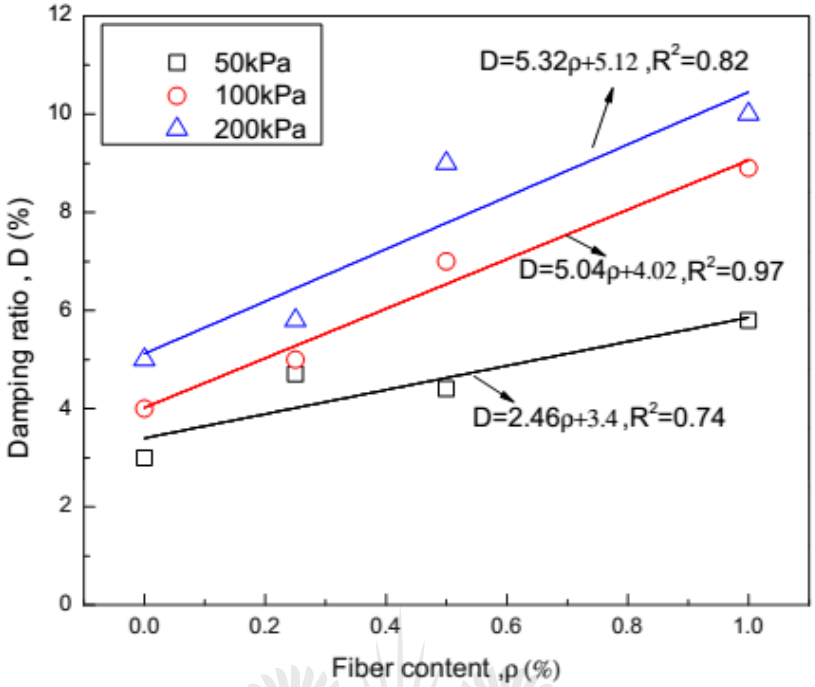

Figure 8.4 : Variation of damping ratio with fiber content

Figure 8.5 presents variation of damping ratio with shear strain for unreinforced and reinforced soil. It is noted that damping ratio increases with increase in shear strain for both soil types. It is shown that beyond 1% strain, damping ratio does not increase significantly.

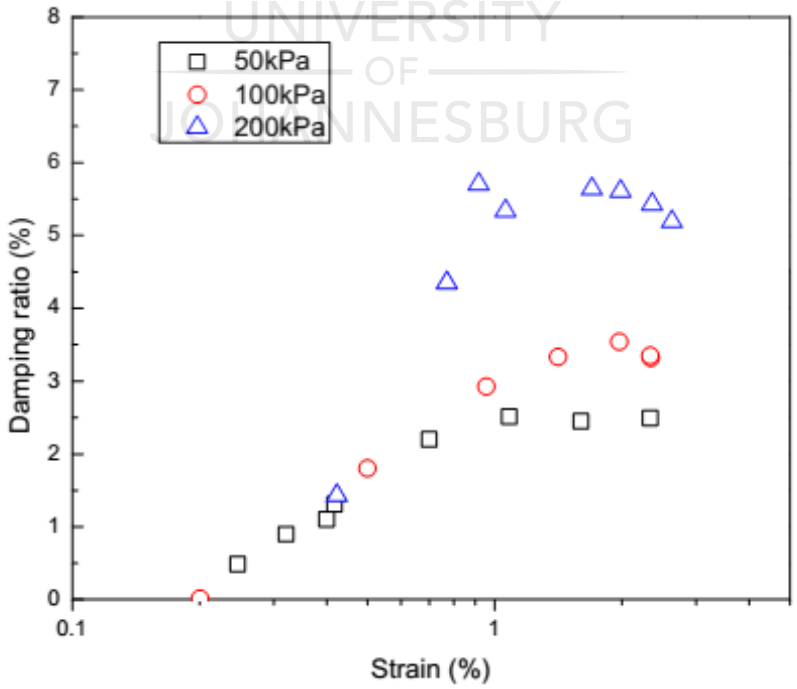

(a)

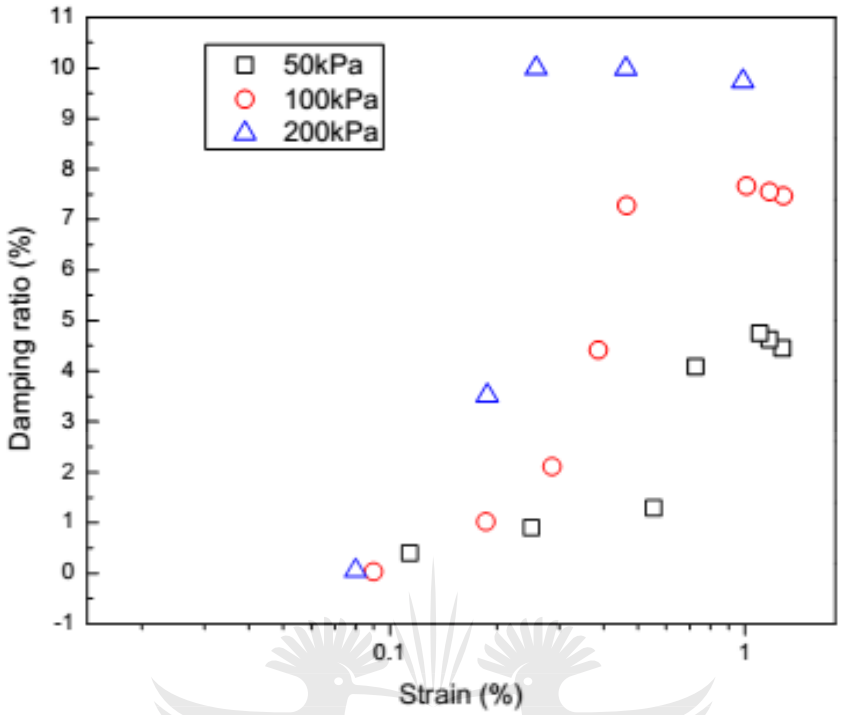

(b)

Figure 8.5: Variation of damping ratio with shear strain (a) Unreinforced soil (b) Reinforced soil

The damping ratio depends on the level of confinement. The scatter of the data was attributed to the variation of the macro structure of the soil composites.

The hysteresis loops of unreinforced and reinforced soil with 1% fiber content for the first cycle are shown in figures 8.6a and b, respectively. It is seen that the loops are more asymmetrical. It is reported (Kumar et al., 2017) that the hysteresis loops become more asymmetrical with high applied strain level. The asymmetrical shape of the loops was therefore due to the high strain level during cyclic shearing

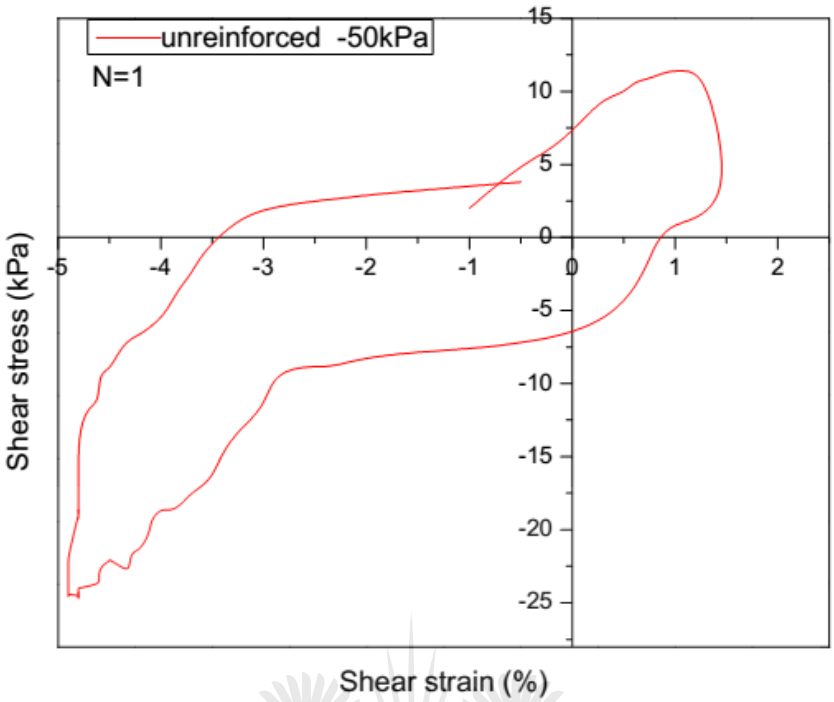

(a)

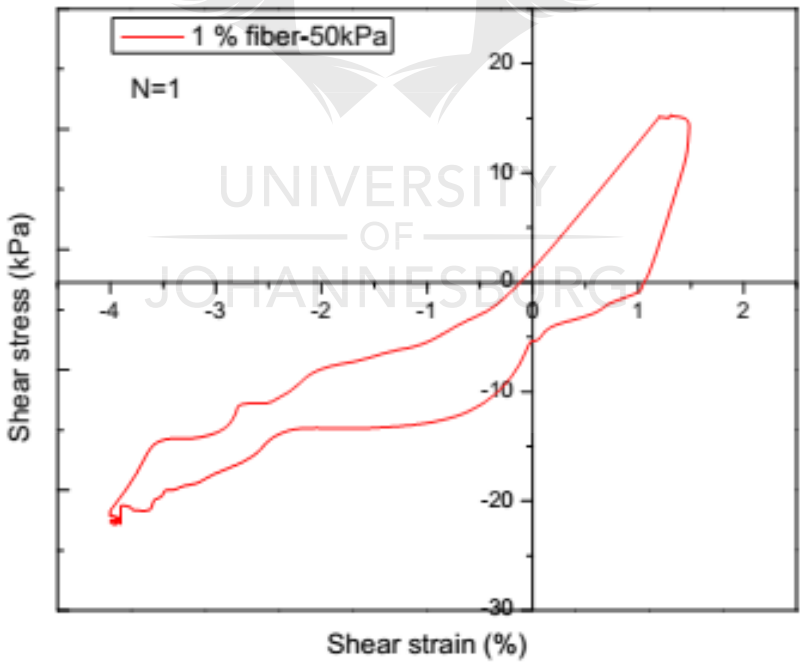

(b)

Figure 8.6: Hysteresis loops for the 1st cycle (a) Unreinforced soil (b) Reinforced soil at constant confining pressure

8.3.3 Effects of fiber inclusion on induced strain

The variation of permanent strain with fiber inclusion is shown in figure 8.7. It is evident that fiber inclusion causes decrease in permanent strain. The increase in confining pressure reduces values of the permanent strain. With fiber content of 1%, permanent strain reduces by 30%, 10% and 25% for the confining pressures of 50kPa, 100kPa and 200kPa, respectively. The fibers endowed the soil with resilience to deformation. This could be attributed to the interweaving of the fiber at high fiber content that in turn restrained the soil matrix from undergoing considerable deformation.

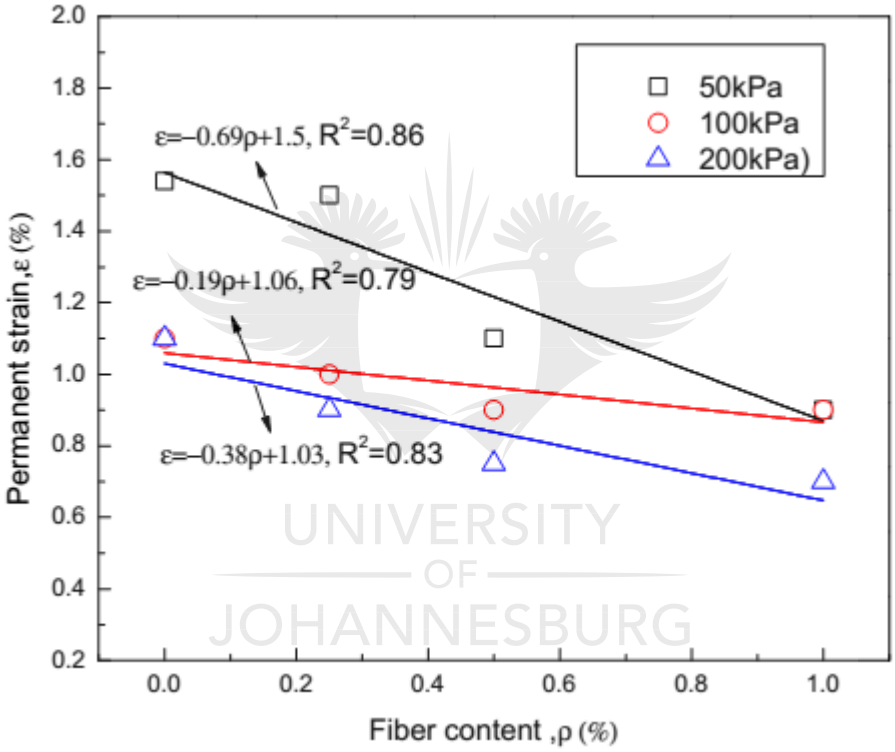

Figure 8.7: Variation of permanent strain with fibers content

The effect of fiber content on the cumulative strain is presented in figure 8.8. It is noted that increase in fiber content causes reduction in cumulative strain. The increase in confining pressure reduces values of the cumulative strain. Fiber content of 1% causes strain reduction of 68%, 66% and 65% for confining pressures of 50kPa, 100kPa and 200kPa, respectively.

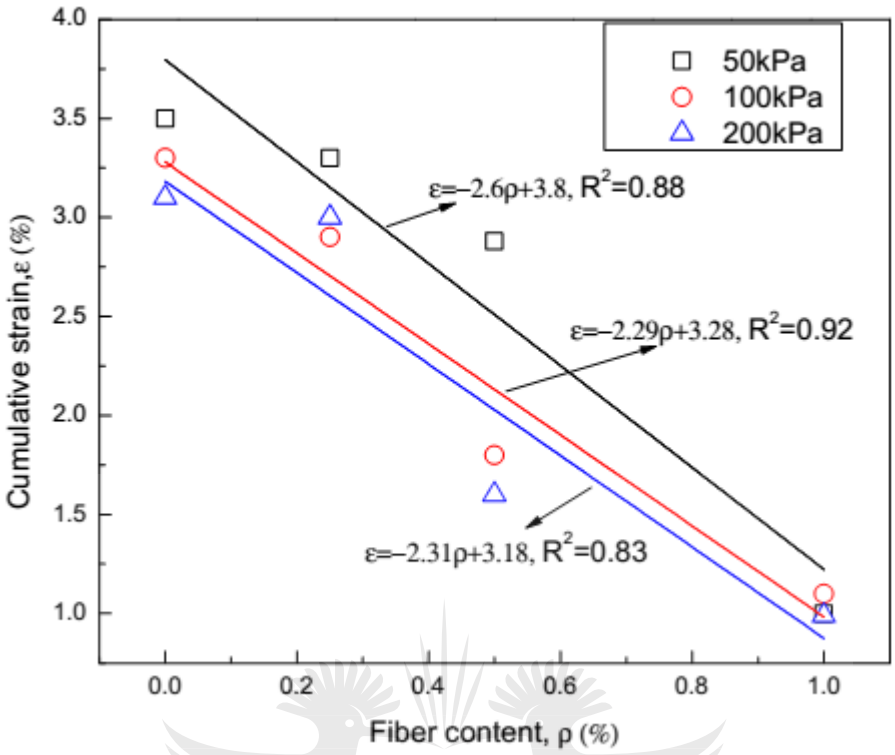

Figure 8.8: Variation of cumulative strain with fibers content

Fibers in this study provided resistance to deformation and hence reduced magnitude of permanent deformation of the specimens. The permanent deformation of the specimens at the first cycle resulted in the insignificant specimens' deformation during succeeding cycles. This was evidenced by the variation of dynamic deviator stress with number of cycles in figures 8.9a-c.

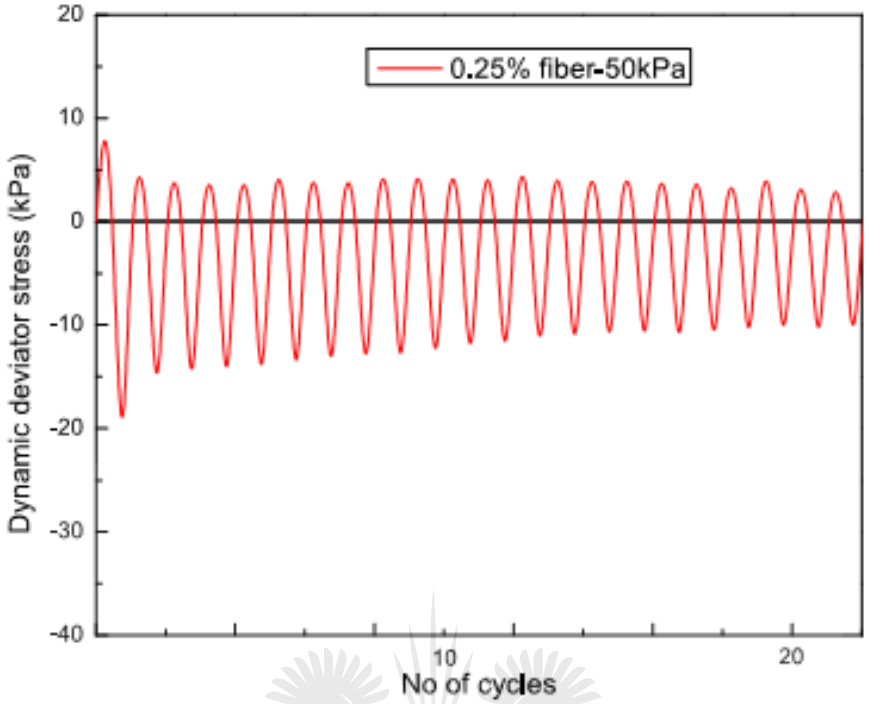

(a)

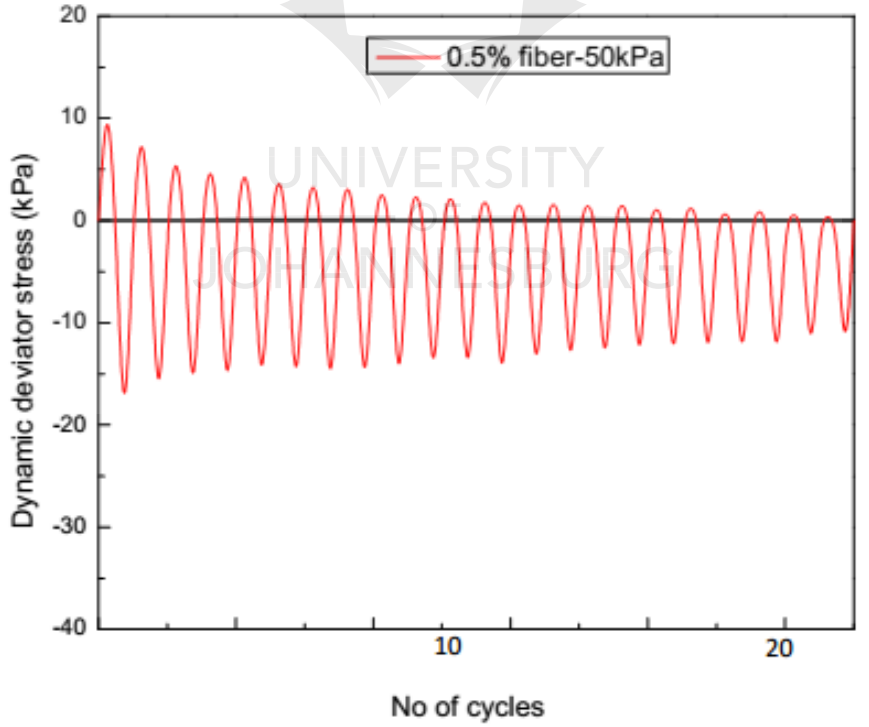

(b)

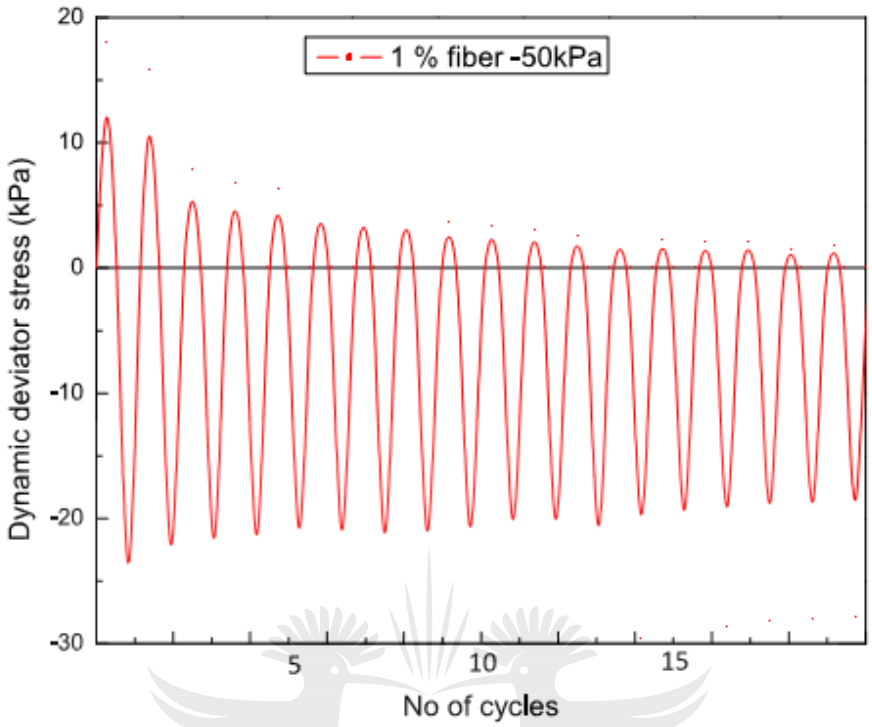

(c)

Figure 8.9: Variation of deviator stress with number of cycles

It is shown that deviator stress reduced with an increase in number of cycles irespective of fiber content. The first 5 cycles contribute significantly to the deformation of the specimens. The deviator stress reduces to some value that is indicative of permanent deformation of the specimen. Therefore, it can be deduced that the first cycle in the cyclic loading is suitable for the evaluation of the intrinsic dynamic properties of the soil. This was also recommended elsewhere (Vucetic and Mortezaie, 2015).

8.3.4 Evaluation of liquefaction potential

The cyclic liquefaction is considered to occur when pore pressure ratio becomes unity and when double amplitude axial deformation greater than 5 % occurs (Alibolandi and Moayed, 2015). In this study, liquefaction potential was evaluated for both unreinforced and reinforced soil at constant confining pressure of 50kPa. The increase in pore pressure ratio with the number of cycles is shown in figure 8.10.

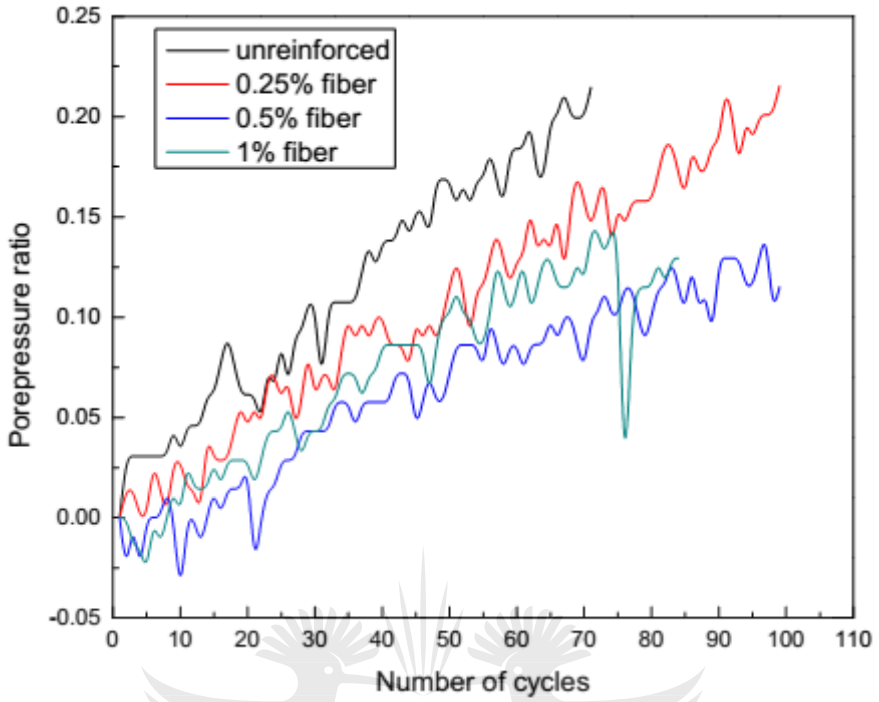

Figure 8.10: Variation of pore pressure ratio with number of cyclic cycles

It is noted that pore pressure ratio increases with number of cycles. The fiber inclusions cause reduction in pore pressure ratio. Furthermore, both unreinforced and reinforced soil specimens show high resistance to liquefaction as the maximum pore pressure ratio is indicated to be 0.2 far below 1, which is a direct indication of liquefaction.

It is reported (Alibolandi and Moayed, 2015; Monkul and Yamamuro, 2011; Naeini and Baziar, 2004; Naeini and Gholampoor, 2014; Sadrekarimi, 2013) that soil with high fine content such as clay or silt exhibits high resistance to liquefaction. Fiber inclusion increases resistance to liquefaction also reported elsewhere (Maheshwari et al., 2012; Noorzad and Amini, 2014). The resistance to liquefaction of unreinforced soil was attributed to high fine content of the soil (see Fig 3.1) and fibers further enhanced resistance to liquefaction by reducing rate of pore pressure increase.

8.3.5 Post cyclic shear behaviour

Post cyclic behaviour of soil is fundamentally important when analysing post earthquake performance of the earth structures. Figure 8.11 presents the post cyclic shear behaviour of the

reinforced and unreinforced soil. It is evident that fiber reinforced soil exhibits considerable ductility. However, the deviator stress at 1% fiber content is erratic at low strain level.

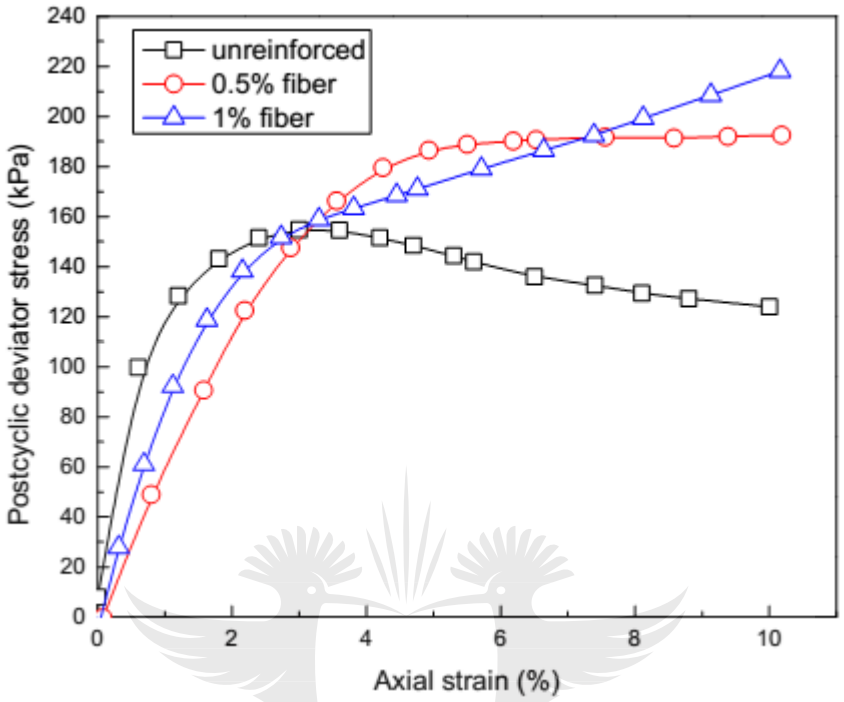

Figure 8.11: Post cyclic monotonic shear strength of the unreinforced and fiber reinforced soil.

The two stage stress-strain relationship is shown for all specimens. The fiber reinforced composites indicate strain hardening in the plastic phase while unreinforced soil indicates strain softening behaviour and relatively high stiffness. Toughness and energy absorbing capacity of soil are the important indicators of soil performance under dynamic or seismic loading (AI Wahab and Heckel, 1995). The aforementioned parameters also govern the behaviour of soil during aftershocks. Toughness and energy absorption capacity depend on the shape of the stress-strain curve for that soil.

The models used to estimate energy absorbing capacity, toughness and post cyclic static energy ratio of the soil are shown in figure 8.12a-c.

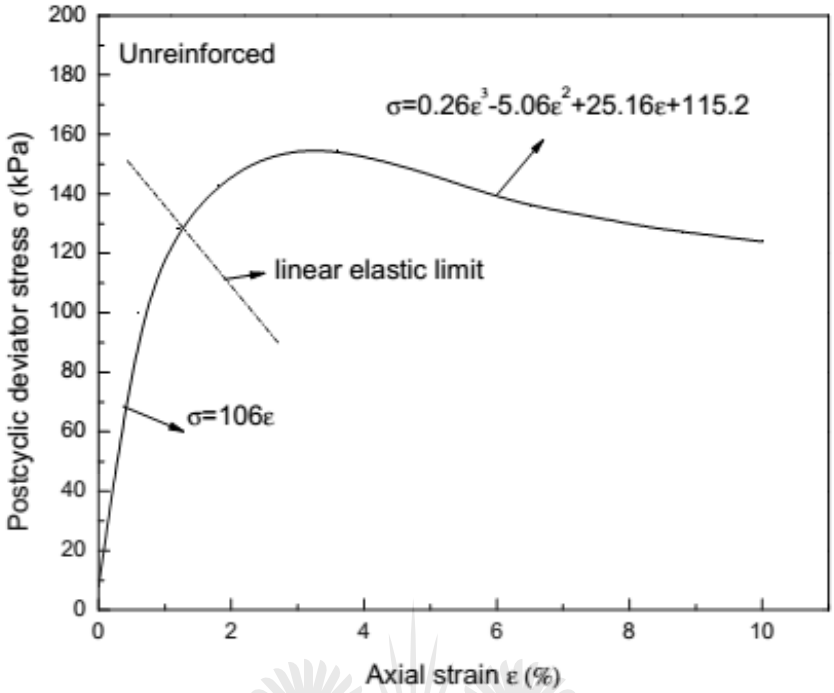

(a)

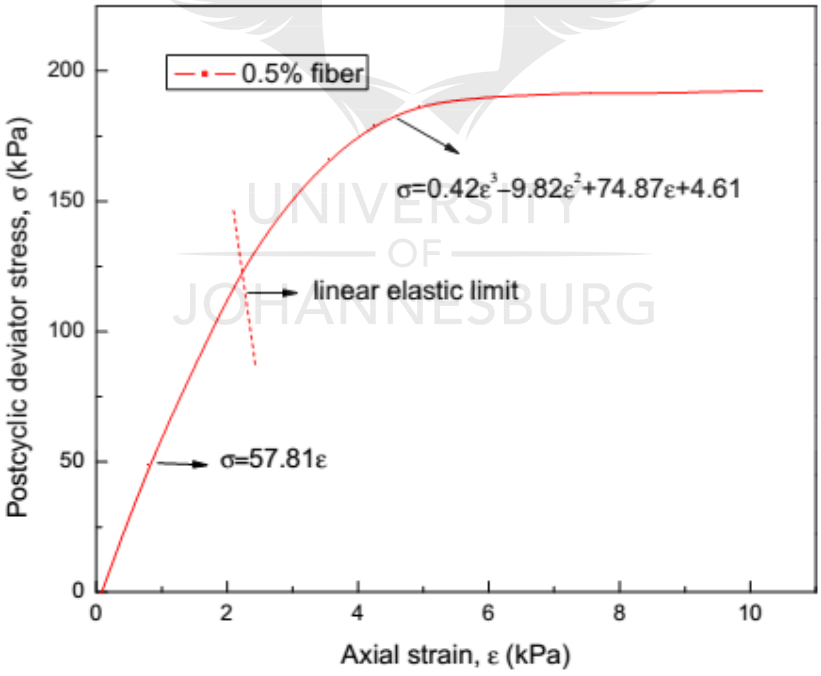

(b)

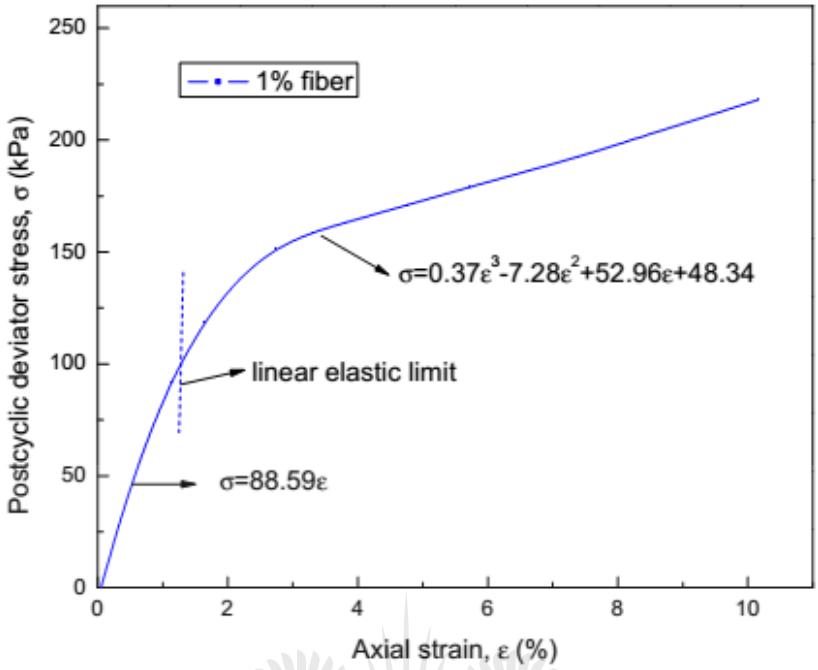

(c)

Figure 8.12: The models for estimating post cyclic properties (a) Unreinforced (b) 0.5% fiber content (c) 1% fiber content

By integrating the curve functions between 0 to 10% strain, the post cyclic energy absorbing capacity of unreinforced soil, 0.5% fiber content and 1% fiber content were found to be 1.3kJ, 1.5kJ and 1.6kJ, respectively. It is evident that fiber inclusion endowed the soil with high energy absorbing properties after cyclic loading. It is anticipated that in an event of aftershock, the fiber reinforced soil will exhibit higher resilience to shear failure than unreinforced soil. The variations of toughness and post cyclic static energy ratio with fiber content are shown in figure 8.13a-b.

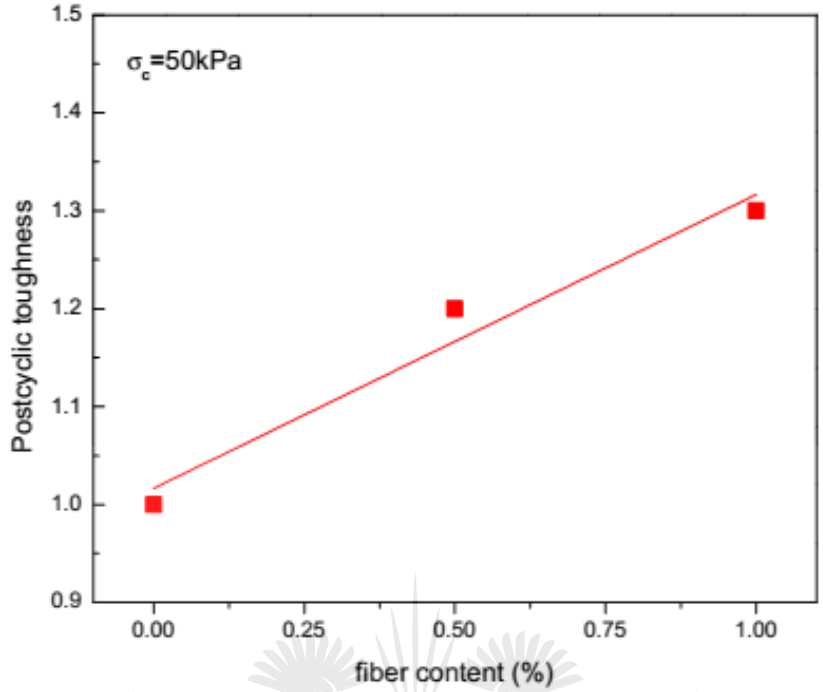

(a)

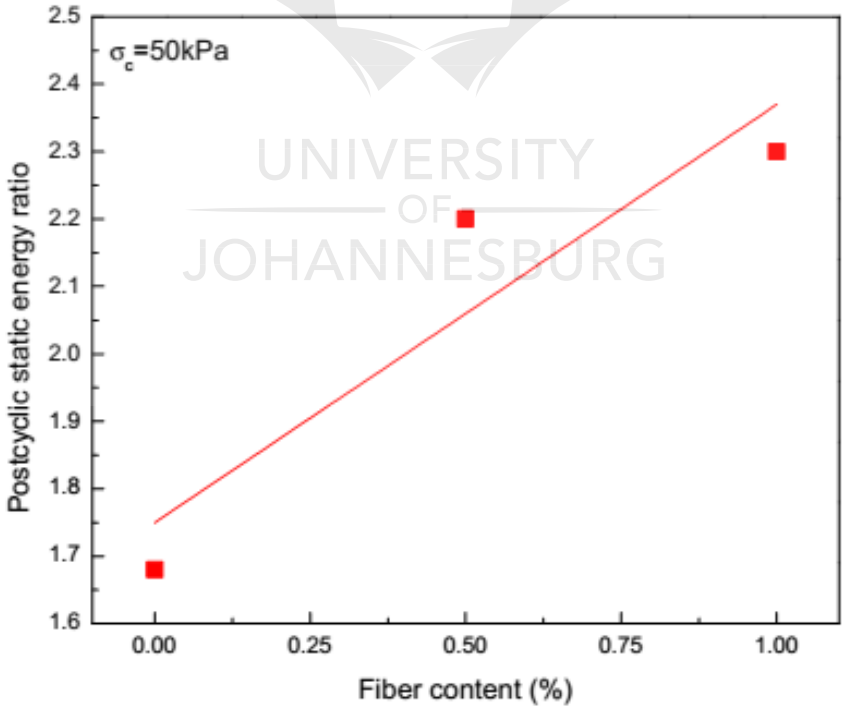

(b)

Figure 8.13: (a) Variation of post cyclic toughness with fiber content (b) Variation of post cyclic energy ratio with fiber content

It is shown that increase in fiber content causes an increase in both post cyclic toughness and static energy ratio. This implies that after cyclic loading, i.e., earthquake, fiber reinforced soil will possess considerable resilience to deformation. This in turn reduces post earthquake damage to the earth structures and also facilitates evacuation. In respect of cyclic traffic load, post cyclic resilience of fiber reinforced soil ensures longevity of the pavement even on the occurrence of sudden heavy loading. The relationships between post cyclic toughness and static energy ratio with dynamic damping ratio are shown in figure 8.14a and b.

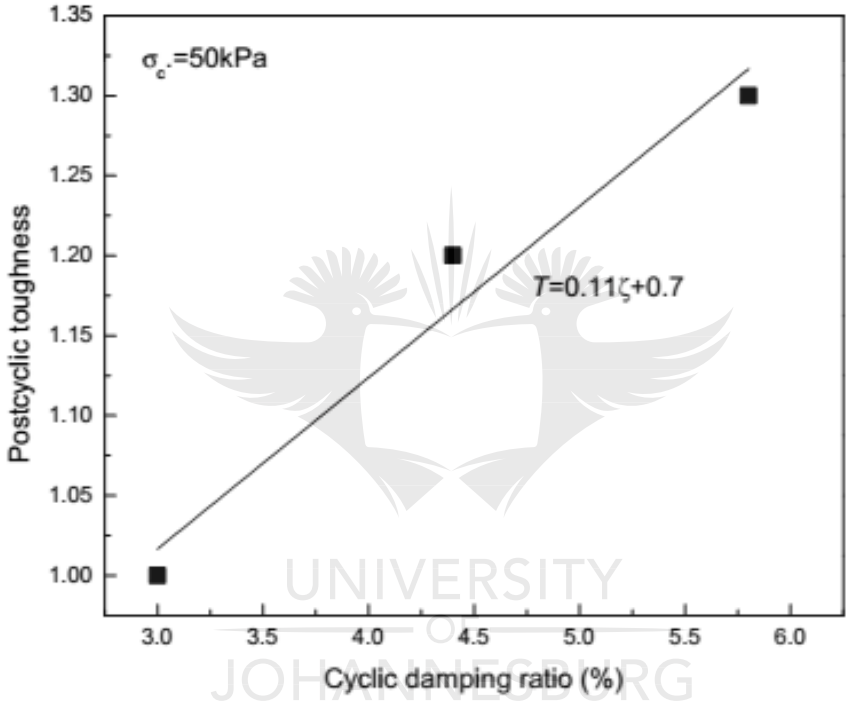

(a)

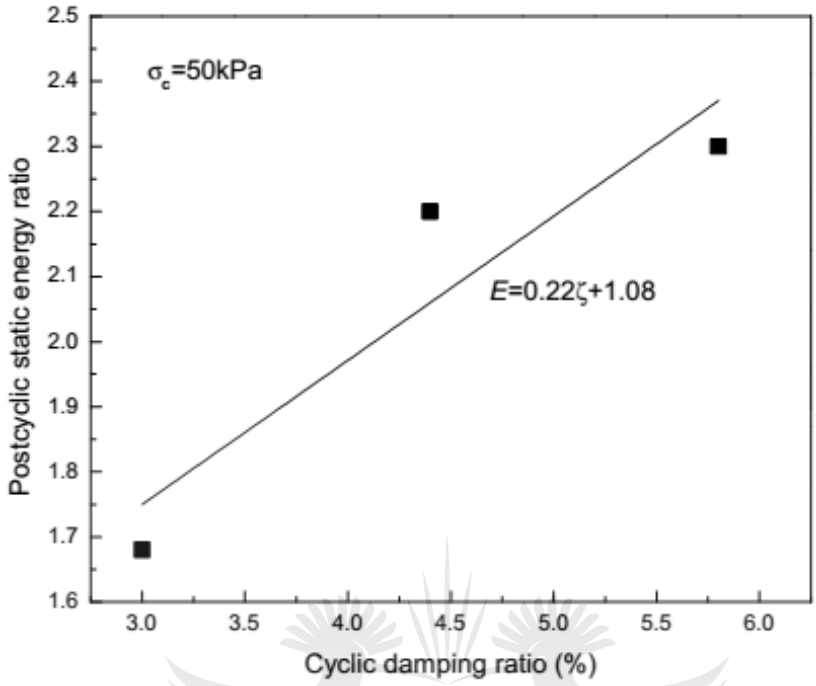

(b)

Figure 8.14: The relationships between dynamic damping ratio and post cyclic properties (a) Toughness (b) Static energy ratio

It is noted that linear relationship is exhibited for both post cyclic static energy ratio and toughness. This implies that post cyclic behaviour is the function of dynamic damping ratio since damping properties of soil are indicative of strain energy stored in the material.

Conclusions

Based on the acquired test results, the following key conclusions are drawn;

1. The fiber inclusions cause increase in shear modulus to fiber content of 0.5% beyond which modulus reduced. The reduction in modulus is attributed to the loss of stiffness of the soil composite due to high percentage of voids. The shear modulus is improved by increasing level of confining pressure.
2. Fiber inclusions enhance damping ratio of the composite due to an improved resistance of the composite to deformation. An increase in confining pressure causes enhanced damping properties.
3. Both permanent strain and cumulative strain reduce with fiber inclusion due to improved resilience to deformation.

4. The reinforced soil exhibits high resistance to liquefaction and high fine content of unreinforced soil improves resistance to liquefaction.
5. Increase in fiber content causes an increase in post cyclic energy absorbing capacity, toughness and static energy ratio of the soil.
6. Linear relationship is indicated between cyclic damping ratio and both post cyclic energy ratio and toughness.
7. In practice, natural fiber inclusion is the seismic retrofitting technique for the earthen structures. This is due to the resilience of the fiber reinforced soil composite to deformation. Resistance to liquefaction of fiber reinforced soil is beneficial to maintain integrity of foundation during earthquake events. It is anticipated that fiber reinforced earthen construction would exhibit resilience to deformation during aftershocks and ensure safe evacuation as evidenced by high post cyclic energy absorbing capacity and toughness, and this is beneficial for the evacuation of people and property. The fiber reinforced soil can be effective used as in-fill for seismic wave barrier walls due to its good damping properties.

References

AI Wahab .R.M and Heckel.G.B .(1995). *Static and Dynamic Strength Properties of a FiberReinforced Compacted Cohesive Soil*. Paper presented at the International Conference on Recent Advances in Geotechnical Earthquake Engineering and Soil Dynamics, Missouri University of Science and Technology.

Alibolandi .M and Moayed.R. (2015). Liquefaction potential of reinforced silty sands. *International Journal of Civil Engineering,, 13,* 195-202.

Amir-Farya.B and Sherif Aggour.M. (2015). Effect of fibre inclusion on dynamic properties of clay. *Geomechanics and Geoengineering*. doi: DOI:10.1080/17486025.2015.1029013

Aqeel Al Adili et al. (2012). Strength of soil reinforced with fiber materials (papyrus). *Soil Mechanics and Foundation Engineering, 48* (6), 241-247.

Blondet et al. (2004). *Earthquake resistant buildings.* Paper presented at the 13th World Conference on Earthquake Engineering Vancouver, B.C., Canada

Das B.M and Ramana.G.V .(2011). *Principles of soil dynamics*. Stamford, USA: Cengage Learning.

El Mohtar et al. (2013). Combined Resonant Column and Cyclic Triaxial Tests for Measuring Undrained Shear Modulus Reduction of Sand With Plastic Fines. *Geotechnical tesing Journal, 36*(4), 1-9.

Ghayoomi et al. (2017). Cyclic Triaxial Test to Measure Strain-Dependent Shear Modulus of Unsaturated Sand. *Int J Geomechanics 17*(9).

Goda et al. (2018). *Scenario-based seismic risk assessment for Malawi using improved information on earthquake sources and local building characteristics. 1*. Paper presented at the 6th European Conference on Earthquake Engineering (16ECEE), Thessaloniki, Greece.

Hardin. B.O and Drnevich.V.P. (1972). Shear modulus and damping in soils: measurement and parameter effects. *Journal of Soil Mechanics and Foundations Division, 6*, 603-624.

Ibraim. E and Fourmont.S. (2006). *Behaviour of sand reinforced with fibers*. Paper presented at the Soil Stress-Strain Behavior: Measurement, Modeling and Analysis Geotechnical Symposium, Roma, Italy.

Indraratna et al. (2016). Laboratory assessment of the role of particle size distribution on the deformation and degradation of ballast under cyclic loading. *Journal of Geotechnical and Geoenvironmental Engineering 142*(7), 04016016.

Kloukinas et al. (2019). *Strength of materials and masonry structures in Malawi*. Paper presented at the The Seventh International Conference on Structural Engineering, Mechanics and Computation, Cape Town, South Africa.

Kokusho.T. (1980). Cyclic triaxial test of dynamic soil properties for wide strain range. . *Soils and Foundations, 20*, 45–60.

Kramer.S.L. (1996). *Geotechnical earthquake engineering*. New Jersey: Prentice Hall.

Kumar et al. (2017). Evaluation of dynamic properties of sandy soil at high cyclic strains. *Soil Dynamics and Earthquake Engineering, 99*, 157-167.

Maheshwari et al. (2012). Effects of reinforcement on liquefaction resistance of Solani sand. *Journal of Geotechnical and Geoenvironmental Engineering, 138*(7), 831–840.

Monkul.M.M and Yamamuro.J.A. (2011). Influence of silt size and content on liquefaction behavior of sands. *Canadian Geotechnical Journal, 48*, 931-942.

Naeini S.A and Baziar. M.H. (2004). Effect of fines content on steadystate strength of mixed and layered samples of a sand,. *Journal of Soil Dynamics and Earthquake Engineering,, 24*, 181-187.

Naeini and Gholampoor.N. (2014). Cyclic behavior of dry silty sand reinforced with a geotextile. *Geotextile Geomembranes, 42*, 611-619.

Noorzad.R and Amini.F. (2014). Liquefaction resistance of babolsar sand reinforced with randomly distributed fibers under cyclic loading. *Soil Dynamics and Earthquake Engineering, 66,* 281-329.

Orakoglua et al. (2017). Dynamic behavior of fiber-reinforced soil under freeze-thaw cycles. *Soil Dynamics and Earthquake Engineering, 101*, 269–284.

Prabakar.J and Sridhar.RS (2002). Effect of random inclusion of sisal fibre on strength behaviour of soil. *Construction and Building Materials, 16*, 123-131.

Sadeghi.M.M and Beig.F.H (2014). Dynamic behavior of reinforced clayey sand under cyclic loading. *Geotextiles and Geomembranes, 42*(5), 564-572.

Sadrekarimi.A (2013). Influence of fines content on liquefied strength of silty sands. *Soil Dynamics and Earthquake Engineering, 55*, 108-119.

Sayida.M.K (2009). *Behaviour of Black Cotton Soil Reinforced with Sisal Fibre.* Paper presented at the 10th National Conference on Technological Trends (NCTT09) India.

Seed H.B and Idriss.I.M.(1970). Soil moduli and damping factors for dynamic response analysis. California: Earthquake Engineering Research Centre, University of California Berkeley.

Vucetic. M and Dobry.R. (1991). Effect of soil plasticity on cyclic response *Journal of Geotechnical Engineering* 117: 89–107.

Vucetic.M and Mortezaie. A. C. (2015). Cyclic secant shear modulus versus pore water pressure in sands at small cyclic strains. *Soil Dynamics and Earthquake Engineering.* 70:60- 72.

Wichtmann et al. (2005). Strain accumulation in sand due to cyclic loading: drained triaxial tests. *Soil Dyn Earthq Eng* 25 (12):967-979.

9 CHAPTER NINE-CONSTITUTIVE MODEL FOR NONLINEAR ELASTIC BEHAVIOUR OF FIBER REINFORCED SOIL UNDER DYNAMIC LOADING: EFFECTS OF MATERIAL ANISOTROPY AND DENSITY

9.1 Introduction

Several models have been proposed for the dynamic properties of unreinforced soil (Hardin and Drnevich, 1972; Kondner and Zelasko, 1963; Matasović and Vucetic, 1993; Vucetic and Dobry, 1991). However, Muge Orakoglu et al (Orakoglua et al., 2017) proposed a model to describe dynamic behaviour of fiber-reinforced soil under freeze-thaw cycles. The model showed a significant influence of fibers on both initial tangential modulus and ultimate cyclic stress of the fiber reinforced soil. Li and Ding (Li and Ding, 2002) formulated a model to describe nonlinear elastic behaviour of fiber reinforced soil under cyclic loading by employing hyperbolic function with two constants describing initial elastic modulus and ultimate cyclic stress. The model constants were assumed to be functions of fiber content, confining pressure and number of cycles. The model showed that initial elastic modulus was sensitive to fiber content and confining pressure. The initial elastic modulus rapidly reduced with increase in loading repetition. However, Li and Ding model did not include effect of fiber distribution orientation, density and fiber aspect ratio. The model did not incorporate strength anisotropy of the fiber reinforced soil. The aforementioned properties of fiber reinforced soil have a bearing on the elastic modulus and the ultimate cyclic stress of the reinforced soil.

This study aims at developing a more updated model to describe nonlinear elastic behaviour of fiber reinforced soil under cyclic loading, by incorporating effects of fiber orientation distribution, density and aspect ratio apart from fiber content, number of cycles and confining pressure. The formulation utilises Li and Ding approach. The fiber reinforced soil is assumed to be composed of fibers lying horizontal to be bedding plane of soil layers. Fiber orientation distribution is assumed to be axisymmetric to the layers of the compacted soil. The model is calibrated by linear regression with multiple variables. The effects of the incorporated variables are evaluated by the variation of the model calibration constants. The calibration of the model utilises data used by Li and Ding in order to provide common basis for comparison.

9.2 Background

The ability of fibers to effectively mobilise tensile resistance depends on their orientation relative to the direction of tensile strains. Therefore, fibers that are orientated in the direction of tensile strain are more effective. The orientation assumed by fibers depends on the specimen mixing and fabrication procedure such as moist tamping.

9.2.1 Distribution of fiber orientation

The non-uniform fiber orientations dictate stress–strain behaviour of the specimen as a result of material anisotropy. A fiber orientation distribution function was proposed by (Michalowski and Cermak, 2002) to describe non- uniform distribution of fiber orientation, and can also be used as a modelling tool to explain the anisotropic constitutive features of fiber reinforced soil specimens subjected to a particular loading condition. The form of the fiber orientation distribution function based on the assumption that the fiber distribution is axisymmetric with respect to the vertical axis of the compacted layers is adopted. With reference to the spherical coordinates in figure 9.1, a generalised fiber orientation distribution function $f(\theta)$ which represents the volumetric concentration of fibers in an infinitesimal volume dV having an angle θ to horizontal, is of the form of equation 9.1 (Diambra et al., 2007; Michalowski and Cermak, 2002).

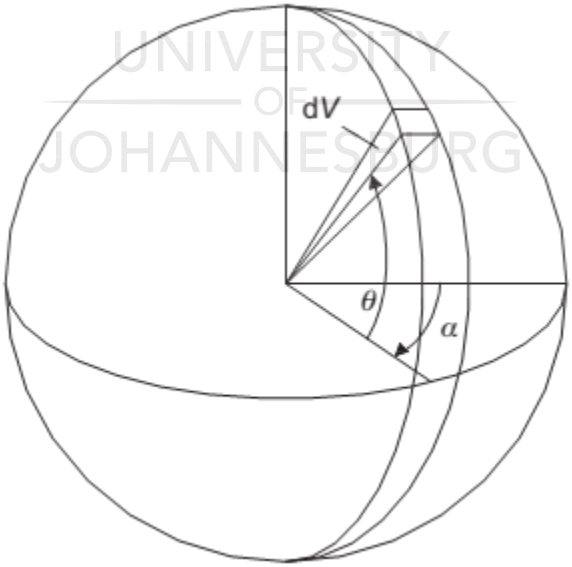

Figure 9.1:Sphere and coordinates used to define orientation distribution function adapted from (Diambra et al., 2007).

$$f(\theta) = \rho_f \left(A + B\left|cos^n \theta\right|\right) \tag{9.1}$$

where $\rho_{.fv}$ is the average volumetric fiber concentration defined by equation 9.2.

$$\rho_f = \frac{v_f}{v_s} \tag{9.2}$$

where v_f and v_s are volume fraction of fibers and soil, respectively. Constants Z, B and n in Eq1are defined by equation 9.3.

$$B = \frac{1 - A}{\int_0^{\pi/2} \cos^{n+1}(\theta) d\theta} \tag{9.3}$$

When B=0, A=1 and fiber orientation distribution function becomes isotropic, $f(\theta) = \rho_f$. Alternatively, B may be determined by equation 9.4 for any positive even integer of n.

$$B = (1 - A)\frac{(1-n)!!}{n!!} \tag{9.4}$$

where double factorial (n!!=2, 4, 6 …. n) and (n+1=3,5,7….. n+1).

The average fiber concentration is expressed as equation 9.5.

$$\rho_{fv} = \frac{1}{V}\int_V \rho(\theta) dV \tag{9.5}$$

The fiber orientation distributions for A=0 and various n values (0.4, 0.5 and 2) are shown in Fig 9-1. The more convenient form of the fiber distribution function is obtained for n=2, A=0 and θ=0, representing a more realistic fiber distribution that is horizontal to the bedding plane and no fibers are orientated in vertical direction. Therefore, from equations 9.1 and 9.4, a more practical fiber distribution function can be presented by equation 9.6 for n=2 and B=3/2.

$$\rho(\theta) = \frac{3}{2}\cos^n(\theta) \tag{9.6}$$

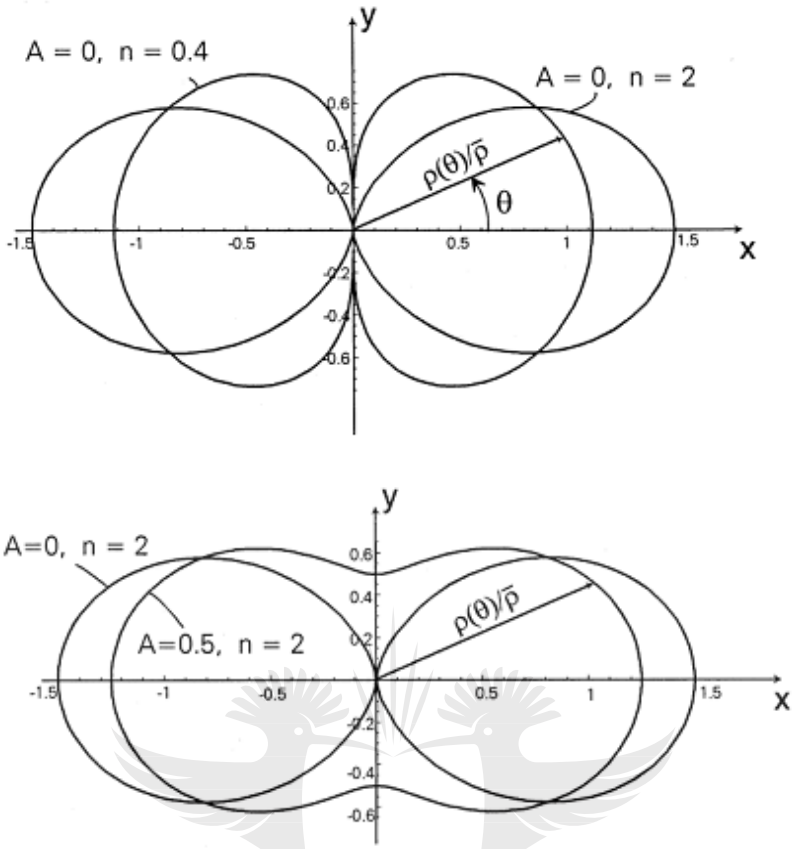

Figure 9.2: Fiber orientation distribution adapted from (Michalowski and Cermak, 2002).

9.2.2 Determination of soil dynamic parameters

The dynamic shear stress and dynamic shear strain of soil can be determined from the equation 9.7 and equation 9.8, respectively.

$$\tau_d = \frac{\sigma_d}{2} \tag{9.7}$$

$$\gamma_{dy} = \varepsilon_d(1+\mu) \tag{9.8}$$

where σ_d and ε_d are the axial dynamic shear stress and axial cyclic strain, respectively.

The dynamic shear stress and strain are expressed by hyperbolic function according to Hardin model (Hardin and Drnevich, 1972) in equation 9.9.

$$\tau_i = \frac{\gamma_i}{a + b\gamma_i} \tag{9.9}$$

where a and b are the fitting parameters and a > 0 and b > 0.

Kondner and Zelasko(Kondner and Zelasko, 1963) studied the stress and strain curves of many soils and expressed dynamic shear stress with hyperbola as equation 9.10.

$$\tau_i = \frac{G_i \gamma}{1 + \frac{G_i}{\tau_{ult}} \gamma} \tag{9.10}$$

where G_i is the initial tangential modulus at $\gamma \approx 0$ and τ_{ult} is the dynamic ultimate stress under dynamic loading. Matasović and Vucetic(Matasović and Vucetic, 1993) improved Kondner and Zelesko function by introducing two curve fitting parameters shown in equation 9.11.

$$\tau_i = \frac{G_i \gamma}{1 + \beta \left(\frac{\gamma}{\gamma_f} \right)^n} \tag{9.11}$$

where γ_f is the reference strain.

From the hysteresis loop of the dynamic shear stress and dynamic shear strain of soil, the slope of loop is the dynamic shear modulus which is expressed as equation 9.12.

$$G_d = \frac{\tau_d^*}{\gamma_d^*} \tag{9.12}$$

where τ_d^* and γ_d^* are the dynamic shear stress and strain amplitude, respectively. The dynamic shear modulus as described by Hardin and Matasović is shown in equation 9.13 and equation 9.14, respectively.

$$G_d = \frac{1}{a + b\gamma_i} \tag{9.13}$$

$$G_d = \frac{G_o}{1 + \beta \left(\frac{\gamma}{\gamma_f} \right)^n} \tag{9.14}$$

where G_d is the dynamic shear modulus at $\gamma \approx a$ and G_o is the initial shear modulus.

9.3 Constitutive model for nonlinear elastic behaviour of fiber reinforced soil

The previous proposed model was developed based on the assumption that the fiber distribution was isotropic and uniformly distributed. The effects of fiber orientation, composite density and fiber aspect ratio were neglected. However, fiber reinforced soil exhibits strength anisotropy due to the non-uniform distribution of fibers emanating from material preparation protocol. In practice, it is impossible to obtain uniform distribution of fibers as the mixing of soil composite is done by machines. For the purpose of design of fiber reinforced geosystems, a realistic approach is to utilise models that incorporate effects of strength anisotropy of the fiber reinforced soil. The aforementioned limitations in the published model prompted an attempt to develop a more improved model by addressing identified limitations.

9.3.1 Formulation of the model with fiber distribution anisotropy and density

The shear stress versus shear strain of the fiber reinforced soil under dynamic loading can be presented in terms of the second invariants of deviatoric tensors given by equation 9.15.

$$\sigma^s = G_d \varepsilon^s \tag{9.15}$$

where $\sigma^s = \sqrt{3J_2}$ and $\varepsilon^s = \sqrt{3I_2}$, J_2 and I_2 are the second order invariants of stress and strain tensors, respectively given by equation 9.16 and equation 9.17.

$$J_2 = \frac{1}{6}\left[(\sigma_1 - \sigma_2)^2 + (\sigma_2 - \sigma_3)^2 + (\sigma_3 - \sigma_1)^2\right] \tag{9.16}$$

$$I_2 = \frac{1}{6}\left[(\varepsilon_1 - \varepsilon_2)^2 + (\varepsilon_2 - \varepsilon_3)^2 + (\varepsilon_3 - \varepsilon_1)^2\right] \tag{9.17}$$

In a dynamic triaxial test, the principal quasi triaxial stresses are such that $\sigma_1 \neq (\sigma_3, \sigma_2)$, $\sigma_2 = \sigma_3$ therefore, equation 9.16 and 9.17 can be reduced to $J_2 = \frac{1}{3}(\sigma_1 - \sigma_3)^2$ and $I_2 = \frac{1}{3}(\varepsilon_1 - \varepsilon_3)^2$. Stress- strain relationship in equation becomes equation 9.18 and simplified as equation 9.19.

$$\sqrt{J_2} = G\sqrt{I_2} \tag{9.18}$$

$$(\sigma_1 - \sigma_3) = G(\varepsilon_1 - \varepsilon_3) \tag{9.19}$$

Shear modulus G_d is a function of mechanical properties of the reinforced soil, i.e., initial shear modulus and strength that are also functions of fiber properties, distribution orientation and composite relative density. The variation of dynamic shear modulus with fiber properties, orientation distribution and composite relative density is presented in the form of equation 9.20.

$$G_d = \psi\left(\frac{3}{2}\rho_f \cos^2\theta + 1\right)\left(\frac{\sigma_c}{P_a}\right)e^{-\beta\rho_f}\, dN \tag{9.20}$$

where ψ is a model parameter, $\left(\frac{3}{2}\rho_f \cos^2\theta + 1\right)$ is the function of fiber content and orientation distribution, θ is fiber orientation angle in (rad), $\left(\frac{\sigma_c}{P_a}\right)$ is the function of confining pressure P_a=1kPa is atmospheric pressure, $e^{-\beta\rho_f}$ is the function of composite's relative density, β is the fiber aspect ratio, ρ_f is fiber content in (%) and N is the function of number of cycles. $e^{-\beta\rho_f}$ is the mathematical decay function, representing decrease in composite's relative density with fiber content and γ_d is relative density of unreinforced soil.

To formulate the dynamic shear modulus function in quasi-triaxial space, a hyperbolic function suggested by (Hardin and Drnevich, 1972), equation 9.13 is adopted such that constants a=A and b=B, are the functions of confining pressure σ_c, fiber content ρ_f, fiber orientation distribution function $\cos^n\theta$, number of cycles N_c and composite's relative density η. The hyperbolic function therefore takes a form of equation 9.21 and equation 9.22·

$$G_d = \left(\frac{\sigma_1 - \sigma_3}{\varepsilon_1 - \varepsilon_3}\right) = \frac{1}{A(\sigma_c, N, \rho_f, \cos^n\theta, \eta) + B(\sigma_c, N, \rho_f, \cos^n\theta, \eta)\varepsilon_d} \tag{9.21}$$

$$\frac{1}{G_d} = \left(\frac{\varepsilon_1 - \varepsilon_3}{\sigma_1 - \sigma_3}\right) = A(\sigma_c, N, \rho_f, \cos^n\theta, \eta) + B(\sigma_c, N, \rho_f, \cos^n\theta, \eta)\varepsilon_d \tag{9.22}$$

Equation 9.22 shows linear relationship between dynamic shear modulus $1/G_d$ and dynamic shear strain

ε_d such that A can be determined as an intercept and B as the slope of the best-fit hyperbola for dynamic shear stress-strain curve $(1/G_d - \varepsilon_d)$. The constants A and B represent initial tangential shear modulus $\frac{1}{G_i}$ and dynamic ultimate shear stress $\frac{1}{\sigma_{ult}}$, respectively. The linear relation allows direct calibration of parameters from the experimental results. In this study, parameters A and B are assumed to take a form of equation 9.23 and equation 9.24, respectively.

$$A(\sigma_c, N, \rho_f, \cos^n\theta, \eta) = \psi_1 \left(\frac{\sigma_c}{P_a}\right)^{a_1} \left(\frac{3}{2}\rho_f \cos^2\theta + 1\right)^{a_2} \left(e^{-\beta\rho_f}\gamma_d\right)^{a_3} (N)^{a_4} \quad (9.23)$$

$$B(\sigma_c, N, \rho_f, \cos^n\theta, \eta) = \psi_2 \left(\frac{\sigma_c}{P_a}\right)^{b_1} \left(\frac{3}{2}\rho_f \cos^2\theta + 1\right)^{b_2} \left(e^{-\beta\rho_f}\gamma_d\right)^{b_3} (N)^{b_4} \quad (9.24)$$

where a_i (i = 1,….,4) and b_i (i = 1,…,4) are constants obtained from dynamic triaxial tests. P_a is atmospheric pressure (kPa) for dimensionless term $\frac{\sigma_c}{P_a}$ and other parameters are as described in the previous section.

9.3.2 Calibration of model parameters

The constitutive model parameters are calibrated by employing linear hyperbolic function in equation 9.22, using data presented in the literature (Li and Ding, 2002) of dynamic triaxial tests of fiber reinforced soil. This is done by firstly finding logarithms of equation 9.23 and equation 9.24. The corresponding logarithmic expressions are shown in equation 9.25 and equation 9.26.

$$\log A = \log\psi_1 + a_1 \log\left(\frac{\sigma_c}{P_a}\right) + a_2 \log\left(\frac{3}{2}\rho_f \cos^2\theta + 1\right) + a_3 \log\left(e^{-\beta\rho}\gamma_d\right) + a_4 \log(N) \quad (9.25)$$

$$\log B = \log\psi_2 + b_1 \log\left(\frac{\sigma_c}{P_a}\right) + b_2 \log\left(\frac{3}{2}\rho_f \cos^2\theta + 1\right) + b_3 \log\left(e^{-\beta\rho}\gamma_d\right) + b_4 \log(N) \quad (9.26)$$

The linear regression with multiple variables is adopted to determine coefficients a_i and b_i, assuming that fibers lie horizontally and parallel to the bedding plane during compaction, such that $\theta = 0$. The data used to calibrate model parameters is shown in Table 9.1 with fiber aspect ratio of 250.

Table 9.1 : Data for calibrating model parameters adapted from (Li and Ding, 2002), $\theta = 0$, β=250, γ_d =1.66

Specimen ID	ρ	σ_o	N	logA	logB	$log\left(\frac{\sigma_c}{P_a}\right)$	$log\left(\frac{3}{2}\rho_f + 1\right)$	$log\left(e^{-\beta\rho_f}\gamma_d\right)$	log N
1	0.2	50	10	-7.15	-2.51	1.7	0.001300933	0.002960847	1
2	0.2	100	10	-7.34	-2.57	2	0.001300933	0.002960847	1
3	0.2	150	10	-7.44	-2.64	2.18	0.001300933	0.002960847	1
4	0.2	50	50	-7	-2.49	1.7	0.001300933	0.002960847	1.7
5	0.2	100	50	-7.19	-2.54	2	0.001300933	0.002960847	1.7
6	0.2	150	50	-7.3	-2.6	2.18	0.001300933	0.002960847	1.7
7	0.2	50	100	-6.94	-2.48	1.7	0.001300933	0.002960847	2
8	0.2	100	100	-7.13	-2.52	2	0.001300933	0.002960847	2
9	0.2	150	100	-7.23	-2.59	2.18	0.001300933	0.002960847	2
10	0.5	50	10	-7.22	-2.55	1.7	0.003245055	-0.322760014	1
11	0.5	100	10	-7.4	-2.59	2	0.003245055	-0.322760014	1
12	0.5	150	10	-7.51	-2.68	2.18	0.003245055	-0.322760014	1
13	0.5	50	50	-7.07	-2.55	1.7	0.003245055	-0.322760014	1.7
14	0.5	100	50	-7.26	-2.59	2	0.003245055	-0.322760014	1.7
15	0.5	150	50	-7.37	-2.67	2.18	0.003245055	-0.322760014	1.7
16	0.5	50	100	-7.01	-2.54	1.7	0.003245055	-0.322760014	2
17	0.5	100	100	-7.2	-2.57	2	0.003245055	-0.322760014	2
18	0.5	150	100	-7.3	-2.66	2.18	0.003245055	-0.322760014	2
19	0	50	10	-7.1	-2.47	1.7	0	0.220108088	1
20	0	100	10	-7.29	-2.54	2	0	0.220108088	1
21	0	150	10	-7.4	-2.6	2.18	0	0.220108088	1
22	0	50	50	-6.95	-2.46	1.7	0	0.220108088	1.7
23	0	100	50	-7.14	-2.52	2	0	0.220108088	1.7
24	0	150	50	-7.25	-2.58	2.18	0	0.220108088	1.7
25	0	50	100	-6.89	-2.45	1.7	0	0.220108088	2
26	0	100	100	-7.08	-2.51	2	0	0.220108088	2
27	0	150	100	-7.19	-2.56	2.18	0	0.220108088	2

The calibrated model coefficients for both initial shear modulus and ultimate shear stress are shown in Table 9.2.

Table 9.2: Calibrated model coefficients

Parameter	Model coefficients				
Initial shear modulus A	ψ_1	a_1	a_2	a_3	a_4
	0.00302	-0.62	-381	-2.07	0.21
Ultimate shear stress B	ψ_2	b_1	b_2	b_3	b_4
	0.02	-0.24	1298	7.9	0.029

The calibrated models for initial shear modulus A and ultimate shear stress B are given by equation 9.27 and equation 9.28, respectively.

$$A = \frac{1}{G_i} = 3.02x10^{-3}\left(\frac{\sigma_c}{P_a}\right)^{-0.62}\left(\frac{3}{2}\rho_f + 1\right)^{-381}\left(1.66e^{-250\rho_f}\right)^{-2.07}(N)^{0.21} \tag{9.27}$$

$$B = \frac{1}{\sigma_{ult}} = 0.02\left(\frac{\sigma_c}{P_a}\right)^{-0.24}\left(\frac{3}{2}\rho_f + 1\right)^{1298}\left(1.66e^{-250\rho_f}\right)^{7.9}(N)^{0.029} \tag{9.28}$$

In order to decouple synergic effects of fiber distribution orientation and density on the model sensitivity, decoupling coefficients related to density, $\mu_1 = \gamma_d^{\,1-a_3}$ and $\mu_2 = \gamma_d^{\,1-b_3}$ for initial shear modulus and ultimate shear stress, respectively are introduced. Therefore equation 9.27 and equation 9.28 are expressed as equation 9.29 and equation 9.30.

$$A = \frac{1}{G_i} = 3.02x10^{-3}\left(\gamma_d^{\,3.07}\right)\left(\frac{\sigma_c}{P_a}\right)^{-0.62}\left(\frac{3}{2}\rho_f + 1\right)^{-381}\left(\gamma_d e^{-250\rho_f}\right)^{-2.07}(N)^{0.21} \tag{9.29}$$

$$B = \frac{1}{\sigma_{ult}} = 0.02\left(\gamma_d^{\,-6.9}\right)\left(\frac{\sigma_c}{P_a}\right)^{-0.24}\left(\frac{3}{2}\rho_f + 1\right)^{1298}\left(\gamma_d e^{-250\rho_f}\right)^{7.9}(N)^{0.029} \tag{9.30}$$

It can be noted that when fiber content is zero, the impact of fibers is eliminated. However, contribution of density is equivalent to that of unreinforced soil.

For β=250 and γ_d=1.66, the general constitutive model with anisotropic fiber distribution for dynamic shear modulus is given by equation 9.31.

$$G_d = \frac{1}{0.014\left(\frac{\sigma_c}{P_a}\right)^{-0.62}\left(\frac{3}{2}\rho_f + 1\right)^{-381}\left(1.66e^{-\beta\rho_f}\right)^{-2.07}(N)^{0.21} + \left(6.05x10^{-4}\left(\frac{\sigma_c}{P_a}\right)^{-0.24}\left(\frac{3}{2}\rho_f + 1\right)^{1298}\left(1.66e^{-\beta\rho_f}\right)^{7.9}(N)^{0.029}\right)\varepsilon_d} \quad (9.31)$$

9.3.3 Parametric study and discussion

The impact of model variables on sensitivity is evaluated by performing parametric study with varying model variables. Figures 9.3a and b show the impact of fiber content and confining pressure on the sensitivity of the model parameters.

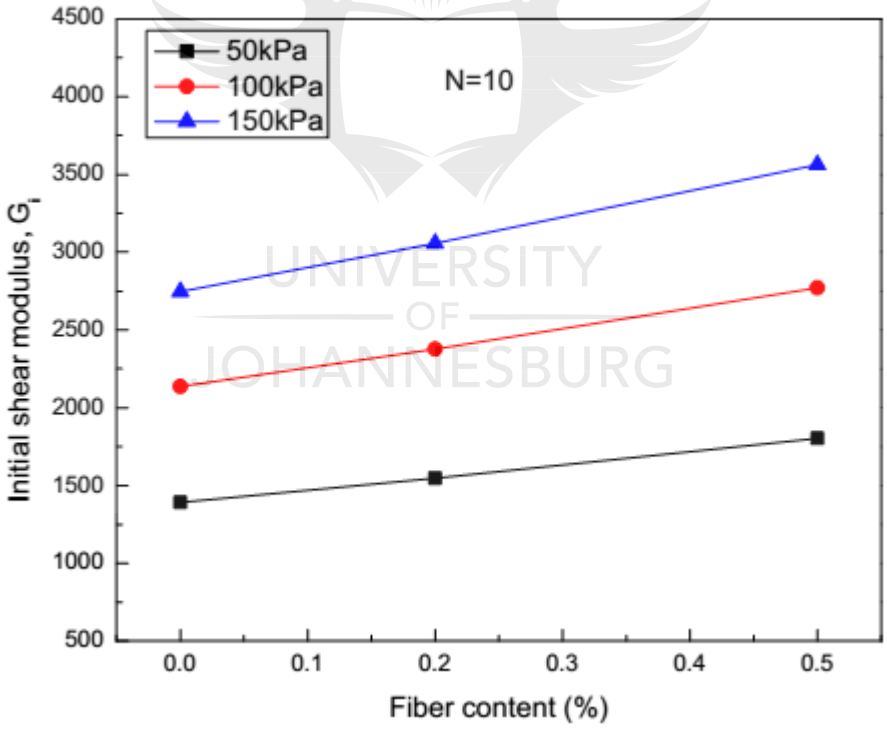

(a)

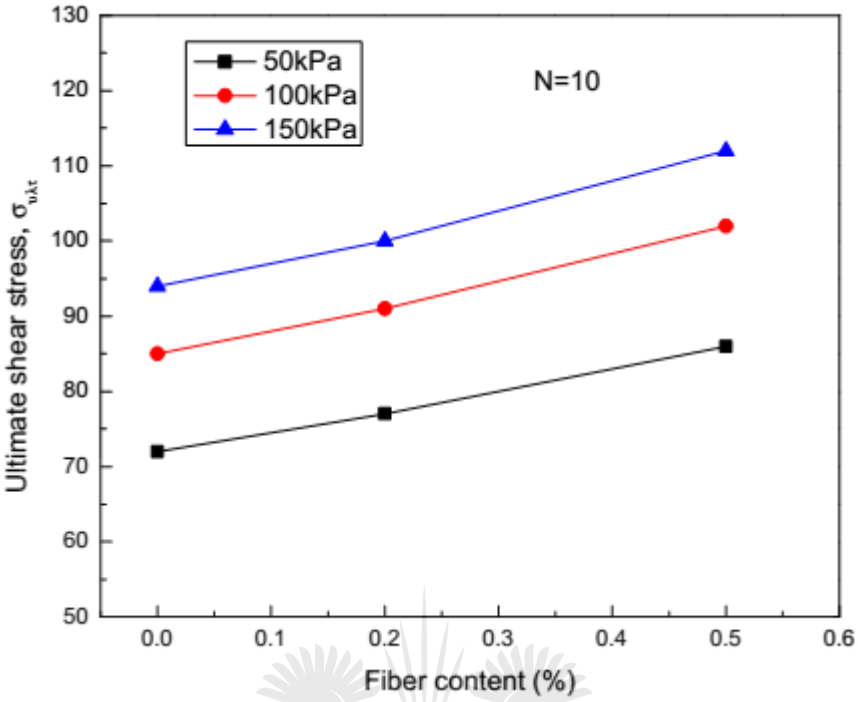

(b)

Figure 9.3: Impact of fiber content on the model parameters (a) Initial shear modulus (b) Ultimate shear stress.

It is shown that an increase in the initial shear modulus value of about 30% occurs with increase in fiber content to 0.5%. On the other hand, an increase in ultimate shear stress of about 18% occurs with increase in fiber content to 0.5%. The parameter values are increased with confining pressure. This implies that initial shear modulus is more sensitive to change in fiber content than ultimate shear stress and also with increase in confining pressure.

Figures 9.4a and b show impact of number of cyclic cycles on sensitivity of the model parameters.

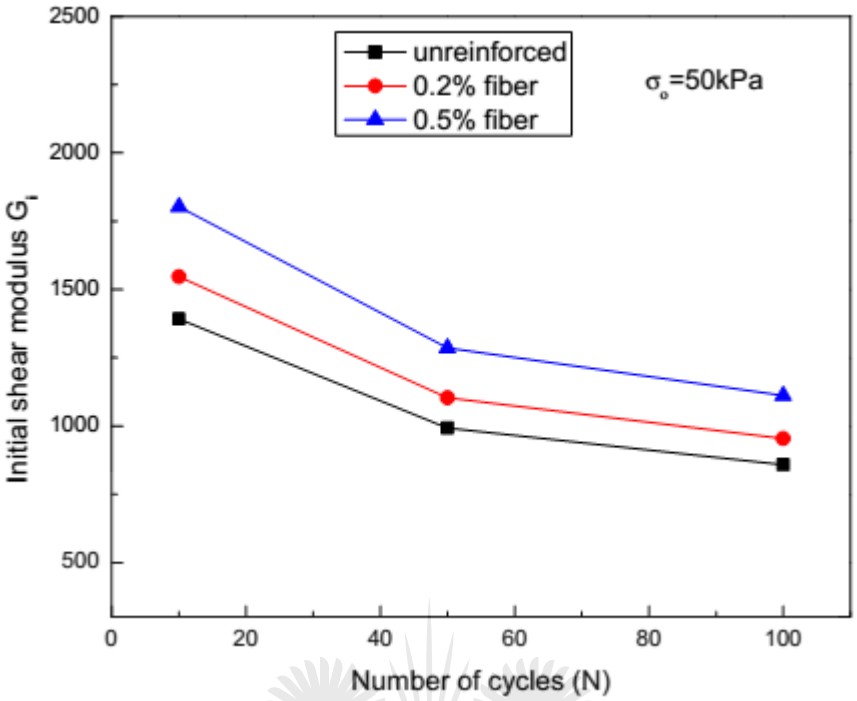

(a)

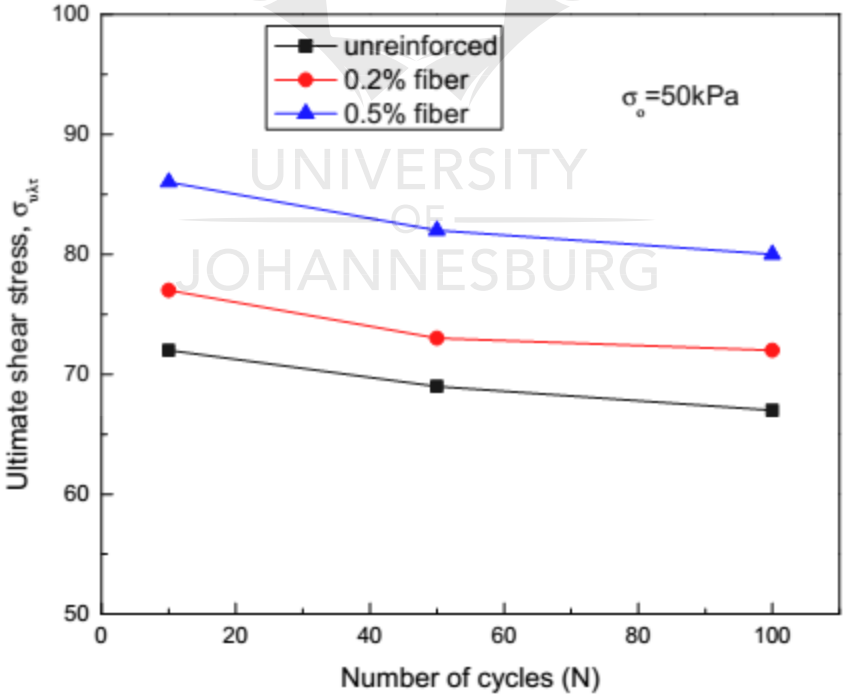

(b)

Figure 9.4: Impact of number of cycles on the model parameters (a) Initial shear modulus (b) Ultimate shear.

It is shown that initial shear modulus increases to about 38% when increase in number of cyclic cycles is 100. On the other hand, decrease in the ultimate shear stress of about 7% occurs with increase in number of cyclic cycles to 100. The parameter values are increased with fiber content. This implies that initial shear modulus is more sensitive to periodic loading than ultimate shear and weakens with progression in periodic loading.

9.3.4 Comparative analysis of isotropic and anisotropic constitutive models

The calibrated constitutive model for the isotropic fiber reinforced soil, assuming that effects of fiber orientation distribution and composite's relative density are negligible is given by equation 9.32 and equation 9.33.

$$A = \frac{1}{G_i} = 5.1x10^{-7}\left(\frac{\sigma_c}{P_a}\right)^{-0.62}\left(\rho_f + 1\right)^{-53}\left(N\right)^{0.21} \tag{9.32}$$

$$B = \frac{1}{\sigma_{ult}} = 7.9x10^{-3}\left(\frac{\sigma_c}{P_a}\right)^{-0.24}\left(\rho_f + 1\right)^{-36}\left(N\right)^{0.029} \tag{9.33}$$

The comparison of impact of variables on model parameters is shown in Table 9.3.

Table 9.3: Comparison of impact of variables on model parameters for isotropic and anisotropic cases, N=10

Fiber content	Isotropic		Anisotropic	
	Initial shear modulus ($x10^3$)	Ultimate shear stress ($x10^3$)	Initial shear modulus($x10^3$)	Ultimate shear stress($x10^3$)
0	13670	0.302	1.4	0.072
0.2	15198	0.325	1.6	0.077
0.5	17807	0.362	1.8	0.086

It is shown that assuming isotropic case to fiber reinforced soil exaggerates the impact of variables on model parameters.

The applicability of the models (isotropic and anisotropic) was verified by predicting shear modulus degradation of the soil composite with varying shear strain at various fiber content and density. The high- strain cyclic triaxial tests were performed on the fiber reinforced composite (0.2% fiber content) and unreinforced soil with average density of 1.9g/cm ^{3}. The maximum

shear modulus of the tested soil composite was estimated using equation 8.3. The normalised shear modulus of the tested soil and the data from the literature were plotted together in order to assess prediction accuracy of the models. Figure 9.5 shows estimated normalised shear moduli by the models with 10 cyclic cycles and also normalised shear modulus curves from the experimental results and literature.

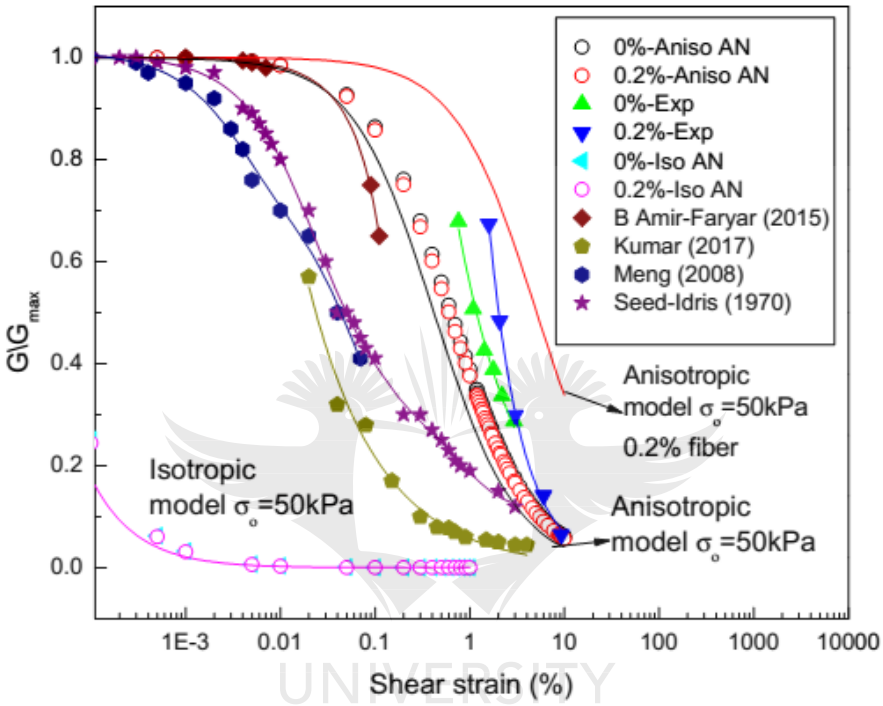

(a)

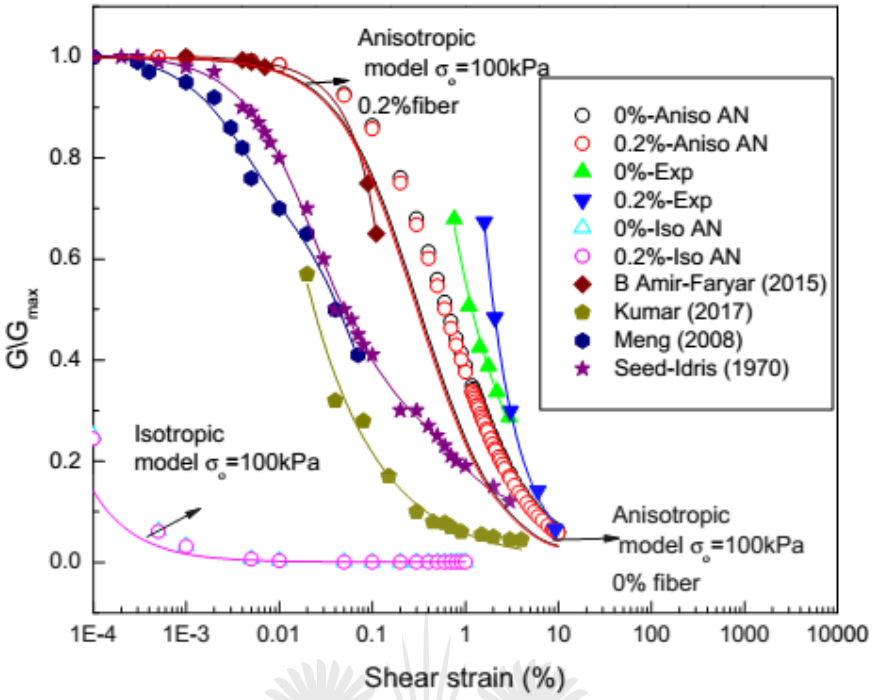

(b)

Figure 9.5: Predicted normalised shear modulus (a) at confining pressure of 50kPa (b) at confining pressure of 100kPa and 10 number of cycles.

It is noted that anisotropic model is relatively accurate at high strain levels while isotropic model shows significant modulus degradation at very low strain. Increase in confining pressure causes marginal shift of the on-set of modulus degradation towards low strain values. The predicted modulus degradation with larger number of cyclic cycles (100) is shown in figure 9.6.

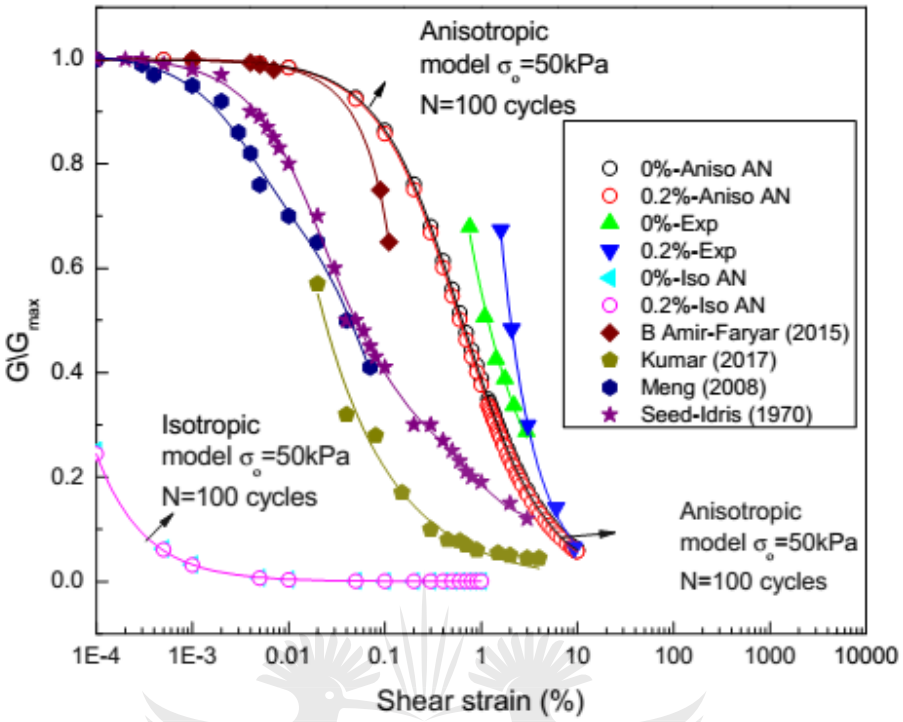

Figure 9.6: Predicted modulus degradation with large number of cyclic cycles (100).

It is noted that the on-set of modulus degradation shifts towards high strain value with large number of cyclic cycles for anisotropic model. On the other hand, modulus degradation shifts towards low strain value for isotropic model. The effect of soil density on the modulus degradation is shown in figure 9.7.

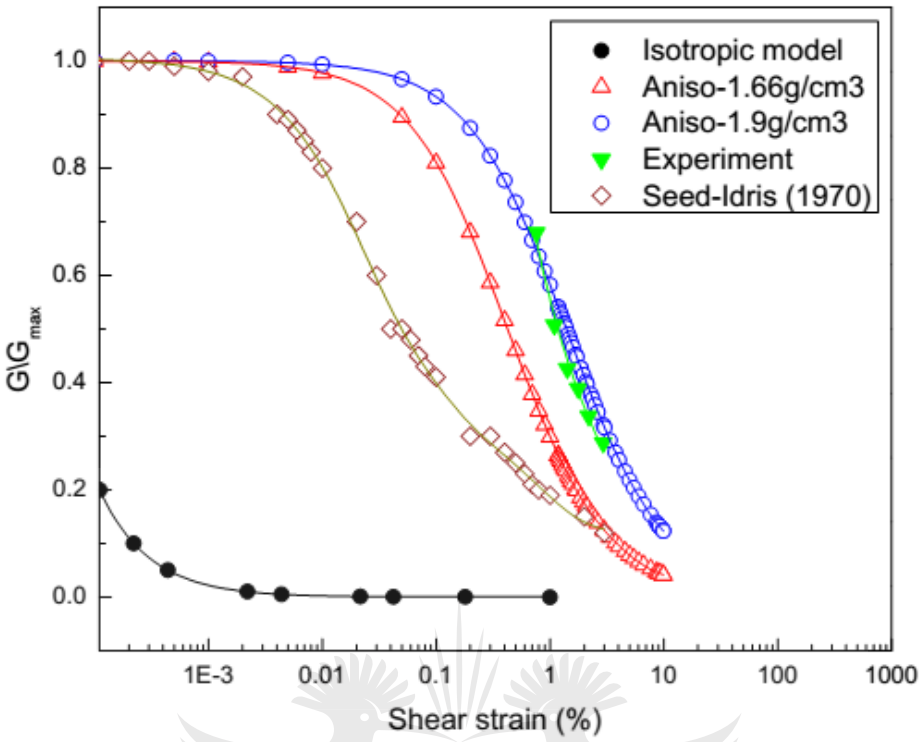

Figure 9.7: Predicted modulus degradation with various soil density.

It is noted that the on-set of shear modulus degradation shifts towards high strain values with increase in soil density. This agrees with typical dynamic response of the soil. In dense soil, the shear modulus degrades with relatively high applied strain amplitudes.

Conclusions and comments

An attempt to formulate constitutive model for non- linear elastic behaviour of fiber reinforced soil under dynamic loading is undertaken. Hardin hyperbolic function is adopted to present the nonlinear stress–strain curve under cyclic loading. The anisotropic properties of soil composite are incorporated by introducing fiber orientation distribution function that is coupled with decay of composite density with increase in fiber content. Nonlinear elastic modulus is assumed to be a function of shear strain and two dependent variables, representing initial tangential modulus and ultimate cyclic loading stress, respectively. Ten constitutive coefficients of the nonlinear elastic model with anisotropic soil properties are calibrated using testing curves from triaxial shear tests presented in the literature. The calibration of parameters is determined using the linear regression with multiple variables. The impact of model variables on the sensitivity of model parameters is evaluated by parametric study. The comparative analysis between isotropic and anisotropic composite scenarios is performed. It is shown that initial tangential shear model is

more sensitive to change in fiber content and confining pressure than ultimate cyclic shear stress. The initial modulus and ultimate shear stress reduce with increase in number of cycles. If the soil composite is assumed to be isotropic, the model variables are overestimated. This implies that incorporating anisotropic properties of soil composite is a more realistic approach to estimate nonlinear elastic behaviour of fiber reinforced soil under dynamic loading. The prediction of shear modulus degradation with anisotropic model is relatively accurate at high strain level while isotropic model shows high sensitivity at very low strain levels.

This work is the first attempt to present anisotropic nonlinear elastic behaviour of fiber reinforced soil and is an extension to what was proposed in the literature for isotropic behaviour. The proposed model is a convenient tool for analysing behaviour of fiber reinforced soil under dynamic loading for geosystems design purposes. However, model parameters are subjective to fiber properties (length and diameter) and the type of soil.

References

Diambra et al. (2007). Determination of fibre orientation distribution in reinforced sands. *Ge´otechnique, 57*(7), 623–628. doi: doi: 10.1680/geot.2007.57.7.623

Hardin B.O and Drnevich.V.P. (1972). Shear modulus and damping in soils: measurement and parameter effects. *Journal of Soil Mechanics and Foundations Division, 6*, 603-624.

Kondner .R.L and Zelasko. J.S. (1963). *A hyperbolic stress–strain formulation of sands*

(1) 289-324; 1963. Paper presented at the 2nd Pan-American Conference on Soil Mechanics and foundation Engineering Sao Paulo, Brazil.

Li.J and Ding.DW (2002). Nonlinear elastic behavior of fiber reinforced soil under cyclic loading. *Soil Dynamic and Earthquake Engineering, 22* (22), 977–983.

Matasović. N and Vucetic.M. (1993). Cyclic characterization of liquefiable sands. *J Geotech Eng, 119*(11), 1805–1822.

Michalowski.R.L and Cermak.J. (2002). Strength anisotropy of fiber reinforced sand. *Computers and Geotechnics, 29*, 279-299.

Orakoglua et al. (2017). Dynamic behavior of fiber-reinforced soil under freeze-thaw cycles. *Soil Dynamics and Earthquake Engineering, 101*, 269–284.

Vucetic and Dobry. (1991). Effect of soil plasticity on cyclic response *Journal of Geotechnical Engineering, 117*, 89–107.

10 CHAPTER TEN-EFFECTS OF SISAL FIBER INCLUSIONS AND PRE-COMPRESSION ON THE STRENGTH PROPERTIES OF LIME–FLY ASH STABILISED SOIL

10.1 Introduction

The compressibility of fly ash is highly affected by lime dosage and duration of load increments. The addition of lime to fly ashes triggers hydration process that in turn causes formation of cementitious compounds that are responsible for enhanced cementation of particles. The lime-fly ash mixtures exhibit low compressibility and high equilibrium void ratio values. On the other hand, longer duration of load increments allows considerable curing time for the pozzolanic reaction between lime and fly ash. Ultimately, the improved stiffness and strength due to pozzolanic reaction offer resistance of fly ash to compression (Moghal and Sivapullaiah, 2011).

To allow pozzolanic reaction to occur in fly ash mixtures, an activator such as Portland cement or lime is added in ratio of 1: 2 to raise the pH up to 12.4. In some cases, the self-cementing fly ash possesses calcium oxide (CaO) in concentrations typically ranging from 20 to 30 percent which allow pozzolanic reaction to occur. Lime can also be added when concentration of calcium oxides is insufficient to facilitate pozzolanic reaction

Using fly ash for soil stabilisation, promotes sustainable construction through reduction of energy use and emissions of greenhouse gases (Tastan et al., 2011). Although field mechanised mixing and compression of lime-fly ash mixtures may promote carbon foot print emission, the application of natural fibers in construction ensures the balance between emitted and consumed carbon. Spreading moist fly ash and hydrated lime using surfacing paver is an ideal approach to reducing dust emission during mixing operations.

The aim of the investigation was to evaluate strength development and resilience of lime-fly ash fiber reinforced soil when subjected to premature uniaxial loading, typically experience during construction work.

10.2 Materials and experimental programme

10.2.1 Materials

The soil sample used in this study was prepared and characterised as in section 3.1.1 according to ASTM D1140-17 (ASTM D1140-17, 2017). The soil properties are summarised in Table 3.1.

Sisal fibers with length of 25mm were used. The summary of the fiber properties is shown in Table 3.3. Commercially available hydrated lime and fly ash (class F) were used for soil stabilisation. The chemical compositions of lime and fly ash are summarised in Table 3.4.

The minimum lime demand for the soil was approximated by conducting Eades-Grim test according to ASTMD 6276 (ASTM D6276, 2019) and was found to be 7% of lime. The mix design for stabilising agents was 1:2 of lime and fly ash respectively according to (Kumar et al., 2007).

10.2.2 Sample preparation

The fiber dosages were determined by percentage dry weight of soil. The fiber dosages used herein were 0.25%, 0.5%, 0.75% and 1%. In preparing the sample, designated fiber content was manually mixed with the stabilised soil in dry state using hands. Great care was taken to achieve uniform distribution of fibers. After dry mixing, water of equivalent optimum moisture content of 11% was added to the soil-fiber composite and mixed thoroughly until a homogeneous soil composite was formed. The mixture of the soil composite was allowed to mellow for 1h in a waterproof and airtight plastic bag prior to specimen fabrication to allow the sample reach equilibrium state prior to curing. The moisture content of ± 2% (OMC) was applied to provide for marginal loss of moisture during specimen preparation.

10.2.3 Specimen preparation for compression test

After mellowing the sample, specimens were prepared in the mould of diameter 55mm and height 120mm, by static compaction of the soil composite into 3 layers using hydraulic jack mounted with pressure gauge. The top surface of each layer was ripped and scarified before adding a succeeding layer in order to create a continuous mass of the composite. To achieve average maximum dry density as obtained by Proctor compaction test, compaction pressure 0f 5MPa was used to compact all specimens. The specimens were extruded by the jack at a constant displacement of 1mm/stroke. Immediately after extrusion, specimens were wrapped and sealed in an airtight plastic bag to prevent carbonation prior to curing.

The damp cloth was placed underneath the specimen to control loss of hydration moisture during curing. The specimens were eventually cured in an oven at 40^{o}C.

Accelerated curing at 40^{o}C was employed to expedite pozzolanic reactions in order to simulate long term field conditions (ASTM D5102, 2009; Little, 1999a). Literature has established that curing at 40^{o}C promotes progression of pozzolanic reactions in order to achieve, within 7days, equivalent 28day strength of lime stabilised soil cured at room temperature. The immediate cation exchange in the soil due to addition of lime was allowed to reach steady state so that it could not affect subsequent strength development during accelerated curing. It should be acknowledged that natural fibers mainly consist of natural lignocellulosic polymer. Although they are sensitive to temperature changes, they show thermal degradation at about 200◦C (Bledzki et al., 2002; Saheb and Jog, 1999). The mechanical properties of sisal fibers degrade at temperatures around 100^{o}C. The thermal effects on the longevity of sisal fibers are not significant at temperatures as low as 40^{o}C (Chand and Hashmi, 1993). Since curing temperature (40^{o}C) was far below glass transition temperature of the sisal fiber lignocellulosic polymers, the physiological changes that could affect serviceability of the fibers were insignificant.

10.2.4 Testing programme and pre-compression procedure

The compression test was carried out after 7 days of curing to determine equivalent 28day strength of stabilised soil-fiber composite. The specimens were tested in accordance with ASTM D2166 (ASTM D2166, 2016a) using Quasar 10 universal tensile machine, at the displacement rate of 0.5mm/min. A minimum of three specimens for each fiber dosage was used to determine the average unconfined compressive strength of the composite. In order to determine pre-compression stress levels, specimens of the designated fiber contents were fabricated and cured for 7days. After curing, unconfined compressive strength test was performed on the specimens. The average 7 day strengths of the composite specimens were then obtained. The pre-compression stresses for conditioning the specimens were equal to 10% and 20% of the strength mobilised by unstressed specimens. Pre-compression stress of 30% UCS caused complete failure of the specimens as shown in figure 10.1 and therefore, 20% UCS was set as maximum pre-compression stress level. The pre-compression stress was applied to specimens after 4h, 8h and 24h of accelerated curing.

Figure 10.1: Effects of 30% UCS pre-compression stress.

10.3 Results and discussions

10.3.1 Effects of fiber inclusions on compressive strength

Tensile resistance of the fibers is responsible for strength mobilisation of fiber reinforced soils (Tang et al., 2010b) and the mechanism is enhanced by the strong bond between fibers and soil (Pickering et al, 2016). The results of the effects of fiber inclusions on the compressive strength of the stabilised soil are shown in figure 10.2.

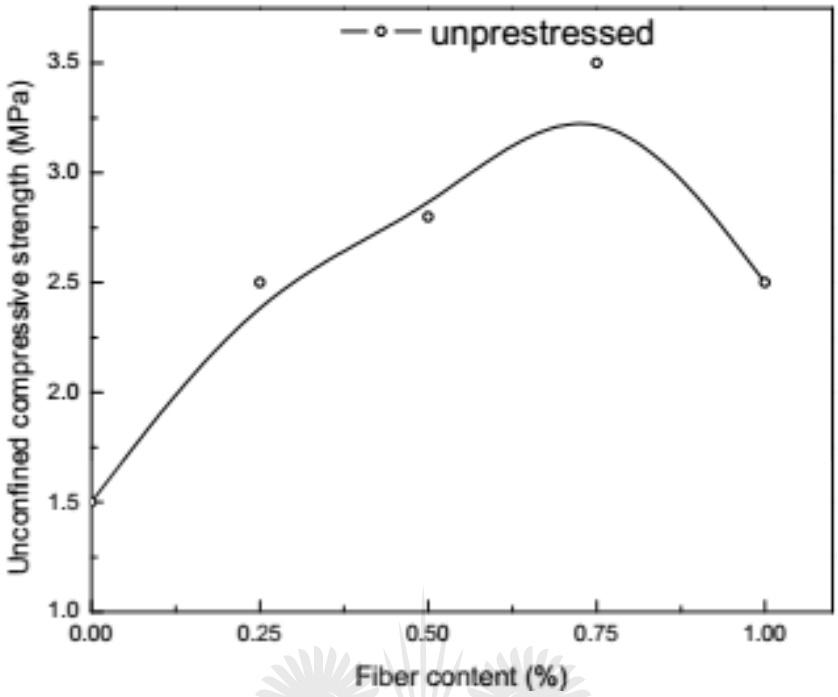

Figure 10.2: Effects of fiber inclusions on the strength.

It is evident that increasing fiber content leads to the improved composite strength up to 0.75% fiber content. The strength drastically decreases at 1% fiber content. It is also noted that strength increases by 169% at 0.75% fiber and drops to 92% at 1% fiber content. The trend agrees with reports by various researchers (Gray and Ohashi, 1983; Maher and Gray, 1990; Park, 2009; Prabakar and Sridhar, 2002; Zornberg, 2002b) on the fiber reinforced soil. In respect of the strength behaviour in Fig 3, the increase in strength of specimens was due to the mobilisation of tensile resistance by fibers coupled with high interfacial strength at the fiber-matrix interface emanating from the physico-chemical and mineralogical changes that occurred during pozzolanic reactions of the stabilised soil. It can be anticipated that during curing process, adhesion of fibers to soil was improved. The decrease observed at 1% fiber was as a result of increased non-uniform distribution of fibers due to high fiber content. Non uniform fiber distribution and orientations reduce macro-interactions between soil and fibers and this in turn reduces capacity of the fibers to mobilise tensile strength (Ahmad et al., 2010a; Diambra et al., 2007).

10.3.2 Effects of composite curing time at pre-compression on strength

Strength behaviour in relation to the curing time at which pre-compression stresses were induced in the composite at various fiber contents is shown in figure 10.3a and b for the stress levels of 10% and 20 % UCS of un-precompressed composite, respectively.

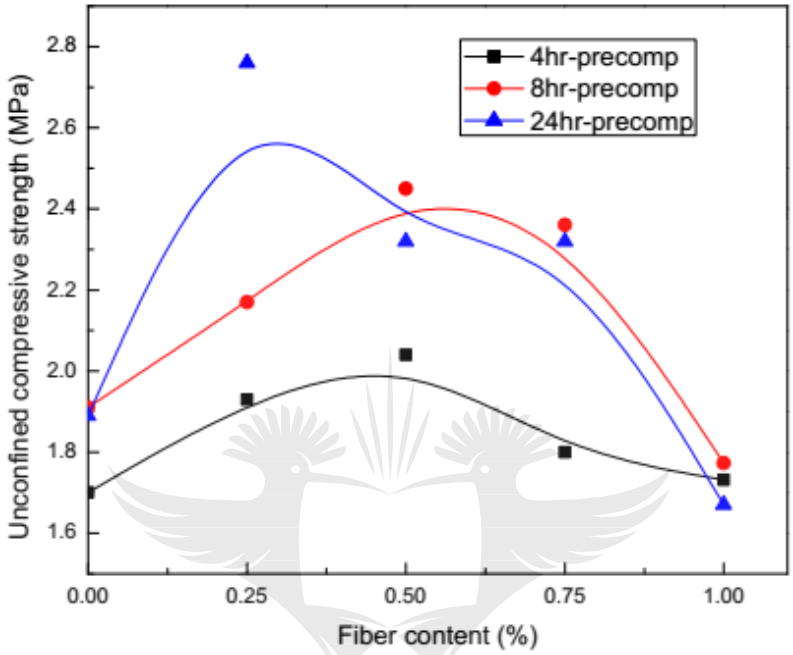

(a)

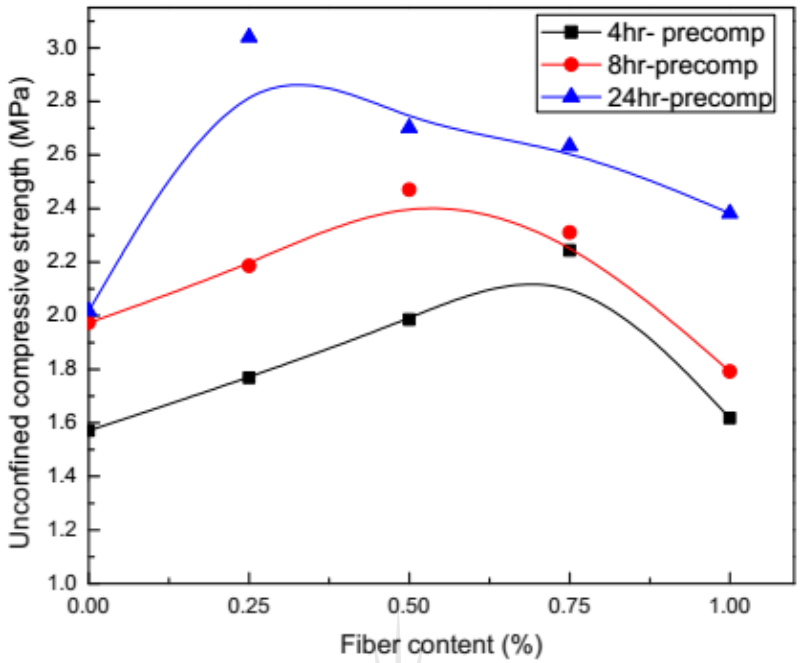

(b)

Figure 10.3: Effects of curing time at pre-compression with fiber inclusions (a) 10% UCS (b) 20% UCS.

It can be noted that strength of the composite is enhanced by the increase in the fiber content to some optimum values for all curing periods, beyond which strength drastically drops. Specimens pre-compressed after 24hrs of curing exhibit significant strength improvements of about 23%and 51% for 10% and 20% pre-compression stress levels respectively. The optimum fiber content for both pre-compression stress levels is 0.25%. The strength improvements are indicated to be in the ascending order of curing time and are more vivid for 20% pre-compression stress. In comparison, strength of 4hr-pre-compressed specimens at 20% pre-compression level is about 10% lower than the same at 10% pre-compression level. The strength reduction is pronounced at high fiber content (1%) for all pre-compression scenarios. Strength enhancement for 24hr pre-compression can be explained in respect of strength development of the composite due to extended pozzolanic reaction and the density of macro cracks induced by the pre-compression stress in the matrix. It is evident that after 24hrs, composite matrix must have developed enough strength to resist pre-compression stresses since pozzolanic reactions are time dependent(Abdulrahman et al., 2014; Al-Swaidani et al., 2016; Basha et al., 2005; Bell, 1996; Jha and Sivapullaiah, 2016b). The development of macro cracks was significantly low in the specimens when the pre-compression was applied at later stages of strength development. On the

other hand, pre-compression at early stages of curing significantly disturbed strength development of the composite. In respect of aforementioned hypotheses, it is obvious that crack density in the matrix was increased by high pre-compression level.

The evolution of damage in the stressed composites occurs in stages. At low applied strain, fibers primarily act as arresters of the macro cracks which nucleate from the internal voids. With further increase in strain, the fibers take over the load carried by the matrix and distribute the strain locally. The fibers then transfer the load back to the matrix through a shear-lag mechanism thus resulting in the homogenisation of macro cracking (Hild et al., 1997; Matzenmiller et al., 1995; Mobasher et al., 1990; Surendra et al., 1991). It is reported that suppressing crack localisation may lead to the enhanced tensile strength of the matrix. The matrix cracking causes the reduction in stiffness especially when subjected to tension and increases with crack closure due to compression. Therefore evolution of strength by 0.25% fiber content at 24hr pre-compression could be due synergic effect of enhanced tensile strength of the soil by the suppression of crack localisation and the closure of macro cracks due to matrix compression associated with pre-compression. On the other hand, drastic reduction in strength at 1% fiber content was due to combined effect of fiber slipping and debonding due to pre-compression and the reduced macro mechanical interaction of fibers and matrix. It can be deduced that matrix cracking was the controlling effect at early stage of curing (4hr). The strength behaviour of the composite at various fiber contents are shown in figure 10.4a and b.

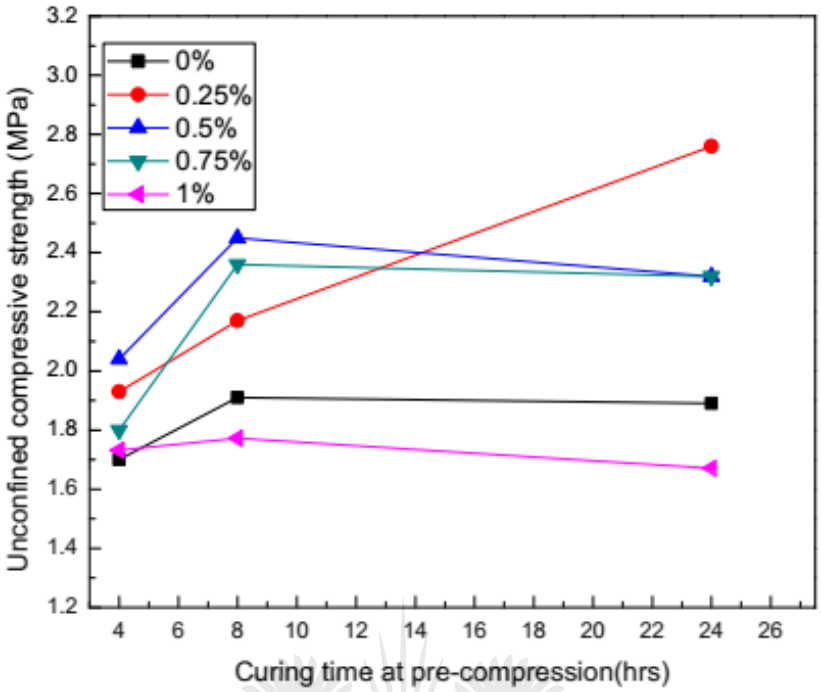

(a)

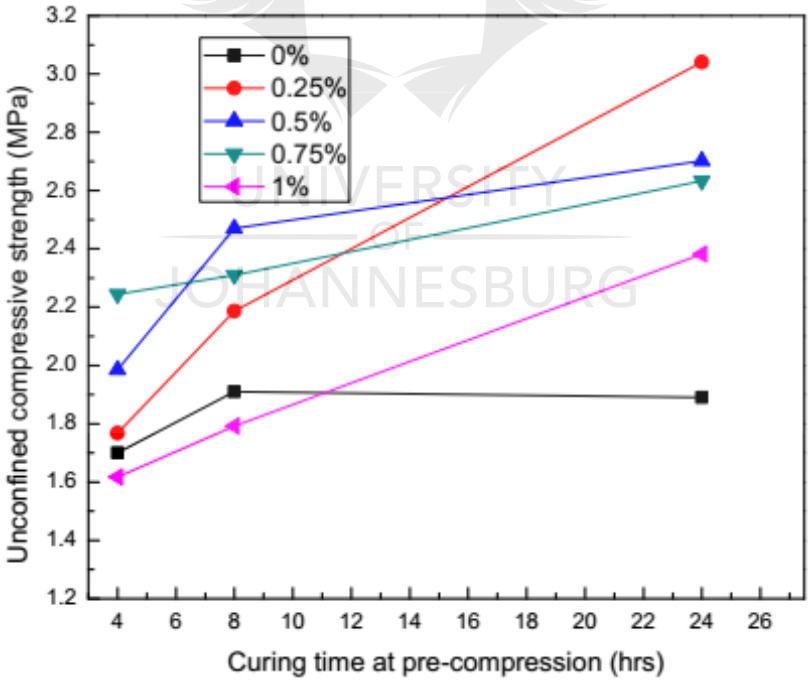

(b)

Figure10.4 : Strength behaviour of the composite at various fiber contents and curing time (a) 10% UCS (b) 20% UCS.

It can be seen that irrespective of the applied pre-stress levels, pre-compressing the stabilised composite at 0.25% fiber content offers significant strength benefits especially when strains are induced after a considerable curing period.

10.3.3 Effects of pre-compression stress level

The effects of pre-compression stress levels were investigated by comparing the strength evolution of low and highly pre-compressed composites at the same fiber content and curing time. In this case, fiber contents in the order of 0%, 0.25%, 0.5% and 1% were used since double fiber increments would offer a better sensitivity of fiber inclusions. Figures 10.5a-d show the effects of increasing pre-compression stress up to 20% UCS.

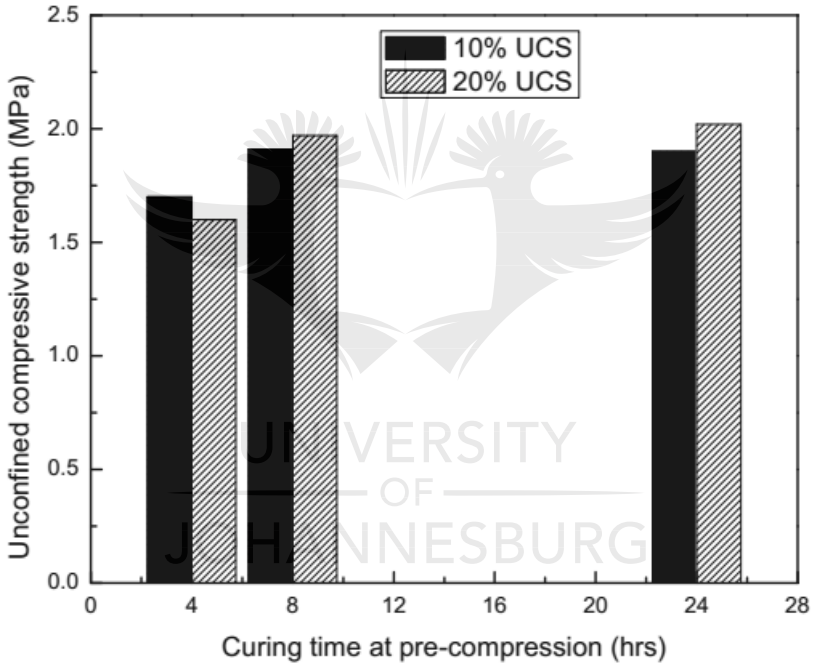

(a)

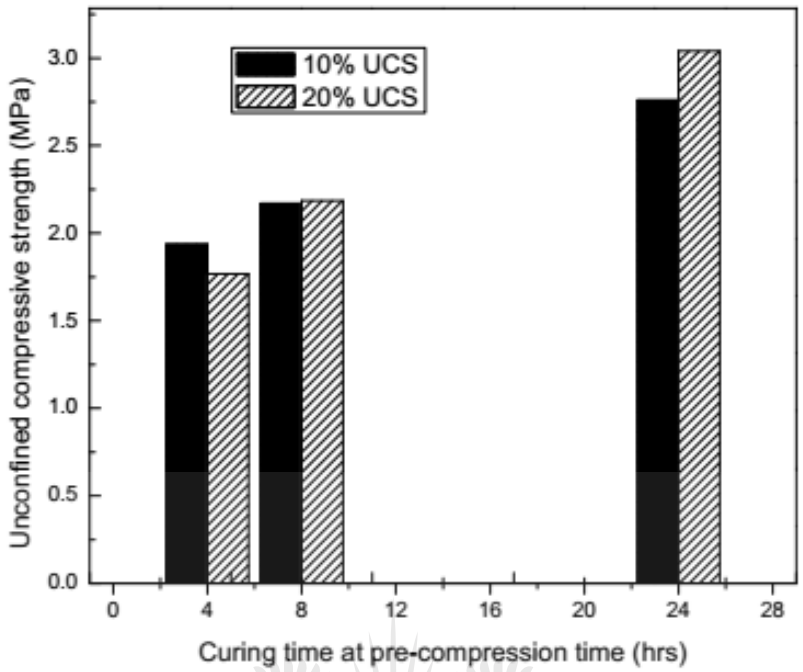

(b)

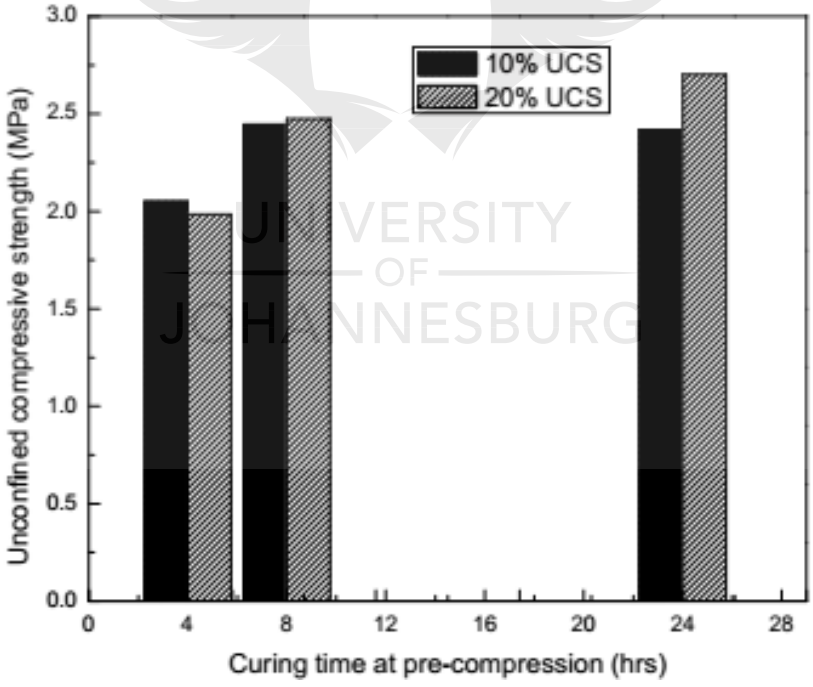

(c)

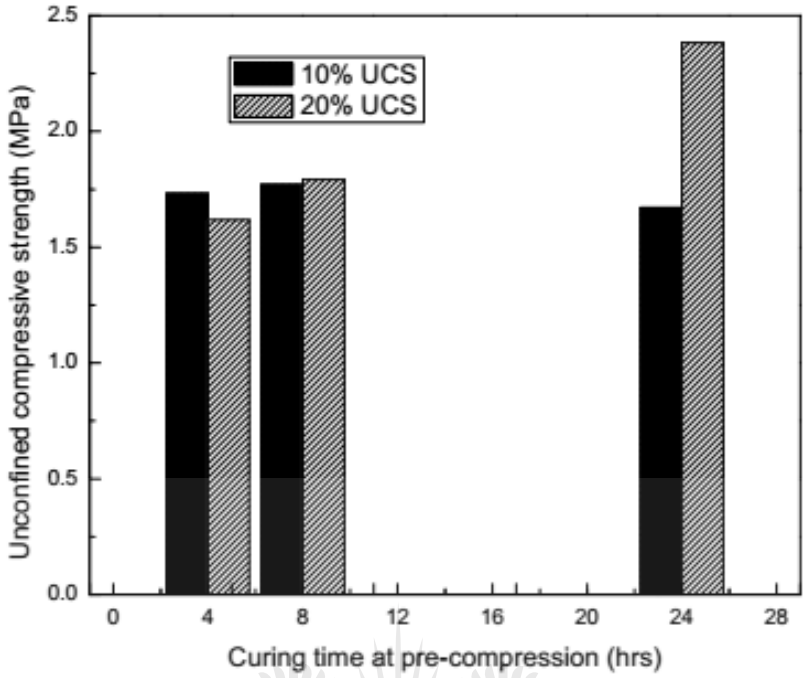

(d)

Figure 10.5: Effects of pre-compression stress level (a) 0% (b) 0.25% (c) 0.5% (d) 1% fiber contents.

It can be seen that increasing pre-compression stress to 20% UCS at early stage of curing (4h) leads to the decrease in the ultimate strength which is shown to be pronounced at high fiber content. With progression of curing, high pre-compression stress (20% UCS) gradually improves strength and a significant improvement of about 42%relative to 10%UCS, is exhibited at 24h curing period. On the other hand, 10% UCS shows stability of strength with the increase in fiber content and curing time. The effect of pre-compression is insignificant at 8h curing time for both pre-compression levels. As already alluded to, the degradation of strength at early stage is attributed to the increase in the crack density induced by the pre-compression strains which undermine fiber-matrix interfacial strength. The cracks propagated along the edges of the fibers were responsible for pre mature debonding and sliding at fiber-matrix interface when high strain level was applied to the specimens (Matzenmiller et al., 1995). The strength gain of the composite with curing time (pozzolanic effects) was responsible for the stability exhibited by 10%UCS pre-compression stress. It can be anticipated that the strength gain by high pre-compression at later stage of curing was due to the improved matrix stiffness and tensile effects of fibers emanating from the compression of the composite. The locked–in tension (strain

energy) in fibers resulted into the significant strength increase at 1% fiber content for 20% UCS pre-compression (Surendra et al., 1991).

The effects of pre-compression on the composites can further be verified by applying the theory of tensile behaviour of cementitious fiber composites and associated crack models proposed by (Yang et al., 1991). The fibers in this case are assumed to be strong and embedded in the brittle soil matrix such that cracks generated by tensile stress in the matrix are ellipsoidal in shape. Furthermore, perfect bond is assumed to exist at the fiber–soil interface so that applied stress required to initiate matrix cracking for non-steady crack state is given by equation 10.1.

$$\sigma_a = \left[\frac{\pi\gamma_c G_{fm}}{2(1-\nu_c)a}\right]^{\frac{1}{2}}\left(1+\frac{2a}{3r_f}V_f\right)^{\frac{1}{2}}\left(1+\frac{a}{r_f}V_f\right) \qquad (10.1)$$

where γ_c and ν_c are average shear modulus and Poisons ratio, respectively, of the composite. G_{fm} is the fracture resistance of the soil matrix, a is the crack length, V_f and r are fiber volume fraction and radius, respectively. Increasing applied stress causes crack to propagate through the matrix until it reaches the length at which debonding and sliding occur at the fiber-matrix interface. The applied stress at which sliding and debonding are initiated is given by equation 10.2.

$$\sigma_a = \left[\frac{4r_f E_f G_{fi}}{a^2}\right]^{\frac{1}{2}}\left(1+\frac{a}{r_f}V_f\right) \qquad (10.2)$$

where G_{fi} is the critical interface debonding energy release rate and E_f is elastic modulus of the fibers. Sliding and debonding increase with further crack propagation and when crack length is very long, say $a \to \infty$ then condition in equation 10.3 exists.

$$\lim_{a\to\infty}\frac{a}{r} = \infty \qquad (10.3)$$

When condition 4 is applied to equations 10.1 and 10.2, the asymptotic stress values as $\frac{a}{r} \to \infty$ are given by equations 10.4a and b.

$$\sigma_i \approx \left[\frac{3\pi V_f G_{fm}\gamma_c}{2(1-\nu_c)r_f}\right]^{\frac{1}{2}} \quad , \quad \sigma_d \approx V_f\left[\frac{8E_f G_{fi}}{r_f}\right]^{\frac{1}{2}} \qquad (10.4a, b)$$

It can be seen in (equations 10.4a and b) that $\sigma_d > \sigma_i$ and asymptotic stress values are proportional to fiber volume fraction. Equating equations 10.1 and 10.2 yields critical fiber volume fraction for debonding of fiber-matrix interface with steady state cracking, given by equation 10.5.

$$V_{fc} = \frac{3\pi\gamma_c G_{fm}}{16E_f(1-\nu_c)G_{fi}} \qquad (10.5)$$

Debonding occurs when $V_f < V_{fc}$ and the vice versa holds. V_{fc} depends on the fiber and matrix properties, and is independent of fiber radius (Surendra et al., 1991; Yang et al., 1991).

Since fibers used herein were randomly distributed, it is assumed that fiber lengths stretched across tension zones as continuous filaments. The fiber orientations were predominantly horizontal due to static compaction, such that fibers offered matrix confinement to lateral deformation. The stabilised soil/matrix properties were assumed homogeneous in all directions. In this study, 60 specimens were prepared at moisture content of 14% of the combined mass of soil and fibers in the mould of 55mm diameter and 120mm height. The average mass of the fabricated specimens was 590g that comprised of soil, fiber and water. The expression of the specimens' mass is given by equation 10.6

$$m_c = 1.14(m_s + m_f) \qquad (10.6)$$

where m_f is total mass of fibers and m_s is mass of the stabilised soil. It should be recalled that fiber content in this study was determined by percentage by dry mass of the soil (see equation .3.1). Therefore, the equivalent volume fraction of the fibers can be determined by utilising its density which is $1.4 g/cm^3$ (Pickering et al., 2016). The fiber volume fraction is given by equation 10.7.

$$\rho_f = \frac{V_f}{V_c} \qquad (10.7)$$

where v_c is volume of the composite and v_f is volume of fibers. The corresponding fiber volume fractions of 0.25%, 0.5%, 0.75% and 1% were computed and found to be in the order of 0.3%, 0.6%, 0.9% and 1.2% respectively. Since strength development in the stabilised soil is time dependent, critical interface debonding energy G_{fi} and matrix fracture resistance G_{fm} were assumed to increase with curing time. The 28day fracture resistance of lime stabilised soil is 0.011N/mm according to (Masashi et al., 1999). The existing reports show that interface debonding energy is approximately as 70% of matrix fracture resistance for cementitious composites (see examples in (Surendra et al., 1991; Yang et al., 1991). Incorporating variation of strength in the stabilised soil specimens with time, assuming that 90% of specimen's strength was gained after 5days of accelerated curing at 40^{o}C , the matrix fracture resistance and the interface debonding energy at a specified curing time were computed using equation 10.8 and equation 10.9, respectively.

$$G_{mt} = 0.0083tG_{fm} \tag{10.8}$$

$$G_{fi} = 0058tG_{mt} \tag{10.9}$$

where t is curing time in hours and G_{mt} is matrix fracture resistance at a given curing time. Therefore, matrix fracture resistances for 4h, 8h and 24h were calculated as 0.0004N/mm, 0.0007N/mm and 0.0022N/mm, respectively whereas corresponding interface debonding energies were found to be 0.0003N/mm, 0.0005N/mm and 0.0015N/mm, respectively. The shear moduli of composite were computed using equation 10.10

$$\gamma_c = \frac{E_c}{2(1+v_c)} \tag{10.10}$$

The Poisons ratio was taken as 0.3 and properties of fibers were adapted from Table 3.3. The summary of elastic moduli and critical fiber volume fractions for 4hr and 24hr curing periods is shown in Table 10.1.

Table 10.1: Elastic moduli and critical fiber volume fractions

Fiber Volume fraction (%)	4h-Precompression				24h-Precompression			
	10% UCS		20% UCS		10% UCS		20% UCS	
	E_c (MPa)	V_{fc} (%)	E_c (MPa)	V_{fc} (%)	E_c (MPa)	V_{fc} (%)	E_c (MPa)	V_{fc} (%)
0.3	80	0.15	88	0.17	162	0.33	111	0.23
0.6	67	0.13	63	0.12	67	0.14	76	0.16
0.9	94	0.18	56	0.11	80	0.17	69	0.12
1.2	50	0.09	55	0.10	52	0.11	60	0.12

It can be seen that the critical fiber volume fraction is less than actual volume fraction for all fiber contents except for specimens with 0.3% fiber volume fraction at 10% UCS pre-compression stress level after 24h of curing. In this case, it implies that the fiber-matrix interface for the specimens remained intact until a point where the matrix sustained maximum stress. The cracking and debonding criteria with respect to pre-compression stresses are shown in Figure 10.6a and b for 4h and 24h curing periods, respectively.

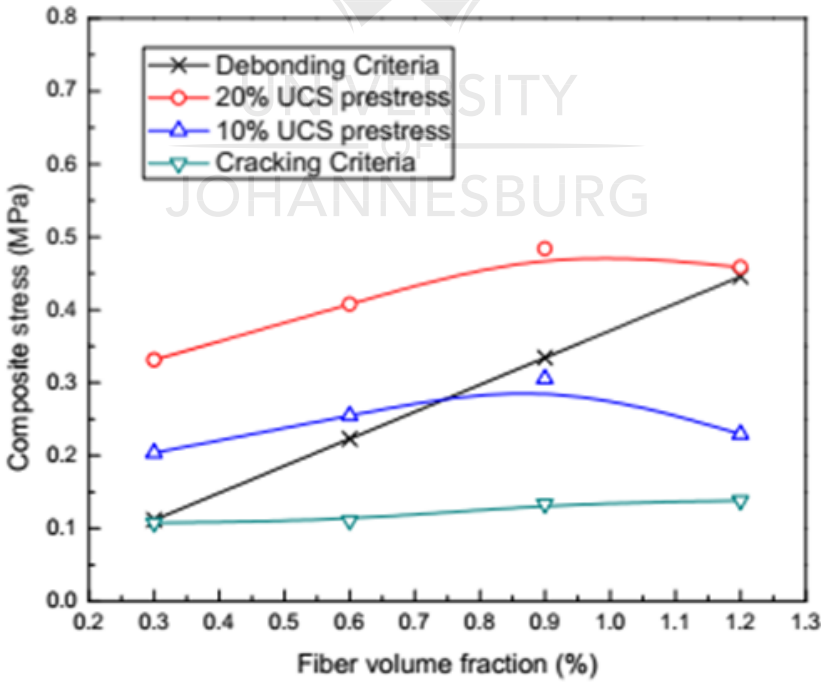

(a)

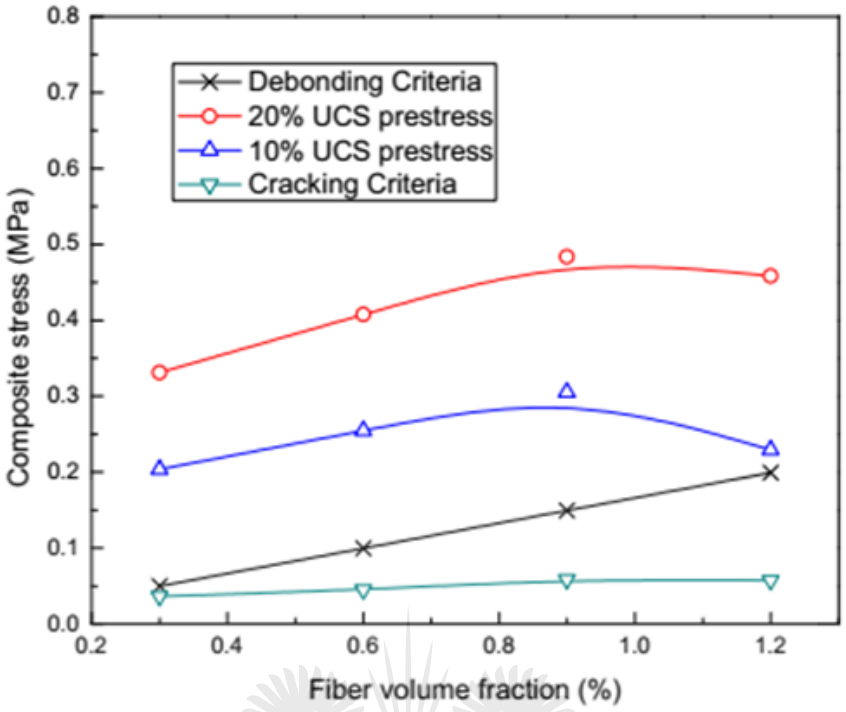

(b)

Figure 10.6: Analytical composite cracking and debonding stresses and applied pre-compression stresses (a) 4 h (b) 24h.

It is evident in figures. 10.6a and b that predicted debonding and cracking stresses are lower than applied pre- compression stresses for 4h curing period at both pre-compression levels. On the other hand,pre-compression after 24h shows that 20% UCS pre-compression stress level leads to debonding at all fiber volume fractions. The 10% UCS pre-compression stress level shows debonding at lower fiber volume fractions (0.3% and 0.6%) and matrix cracking at higher fiber volume fractions (0.9% and 1.2%.). The prediction is in agreement with the composite behaviour exhibited by specimens pre-compressed after 4hr in figure 10.3. The crack model used herein utilises fiber volume fraction as critical parameter and it does not include effects of fiber orientation and discontinuities.

10.3.4 Compressive strength of un-precompressed versus pre-compressed composites

The comparative analysis of 7day strength behaviour of un-precompressed and pre-compressed composites is shown in Tables 10.2a and b for 10%UCS and 20% UCS, respectively. The variance hereto refers to the difference in strength between the unconditioned and conditioned specimens. The positive sign indicates strength gain and negative signifies reduced strength.

Table 10.2a: Difference in strength between un-precompressed and pre-compressed composite under 10% UCS stress level

Fiber content (%)	7 day compressive strength (MPa)						
	Un-precompressed	Pre-compression					
		4h	Variance*	8h	Variance*	24h	Variance*
0	1.30	1.70	+0.4	1.91	+0.61	1.89	+0.59
0.25	2.50	1.90	-0.6	2.17	-0.33	2.76	+0.26
0.5	2.80	2.04	-0.76	2.45	-0.35	2.32	-0.48
0.75	3.50	1.80	-1.7	2.36	-1.14	2.32	-1.18
1	2.50	1.73	-0.8	1.77	-0.73	1.67	-0.83

*Variance is the difference in strength between pre-compressed and un-precompressed+ increase, - decrease

Table 10.2b: Difference in strength between un-precompressed and pre-compressed composite under 20% UCS stress level

Fiber content (%)	7 day compressive strength (MPa)						
	Un-precompressed	Pre-compression					
		4h	Variance*	8h	Variance*	24h	Variance*
0	1.30	1.57	+0.27	1.97	+0.67	2.01	+0.71
0.25	2.50	1.77	-0.73	2.19	-0.31	3.04	+0.54
0.5	2.80	1.99	-0.81	2.47	-0.33	2.70	-0.1
0.75	3.50	2.24	-1.26	2.31	-1.19	2.63	-0.87
1	2.50	1.62	-0.88	1.79	-0.71	2.38	-0.12

It is evident from the tables that compressive strengths of un-precompressed specimens are higher than pre-compressed specimens for fiber contents greater than 0.25%. The reduction in strength is more pronounced for 0.75% fiber content for both pre-compression stress levels. The macro-mechanical interlock between fibers and soil particles is the typical reinforcement mechanism in fiber reinforced soils. The efficiency of the mechanism depends on the friction and cohesion at fiber-matrix interface (Ahmad et al., 2010a; Wu et al., 2014b). The friction and cohesion at fiber-matrix interface are enhanced by pozzolanic products due to lime addition as fiber-matrix contact points are increased (Moghal et al., 2017). The disturbance to the bonding of pozzolanic products with fibers would compromise adhesion at fiber-matrix interface and in turn reduce strength gain of the soil composite. Therefore, application of pre-compression stress in the present study obviously caused redistribution of interfacial strength and fiber-matrix debonding. These phenomena were responsible for the lower strength values exhibited by pre-compressed specimens. The pronounced reduction in strength by 0.75% fiber content was due to

the high degree of debonding caused high applied pre-compression stress. The progression of curing could not recover the adhesion at fiber-matrix interface after extended curing time.

In addition, the unreinforced composites benefit from pre-compression irrespective of pre-stress level and curing period, however, strength improvement is relatively low with short curing period at high pre-compression stress level. The low fiber content (0.25%) also shows strength benefits at relatively longer curing period (24h) regardless of pre-compression stress level. The high fiber contents and short curing periods show undesirable effects of pre-compression. It can be deduced therefore that the synergic effects of pre-compression and fiber content are to enhance strength in the stabilised soil composite at low fiber content only when the composite gains considerable strength. The strength gain registered in unreinforced composite specimens was due to the densification of the soil with applied pre-compression load that led to the decrease in void ratio and in turn enhanced shearing resistance of the soil. Fiber inclusion is reported to reduce compressibility of lime amended soil (Moghal and Sivapullaiah, 2011), this implies that high fiber content offered considerable resistance to compressibility and this explains the reduced strength exhibited by pre-compressed specimens at high fiber content. Furthermore, low strength gain with short curing period could be due to evolution of macro cracks whose effects were suppressed by the progression of strength development (pozzolanic reaction). It should also be mentioned that the presence of moisture in both the fibers and matrix at early stage of curing contributed, somehow to the debonding and sliding of fibers during pre-compression. The presence of moisture in the natural fibers reduces strength in the fiber composite as reported in the literature (Pickering et al., 2016; Prabakar and Sridhar, 2002). In addition, at high fiber content, reduced macro-mechanical interaction of fibers and matrix accounted for the overall strength reduction in the composite (Ahmad et al., 2010a)

10.3.5 Stress-strain relationship and failure modes of the composite

The macro structural modification of the soil with fibers leads to the changes in the stress strain behaviour and failure modes of the composite as reported by many investigators (Al-Refeai, 1991; Bouhicha et al., 2005; Ghavami et al., 1999a; Maher and Gray, 1990; Park, 2009; Tang et al., 2007). Figure 10.7 shows the stress-strain relationship and associated failure modes of the composite pre-compressed with 20% UCS after 24h of curing for unreinforced soil, 0.5% and 1% fiber contents.

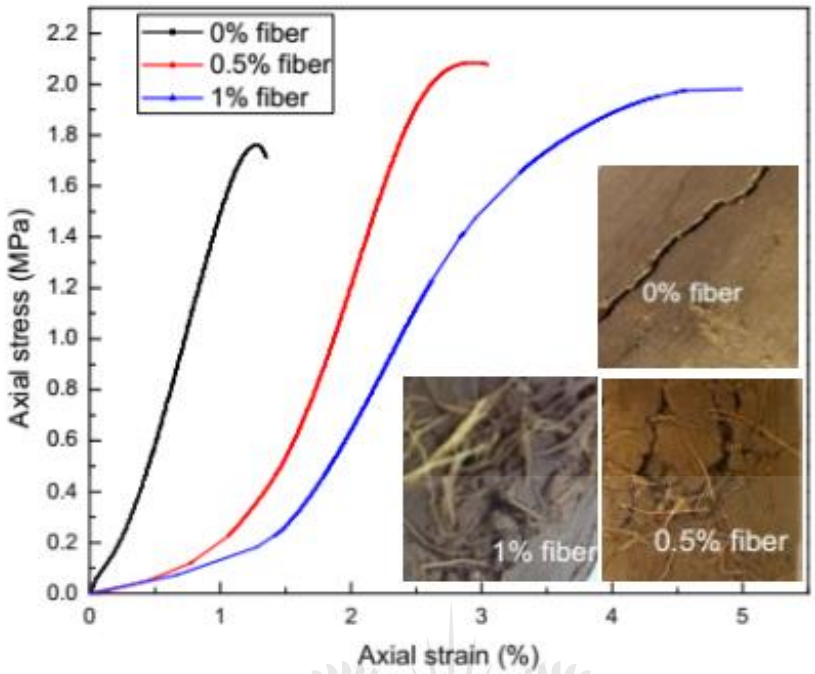

Figure10.7: Strain-strain relationship and typical failure modes.

The effects of high pre-compression stress and 24h curing on specimen's behaviour were more vivid as evidenced by the results in the previous sections. The fiber contents selected herein exhibited representative stress-strain behaviour and typical failure modes.

It can be seen figure 10.7 that unreinforced soil exhibits high stiffness and brittle failure which is characterised by the diagonal crack. This behaviour has also been reported by (Tang et al., 2007). Increasing fiber content endows the composite with ductile behaviour as depicted by stress-strain relationship of 0.5% and 1% fiber contents. It can be concluded that fiber composites specimens sustained considerable deformation before failure and the failure mode was characterised by squashing and crushing which is indicative of ductile behaviour of the material. It should be highlighted that the synergic effect of pre-compression and fiber inclusions on failure mode was not obvious.

Conclusions

In this investigation, lime-fly ash stabilised soil was used to study the effects of fiber inclusions and pre-compression on the strength properties of the pre-compressed composite. The randomly distributed sisal fibers were used as reinforcing elements of the stabilised soil. The pre-compression stress equivalent to 10% and 20% of the 7 day strength mobilised by the un-precompressed composite was applied to the specimens with designated fiber content, at varying

curing time. The synergic effects of pre-compression and fiber inclusions on the strength of the conditioned composite were determined after 7 days of curing period by unconfined compression tests. Based on the acquired results, the following conclusions are drawn:

1. Fibers inclusions increase strength and ductility of the composite. This is attributed to the high tensile resistance mobilised by the fibers.
2. Lower strengths are mobilised by pre-compressed composite in comparison with un-precompressed composite. This is attributed to redistribution of fiber-matrix bond strength and the evolution of macro cracks that reduce stiffness of the composite.
3. Damaging effects of pre-compression are reduced when pre-compression stresses are induced at longer period of curing. This is due to time related strength gain of the composite (pozzolanic reaction) that endows the matrix with resistance to compression.
4. Pre-compression can improve mechanical properties when applied to composite at low fiber content.
5. The crack model for damage mechanism in cementitious fiber composite can predict with reasonable accuracy the strength behaviour of fiber composites that are pre-compressed after short period of curing.
6. In practice, the use of heavy machinery in fly ash stabilised earthen construction may reduce ultimate strength of the foundation structure. Pre mature loading of the stabilised earthen walls may compromise characteristic strength of the structural element. Therefore, light weight tools are recommended for construction of stabilised earthen foundation in order to minimise ultimate strength reduction due to excessive premature loading. Superimposed loading should be applied when the stabilised material is fully cured, i.e., at least after 28 days of curing. From the design point of view, characteristic strength of fiber reinforced soil must be reduced by material reduction factor, preferably 1.2 to cater for lower ultimate strength of the material.

References

Abdulrahman et al. (2014). Soil–water characteristic curve of lime treated gypseous soil. *Journal of applied clay sciennce, 102* 128-138.

Ahmad et al. (2010). Performance evaluation of silty sand reinforced with fibres. *Geotextiles and Geomembranes, 28*, 93–99.

Al-Refeai .O (1991).Behaviour of granular soils reinforced with discrete randomly oriented inclusions. *Geotextile Geomembranes, 10*, 319–333.

Al-Swaidani et al.(2016). Effect of adding natural pozzolana on geotechnical properties of lime stabilized clayey soil. *Journal of rock mechanics and geotechnical engineering,8* 714-725.

ASTM D1140-17. (2017). Standard Test Methods for Determining the Amount of Material Finer than 75-µm (No. 200) Sieve in Soils by Washing. West Conshohocken PA: *ASTM International.*

ASTM D2166. (2016). Standard Test Method for Unconfined Compressive Strength of Cohesive Soil. West Conshohocken, PA: , *ASTM International.*

ASTM D5102. (2009). Standard Test Method for Unconfined Compressive Strength of Compacted Soil-Lime Mixtures. West Conshohocken, PA.

ASTM D6276. (2019). Standard Test Method for Using pH to Estimate the Soil-Lime Proportion Requirement for Soil Stabilization. West Conshohocken, PA: *ASTM International.*

Basha et al. (2005). Stabilization of residual soil with rice husk ash and cement. *Construction and Building Materials, 19*(6), 448-453.

Bell.F.G. (1996).Lime stabilization of clay minerals and soils. *Engineering Geology, 42* 223-237.

Bledzki et al. (2002). Natural and Wood Fiber Reinforcement in Polymers. *Rapra Review Reports, 13*, 1-144.

Bouhicha et al. (2005). Performance of composite soil reinforced with barley straw. *Cement & Concrete Composites, 27*, 617–621.

Chand N and Hashmi. S. (1993). Mechanical properties of sisal fibre at elevated temperatures *J Mater Sci, 28*, 6724-6728.

Diambra et al. (2007). Determination of fibre orientation distribution in reinforced sands. *Ge´otechnique, 57*(7), 623–628. doi: doi: 10.1680/geot.2007.57.7.623

Ghavami et al. (1999). Behaviour of composite soil reinforced with natural fibers. *Journal of cement concrete composite, 21*, 39-48.

Gray D.H and Ohashi. (1983). Mechanics of fiber reinforcement in sand. *Journal of Geotechnical Engineering, 109*(3), 335–353.

Hild et al. (1997). On the mechanical behavior of fiber-reinforced composites *Composite structures, 39*(3-4), 213-287.

Jha A.K. and Sivapullaiah.P.V. (2016).Volume change behavior of lime treated gypseous soil influence of mineralogy and microstructure. *Journal of Aplplied Clay Science, 119*, 202-212.

Kumar et al. (2007). Influence of fly Ash, lime, and polyester Fibers on compaction and strength properties of expansive Soil. *Journal of Materials in Civil Engineering, 19*, 242-248.

Little.D.N. (1999). *Evaluation of structural properties of lime stabilised soils and aggregates*. Arlington: National lime association

Maher. H and Gray.H. (1990). Static response of sand reinforced with randomly distributed fiber. *Journal of Geotechnical Engineering, 116*, 1661–1677.

Masashi et al. (1999). Engineering Properties of soil stabilised by ferrum lime and used for the application of road base. *Soils and Founadtions, 39*(1), 31-41.

Matzenmiller et al. (1995). A constitutive model for anisotropic damage in fiber-composites. *Mechanics of Materials, 20*, 125-152

Mobasher et al. (1990). Micro cracking in fiber reinforced concrete. *Cement and concrete Reseach, 20*, 665-676.

Moghal.A.A. and Sivapullaiah.P.V.(2011). Effect of pozzolanic reactivity on compressibility characteristics of stabilised Low Lime Fly Ashes. *Geotechnical and Geological Engineering, 29*, 665-673.

Moghal et al. (2017). Target reliability approach to study the effect of fiber reinforcement on UCS behavior of Lime treated semiarid Soil. *Journal of Materials in Civil Engineering 29*(6), 04017014-04017011-04017015.

Park.S.S.(2009).Effect of fiber reinforcement and distribution on unconfined compressive strength of fiber-reinforced cemented sand. *Geotextiles and Geomembranes, 27*,162–166.

Pickering et al. (2016). A review of recent developments in natural fibre composites and their mechanical performance. *Composites: Part A 77, 83*, 98–112.

Prabakar.J and Sridhar.S.R. (2002). Effect of random inclusion of sisal fibre on strength behaviour of soil. *Construction and Building Materials, 16,* 123-131.

Saheb.D.N and Jog.J.P. (1999). Natural fiber polymer composites: a review. *Advances in Polymer Technology,, 18*(4), 351-363.

Surendra et al. (1991). Mechanical Behavior of Fiber- Reinforced Cement-Based Composites. *Journal of the American Ceramic Society, 74*(11), 2727-2738, 2947-2753.

Tang et al. (2007). Strength and mechanical behavior of short polypropylene fiber reinforced and cement stabilized clayey soil. *Geotextiles and Geomembranes, 25*(5), 194-202.

Tang et al. (2010). Interfacial shear strength of fiber reinforced soil. *Geotextiles and Geomembranes, 28,* 54–62.

Tastan et al. (2011). Stabilization of Organic Soils with Fly Ash. *Journal of Geotechnical and Geoenvironmental Engineering, 137*(9), 819-833.

Wu et al. (2014). Investigation of mechanical properties of randomly distributed sisal fibre reinforced soil. *Materials Research Innovations, 18*(2), 953-959. doi: DOI 10.1179/1432891714Z.000000000511

Yang et al. (1991). Micromechanical theory and uniaxial tensile tests of fiber reinforced cement composites. *Materials Research Society, 6*(11), 2463-2473.

Zornberg.G.J (2002). Discrete framework for limit equilibrium analysis of fibre-reinforced soil. *Géotechnique, 52*(8), 593-604.

11 CHAPTER ELEVEN-COMPRESSIVE AND TENSILE STRENGTH PROPERTIES OF PRE-COMPRESSED AND SOAKED SISAL FIBER REINFORCED LIME–FLY ASH STABILISED SOIL

11.1 Introduction

Studies of stabilised and unstabilised fiber reinforced soil have adapted unconfined compression test as a measure of soil mechanical performance (Baldovino et al., 2018; Hejazi et al, 2012). Compared with compressive or shear strength, tensile strength of the soil is basically assumed to be zero, or insignificant in geotechnical engineering practice because of its relatively low value (Jian et al., 2014). In fact, the tensile strength of soil is difficult to be precisely measured due to lack of satisfying laboratory techniques. The tensile strength of soil is, however, an important mechanical parameter in the design of geosystems, i.e., slopes, embankments and foundations, where tensile cracks are likely to occur (Albrech and Benson, 2001; Miller et al., 1998; Morris et al, 1992). The tensile properties of soil improve with fiber inclusions. The strength index of lime stabilised soil is increased with an increase in lime content (Baldovino et al., 2018; Consoli et al., 2012, 2014). It is imperative therefore to investigate the compressive and tensile behaviours of stabilised natural fiber reinforced soil composites under severe environments, i.e., high moisture exposures. The durability properties during long-term environmental exposure are crucial for material design of its outdoor applications (Liao, 2003). In practice, during subgrade or foundation construction, the stabilised soil composite can be loaded prematurely when exposed to heavy construction machinery. The effects of premature loading on the ultimate strength gain of stabilised soil composites have not been comprehensively reported in literature. The investigations into the performance of pre-loaded soil composite under severe wet environments have not received attention. Moreover, properties of the stabilised soil composite dictate the empirical design of structural layers for the geosystems. Therefore, an insight into the behaviour of pre-loaded soil composite materials exposed to severe environments could provide guidelines for the mechanistic ultimate and serviceability limit state designs of geosystems. The objective of this study was to detail the mechanical behaviour, in particular the strength and resilience of pre-loaded stabilised soil composite under severe wet environments. Of special interest were compressive, tensile strengths, and the macro structural integrity of soaked and crushed specimens after reloading.

11.2 Materials and experimental programme

11.2.1 Materials

The soil sample used in this study was prepared and characterised as in section 3.1.1 according to ASTM D1140-17 (ASTM D1140-17, 2017). The particle size distribution of the soil is shown in figure 3.1. Sisal fibers with length of 25mm were used. The summaries of the fiber and soil properties are indicated in Table 3.1 and Table 3.3, respectively on chapter 3.

11.2.2 Sample preparation

The fiber dosages were determined by percentage dry weight of soil. The fiber dosages used herein were 0.25%, 0.5%, 0.75% and 1%. Sample preparation procedure highlighted in section 10.1.1 on chapter 10 was adopted.

11.2.3 Specimen preparation for compression test

The specimens were prepared in the 55mm diameter mould and 120mm height, by static compaction of the soil composite into 3 layers using hydraulic jack mounted with pressure gauge. The compaction pressure of 5MPa was used and extra care was taken to control quality of the specimens. Curing protocol highlighted in the previous section 10.2.3 on chapter 10 was adopted.

A durability assessment of the soil-lime-fly ash specimens was carried out by subjecting the specimens to 24h capillary soaking for the measurement of resistance to loss in strength due to moist conditions, which is typical in tropical regions. Capillary soaking was conducted by firstly, removing the cured specimens from the plastic wraps and subsequently wrapping them with wet absorptive fabric. The specimens were thereafter placed on the porous stone filled in the dish. The water level was kept at the top of the porous stone and in contact with the fabric wrap throughout the capillary soaking as shown in figure 11.2.

Figure 11.1: Capillary soaking of specimens.

The pre-compression was performed in the similar approach as in section 10.2.4 on chapter 10. The pre-compression stress was applied to specimens after 4h and 24h of accelerated curing. The pre-compression load levels are shown in Table 11.1.

Table 11.1: Pre-compression loads for specimens

Fiber content	Pre-compression load (N)	
%	10% UCS	20%UCS
0	200	400
0.25	300	600
0.5	400	800
1	350	700

11.2.4 Unconfined compression test programme

The compression test was carried out on the soaked stabilised soil-fiber composite to determine strength properties of the conditioned specimens. The specimens were tested in accordance with ASTM D2166 (ASTM D2166, 2016a) using Quasar 10 universal tensile machine, at a displacement rate of 0.5mm/min. In order to determine percentage residual strength, specimens of the designated fiber content were initially loaded beyond peak stress. The specimen was

automatically unloaded when strain value reached 10% in excess of yield strain (strain at peak stress). The strain tolerance for unloading point was adapted to ensure that the entire specimen exhibited plastic behaviour so that elastic recovery could not affect the residual strength values. The unloading crosshead speed was kept equal to initial displacement rate. The percentage residual strength was thereafter computed using equation 11.1 .

$$P_r = \frac{Q_r}{P} x100 \qquad (11.1)$$

where P is the initial maximum sustained load and Q_r is the maximum sustained load after reloaded. To avoid effects matrix suction on residual strength, permanently deformed specimens were reloaded within 3s after unloading. A minimum of three specimens for each fiber dosage and testing condition was used to determine the average strength of the conditioned specimens.

11.2.5 Split tensile test programme

Split tensile test was conducted in accordance with Brazilian standard NBR 7222 (ABNT, 1983). The cylindrical specimens of size similar to those for compression test were used. The specimen preparation and curing protocols were as described in section 11.2.2 and 11.2.3, respectively. The test was conducted using the tensile machine that was used for compression test at displacement rate of 0.5mm/min. The soaked specimens were placed horizontally between the bearing blocks of the compression testing machine. Strips of mild steel of 5 mm thick, 8mm wide, and 55 mm long were placed on the upper and lower load bearing parts of the specimen to ensure uniform bearing pressure. The maximum load was recorded and the split tensile strength was computed using equation 11.2.

$$P = \frac{2F}{\pi D_s L} \qquad (11.2)$$

where F is the maximum recorded load, D_s is the diameter of the specimen and L is the height of the specimen.

11.3 Results and discussions

11.3.1 Effects of soaking on the compressive strength

The effects of soaking were investigated by compression test at various fiber dosages. The variation of compressive strength at various fiber contents for soaked and unsoaked specimens is presented in figure 11.3.

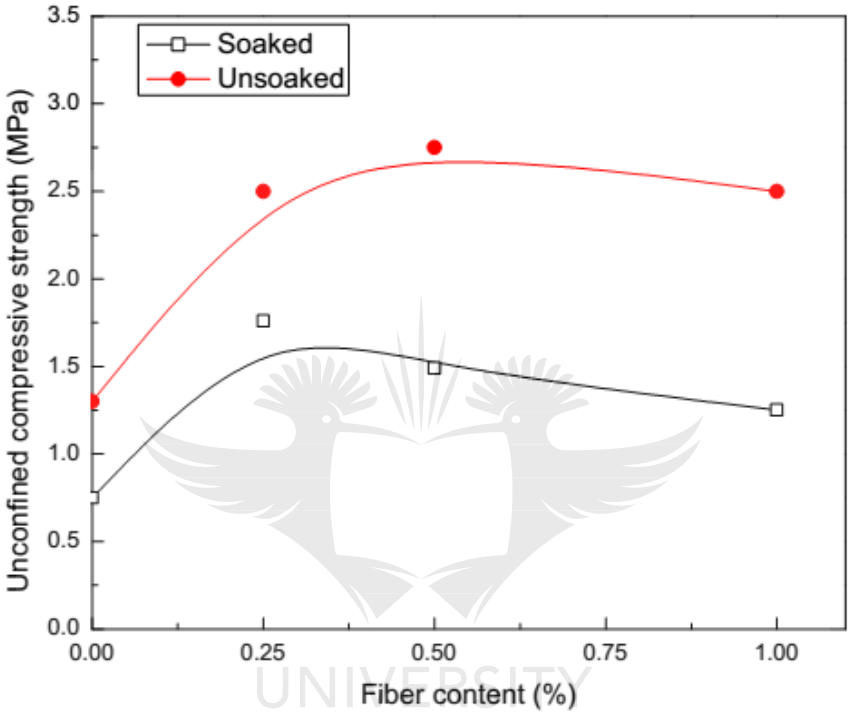

Figure 11.2: Variation of compressive strength of soaked and unsoaked specimens.

As shown in figure 11.4, fiber inclusion causes an increase in strength of the composite followed by the decrease at high fiber content. The increase in strength was attributed to the strength mobilised by the mechanical interlock and cohesion between fibers and cementitious compounds of the stabilised soil. The decrease in strength at high fiber content was due to the evolution of fiber-fiber mechanical interaction that was associated with low strength mobilisation (Ahmad et al., 2010b). The optimum strength gain was indicated at 0.25% fiber content for soaked specimens and 0.5% for unsoaked specimens. It is evident that soaked specimens mobilised lower strength values than unsoaked specimens. This behaviour was similar to the trend reported elsewhere (Little, 1999b; Osinubi, 1998b). The percentage loss of strength was 38%, 28%, 45% and 47% for unreinforced soil, 0.25%, 0.5% and 1% fiber contents, respectively. The registered

average strength loss (40%) was higher than 20% which was reported in the previous investigations (National Lime Association, 2006). It should be acknowledged that moisture offered lubrication at fiber-matrix interface and impaired fiber-matrix macro-mechanical interaction (Tang et al, 2010). Furthermore, the moisture caused loss of cohesion at fiber-matrix interface and reduced matric suction. In addition, the hydrophilicity of natural fibers was responsible for the degradation of fiber mechanical properties that ultimately reduced strength of the composite (Pickering et al., 2016).

11.3.2 Effects of fiber inclusions on compressive strength of soaked composite.

The effects of fiber inclusions on compressive strength of soaked specimens are indicated in figures 11.4a and b.

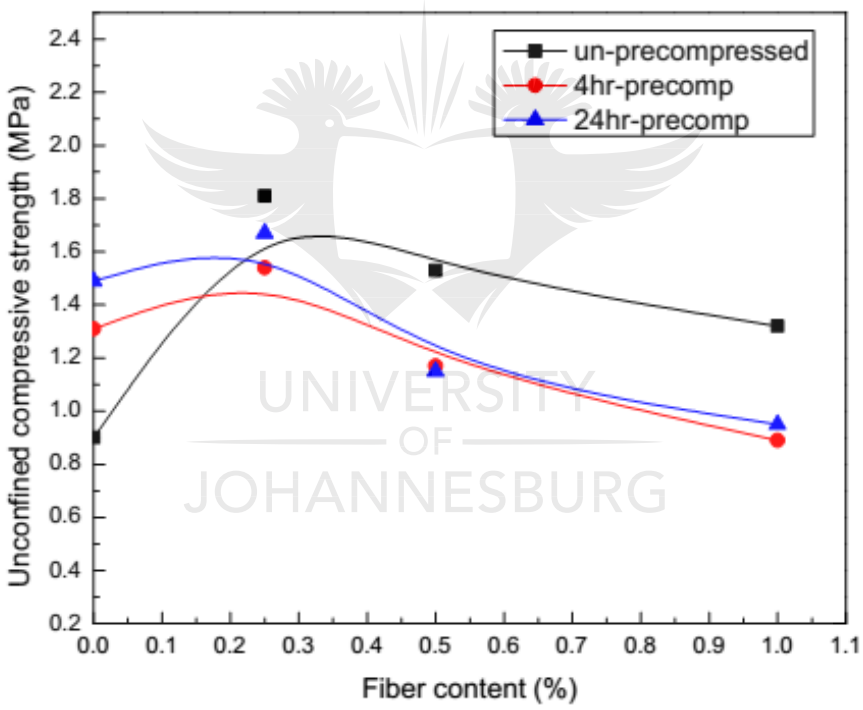

(a)

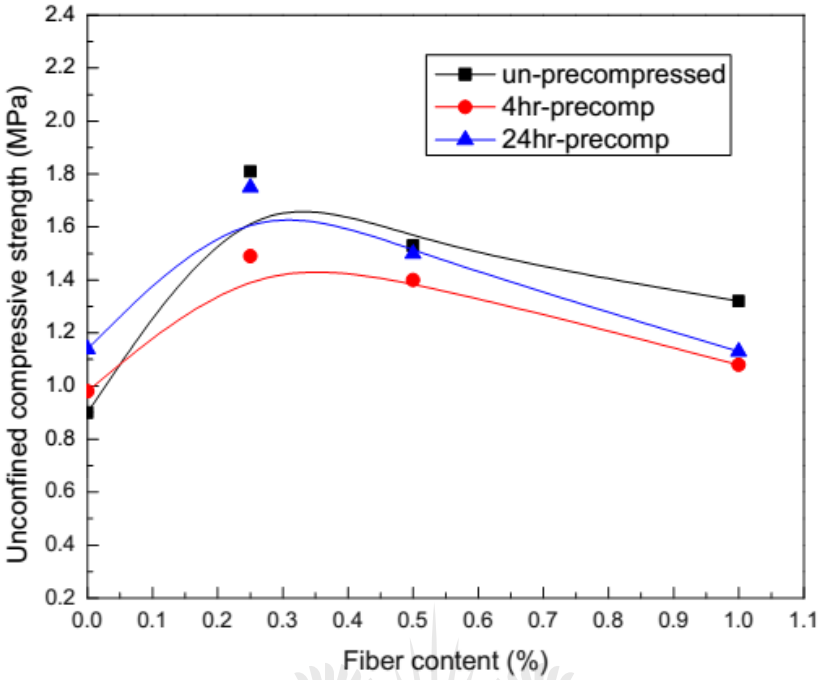

(b)

Figure 11.3: Variation of UCS with fiber contents at various curing time at pre-compression (a) 10%UCS (b) 20% UCS.

It is noted that fiber inclusion increases unconfined compressive strength to optimum values and then decreases with further increase in fiber content. For 10% UCS pre-compression stress level, strength gains of 18% and 12% are registered at 0.25% fiber content after 4h and 24h, respectively. The decrease of about 32% and 40% relative to unreinforced specimens is indicated at 1% fiber content. On the other hand, 20% UCS pre-compression stress level shows similar trend, however at 1% fiber content, the specimens still exhibit improved strength relative to unreinforced specimens. In comparison, the strength gains of 20% and 17% relative to unreinforced specimens are shown after 4h and 24h, respectively.

The maximum strength gains for both pre-compression stress levels are registered after 24h of curing. The initial strength gains of the specimens in this investigation were attributed to the strength mobilised by the fibers as a result of the mechanical interaction with cementitious compounds and enhanced shear resistance of the soil matrix due to pre-compression. This mechanical interaction mechanism is well documented in previous studies (Tang et al, 2007a, 2010). The contribution of suction to strength was insignificant due to the 24h soaking of the specimens. The enhanced strength after 24h of curing was due to the improved resistance of the

soil composite to compression because of strength gain by pozzolanic reaction. This phenomenon was also reported elsewhere (Moghal and Sivapullaiah, 2011; Moghal et al., 2017). The resilience by 20% UCS pre-compressed specimens could be the effect of increased stiffness of soil matrix and strain energy induced in fibers after pre-compression. The comparison of strength evolution of un-precompressed and pre-compressed specimens for both scenarios is shown in Tables11.2a and b.

Table 11.2: Comparison of compressive strength evolution between un-precompressed and pre-compressed specimens with 10% UCS.

Fiber content %	Soaked 7 day compressive strength (MPa)				
	Un-precompressed	Pre-compressed			
		4h	Variance* (%)	24h	Variance* (%)
0	0.9	1.31	+45	1.49	+65
0.25	1.81	1.54	-15	1.67	-8
0.5	1.53	1.17	-24	1.15	-25
1	1.32	0.89	-33	0.90	-31

* Variance is the difference between un-precompressed strength and pre-compressed strength expressed as percentage of un-precompressed strength

Table 11.2b: Comparison of compressive strength evolution between un-precompressed and pre-compressed specimens with 20% UCS stress level

Fiber content %	Soaked 7 day compressive strength (MPa)				
	Un-precompressed	Pre-compressed			
		4h	Variance* (%)	24h	Variance* (%)
0	0.9	0.91	+1	1.14	+26
0.25	1.81	1.49	-18	1.79	-2
0.5	1.53	1.40	-9	1.50	-2
1	1.32	1.08	-18	1.13	-14

*Variance is the difference between un-precompressed strength and pre-compressed strength expressed percentage of un-precompressed strength

It is evident from the tables that compressive strengths of un-precompressed specimens are higher than pre-compressed specimens. Approximately 20% strength reduction is exhibited by the pre-compressed specimens. Fiber inclusion causes further reduction in strength. In this investigation, the macro-mechanical interlock between fibers and soil particles was the typical reinforcement mechanism in fiber reinforced soil. The efficiency of the mechanism was the function of friction and cohesion at fiber-matrix interface (Ahmad et al., 2010b; Tang et al, 2007a; Wu et al., 2014a). The friction and cohesion at fiber-matrix interface was enhanced by pozzolanic products due to lime addition as fiber-matrix contact points were increased (Moghal et al., 2017). Any disturbance to the bonding process of pozzolanic products to fibers as curing progressed would compromise adhesion at fiber-matrix interface. This would ultimately reduce strength mobilisation of the fiber composite. The application of pre-compression stress caused redistribution of bond strength and fiber-matrix debonding. The pre-compression initiated macro crack development along fiber-matrix interface and altered bonding process. The development of macro cracks was significantly low in the specimens when the pre-compression was applied at later stage of curing (24h). On the other hand, pre-compression at early stage (4h) of curing significantly disturbed strength development of the composite. In respect of aforementioned hypotheses, it is obvious that crack density in the matrix was increased by high pre-compression level and was accompanied by the localised debonding of fiber-matrix interface (Kafodya and Okonta, 2018). The strength gain by unreinforced specimens was due to soil densification as a result of compression that in turn caused increased shear resistance, and ultimately improved unconfined compressive strength. The synergic effects of matrix stiffness and high resistance to compression of the composite after extended curing period were responsible for high strength gain registered by 20% UCS pre-compressed and 24h cured specimens.

11.3.3 Effects of fiber inclusions on tensile strength of soaked composite.

The split tensile strengths for both pre-compression scenarios are shown in figures 11.4a and b for 10% UCS and 20% UCS pre-compression stress levels, respectively.

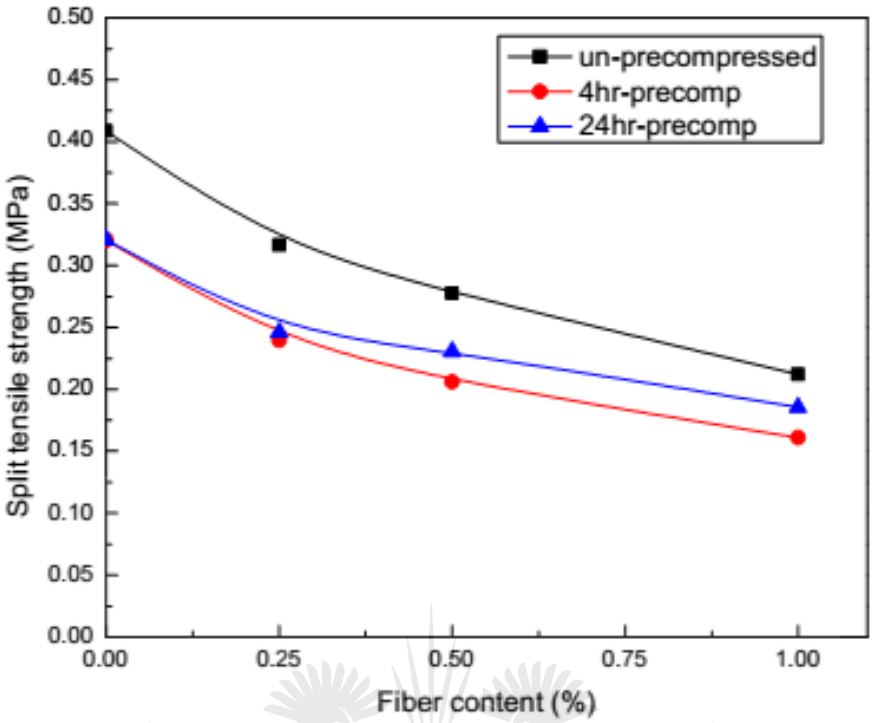

(a)

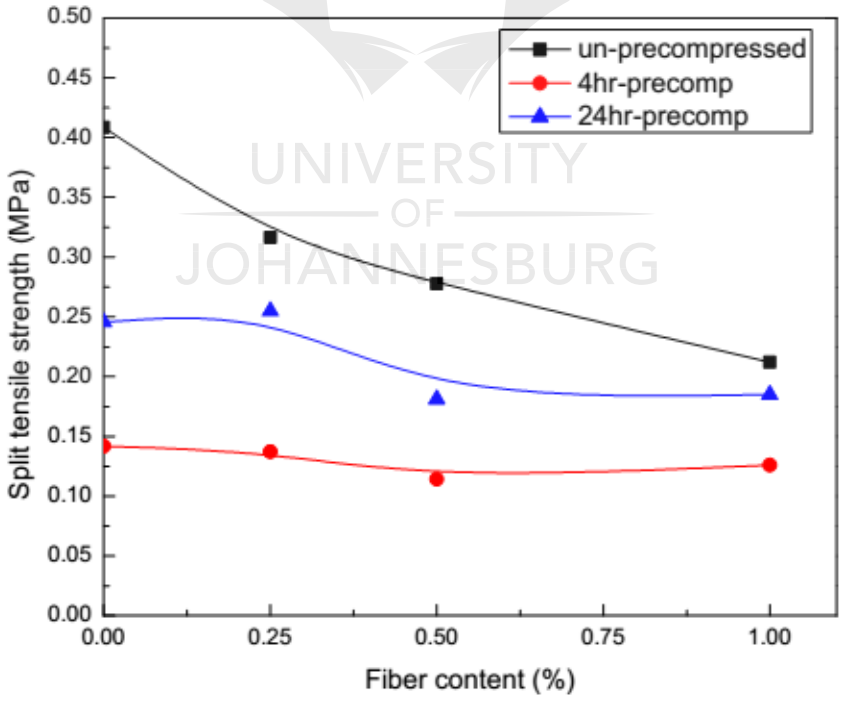

(b)

Figure 11.4: Variation of split tensile strength with fiber contents (a) 10%UCS (b) 20% UCS.

It is noted that pre-compression causes reduction in split tensile strength for both pre-compression cases. As shown in figures 11.4a and b, approximately 20% strength reduction is exhibited for both pre-compression cases. It is evident that increase in the fiber inclusions leads to further reduction in split tensile strength. For 10% UCS pre-compression stress level, 50% and 11% strength reductions, relative to unreinforced specimens are shown at 1% fiber content after 4h and 24h curing time, respectively. On the other hand, about 7% and 24% strength reductions are indicated for specimens under 20% UCS pre-compression stress level. As already alluded to, adhesion at fiber-matrix interface and interfacial friction resistance were the fundamental parameters that dictated the resistance of fibers to slippage. In this case, weak bond and low frictional resistance culminated into low tensile resistance of the composite (Tang et al, 2010; Yetimoglu and Salbas, 2003).

Fundamentally, increasing volume of fibers caused changes in the volume of solids and voids within a given volume of the composite. The addition of fibers essentially provided resistance to compaction and prevented dense packing of grains while creating voids along the peripheral of the fibers. In this respect, fiber reinforced soil possessed both macro voids as a result of packing of a smaller number of solids and micro voids emanating from the inability of fibers to form perfect bond with soil particles (Ibraim and Fourmont, 2006). The aforementioned phenomena, in turn increased volume of voids in the composite. Since the specimens in the present study were compacted and tested at almost saturated condition, it can be deduced that moisture filled the micro and macro voids of the composite and in turn reduced friction and mechanical interaction at fiber matrix interface. High fiber content increased volume of voids and suppressed particle-fiber interaction. These mechanisms substantiate the pronounced strength reduction with fiber inclusions exhibited by both un-precompressed and pre-compressed specimens. Applying fiber slippage and force equilibrium theories, and adopting the split tensile model for fibers shown in figure 10.6, the tensile resistance of the stabilised composite could be analysed with the following assumptions (1) constant shear stress exists along the length of the fiber (2) fiber diameter does not change with tensile loading (3) fibers are flexible with circular cross-section, of uniform diameter and are linearly elastic (4) stabilised soil matrix offers resistance to tension.

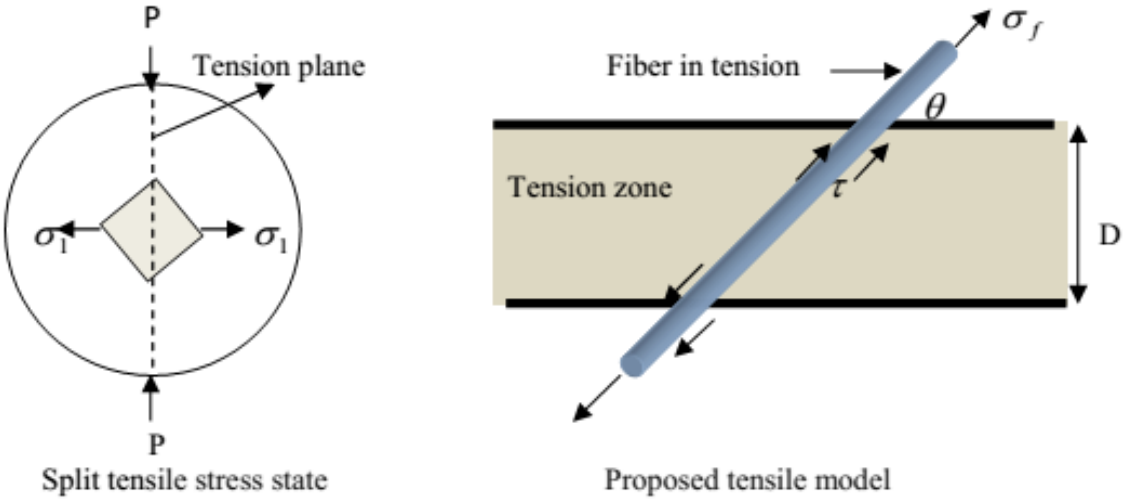

Figure 11.5: Proposed tensile model at tension zone.

Using force equilibrium theory, at the incipient of fiber slippage, the maximum tensile stress induced in the fiber due to full anchorage at fiber ends is given by equation 11.3.

$$\sigma_f = 2\sigma_\theta \frac{L}{D} \tan\delta \sin\theta \qquad (11.3)$$

where σ_θ is the effective normal stress on the fiber inclined to the horizontal at an angle θ, L and D are length and the diameter of the fiber, respectively and δ is fiber-soil friction angle. The term $\sin\theta$ is an empirical scalar that accounts for the fiber orientation. From equation 11.3, when θ=0, it implies that fibers lie parallel to tension plane and corresponding induced tensile stress $\sigma_f = 0$, which indicates that fibers are not stretched and have no tension because shear mobilisation does not take place in the absence of fiber ends anchorage. For θ=90°, $\sin\theta$=1 which implies that fibers are normal to the tension plane, the maximum induced tension takes place due to full anchoring of fiber ends. In figure 11.5, tangential stress can be expressed by equation 11.4.

$$\tau = \sigma_\theta e^{-0.5v_f} \tan\delta \qquad (11.4)$$

where $e^{-0.5v_f}$ accounts for the reduced tangential stress due to moisture impaired fiber-fiber interaction and v_f is fiber volume fraction at tension zone, assuming that 50% fiber volume fraction effectively mobilise tensile resistance. Since stabilised soil is considered to resist

tension, total resistance to applied split tensile stress T_R at the tension plane prior to fiber slippage is given by equation 11.5.

$$T_{Rf} = \varepsilon E_s e^{-v_v} + 2\sigma_\theta \frac{L}{D} e^{-0.5v_f} \tan\delta \sin\theta \quad (11.5)$$

where ε is soil matrix strain, E_s is elastic modulus of the matrix and v_v is the matrix void space. Fiber inclusion increases resistance to soil matrix compaction and compression, hence increases volume of matrix voids (Ibraim and Fourmont, 2006). In this respect $v_v = \alpha v_f$ where α is the proportionality constant. Applying rule of mixture for composites, and assuming that perfect bond exists before fiber slippage; the maximum tensile resistance can be expressed by equation 11.6.

$$T_R = v_m \varepsilon E_s e^{-\alpha v_f} + v_f 2\sigma_\theta \frac{L}{D} e^{-0.5v_f} \tan\delta \sin\theta \quad (11.6)$$

where v_m and v_f are matrix and fiber volumetric fractions, respectively. Equation 11.6 can also be expressed as equation 11.7.

$$T_R = \left(\frac{A - A_f}{A}\right) \varepsilon E_s e^{-\alpha \frac{A_f}{A}} + \left(\frac{A_f}{A}\right) 2\sigma_\theta \frac{L}{D} e^{-0.5\frac{A_f}{A}} \tan\delta \sin\theta \quad (11.7)$$

where A is total area of tension zone of the specimen and A_f is total cross section area of the fibers across tension zone. Taking $\alpha = 0.25$, the variation of normalised tensile resistance with fiber contents at the incipient of slippage is shown in figure 11.6.

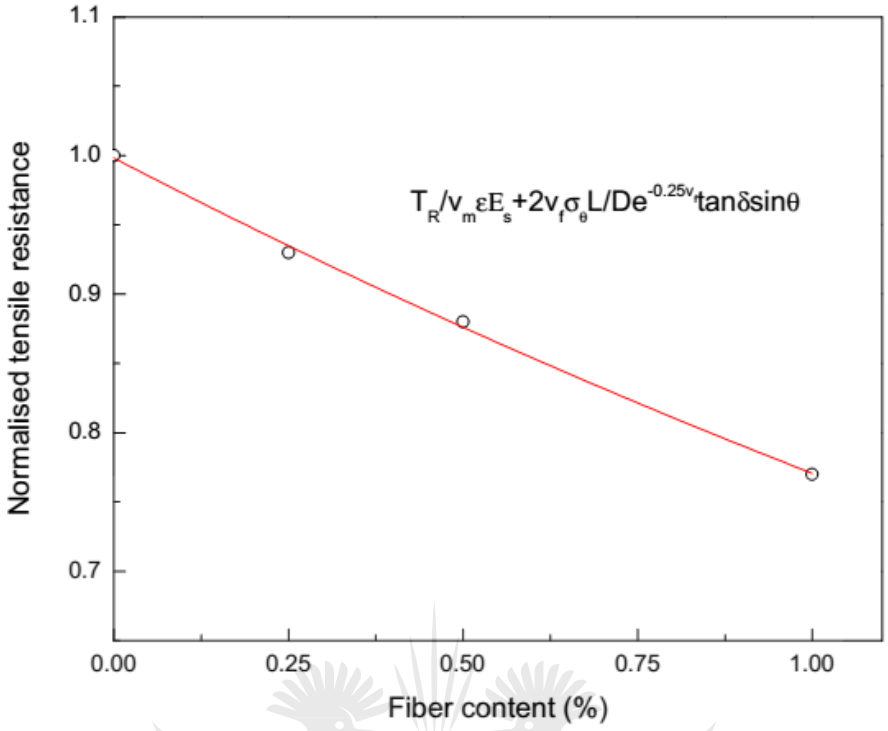

Figure 11.6: .Normalised tensile resistance with fiber content.

The model in figure 11.6 is in agreement with the tensile behaviour exhibited by both pre-compressed and un-precompressed specimens. According to the model, when fiber content is 0 (unreinforced soil), $v_m = 1$ and tensile resistance is equivalent to εE_s, which is tensile resistance of the soil matrix only. The ability of the composite to resist tension depends on matrix elastic modulus, fiber orientation and fiber-matrix friction angle. Non uniform fiber distribution reduces macro structural interaction (Diambra et al., 2007), water ingress at fiber-matrix interface reduces angle of friction (Tang et al, 2010) and water ingress reduces stiffness of both matrix and natural fibers(Pickering et al., 2016).

The comparisons of tensile strength evolution of un-precompressed and pre-compressed specimens are shown in Tables 11.3 and 11.4 for 10% UCS and 20% UCS pre-compression stress levels, respectively.

Table 11.3: Comparison of split tensile strength evolution between un-precompressed and pre-compressed specimens with 10% UCS

Fiber content %	Soaked 7 day split tensile strength (MPa)				
	Un-precompressed	Pre-compressed			
		4h	Variance* (%)	24h	Variance* (%)
0	0.41	0.32	-22	0.32	-22
0.25	0.32	0.23	-28	0.25	-22
0.5	0.28	0.21	-25	0.23	-18
1	0.21	0.16	-24	0.19	-10

*Variance is the difference between un-precompressed strength and pre-compressed strength expressed as percentage of un-precompressed

Table 11.4: Comparison of split tensile strength evolution between un-precompressed and pre-compressed specimens with 20% UCS

Fiber content %	Soaked 7 day split tensile strength (MPa)				
	Un-precompressed	Pre-compressed			
		4h	Variance* (%)	24h	Variance* (%)
0	0.41	0.14	-65	0.25	-39
0.25	0.32	0.14	-56	0.28	-13
0.5	0.28	0.11	-61	0.18	-36
1	0.21	0.13	-38	0.19	-10

*Variance is the difference between un-precompressed strength and pre-compressed strength expressed as percentage of un-precompressed

It is apparent that pre-compressed soil composite specimens exhibit lower strength values than un-precompressed counterparts. Curing time shows insignificant effects on the strength variance for 10% UCS pre-compression stress level. On the other hand, 20% UCS pre-compression stress level increases percentage of variance for specimens after 4h of curing. The pronounced percentage of variance for 4h-precompressed specimens at 20% UCS pre-compression stress level was attributed to the induced damage by pre-compression that was responsible for bond redistribution during pozzolanic reaction. In addition, cracks induced in the soil composite

during pre-compression created void spaces for moisture accumulation during capillary soaking. High moisture content significantly reduced tensile resistance.

11.3.4 Variation of percentage residual compressive and tensile strengths with fiber inclusions

The variation of percentage residual strengths with fiber contents and curing time at which pre-compression stress was applied are shown in Tables 11.5 and 11.6 for 10% UCS and 20% UCS pre-compression stress levels, respectively and for both compressive and tensile strengths.

Table 11.5: Residual strength of specimens with 10% UCS pre-compression

Fiber content (%)	Residual strength (%)			
	Compressive strength		Split tensile strength	
	4h	24h	4h	24h
0	84	79	50	51
0.25	90	85	68	78
0.5	94	86	71	53
1	96	90	27	30

Table 11.6: Residual strength of specimens with 20% UCS pre-compression

Fiber content (%)	Residual strength (%)			
	Compressive strength		Split tensile strength	
	4h	24h	4h	24h
0	90	68	55	52
0.25	89	70	50	80
0.5	87	90	32	50
1	81	95	30	52

As shown in table 11.6, percentage residual strength for compression test decreases with increasing fiber content. Average percentage residual strength of at least 80% for both unreinforced and reinforced specimens in compression is indicated. In comparison, effects of pre-compression stress level on the residual strength are negligible. Furthermore, the effects of curing time vividly show undefined trend for both pre-compression levels. The fiber controlled strength due to fiber intertwining was responsible for an increase in percentage residual strength with increasing fiber content. The specimen's macro-structural modifications, i.e., change in void

space; cracking and deformation after initial loading were responsible for undefined trend for reloaded specimens. It should be highlighted that high residual strength offers benefits to the serviceability of the geosystems. From the design perspective, high residual strength guarantees longevity of geosystems when exposed to severe pre-loading, i.e., heavy or impact load.

On the other hand, specimens under tension in Tables 11.5 and 11.6 exhibit low percentage residual strength. The tensile residual strength increases to maximum and drastically reduces with increasing fiber content. It is clear that 1% fiber content exhibits low residual strength. An average of 50% residual strength is registered by specimens in tension. The effects of curing and pre-compression on the tensile residual strength are negligible due to macro structural modifications of the specimens. It can be deduced that fiber moisture induced slippage during loading endowed the specimens with low tension resistance.

11.3.5 Variation of strength indices $\left(\frac{q_t}{q_u}\right)$ with fiber content and pre-compression

The ratio of split tensile strength to unconfined compressive strength has been used to measure performance of lime or cement amended soil with different variables. It has also been used to establish the relationship between tensile and unconfined compressive strengths. The previous investigations (Consoli et al., 2012, 2014) have established that $\frac{q_t}{q_u}$ is the scalar independent of porosity and amount of stabilising agent. The straight proportionality exists between tensile and compressive strengths of fiber reinforced cemented soil mixtures. Any rational dosage methodology considering the effect of different variables can be centered on tensile or compression tests, once they are intimately related through a scalar $\frac{q_t}{q_u}$. It was indicated that $\frac{q_t}{q_u}$ ratios for various stabilised soil range from 0.1-0.2 (Baldovino et al., 2018; Consoli et al., 2012, 2014). In this present study, the ratios of tensile and compressive strengths were evaluated at various fiber contents, pre-compression level and curing time. The results of variation of $\frac{q_t}{q_u}$ with fiber content are shown in figures11.7 a and b.

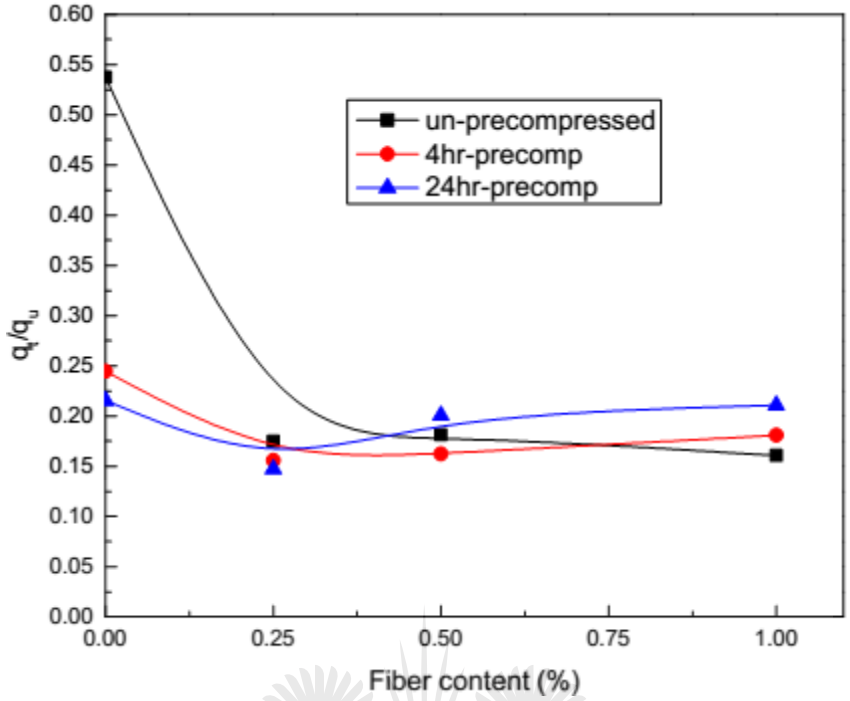

(a)

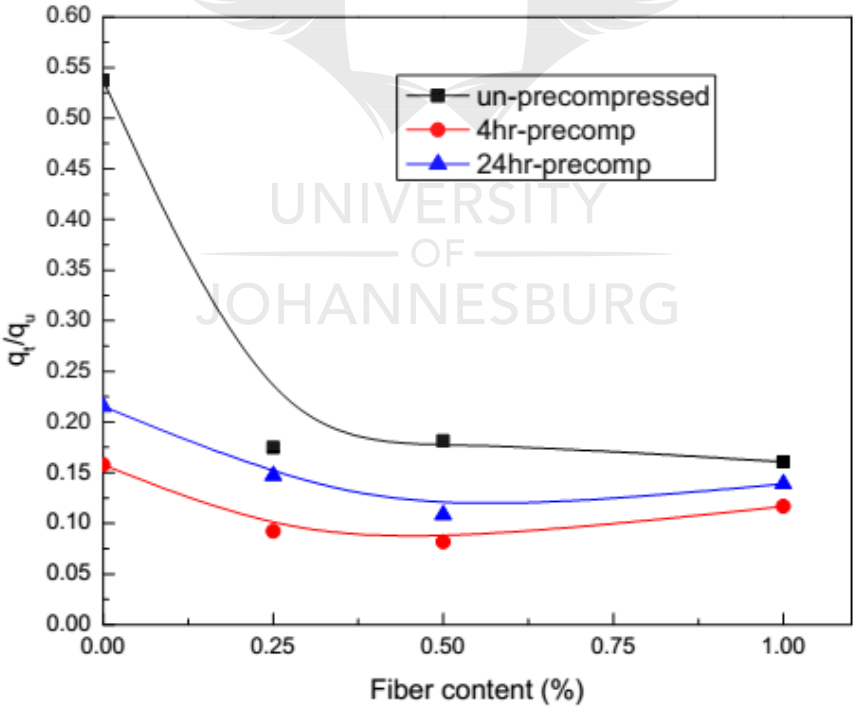

(b)

Figure 11.7: Variation of strength indices of the soaked soil composites (a) 10% UCS (b) 20% UCS.

It can be seen that $\frac{q_t}{q_u}$ ratios decrease with increasing fiber content to the minimum value. For the pre-compressed composite, strength index shows rebound from 0.25% to 1% fiber contents. The similar trend is shown for both pre-compression and un-precompression scenarios however, no rebound is exhibited up to 1% fiber content for un-precompressed composite. Reduction in the index means that soaked sisal fibers in this study did not perform well in tension rather than in compression. However, the compression efficiency declined with fiber inclusion. The summary of the optimum $\frac{q_t}{q_u}$ values is shown in Table 11.7.

Table 11.7: Optimal q_t/q_u values for un-precompressed and pre-compressed specimens

Curing time (h)	$\frac{q_t}{q_u}$		
	Un-precompressed	Pre-compressed	
		10%UCS	20%UCS
	0.18		
4	-	0.16	0.08
24	-	0.15	0.11

It is clear that the values are within the range reported in literature (Consoli et al., 2012, 2014). The pre-compressed composites indicate lower values than un-precompressed. The values further reduce with the increase in pre-compression level. Effects of curing indicate marginal changes. The trend in the table implies that the compression efficiency of stabilised soil composite reduced with the increase in pre-compression. It can therefore be concluded that strength index depends on fiber content and pre-compression level and straight proportionality exists between tensile and compressive strengths beyond optimum strength index or fiber content. Figures11.8a, b and c show the relationship between tensile and compressive strengths of un-precompressed and pre-compressed stabilised composite beyond the optimum index values.

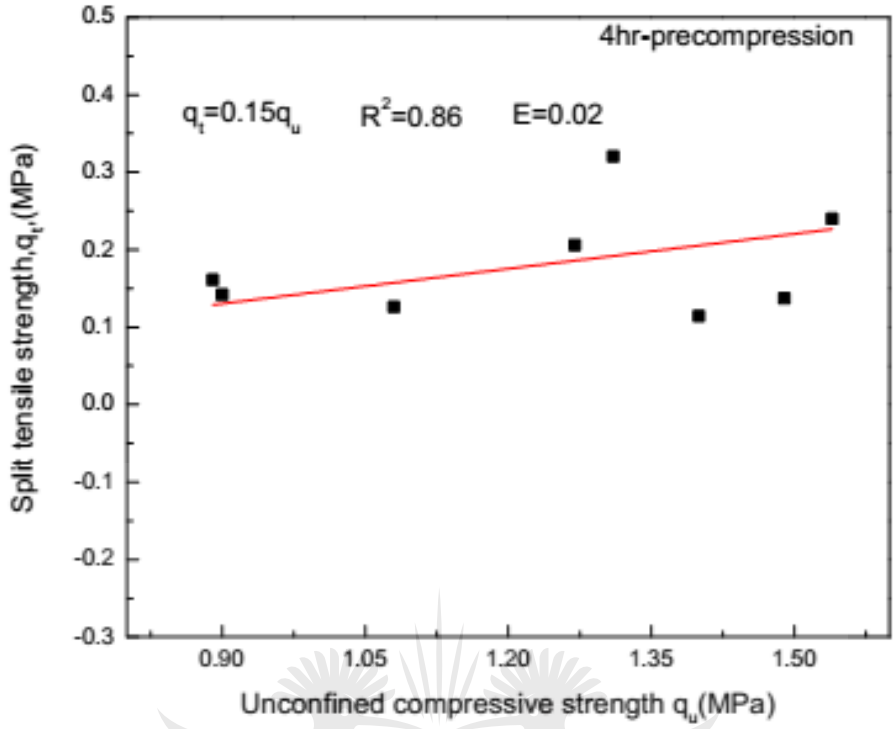

(a)

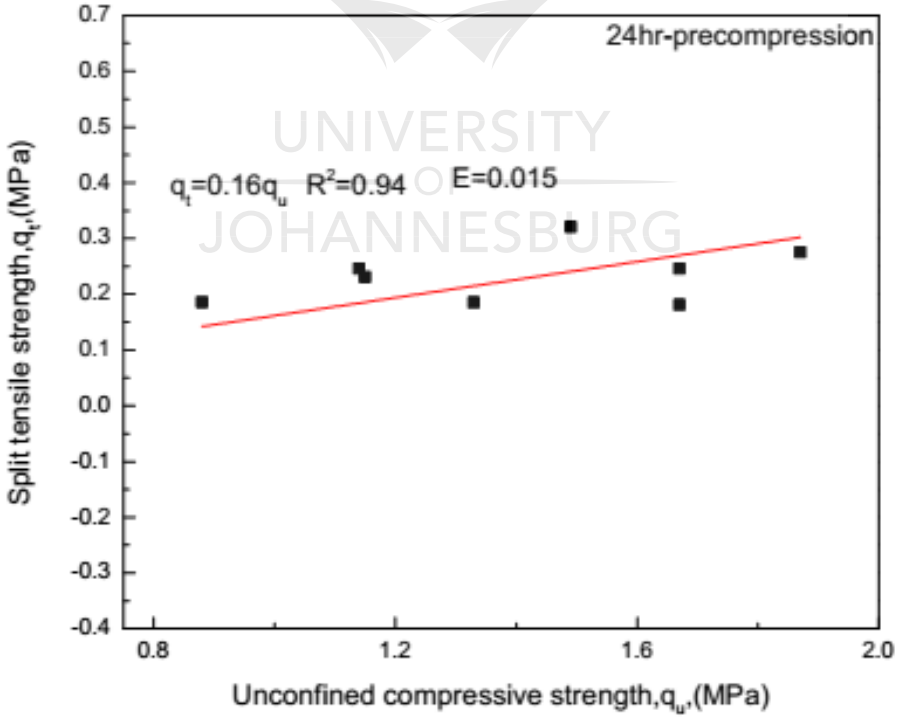

(b)

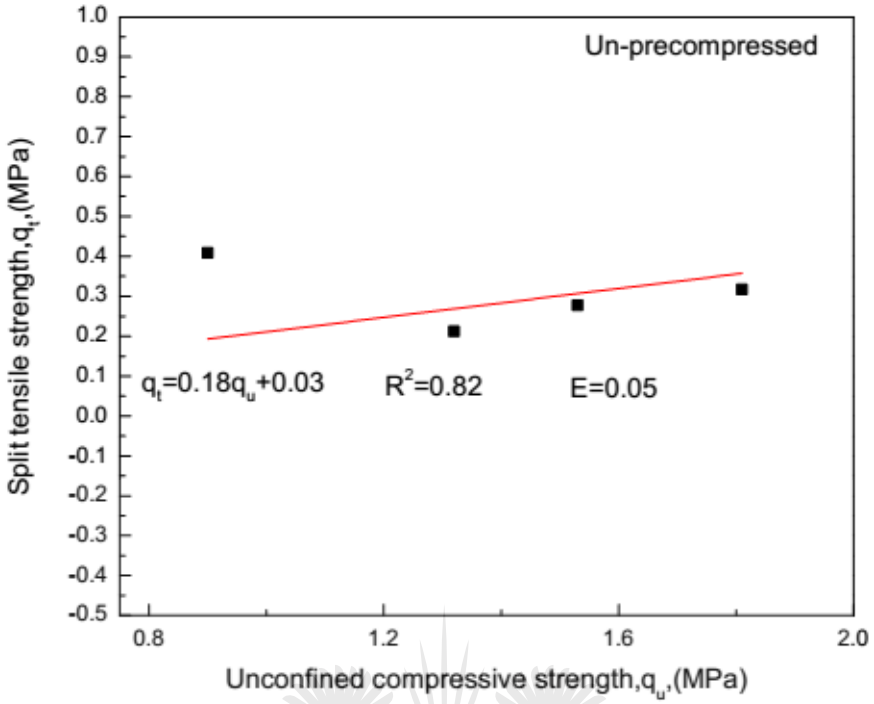

(c)

Figure 11.8: Split tensile and compressive strength relationships beyond optimum indices (a) 4hrs pre-compression (b) 24hr-precompression (c) un-precompressed.

It can be seen that the models substantiate the aforementioned claims and linear proportionality between tensile and compressive strengths beyond optimum fiber content exists.

11.3.6 Load-deformation relationship and failure modes

The representive load-deformation relationships of the unreinforced and reinforced (1% fiber content) stabilised soil for the un-precompressed specimens under tensile and compression are shown in figures 11.9a and b, respectively.

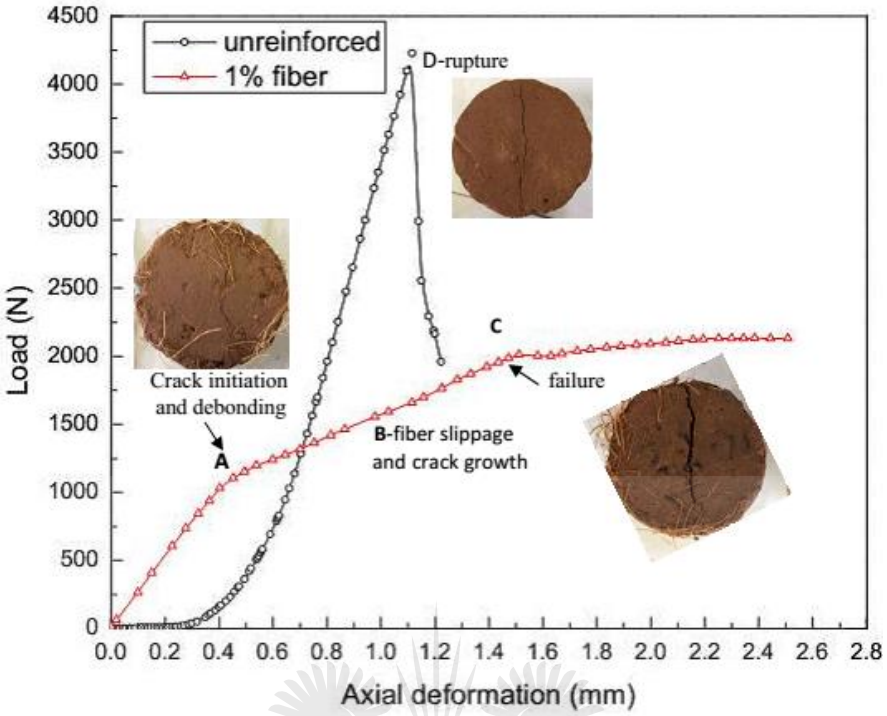

(a)

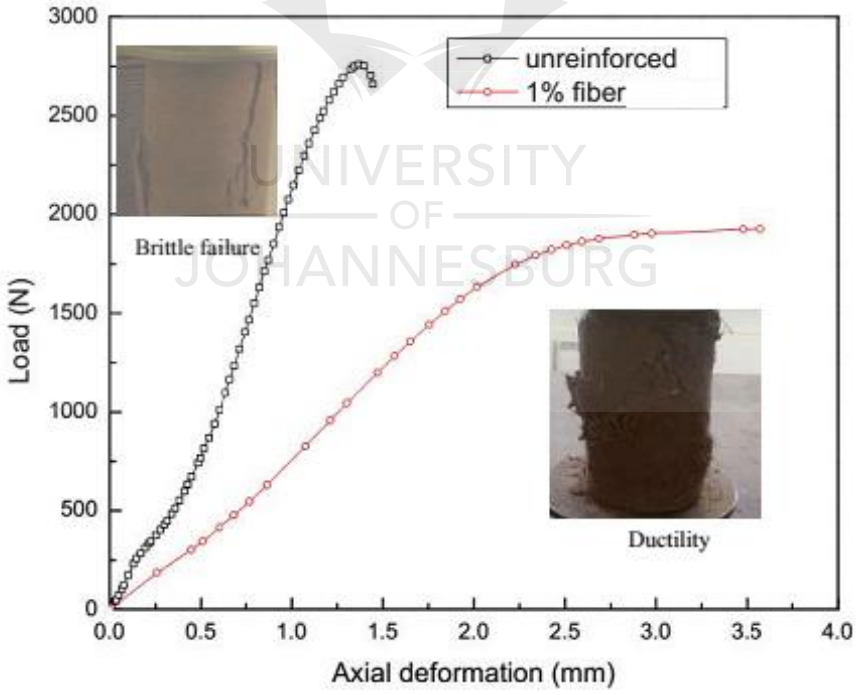

(b)

Figure 11.9: Load-deformation relationship of unreinforced and reinforced soaked lime flyash stabilised soil. (a) split tension behaviour (b) compression behaviour.

It can be seen that unreinforced specimens for tensile test exhibit considerable stiffness relative to reinforced specimen at axial deformation beyond 0.3mm. Material relaxation is indicated below 0.3mm deformation. It is noted that unreinforced stabilised soil is associated with brittle tension failure immediately after peak load as evidence by the macrostructure in figure 11.10a. The behaviour of reinforced specimens (1% fiber content) under tension is characterised by linear relationship between load and deformation to some deformation level (0.3mm) beyond which strain hardening occurs. Furthermore, considerable post peak ductility is exhibited for reinforced specimens. On the other hand, unreinforced specimens in compression also exhibit higher stiffness than reinforced ones. Considerable post peak ductility is shown. The compression failure mode for unreinforced specimen is characterised by specimens' crushing whereas reinforced specimens show multiple planes of failure.

The material relaxation might have been triggered by the expulsion of moisture from the void spaces and particle movement due to the applied load. Brittle behaviour of stabilised soil was also reported elsewhere (Tang et al, 2007a). Strain hardening was attributed to the resistance of the fibers to slippage and elongation. The multiple planes of failure for reinforced specimens in compression were due to the random distribution and orientation of fibers that caused redistribution of the potential planes of weakness.

Conclusions

Based on the acquired results, it is concluded that;

1. Capillary soaking causes loss of strength of about 40% however, fiber inclusion improves compressive strength of soaked specimens relative to unreinforced specimens.
2. In comparison, pre-compressed stabilised soil-fiber composites exhibits lower compressive and tensile strengths than un-precompressed composites. About 20% strength loss of both compressive and tensile strength is registered. This is due to the synergic effects of soil matrix cracking and weak bond at fiber-matrix interface.
3. From the engineering design perspective, the characteristic strength of the stabilised soil should be reduced by the material reduction factor, preferably 1.2 to cater for strength reduction due to premature loading and moisture ingress.
4. Natural fiber inclusion reduces tensile strength of soaked composite due to fiber slippage, low fiber-matrix friction and moisture impaired fiber-fiber interaction.

5. In comparison, soaked natural fiber reinforced soil performs better in compression than in tension. However, strength proportionality of 10% to 17% between tensile and compressive strengths is indicated beyond optimum strength index.
6. From the engineering design point of view, tensile strength of the lime stabilised soil can be taken as 10% of the unconfined compressive strength.
7. Fiber inclusion increases compression residual strength of soaked composite to about 90%. This is as a result of the resilience of fibers to failure. Compressive and tensile strengths of compressed composite are enhanced by extended curing time. This is attributed to the increased resistance of the composite to compression and tension due to pozzolanic reaction.
8. Fiber inclusion improves ductility of the soaked lime-fly ash stabilised soil.
9. In practice, using stabilised fly ash fiber reinforced soil in earthen construction endows the structure with considerable resilience to deformation under moisture exposure. It is anticipated that the stabilised fiber reinforced earthen structure would exhibit significant load carrying capacity when re-loaded after sustaining heavy loading under severe moisture conditions.

References

ABNT. (1983). "Mortar and concrete—Test method for split tensile strength of cylindrical specimens. Rio de Janeiro, Brazil NBR 7222.

Ahmad et al. (2010). Performance evaluation of silty sand reinforced with fibres. *Geotextiles and Geomembranes, 28*, 93–99.

Albrech.B.A and Benson.C.H. (2001). Effect of desiccation on compacted natural clay. Journal of. *Journal of Geotechnical and Geoenvironmental Engineering, 127*(1), 67-75.

ASTM D1140-17. (2017). Standard Test Methods for Determining the Amount of Material Finer than 75-μm (No. 200) Sieve in Soils by Washing. West Conshohocken PA: ASTM International.

ASTM D2166. (2016). Standard Test Method for Unconfined Compressive Strength of Cohesive Soil. West Conshohocken, PA: , ASTM International.

Baldovino et al. (2018). Effects of lime addition on geotechnical properties of sedimentary soil in Curitiba, Brazil. *Journal of rock mechanics and geotechnical engineering, 10*(1),188-194.

Consoli et al. (2012). Parameters controlling tensile and compressive strength of fiber-reinforced cemented Soil. *Journal of Materials in Civil Engineering*.

Consoli et al. (2014). Control factors for the long term compressive strength of lime treated sandy clay soil. *Journal of Transportation Geotechnics, 1*, 129-136.

Diambra et al. (2007). Determination of fibre orientation distribution in reinforced sands. *Ge´otechnique, 57*(7), 623–628. doi: doi: 10.1680/geot.2007.57.7.623

Hejazi et al. (2012). A simple review of soil reinforcement by using natural and synthetic fibers. *Construction and Building Materials, 30*, 100-116.

Ibraim. E and Fourmont.S. (2006). *Behaviour of Sand Reinforced with Fibres*. Paper presented at the Geotechnical Symposium in Rome, Rome.

Jian et al. (2014). Effect of discrete fibre reinforcement on soil tensile strength. *Journal of rock mechanics and geotechnical engineering, 6*, 133-137.

Kafodya.I and Okonta.F.N. (2018). Effects of natural fiber inclusions and pre-compression on the strength properties of lime-fly ash stabilised soil. *Construction and Building Materials, 170*, 737-746.

Little.D.N. (1999). Evaluation of structural properties of lime stabilized soils and aggregates (pp. 49). Arlington: National Lime Association.

Miller et al. (1998). Experimental analysis of desiccation crack propagation in clay liners. *Journal of the American Water Resources Association, 34*(3), 677-686.

Moghal.A.A. and Sivapullaiah.P.V. (2011). Effect of pozzolanic reactivity on compressibility characteristics of stabilised Low Lime Fly Ashes. *Geotechnical and Geological Engineering, 29*, 665-673.

Moghal et al. (2017). Target reliability approach to study the effect of fiber reinforcement on UCS behavior of Lime treated semiarid Soil. *Journal of Materials in Civil Engineering 29*(6), 04017014-04017011-04017015.

Morris et al. (1992). Cracking in drying soils. *Canadian Geotechnical Journal, 29*(2), 263-277.

National Lime Association. (2006). Technical brief:Mixture design and testing procedures for lime stabilized soil. Arlington: National Lime Association.

Osinubi.K.J. (1998). Influence of compactive efforts and compaction delays on lime-treated soil Journal of Transportation Engineering 124(1998) 149-155. *Journal of Transportation Engineering, 124*, 149-155.

Pickering et al. (2016). A review of recent developments in natural fibre composites and their mechanical performance. *Composites: Part A, 77*(83), 98–112.

Tang et al. (2007). Strength and mechanical behavior of short polypropylene fiber reinforced and cement stabilized clayey soil. *Geotextile Geomembranes, 25*(3), 194-202.

Tang et al. (2010). Interfacial shear strength of fiber reinforced soil,. *Geotextiles and Geomembranes, 28*, 54–62.

Thwae.M.M and Liao.K (2003). Durability of bamboo-glass fiber reinforced polymer matrix hybrid composites. *Composites Science and Technology, 63,* 375–387.

Wu et al. (2014). Investigation of mechanical properties of randomly distributed sisal fiber reinforced soil. *Materials research innovation, 18,* 953-959.

Yetimoglu.T and Salbas.O. (2003). A study on shear strength of sands reinforced with randomly distributed discrete fibers. *Geotextiles and Geomembranes, 21,* 103-110.

12 CHAPTER TWELVE-ROLE OF SISAL FIBER INCLUSION IN ADOBE MASONRY CONSTRUCTION

12.1 Introduction

The application of adobe materials faces several constraints due to their brittle behaviour, low tensile strength and deterioration when exposed to moisture. However, the properties of adobe can be improved by mechanical compaction, chemical stabilisation with cement, lime and bitumen, and fiber inclusions such as straw (Islam and Iwashita, 2010; Mesbah et al., 2004). Chemical stabilisation can significantly improve strength and water resistance of adobe. Typically, chemical binders are added at the contents between 4 and 10% of the soil dry weight (Consoli et al., 2012; Moghal et al., 2018). On the other hand, the use of these additives significantly increases both material cost and environmental impact. Alternatively, natural fiber inclusion have been used in earthen construction to increase ductility, tensile strength, post crack strength, erosion resistance, dimensional stability and reduce shrinkage cracks of the material (Walker, 2004).

The previous studies (Binici et al., 2005; Sharma et al., 2015) focused on the solution to improve mechanical properties of adobe bricks with natural fibers and chemical additives. Some of the existing literature (Blondet et al., 2011; Figueiredo et al., 2013) reports much on the seismic behaviour of adobe structures and the development of seismic strengthening solutions. In practice, the performance of adobe masonry in tension and shear is governed by the properties of mortar. Therefore, it is recommended that the strength of mortar should be less than the strength of masonry units (ENV 1992-2, 2006). On the contrary, some proposals have promoted the use of mortars with strengths similar to or greater than the bricks. To date, there is little published scientific data to support these recommendations or published design values for flexural bond strength of adobe brick masonry (Walker, 1999). The study on cement stabilised mortar shows that tensile bond strength of cement mortar and adobe bricks/blocks varies between 0.007 and 0.032MPa and flexural bond strength between 0.004 and 0.014MPa (Walker, 1999). The bonding properties of unstabilised mortar with adobe bricks/blocks have not been extensively reported. In particular, synergic strength contributions of fiber reinforced mortar and adobe bricks/blocks to the global performance of the adobe masonry structures have not been reported in the literature. The adobe masonry structures are poorly constructed in the developing countries

due to lack of design and construction guidelines. This has rendered the structures vulnerable to natural hazards such as earthquakes(Novelli et al., 2019).

This study aimed at providing information on the mechanical properties of fiber reinforced adobe masonry construction for the design of resilient and sustainable low cost infrastructure. Sisal fibers were used to reinforce mud mortar and adobe bricks. The study focused on the investigation into the effect of fiber inclusion in mud mortar and adobe bricks on the strength improvement of the adobe masonry structure. This was achieved by performing series of masonry element tests such as prism, triplet and couplet to determine compressive, shear and tensile strengths, respectively. The uniaxial compression test on wallets and diagonal compression (shear) test on masonry wall panels were performed to determine compressive strength and shear resistance of the adobe masonry structures. A finite element analysis of the wall panels was conducted to evaluate the stress state of the loaded reinforced and unreinforced masonry wall panels. The results of numerical analysis were compared with ASTM and RILEM interpretations using Mohr circles. Finally, design of the masonry walls was carried out according to BS5628 and Eurocode 6 standards in order to estimate load carrying capacity of the full scale adobe wall.

12.2 Materials and experimental programme

12.2.1 Materials

The soil used in this study was locally collected and air dried for 48h. Sisal fibers with length of 25mm were used. The summary of the fiber and soil properties is referred to chapter 3 in Table 3.3 and Table 3.2, respectively.

12.2.2 Experimental programme

The compression test of adobe bricks was carried out using Coopers TC4131 compression machine at the stress rate of 0.5kPa/s according to (ASTM C67-03a, 2003). Compression test on mortar specimens was performed using Quasar 10 universal tensile machine at a loading rate of 0.5mm/min according to (BS EN 1015-11, 1999). The average compressive strength value of 6 tested specimens was determined and taken as representative strength of materials for both bricks and mortar.

The tension capacity of mortar was determined by a series of couplets tests using fabricated test rig. The test set-up for couplets is shown in figure 12.1.

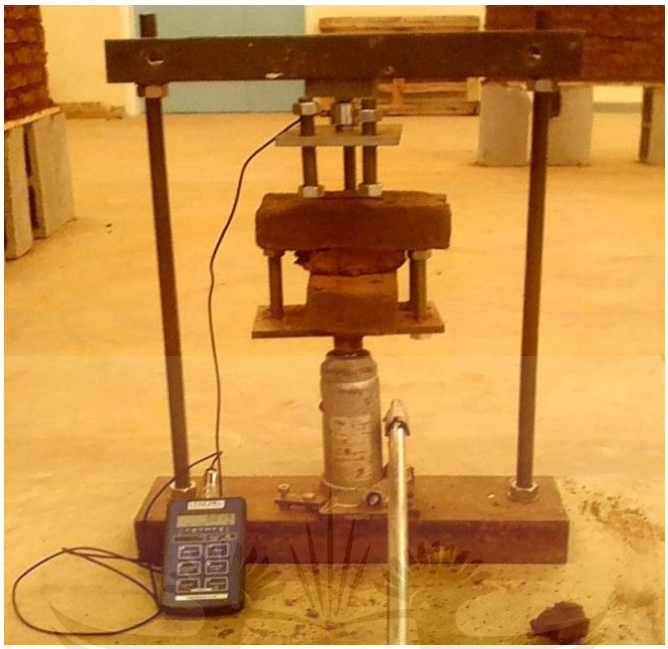

Figure 12.1: Test set-up for mortar couplet test.

The tension bond resistance of the mortar was computed as the sum of measured load and the self-weight of the bottom brick. The tensile bond strength was determined by dividing total load with mortar-brick contact area. The average strength value of 5 specimens of each mortar type was determined and taken as representative strength of the material.

The prism and triplet tests were conducted according to (ASTM C1314-03b, 2003) and (BS EN 1052-3, 2002), respectively. The triplet was realised with three bricks and two mortar joints. The wooden blocks of 50mm width were placed under the lateral bricks and the load was applied on top of the central brick. Three lateral confinement stresses of 0.025kPa, 0.05kPa and 0.1kPa were applied to determine the coefficient of friction and failure criteria of each mortar type. The test set-up for triplets is shown in figure 12.2.

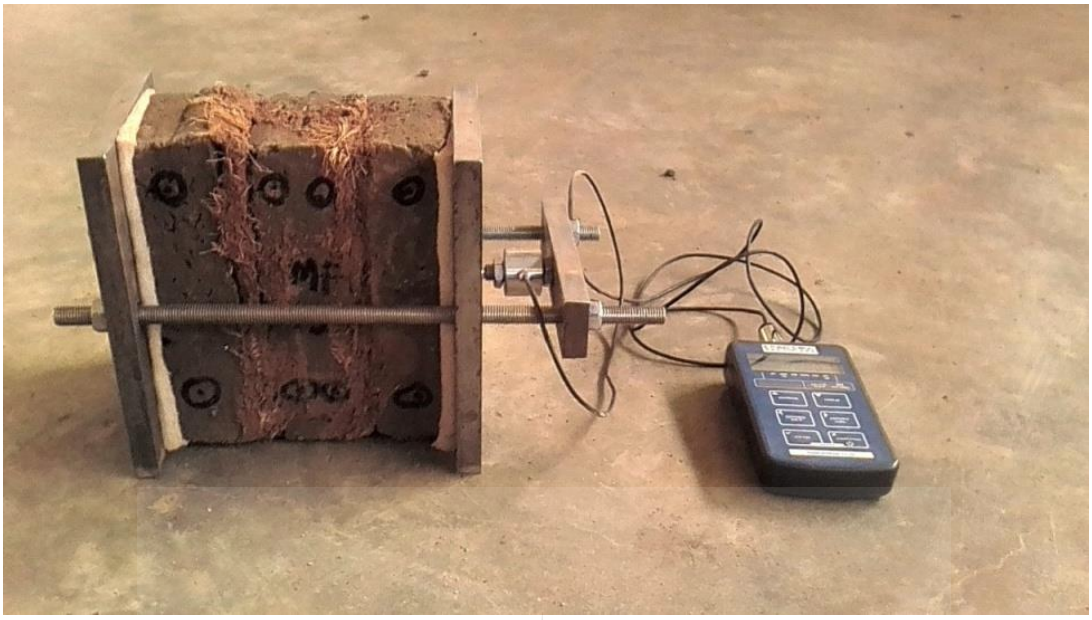

Figure 12.2: Triplet test specimen and confinement frame.

The shear strength of the triplet was computed using equation 12.1.

$$\tau_t = \frac{P_{ult}}{2A_g} \tag{12.1}$$

where P_{ult} is the ultimate load and A_g is the area parallel to the mortar joint.

Diagonal compression test was performed on wall panels to determine shear strength in accordance with (ASTME519-15, 2015). The diagonal compression test set-up is shown in figure 12.3.

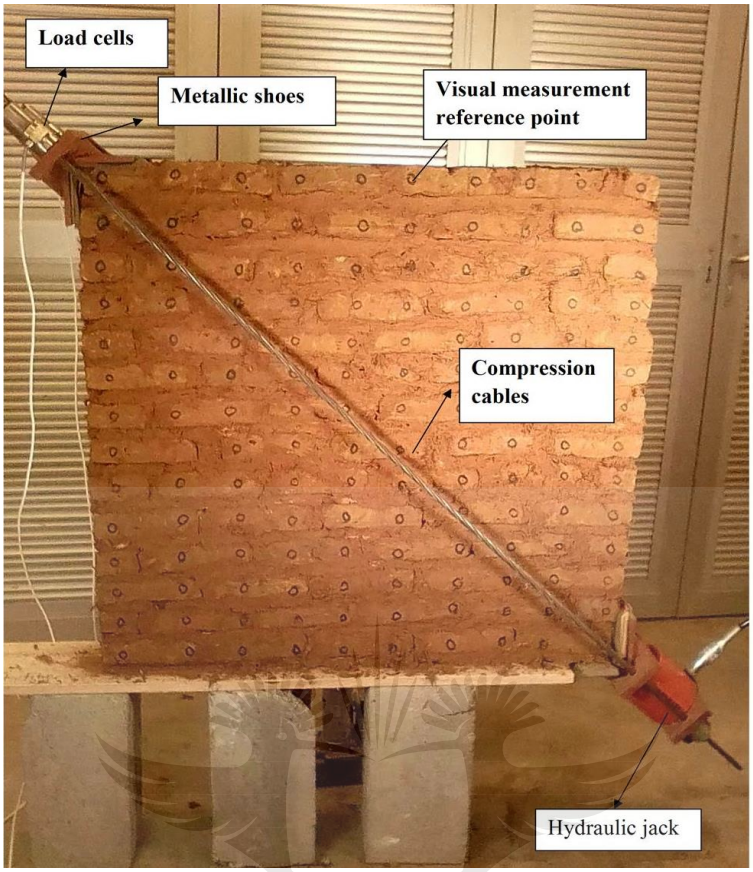

Figure12.3 : Diagonal compression test set-up.

The metallic shoes of length 1/10 of the panel length were anchored to the lower and upper corners of the panel by the tension cables. The load cells and the metallic shoes were fixed to the cables by steel pins. The metallic shoes were used in order to distribute the load on a larger surface area to avoid concentration of compression stresses and, consequently, local failures at the corners. The diagonal compression load was applied on the lower corner of the wall by a hydraulic jack until failure of the panel occurred. Shear strength of the panel was computed using equation 12.2 according to ASTM.

$$\tau_p = 0.707\frac{P_t}{A_p} \qquad (12.2)$$

where P_t is the ultimate failure load and A_p is the net area of the panel.

Displacements and strains of the prism, triplet and wall panel specimens were measured using an Imetrum Video Gauge system, during testing, along with the applied loads measured by

calibrated load cells. All masonry specimens were tested when dry at the prevailing average relative humidity of about 35% ±3. At this prevailing condition, mechanical behaviour of the adobe masonry could not be affected since water vapour in the air was so low that it could not penetrate through the masonry joints which govern the overall behaviour of the masonry construction.

Numerical simulation of the panels was performed by Finite-Element code ANSYS 14 in ANSYS Parametric Design Language (APDL). The objective was to evaluate stress state of the wall panels by linear elastic analysis. Both bricks and mortar were modelled using four node triangular standard elements called Plane 183.These elements have two degrees of freedom per nodes, four Gauss integration points and Lagrangian polynomials as shape functions. The model of the masonry wall was built as a regular inclusion of bricks into a matrix of mortar. The mortar was perfectly bonded to bricks and geometrical configuration and the boundary conditions were identical to the real experimental setup used in the laboratory testing.

The maximum shear loads obtained from the experimental results were applied to the finite element model. The elastic materials properties such as Young's modulus and Poison's ratio that were employed in the finite element analysis are summarised in Table 12.1.

Table 12.1. Material properties employed in finite element analysis of panels

Property	Reinforced mortar	Unreinforced mortar	Bricks	Ref
Elastic Modulus (MPa)	150	350	1500	Experiment
Poison's ratio	0.2	0.2	0.26	

12.3 Results and discussions

12.3.1 Couplet test

The results of couplet test for both reinforced and unreinforced mortar types are shown in Table 12.2 and 12.3.

Table 12.2: Tensile bond resistance of fiber reinforced mud mortar

Specimen Serial	Maximum Tensile capacity (N)	Mean (N)	COV %
RM1	32		
RM2	34	37	11
RM3	40		
RM4	41		
RM5	38		

*RM=Reinforced mortar

Table 12.3: Tensile bond resistance of unreinforced adobe mud mortar

Specimen Serial	Maximum Tensile capacity (N)	Mean (N)	COV %
URM1	20		
URM2	21		
URM3	32	28.2	26
URM4	37		
URM5	31		

*URM=Unreinforced mortar

The tensile capacity values of reinforced specimens range between 32N and 41N while values of unreinforced specimens range between 20N and 37N. The average tensile resistance values for both unreinforced and reinforced mortar types are 28.2N and 37N, respectively. Fiber inclusion causes an increase in tensile capacity of about 31% compared with unreinforced specimens. The coefficient of variation (COV) of unreinforced specimens is 26% while that for reinforced specimens is 11%. This implies that test results of unreinforced specimens exhibited higher dispersion than for reinforced ones. The fiber inclusion in mud mortar reduces shrinkage of the soil and also minimises size of shrinkage cracks (Moghal et al., 2018). The lower resistance exhibited by unreinforced mortar was due to the shrinkage of the mortar that undermined bonding at mortar-brick interface. The presence of shrinkage cracks caused pre-mature failure of

the unreinforced mortar. The variations in the bonding properties of the unreinforced mortar resulted in the high dispersion of test results. On the other hand, the low shrinkage and significant tensile resistance of fibers were responsible for good bonding at the mortar-brick interface and high tensile bond resistance.

12.3.2 Triplet test

The results of triplet tests for reinforced and unreinforced mortar types are shown in Tables 12.4and 12.5, respectively.

Table 12.4: Shear strength of reinforced mortar with various lateral confinement stresses

Specimen serial	Lateral confinement stress (kPa)		
	0.025	0.05	0.1
	Shear strength (MPa)		
1	0.038	0.075	0.105
2	0.035	0.077	0.105
3	0.050	0.075	0.105

Table 12.5:Shear strength of unreinforced mortar with various lateral confinement stresses

Specimen serial	Lateral confinement stress (kPa)		
	0.025	0.05	0.1
	Shear strength (MPa)		
1	0.028	0.035	0.083
2	0.030	0.055	0.085
3	0.038	0.055	0.080

Mohr-coulomb failure criteria for both mortar types are shown in figure 12.4.

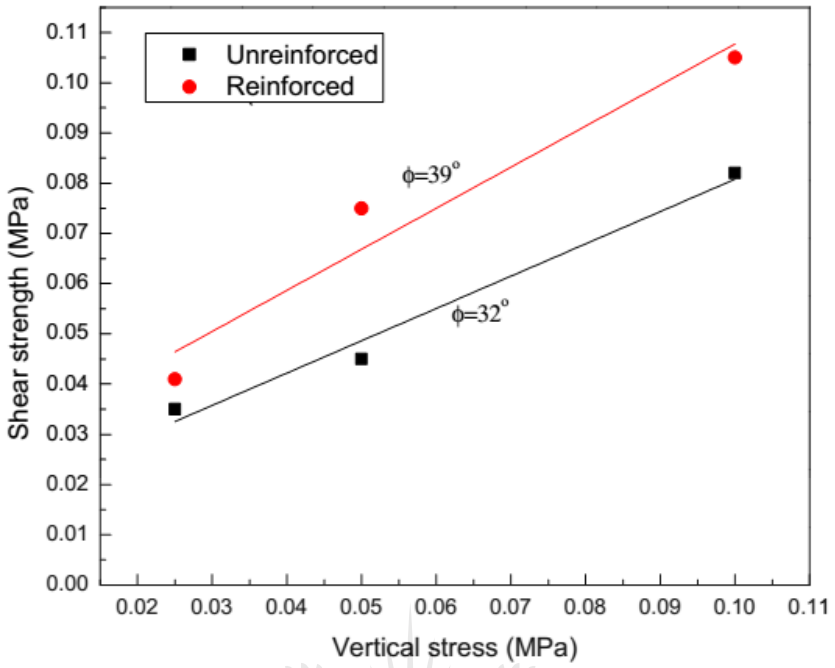

Figure12.4 : Mohr-coulomb failure criteria for triplets with reinforced and unreinforced mortar.

For the reinforced specimens, shear strength with lateral confinement stresses between 0.025kPa and 0.1kPa ranges between 0.035kPa and 0.105kPa. On the other hand, the shear strength of unreinforced specimens with lateral confinement stresses between 0.025kPa and 0.1kPa ranges between 0.028kPa and 0.085kPa. The shear strength values of adobe masonry between 0.014kPa and 0.05kPa are reported in the literature (Erika et al, 2014). The marginal difference between the literature and the test results is attributed to the type of soil and the lateral confinement stresses imposed on the specimens in the present study. The corresponding Mohr-Coulomb failure criteria for both mortar types are shown in figure.12.4. It is shown that an increase in lateral confinement stress causes an increase in shear strength. It is worth noting that the angles of friction for reinforced and unreinforced specimens are 39^{o} and 32^{o}, respectively. In comparison, fiber reinforced specimens indicate an average increase in shear strength of about 22% relative to unreinforced specimens. The cohesion of about 0.037MPa and 0.025MPa for reinforced and unreinforced mortar respectively, are indicated. The angles of friction between 29^{o} and 34^{o,} and cohesion values between 0.037MPa and 0.045MPa for unreinforced adobe specimens are reported in the literature(Erika et al, 2014). It is noted that the test results in the present study are relatively close to what has been reported in the literature. It is evident that fibers endowed the mortar with significant shear strength and friction coefficient. This was

attributed to the mechanical interaction between fibers and soil particles that ultimately mobilised resistance to applied shear. The fibers provided large friction surface area with soil particles hence enhanced friction resistance of the fiber composite.

12.3.3 Prism test

The results of compressive strength and strain of masonry prisms for specimens with unreinforced mortar and bricks (UBUM), specimens with unreinforced bricks and reinforced mortar (UBRM), specimens with reinforced bricks and unreinforced mortar (RBUM) and specimens with reinforced bricks and mortar (RBRM) are shown in figure.12.5.

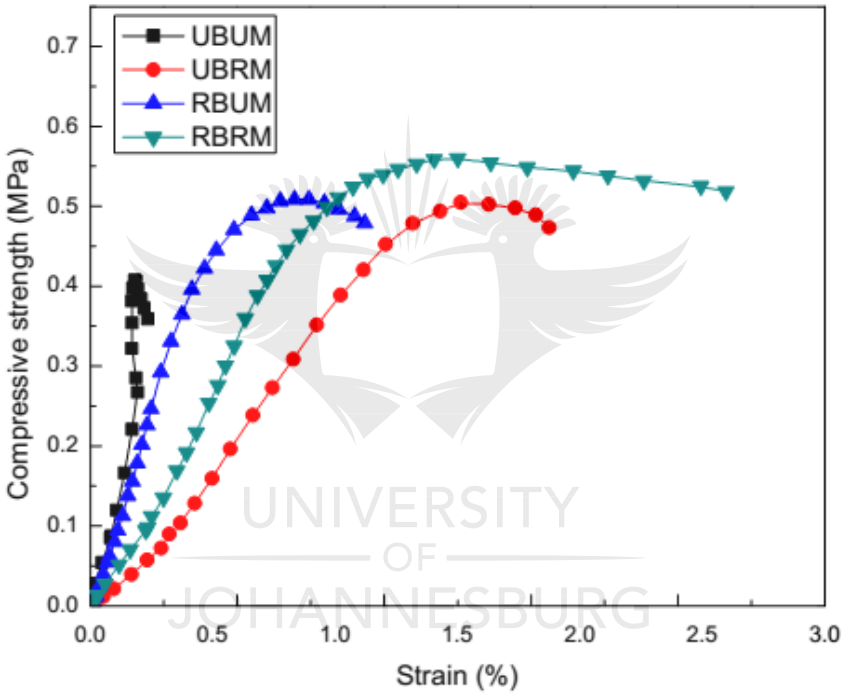

Figure 12.5 : Stress-strain relationship of masonry prisms.

It is shown that compressive strength of reinforced prisms increases linearly to yield strain and reduces to failure strain. The unreinforced prisms fail immediately after reaching yield strain which is an indicative of brittle behaviour. In comparison, prisms with unreinforced mortar mobilise low strength compared with reinforced prisms. It is shown that reinforced prisms exhibit strength increase of a minimum of 25% relative to unreinforced prisms. The ductility increases with fiber inclusion in either the mortar or the bricks. Almost the same compressiv strength of about 0.5MPa is mobilised with fiber inclusion in either the mortar or bricks. The

prisms with fiber reinforced mortar and bricks show the highest ductility and strength of about 0.55MPa.The yield strain values for UBUM, RBUM, UBRM and RBRM are 0.15%, 0.5%, 1.2% and 1.2%, respectively. It is noted that the strength and deformation of the masonry prisms increase with fiber inclusion especially in the mortar. It is reported elsewhere that strength of the masonry increases with an increase in strength of the mortar*(*Nazeer et al., 2018). Some reports (Erika et al, 2014; Wu et al., 2013b) indicate values of prism compressive strength of the traditional adobe in the range between 0.36MPa and 1MPa, and strain between 0.5% and 3%. It is noted that the test results are within the values reported in the literature however, the prism compressive strength of adobe masonry depends on the properties of adobe material. The high load carrying capacity of reinforced mortar was responsible for strength improvement of the masonry prisms. The reinforced bricks provided additional strength to the masonry. It can be concluded that the strength of both bricks and mortar had similar influence on the overall strength of the masonry. The typical failure modes of the masonry prisms with unreinforced mortar and bricks (UBUM), with unreinforced bricks and reinforced mortar (UBRM) and those with reinforced bricks and mortar (RBRM) are shown in figure 12.6. It is noted that typical failure mode of unreinforced masonry is characterised by vertical crack across the bricks and mortar joints. This is also reported elsewhere(Wu et al., 2013b). In case of the partially reinforced prisms (UBRM), the failure mode is characterised by vertical cracks relatively smaller than those of unreinforced prisms. For the fully reinforced prisms (RBRM), the failure is characterised by both vertical and horizontal cracks accompanied by large lateral deformation. The ductility is advantageous to seismic performance of the reinforced masonry. It implies that the reinforced adobe masonry structure would undergo considerable deformation before collapse during earthquake (Tetley and Madabhushi, 2007).

Figure 12.6 : Failure modes of masonry prisms.

It is noted that typical failure mode of unreinforced masonry is characterised by vertical crack across the bricks and mortar. In case of the partially reinforced prisms (with either reinforced mortar or brick), the failure mode is characterised by vertical cracks relatively smaller than those of unreinforced prisms. For the fully reinforced prisms (both mortar and bricks reinforced), the failure is characterised by both vertical and horizontal cracking accompanied by large lateral deformation. The ductility is advantageous to seismic performance of the reinforced masonry. It implies that the reinforced adobe masonry structure would undergo considerable deformation before collapse during earthquake events.

12.3.4 Wallet compression test

The results of the compressive strength of masonry wallets for reinforced (RBRM) and unreinforced specimens (UBUM) are shown in Table 12.6.

Table 12.6: Results of compressive strength of fiber reinforced and unreinforced masonry wallets

Specimen designation	Dimensions h x w x t (mm)	Maximum compressive load (kN)	Compressive strength (MPa)	Mean (MPa)	COV %
RMRB1	480 x 400 x 202	126	1.3		
RMRB2	480 x 401 x 205	124	1.26	1.3	2.7
RMRB3	500 x 400 x 209	140	1.33		
UMUB1	502 x 400 x 210	68	0.65		
UMUB2	515 x 410 x 208	48	0.45	0.53	19
UMUB3	520 x 410 x 210	56	0.51		

The compressive strength values of the reinforced wallets range between 1.26MPa and 1.33MPa with coefficient of variation of 2.7%. On the other hand, compressive strength of unreinforced wallets ranges between 0.45MPa and 0.65MPa with coefficient of variation of 19%. The compressive strength values of adobe wallets between 0.77MPa and 1.72MPa are reported in the literature (Varum et al., 2008). In comparison, the compressive strength results obtained from the tests are within the range reported in the literature. It is worth noting that fiber inclusions in the mortar and bricks cause an average increase in the compressive strength of the wallets of about 145% as compared with unreinforced wallets. The results of fiber reinforced masonry wallets show small variation while the unreinforced masonry wallets indicate large variation. The shrinkage cracks might result in non-uniform material properties and pre-mature failure, and hence were responsible for the scatter of test results for unreinforced wallets. The material homogeneity reduced scatter of the reinforced wallets test results. Failure mode of the reinforced wallets was characterised by large deformation with vertical cracks. On the other hand, unreinforced wallets failed by crushing of the bricks and mortar as shown in figure 12.7.

(a) (b)

Figure 12.7: Failure modes of wallets (a) reinforced (b) unreinforced.

12.3.5 Diagonal compression panel test

The results of diagonal compression shear strength for reinforced (RBRM) and unreinforced (UBUM) panels are shown in Table 12.7.

Table 12.7: Results of diagonal compression test

Specimen designation	Maximum shear strength (τ) (MPa)	Maximum Diagonal Shear load (kN)	Shear modulus (G) (MPa)	Mean shear strength (MPa)	Mean shear modulus (MPa)	COV shear strength %	COV shear modulus %
UBRM1	0.043	73.6	21.76	0.047	41.60	13	47
UBRM2	0.041	70.2	42.21				
UBRM3	0.056	95.8	60.78				
UBUM1	0.016	27.4	6.48	0.014	9.32	12.6	44
UBUM2	0.012	20.5	13.96				
UBUM3	0.014	24	7.52				

The diagonal compression shear strength values of the reinforced panels range between 0.041MPa and 0.056MPa with coefficient of variation of 13%.The diagonal shear modulus of reinforced panels ranges between 21.76 and 60.78 MPa. On the other hand, diagonal compression shear strength of unreinforced panels ranges between 0.012MPa and 0.016MPa with coefficient of variation of 12.6%. The diagonal shear modulus of unreinforced panels is between 6.48MPa and 13.96MPa. It is noted that reinforced panels exhibit an average increase in shear strength and shear modulus of 235% and 346%, respectively compared with unreinforced panels. The shear stress and strain relationships of both reinforced and unreinforced specimens are shown in figure 12.8.

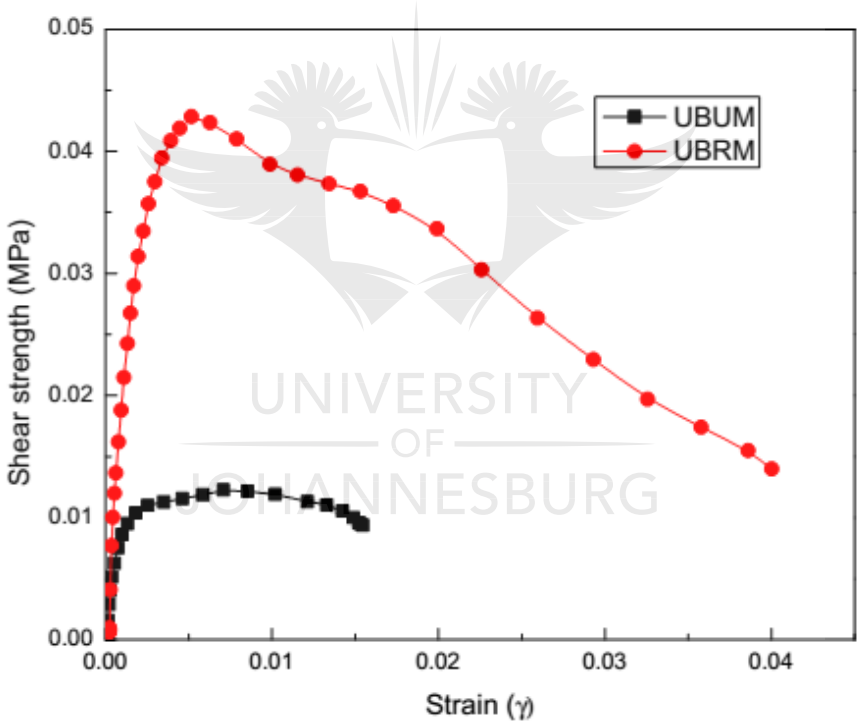

Figure 12.8: Shear strength and strain relationship of panels.

It is noted that wall panels with reinforced mortar exhibit three-fold increase in shear strength and four-fold increase in shear modulus. The reinforced panels exhibit considerable ductility before collapse. The failure modes of both unreinforced and reinforced panel are characterised by the diagonal crack inclined at almost 45^{o} to the horizontal plane of the panel as shown in figure 12.9a and b.

(a)

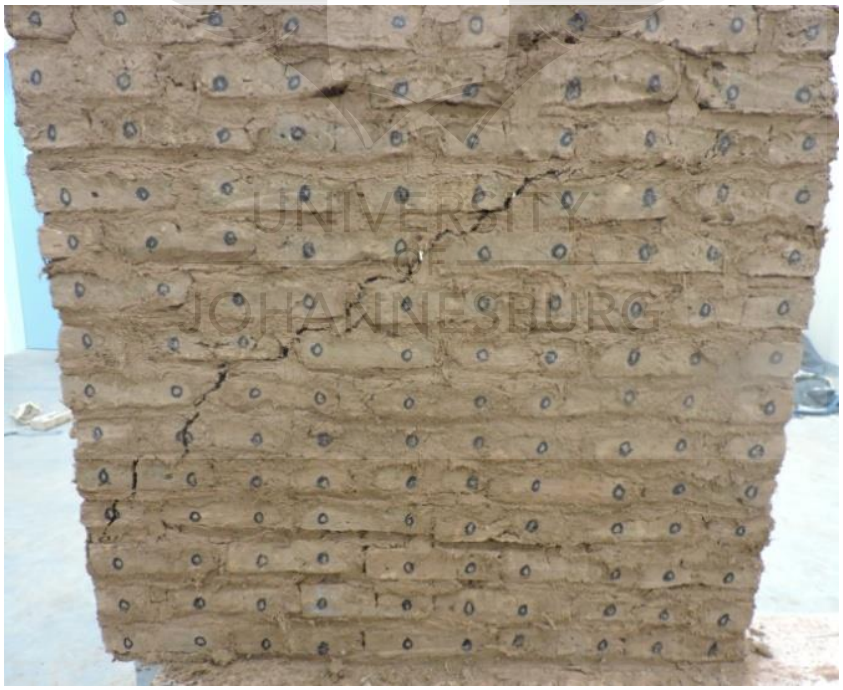

(b)

Figure 12.9: (a) Failure of unreinforced panel (b) Failure of reinforced mortar.

The failure modes indicate that the major principal tensile stress coincides with the inclination of the crack. It is anticipated that reinforced panel would perform better to lateral loading such as seismic loading.

12.3.6 Finite element analysis of the wall panels

Finite element modelling was undertaken by imposing loads from the experimental results (81kN and 25kN for reinforced and unreinforced panels, respectively). The major principal tensile stress was assumed to be concentrated at the center of the panel (Alecci et al., 2013; Brignola et al., 2009; Gabor et al., 2006). The modelling scheme of the panel is shown in figure 12.10 a and b.

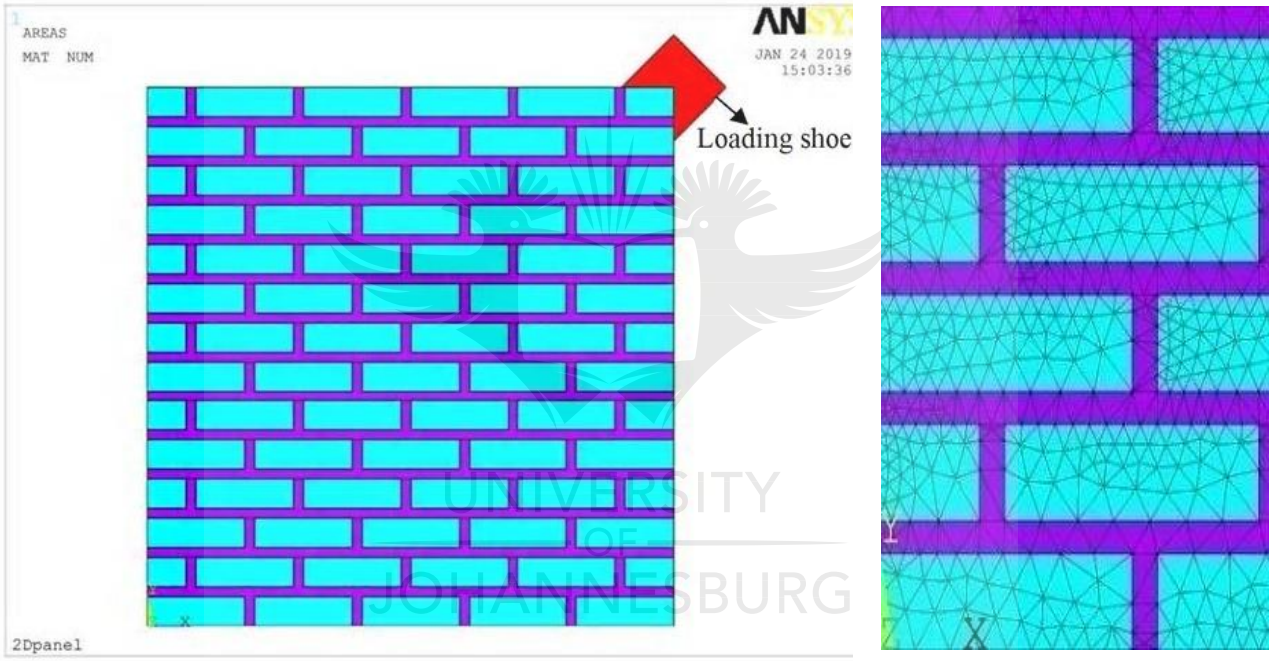

(a) (b)

Figure 12.10: Finite Element Model discretisation scheme.

The results of the finite element linear elastic analysis for unreinforced are shown in figures 12.11a- b and figures 12.12a-b. The results of reinforced panel are shown in Fig 12.13a- b, and figures 12.14a-b.

The finite element results show that the stress and strain are high in the direction inclined at 45^{o} to the horizontal plane of the panel. The normalised principal tensile stresses of about 0.6 and 0.99 for unreinforced and reinforced panels respectively, are indicated. The normalised principal

compressive stresses of about 0.96 and 2.7 for unreinforced and reinforced panels respectively are shown. The corresponding maximum shear stresses of 0.7 and 1.7 for unreinforced and reinforced panels respectively are determined. In the standard interpretation of the masonry diagonal compression test, as provided by ASTM, it is assumed that the stress state at the centre of the panel is of pure shear such that principal tensile stress is equal to shear stress and can be calculated by equation 12.2, and the principal directions coincide with the two diagonals of the panels (Alecci et al., 2013; ASTME519-15, 2015; Brignola et al., 2009). According to RILEM, masonry is assumed as an isotropic and homogeneous material such that stress state at the centre of the specimen is not a pure shear state, although the principal directions still coincide with the two diagonals of the panels (Alecci et al., 2013; Brignola et al., 2009; RILEM LUMB6, 1994).

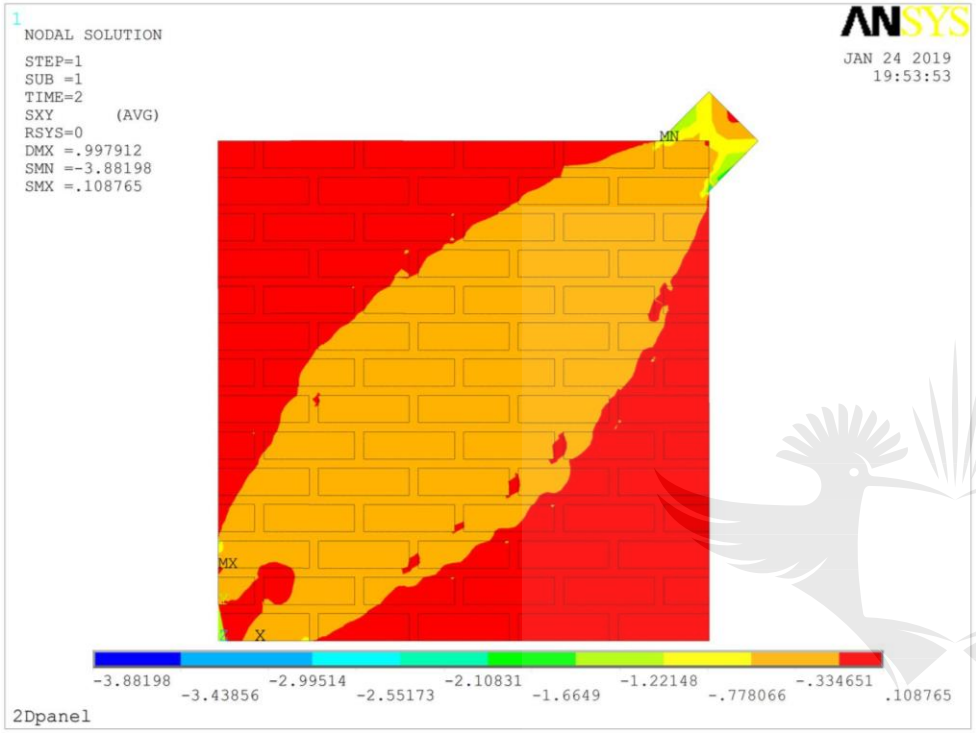

(a)

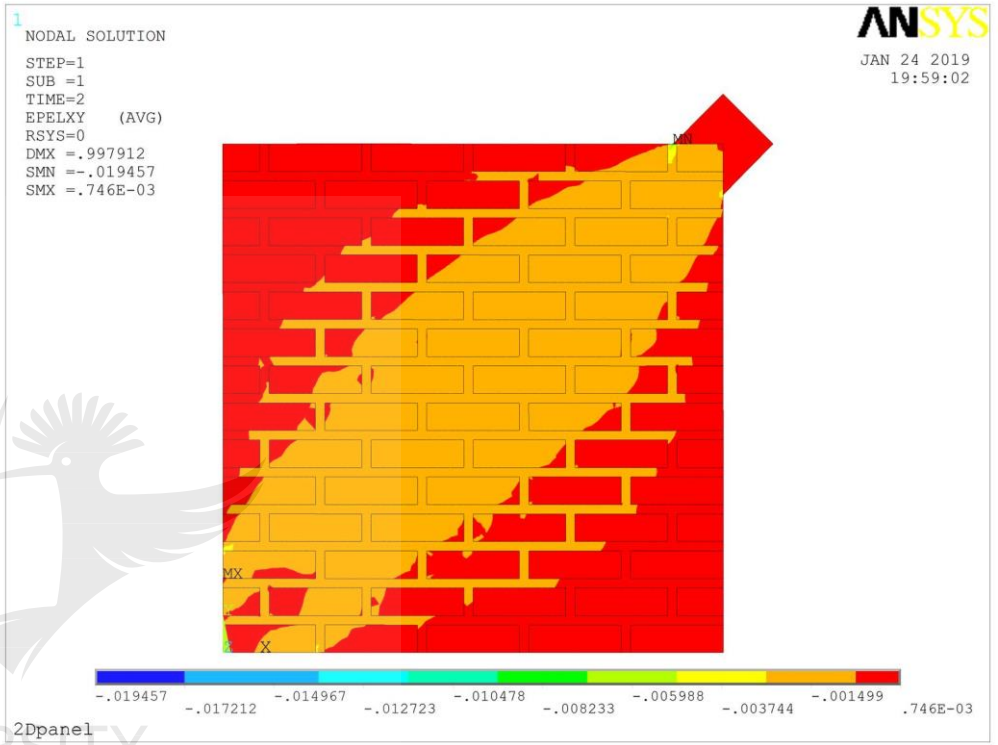

(b)

Figure 12.11: (a) Shear stress distribution of unreinforced panel. (b) Shear strain distribution of unreinforced panel.

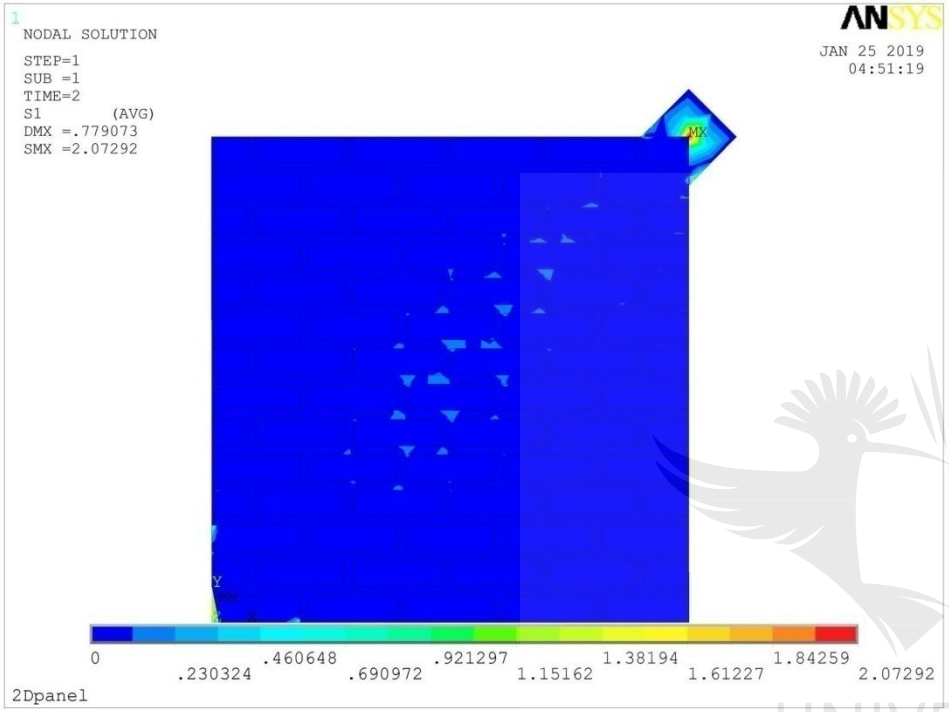

(a)

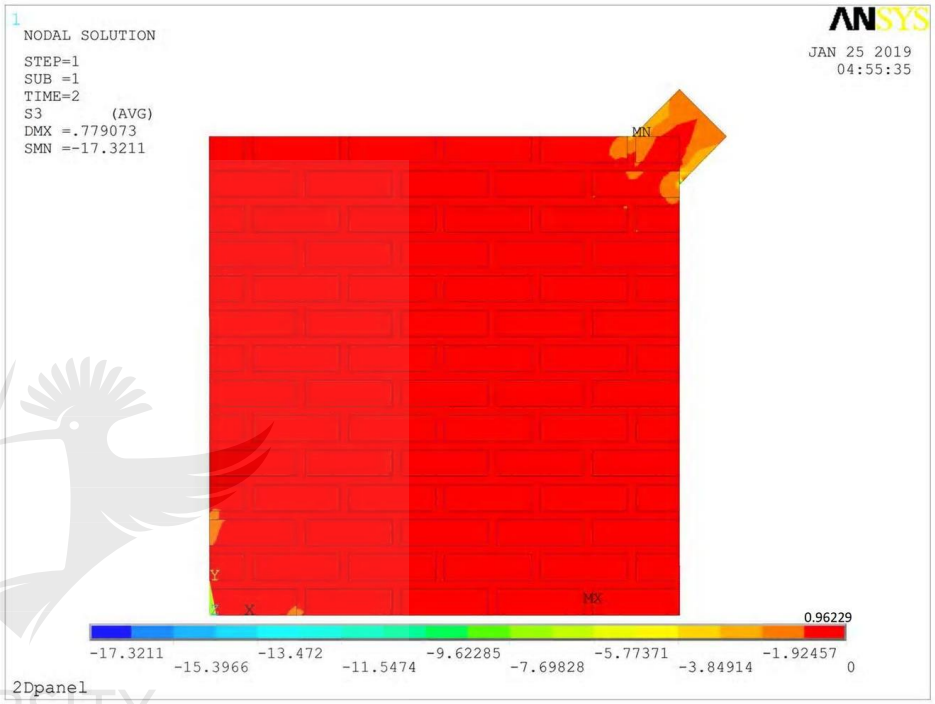

(b)

Figure 12.12: (a) Principal tensile stress distribution of unreinforced panel. (b) Principal compressive stress distribution of unreinforced panel.

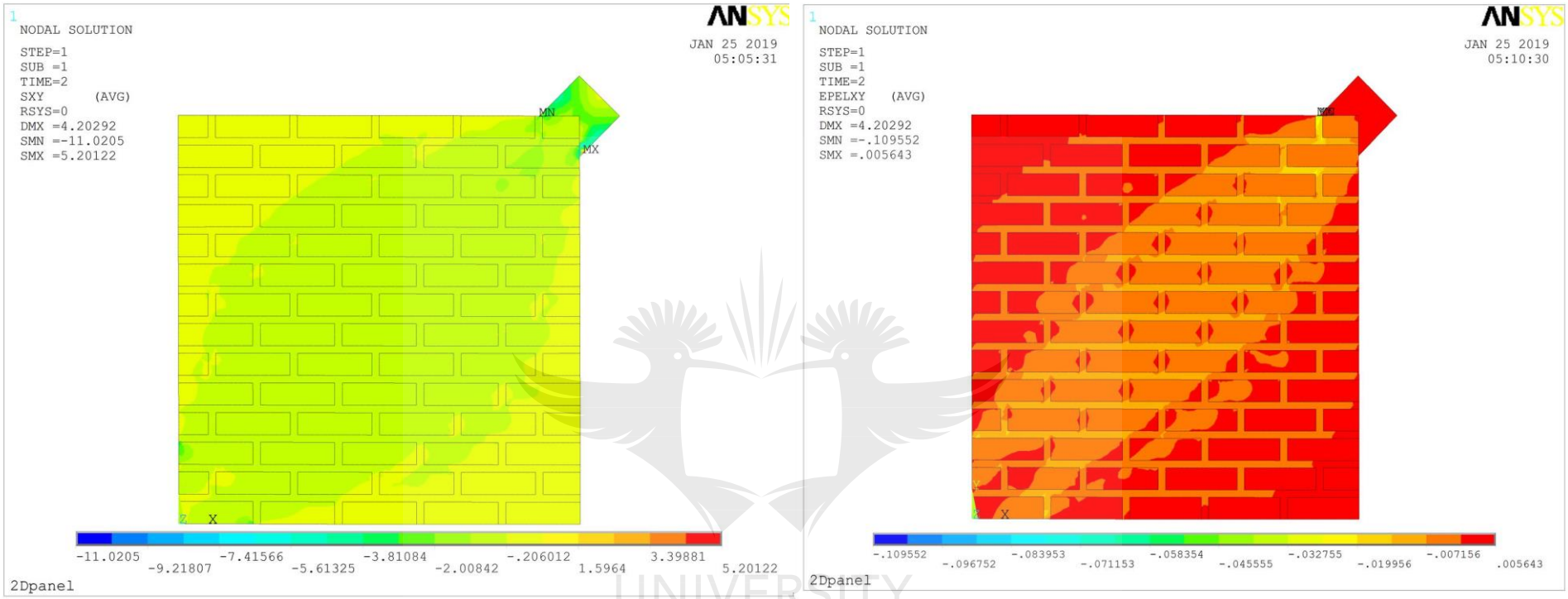

(a) (b)

Figure 12.13:(a) Shear stress distribution of reinforced panel. (b) Shear strain distribution of reinforced panel.

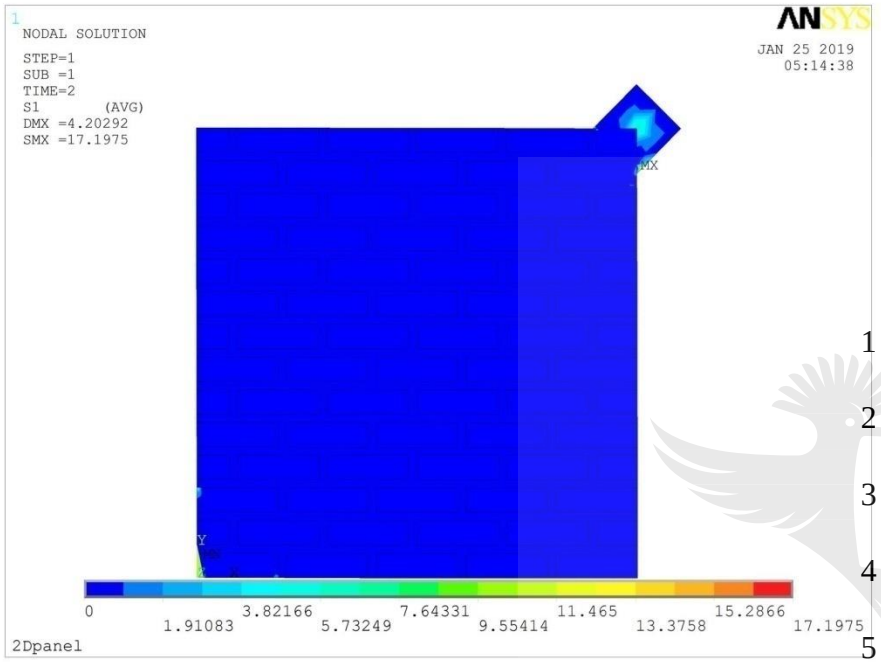

(a)

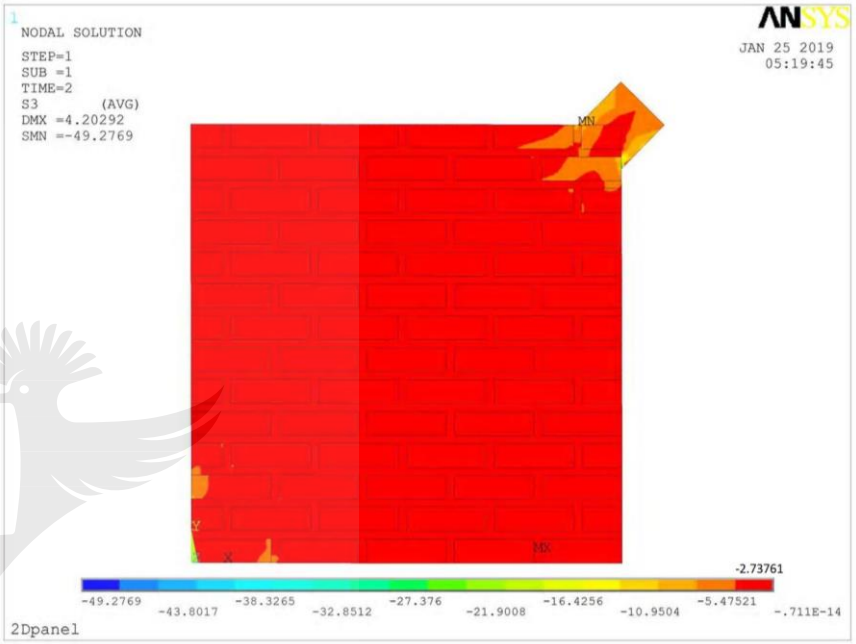

(b)

Figure 12.14:(c) Principal tensile stress distribution of reinforced panel. (d) Principal compressive stress distribution of reinforced panel.

This interpretation gives the values of the principal stress state localised at the centre of the panel given by equation 12.3 and equation 12.4.

$$\sigma_1 = 0.5\frac{P_{ult}}{A_p} \tag{12.3}$$

$$\sigma_3 = 1.62\frac{P_{ult}}{A_p} \tag{12.4}$$

The Mohr circles according to ASTM and RILEM interpretations and the stress state of the simulated reinforced and unreinforced panels are shown in figure 12.15.

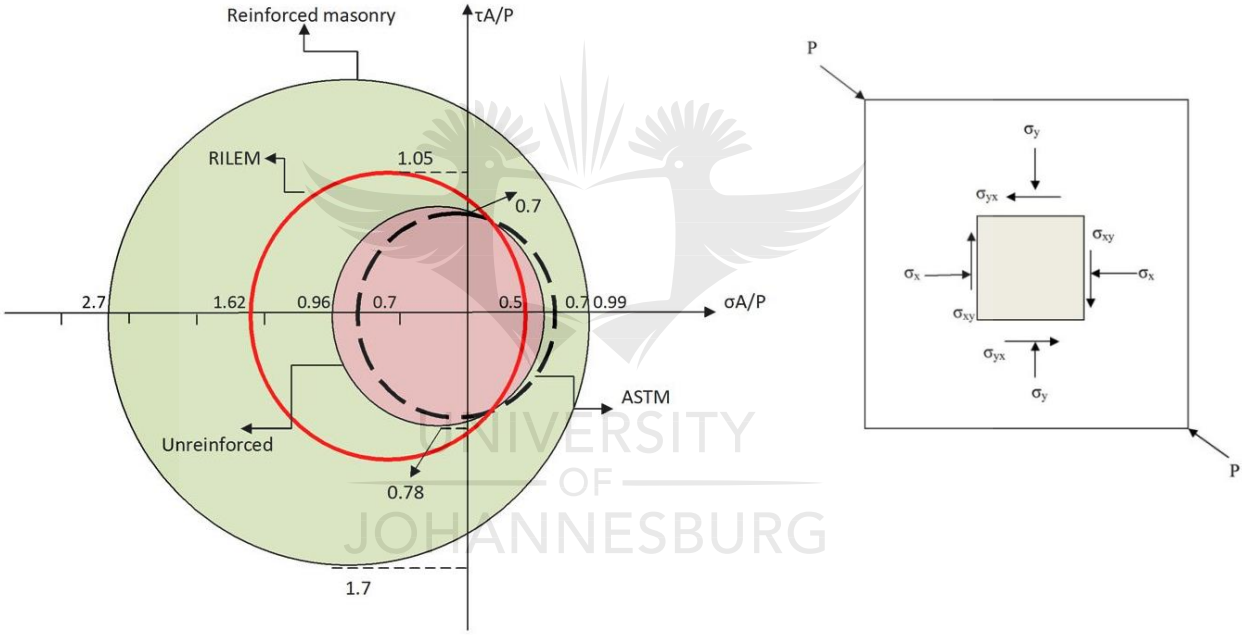

Figure 12.15: Normalised Mohr Circles of failure criteria and stress state at the center of the wall panel.

It can be seen that the numerical analysis results of the reinforced panel agree with RILEM irrespective of the stress values. The stress state of the unreinforced panel shows slight deviation from the ASTM assumption. It can be concluded that the stress state at the center of the panel for both panels is not a pure shear state and can better be described by RILEM interpretation.

12.4 Design of vertically and laterally loaded adobe masonry wall

The typical maximum dimensions of adobe houses in the developing countries are 8x5x2.5m (Novelli et al., 2018). The typical thickness is double brick wall of about 250mm.

12.4.1 Case 1: Vertical Load resistance

The design procedure according to BS5628 (BS 5628-1, 2005) and Eurocode 6(ENV 1992-2, 2006) is adopted. The design assumptions and adobe wall specifications include; wall dimensions of 8m length, 2.5m height and 0.25m thickness, category II of masonry units and normal construction control and material reduction factor of 3 (Table 2.3 of EC6), simple restraint is provided by the roof, load eccentricity at the top of the wall is less than 0.005t (t is the thickness of the wall), the typical slenderness ratio is about 10, typical wall capacity reduction factor is 0.97 (Table 7 BS5628). Vertical load resistance is given by equation 12.5.

$$N_v \leq \frac{\beta f_k t}{\gamma_m} \qquad (12.5)$$

where ,γ_m=3, β=0.97, f_k is characteristic masonry compressive strength.

For unreinforced wall, f_k=0.5MPa (Refer to results of wallet compressive strength), load resistance is $N_v \leq 40$kN/m run of the wall.

For reinforced wall, f_k=1.3MPa, load resistance is $N_r \leq 100$kN/m run of the wall.

12.4.2 Case 2: Lateral shear resistance

Using limit state design approach and maximum vertical load resistance (40N/mm run of unreinforced wall and 100N/mm run of reinforced wall) and assuming that the wall is fully vertically loaded, allowable shear resistance of the wall is given by equation 12.6.

$$F_v = N_v tan\varphi \qquad (12.6)$$

where Φ is the friction angle determined by triplet test, 32^o .and 39^o for unreinforced and reinforced mortar, respectively.

For unreinforced wall, N_v=40kN/m run of the wall and allowable shear resistance is $F_v \leq 25$kN/m run of the wall.

For reinforced wall, N_v=100kN/m run of the wall and allowable shear resistance is $F_v \leq 80$kN/m run of the wall.

Conclusions

The mechanical properties of fiber reinforced and unreinforced adobe masonry were investigated by series of laboratory tests namely, masonry triplet, couplets and prisms tests. The shear strength, tensile bond resistance and compressive strength of the masonry elements were determined. Masonry structural performance was assessed by uniaxial compression and diagonal compression shear tests on wallets and wall panels. Finite element linear elastic analysis was performed to evaluate the stress state condition of both loaded reinforced and unreinforced wall panels. A full scale adobe masonry wall design according to BS5628 and Eurocode 6 standards was conducted using the acquired material properties. Based on the acquired results, the following conclusions are drawn;

1. Fiber inclusion increases tensile resistance of mortar to about 31% of the unreinforced mortar.
2. Fiber reinforcement increases shear strength of the mud mortar and improved friction coefficient from 0.63 to 0.81, representing 22% increase.
3. The compressive strength of the adobe prisms increases by 25% with fiber inclusion in either the mortar or the bricks.
4. The twofold strength increase may be registered by wallets with fiber reinforcement in both the mortar and the bricks.
5. The threefold shear strength and modulus improvements of the wall panels may be achieved with fiber reinforced mortar.
6. The shear stress state in the reinforced and unreinforced wall panel is not a pure shear state and is better described by RILEM interpretation.
7. Fiber reinforced adobe masonry exhibits ductile behaviour and the failure mode of the unreinforced is brittle.
8. The load resistance of the vertically loaded adobe fiber reinforced masonry wall is estimated as 100kN/m run of the wall while unreinforced wall can support load of approximately 40kN/m run of the wall. The shear resistance of reinforced wall is estimated as 80kN/m run and unreinforced wall can support shear load of about 25kN/m run of the wall.

References

Alecci et al. (2013). Shear strength of brick masonry walls assembled with different types of mortar. *Construction and Building Materials, 40*, 1038–1045.

ASTM C67-03a. (2003). Standard test methods for sampling and testing bricks an clay tiles. Conshohocken PA: ASTM.

ASTM C1314-03b. (2003). Standard test method for compressive strength of masonry prisms Conshohocken PA: ASTM.

ASTME519-15. (2015). Standard test method for diagonal tension (shear) in masonry assemblages. Conshohocken PA: ASTM.

Binici et al. (2005). Investigation of fibre reinforced mud brick as a building materia. *Construction and Building Materials, 19*, 313-318.

Blondet et al. (2011). Earthquake resistant of earthen construction: The great contemporary experience of Pontifical Catholic University of Peru. *Inf. constr, 63*(523), 41–50.

Brignola et al. (2009). Identification of shear parameters of masonry panels through the in situ diagonal compression test. *Int J Archit Heritage, 3*(1), 52–73.

BS 5628-1. (2005). Code of practice for structural use of unreinforced masonry. London: BSI.

BS EN 1015-11. (1999). Methods of test for mortar for masonry. Determination of flexural and compressive strength of hardened mortar: BIS.

BS EN 1052-3. (2002). Method of test for masonry :Determination of iniyial shear strength: BSI.

Consoli et al. (2012). Parameters controlling tensile and compressive strength of fiber-reinforced cemented Soil. *Journal of Materials in Civil Engineering*.

ENV 1992-2. (2006). Design of masonry structures: CEN.

Erika et al. (2014). *Mechanical Properties of adobe masonry of historical buildings in Peru*. Paper presented at the 9th International Conference on Structural Analysis of Historical Constructions Mexico City, Mexico

Figueiredo et al. (2013). Seismic retrofitting solution of an adobe masonry wall. *Mater. Struct., 46*(1-2), 203-219.

Gabor et al. (2006). Modelling approaches of the in-plane shear behaviour of unreinforced and FRP strengthened masonry panels. *Composite structures, 74*, 277-288.

Islam.M.S and Iwashita.K. (2010). Earthquake resistance of adobe reinforced by low cost traditional materials. *Journal of Natural disaster science, 32*(1), 21.

Mesbah et al. (2004). Development of a Direct Tensile Test for Compacted Earth Blocks Reinforced with Natural Fibers. *Journal of Materials in Civil Engineering, 16*(1), 95-98.

Moghal et al. (2018). Effect of polypropylene fibre reinforcement on the consolidation, swell and shrinkage behaviour of lime-blended expansive soil. *International journal of geotechnical engineering, 12* (5), 462-471.

Nazeer et al. (2018). Behaviour and strength assessment of masonry prisms. *case studies in construction materials, 8*, 23-38.

Novelli et al. (2018). A Resource on construction in Earthquake Regions *The World Housing Encyclopedia* EERI and IAEE.

Novelli et al. (2019). Seismic Mitigation Framework for Non-engineered Masonry Buildings in Developing Countries: Application to Malawi in the East African Rift *Resilient Structures and Infrastructure*. Singapore: Springer.

RILEM LUMB6. (1994). Diagonal tensile strength tests of small wall specimens 1991 *Rilem recommendations for the testing and use of constructions materials.* (pp. 488–489). London: RILEM.

Sharma et al. (2015). Enhancing sustainability of rural adobe houses of hills by addition of vernacular fiber reinforcement. *International Journal of Sustainable Built Environment, 4*, 348–358.

Tetley.R and Madabhushi.G. (2007). *Vulnerability of adobe buildings under earthquake loading*. Paper presented at the 4th International Conference of Earthquake Geotechnical Engineering Thessaloniki- Greece.

Varum et al. (2008). *Mechanical Characterization of Adobe Masonry Walls* Paper presented at the Terra 2008: The 10th International Conference on the Study and Conservation of earthen archtectural heritage, Bamako Mali.

Walker.P (1999). Bond Characteristics of earth block masonry. *Journal of Materials in Civil Engineering, 11*(3), 249-256.

Walker.P (2004). Strength and Erosion Characteristics of Earth Blocks and Earth Block Masonry. *Journal of Materials in Civil Engineering, 16*(5), 497-506.

Wu et al. (2013). Strength and stress–strain characteristics of traditional adobe block and masonry. *Materials and structures, 46*, 1449–1457.

13 CHAPTER THIRTEEN-CONCLUSIONS

13.1 Research summary

The aim of the research was to assess potential use of natural fiber (sisal) reinforced soil as a construction material for sustainable and resilient earthen construction and also potential application of fly ash for the beneficiation of the waste product to improve durability and strength of earthen construction. In this study, randomly oriented sisal fibers were used as reinforcing elements of soil matrix to investigate mechanical properties, resilience and durability of fiber soil composites. The combined effects of fly ash stabilisation and sisal fiber inclusion were also investigated in order to establish the mechanics behind reinforcing mechanisms of chemically stabilised fiber soil composites. Natural based rosin was used to improve fiber-matrix interfacial and durability properties for long term performance of the composite. The resilience of the fiber soil composite to seasonal moisture changes was also investigated by subjecting the composite to wet and dry cycles. The mechanical properties of the fiber soil composite were tested statically and dynamically in order to establish static and dynamic behaviours with special interest in evaluating interfacial strength, macro structural deformation, fracture mechanisms, shrinkage and swelling and resilience to cyclic loading. The rationale behind dynamic testing was to mimic material behaviour during earthquake or vibrations. The constitutive model for dynamic behaviour of the fiber-soil composite was developed as tool for design of fiber reinforced earth or geo systems. Investigation into the role of fiber inclusion in adobe masonry construction was conducted to aid the establishment of design guidelines of low-cost earthen construction.

13.2 Key conclusions

13.2.1 Macrostructural and strength properties

Increasing fiber content at designated fiber length and content causes decrease in maximum dry density. This is attributed to the low unit weight of fibers. Fiber inclusion improves unconfined compressive strength and ductility of the composite. Increasing fiber length beyond 25mm and corresponding fiber content beyond 0.75% may reduce unconfined compressive strength. This is due to non-uniform distribution of fibers and the reduced fiber–soil interlocking mechanism. The kinematic strain hardening behaviour and the improved ductility are associated with an increase in fiber length and content. Energy based homogenisation can estimate failure shear strength of short fiber and a reasonable accuracy is achieved with low fiber content.

13.2.2 Fiber coating and interfacial strength properties

Interfacial shear strength and interfacial residual shear strength of rosin coated fibers reduce in the presence of moisture. This is attributed to the lubrication at the fiber-matrix interface by the film of moisture. Interfacial shear strength of both coated and uncoated fibers improve with reduced moisture content of the matrix. The coated fibers mobilise higher strength than uncoated at low moisture content. The increased adhesion and mechanical interlock of the coated fibers cause an increase in the interfacial shear strength. High matrix density increases interfacial shear strength and interfacial residual shear strength of both coated and uncoated fibers. This is as a result of high frictional resistance on the fiber surface that enhances mechanical interlock of the fiber and soil matrix. The level of compaction is directly related to the level of strength which is mobilised by the composite.

Unconfined compressive strength of the sisal fiber reinforced soil with coated fibers may be lower than of uncoated fiber at high moisture content and strength is significantly enhanced with drying. Shear-lag analysis can predict fiber axial load transfer with some acceptable value for both coated and uncoated fibers.

13.2.3 Matric suction induced properties

Increasing fiber content of the compacted soil composite reduces matric suction due to an increase in pore size as a result of resistance of soil composite to compaction. Moisture absorption of sisal fibers at high fiber content increases matric suction due to low free moisture. The mechanical properties of soil composites are enhanced by matric suction. Evolution of matric suction in the reinforced soil composite is associated with softening post peak behaviour of the soil composite. Compaction of the soil-fiber composites may have a bearing on the evolution of matric suction.

13.2.4 Desiccating cracking and strength properties

The crack morphology of reinforced soil is characterised by small cell area with irregular shapes, short and thin cracks and non-orthogonal crack intersections. The sisal fiber content dictates rate of moisture loss from the soil. With 0.5% fiber content, the rate of moisture loss may be lower than unreinforced soil. This is attributed to the low free moisture in the composite caused by the absorption of moisture by the fibers. With 1% fiber content, the rate of moisture loss may be greater than unreinforced soil due to increased volume of water pathways created by the fibers.

Crack width and surface area ratio reduce with an increase in fiber content. Crack width reduction of 74% and surface crack reduction of 35% can be achieved at 1% fiber content. Crack growth and shrinkage strain are significantly reduced with fiber inclusion. The growth rate can reduce from 5.8mm/hr for unreinforced soil to 1.2mm/hr at 1% fiber content. The shrinkage can reduce from 5.5% for unreinforced soil to 1% for reinforced soil with 1% fiber content. Increasing thickness of the soil layer leads to large crack width and high rate of moisture loss of the composite. Increasing number of wet and dry cycles causes strength degradation of both reinforced and unreinforced soil due to loss of binding fine particles of the soil. However, reinforced soil indicates considerable resilience to strength degradation.

13.2.5 Cyclic strength properties and analytical model

The fiber inclusions in the soil for earthen construction cause an increase in shear modulus to fiber content of 0.5% beyond which modulus can reduce. The reduction in modulus is attributed to the loss of stiffness of the soil composite due to high percentage of voids. The shear modulus is improved by increasing level of confining pressure. Fiber inclusions enhance damping ratio of the composite due to improved resistance of the composite to deformation. An increase in confining pressure leads to enhanced soil composite damping properties. Both permanent strain and cumulative strain reduce with fiber inclusion due to improved resilience to deformation. Fiber reinforced soil exhibits high resistance to liquefaction. Increase in fiber content causes an increase in post cyclic energy absorbing capacity, toughness and static energy ratio of the soil. Linear relationship is indicated between cyclic damping ratio and both post cyclic energy ratio and toughness.

The non linear behaviour of fiber reinforced soil under dynamic loading can be estimated by incorporating anisotropic properties of soil. The initial tangential shear model is more sensitive to change in fiber content and confining pressure than ultimate cyclic shear stress. The initial modulus and ultimate shear stress reduce with an increase in number of cycles. If the soil composite is assumed to be isotropic, the impact of model variables is overestimated. The proposed revised model for non linear behaviour of fiber reinforced soil under dynamic loading is a convenient tool for analysing behaviour of fiber reinforced soil under dynamic loading for geosystems design purposes. However, model parameters are subjective to fiber properties (length and diameter) and the type of soil. The recommended fiber sizes that accurately fit into

the model are diameters of 0.1mm and any fiber length to produce fiber a corresponding aspect ratio of 250, at engineer's discretion.

13.2.6 Lime- fly ash stabilisation, resilience and durability

Fibers inclusions increase strength and ductility of the stabilised fiber-soil composite. This is attributed to the high tensile resistance mobilised by the sisal fibers. Lower strengths are mobilised by pre-compressed stabilised composite in comparison with un-precompressed stabilised composite. This is attributed to redistribution of fiber-matrix bond strength and the evolution of macro cracks in the matrix that lead to reduction in the stiffness of the composite. Damaging effects of pre-compression are reduced when pre-compression stresses are induced after longer period of curing of the stabilised soil composite. This is due to time related strength gain of the composite (pozzolanic reaction) that endows the matrix with resistance to compression.

Pre-compression can improve mechanical properties when applied to composite at low fiber content. The crack model for damage mechanism in cementitious fiber composite can predict with reasonable accuracy the strength behaviour of stabilised fiber composites that are pre-compressed after short period of curing.

Capillary soaking causes loss of strength of about 40% however, fiber inclusion improves compressive strength of soaked stabilised sisal fiber-soil composites. In comparison, pre-compressed stabilised soil-fiber composites exhibits lower compressive and tensile strengths than un-precompressed stabilised composites. About 20% strength loss of both compressive and tensile strength are registered. This is due to the synergic effects of soil matrix cracking and weak bond at fiber-matrix interface. From the engineering design perspective, the characteristic strength of the stabilised soil should be reduced by the material reduction factor, preferably 1.2 to cater for strength reduction due to premature loading and moisture ingress. Sisal fiber inclusion reduces tensile strength of soaked stabilised composite due to fiber slippage, low fiber-matrix friction and moisture impaired fiber-fiber interaction.

In comparison, soaked stabilised sisal fiber reinforced soil performs better in compression than in tension. However, strength proportionality of 10% to 17% between tensile and compressive strengths is indicated beyond optimum strength index. Fiber inclusion increases compression residual strength of soaked stabilised composite to about 90%. This is as a result of the resilience

of fibers to failure. Compressive and tensile strengths of compressed composite are enhanced by extended curing time. This is attributed to the increased resistance of the composite to compression and tension due to pozzolanic reaction. In practice, using stabilised fly ash- sisal fiber reinforced soil in earthen construction endows the structure with considerable resilience to deformation under moisture exposure. It is anticipated that the stabilised fiber reinforced earthen structure would exhibit significant load carrying capacity when re-loaded after sustaining heavy loading under severe moisture conditions.

13.3 Sisal fiber reinforced adobe earthen construction

In adobe masonry construction, fiber inclusion increases tensile resistance of mortar to about 31% of the unreinforced mortar. Fiber reinforcement increases shear strength of the mud mortar and improves friction coefficient from 0.63 to 0.81, representing 22% increase. The compressive strength of the adobe prisms increases by 25% with fiber inclusion in either the mortar or the bricks. The twofold strength increase is registered by wallets with fiber reinforcement in both the mortar and the bricks. The threefold shear strength and modulus improvements of the wall panels are indicated with fiber reinforced mortar. The shear stress state in the reinforced and unreinforced wall panel is not a pure shear state and is better described by RILEM interpretation. Fiber reinforced adobe masonry exhibits ductile behaviour.

13.4 Field practice recommendations

Longer fiber lengths greater than 25mm are not recommended for application in fiber soil reinforced composite since are not effective in mobilising strength and pose challenges in compaction. In practice, incorporating fibers in earthen construction can endow the foundation structure and walls with significant ductility and strength. Ductility is beneficial for the resilience of the structure to seismic loading. Enhanced compressive strength increases structural performance under sustained gravity loads and may prolong service life of the structure.

In construction, gum rosin can effectively be used to enhance strength properties and potentially long term performance of fiber reinforced earthen walls.

Practically, the evolution of matric suction in the soil-fiber composite during dry spells would enhance strength of the earthen walls and foundation. The effects of tensile stresses associated with suction would be controlled by fiber inclusion. The moisture absorption by fibers would facilitate development of suction induced strength of the earthen structure which is beneficial to

maintain integrity of the structure. In application, fiber length should not be excessively long (preferably 25mm) to avoid creating large soil void volume that would suppress suction induced strength in earthen structure. Fiber inclusion could effectively control desiccation cracking of the soil during drying which is beneficial in maintaining integrity of wall and foundation of the earthen structures.

Practically, sisal fiber inclusion is the seismic retrofitting technique for the earthen structures. This is due to the resilience of the fiber reinforced soil composite to deformation. Resistance to liquefaction of sisal fiber reinforced soil is beneficial to maintain integrity of foundation during earthquake events. It is anticipated that fiber reinforced earthen construction would exhibit resilience to deformation during aftershocks as evidenced by the high post cyclic energy absorbing capacity and toughness, and this is beneficial for the evacuation of people and property. The fiber reinforced soil can effectively be used as in-fill for seismic wave barrier walls due to its good damping properties.

The use of heavy machinery in fly ash stabilised earthen construction may reduce ultimate strength of the foundation structure. Pre mature loading of the stabilised earthen walls may compromise characteristic strength of the structural element. Therefore, light weight tools are recommended for construction of stabilised earthen building foundation in order to minimise ultimate strength reduction due to excessive premature loading. Superimposed loading should be applied when the stabilised materials are fully cured, i.e., at least after 28 days of curing. From the design point of view, characteristic strength of fiber reinforced soil must be reduced by material reduction factor, preferably 1.2 to cater for lower ultimate strength of the material. From the design point of view, tensile strength of the stabilised soil could be taken as 10% of the unconfined compressive strength.

A typical sisal fiber reinforced adobe masonry wall can support vertical load of about 100kN/m run of the wall and shear of shear forces of about 80kN/m run. It is therefore anticipated that fiber reinforced adobe earthen construction can exhibit resilience during earthquake events.

APPENDEX A-PROPOSED DESIGN AND CONSTRUCTION GUIDELINES OF FIBER REINFORCED SOIL FOR RESILIENCE AND SEISMIC RETROFFITING

1. Proposed foundation details of low-cost buildings for seismic robustness

Based on the post peak and dynamic behaviour of the fiber reinforced soil, it is proposed that the foundations plinth of the low-cost buildings should be filled with well mixed randomly distributed fiber reinforced soil compacted to at least 95% MDD and also wave barrier wall should filled with compacted fiber reinforced soil for dynamic energy absorption. The construction details are shown in figure 1.

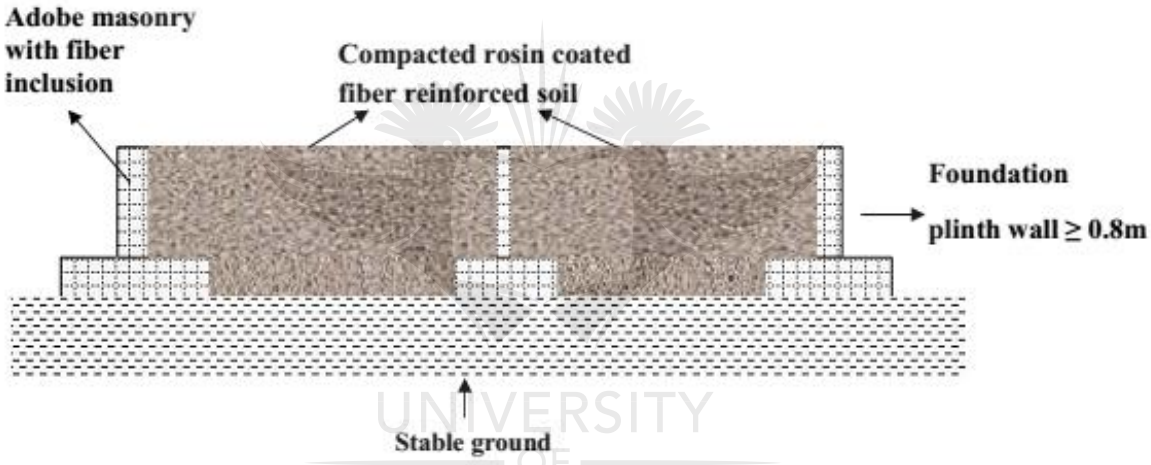

Figure 1.Proposed foundation details for seismic retrofitting of earthen structures

The proposed details endow the foundation with considerable ductile and resilience to deformation. The wave barrier walls with compacted fiber reinforced soil ensures substantial seismic energy absorption or attenuation.

1. Limit state design or load and resistance factor foundation design on stabilised, pre-compressed and soaked fiber reinforced soil

The general criteria should be adopted as in equation 1 and material reduction factor of 1.2 should be used to cater for strength degradation due to pre mature loading together with the factors for material strength variability.

$$\alpha S \leq \frac{R}{\gamma_m} \quad (1)$$

where R is the material resistance and S is the applied variable or permanent loading, α is the load factor and γ_m is the material strength reduction factor. For instance, when sizing the foundation on the stabilised fiber reinforced soil, the ultimate net bearing capacity of the soil may be factored by 0.83 for material strength reduction due to pre mature loading during construction and 0.8 as performance factor to cater for errors in calculation and construction. The design formula may be given by equation 2

$$\alpha S \leq \frac{R}{\gamma_m \gamma_p} \quad (2)$$

where γ_p is the performance factor equal to 1.3 and $\gamma_m = 1.2$. The design strength may be computed as equation 3.

$$\alpha S \leq 0.67 q_{ult} \quad (3)$$

where q_{ult} is the ultimate bearing capacity of the stabilised soil.

APPENDIX B-SUPPLIMENTARY DATA FOR CHAPTER 3

Recorded specimens' density data

Specimen serial	Mass g	Bulk density kg/m^3	Dry density kg/m^3
1	589.5	2067.7	1846.15
2	566	1985.27	1772.56
3	591	2072.96	1850.85
4	575	2016.84	1800.74
5	600	2104.53	1879.04
6	591.5	2074.71	1852.42
7	564	1978.26	1766.30
8	568.5	1994.04	1780.39
9	609.5	2137.85	1908.79
10	559.5	1962.47	1752.20
11	589.5	2067.7	1846.15
12	592.5	2078.22	1855.55
13	578	2027.36	1810.14
14	587.5	2060.68	1839.89
15	563.5	1976.50	1764.73
16	574.5	2015.09	1799.18
17	576	2020.35	1803.88
18	582	2041.39	1822.67
19	561.5	1969.49	1758.47
20	568	1992.29	1778.82
21	581.5	2039.64	1821.10
22	581	2037.88	1819.53
23	581.5	2039.65	1821.10
24	568.5	1994.04	1780.39
25	581.5	2039.64	1821.10
26	587.5	2060.68	1839.89
27	590.5	2071.20	1849.29
28	575	2016.83	1800.74
29	567	1988.77	1775.69
30	599.5	2102.77	1877.47
31	584.5	2050.16	1830.50
32	611	2143.11	1913.49
33	594.5	2085.23	1861.81
34	568.5	1994.04	1780.39
35	565	1981.76	1769.43
36	563.5	1976.50	1764.73
37	592.5	2078.22	1855.55
38	594	2083.48	1860.25
39	611.5	2144.86	1915.05
40	620.5	2176.43	1943.24
41	616	2160.64	1929.15

42	606	2125.57	1897.83
43	609.5	2137.84	1908.79
44	617	2164.15	1932.28
45	614.5	2155.38	1924.45
46	615.5	2158.89	1927.58
47	605	2122.06	1894.70
48	616	2160.64	1929.15
49	616	2160.64	1929.15
50	610.5	2141.35	1911.92
51	606.5	2127.32	1899.39
52	621.5	2179.94	1946.37
53	610.5	2141.35	1911.92
54	606	2125.57	1897.83
55	609.5	2137.84	1908.79
56	605.5	2123.81	1896.26
57	605	2122.06	1894.70
58	607.5	2130.83	1902.53
59	605	2122.06	1894.70
60	622.5	2183.44	1949.50
61	590.5	2071.20	1849.29
62	608	2132.58	1904.09
63	601.5	2109.78	1883.74
64	600.5	2106.28	1880.60
65	585	2051.91	1832.06
66	578	2027.36	1810.14
67	590	2069.45	1847.72
68	589.5	2067.69	1846.15
69	600	2104.52	1879.04
70	585	2051.91	1832.066

APPENDIX C- PUBLISHED ARTICLES

Construction and Building Materials 170 (2018) 737–746

Contents lists available at ScienceDirect

Construction and Building Materials

journal homepage: www.elsevier.com/locate/conbuildmat

Effects of natural fiber inclusions and pre-compression on the strength properties of lime-fly ash stabilised soil

Innocent Kafodya, F. Okonta *

Civil Engineering Science Department, University of Johannesburg, P.O Box 524, Auckland Park 2006, South Africa

HIGHLIGHTS

- Pre-compression reduces unconfined strength of fiber reinforced lime-fly ash stabilised soil.
- Mechanical properties of fiber reinforced stabilised soil improve with fiber inclusions.
- Fully cured lime-fly ash stabilised soil composite offers considerable resistance to compression.
- Ductility of the fiber-soil composite significantly improves with fiber inclusions.

ARTICLE INFO

Article history:
Received 10 November 2017
Received in revised form 18 February 2018
Accepted 25 February 2018

Keywords:
Fiber
Composite
Strength
Soil stabilisation

ABSTRACT

In this study, the synergic effects of pre-compression and fiber inclusions, on the mechanical behaviour of lime fly ash stabilised soil were investigated. Randomly distributed 25 mm sisal fibers were mixed with stabilised soil at the contents of 0%, 0.25%, 0.5%, 0.75% and 1% by dry mass of the soil. Both fiber composite and unreinforced soil specimens were subjected to the pre-compression stresses equivalent to 10% and 20% of the strength mobilised by the un-precompressed specimens. The pre-compression stresses were applied after 4 h, 8 h and 24 h of accelerated curing at 40 °C, after which the conditioned specimens were allowed to continue curing under constant conditions. The 7 day strength of the fully cured composites was determined by a series of unconfined compression tests. The results revealed that optimum strength of 3.5 MPa was mobilised by un-precompressed specimens at 0.75% fiber content. Pre-compression with 10% UCS showed maximum strength of 2.8 MPa at 0.25% fiber content whereas 20% UCS indicated optimum strength of 3.04 MPa at 0.25% fiber content. In comparison, pre-compressed specimens exhibited lower strength values than un-precompressed specimens. This was attributed to the redistribution of bond strength, evolution of matrix cracking and fiber-matrix interfacial debonding. The maximum strengths of specimens for both pre-compression levels occurred after 24 h of curing. This was due to the progressive strength development that endowed the composite with some resistance to compression that was responsible for matrix cracking and debonding. Fiber inclusions significantly improved ductility of the stabilised soil. The theoretical crack model of damage mechanisms in cementitious fiber composites can predict strength behaviour of composites that were pre-compressed after short period of curing.

1. Introduction

Lime stabilisation technique has been applied for ages in construction of improved subbases and subgrade of railways, highways and airfields embankments [1,2]. In practice, the technique is effectively applied to expansive or clayey soils. Lime stabilisation improves plasticity index, swelling, shrinkage, permeability and typical engineering properties such as shear strength and, compressibility of soil [1,3–8]. The combined addition of lime and fibers increases the efficiency to transfer load from matrix to fibers especially at extended curing time and also significantly affects the rate of unconfined compressive strength gain of the soil [9,10]. Literature has shown that compressibility of fly ash is highly affected by lime dosage and duration of load increments. The addition of lime to fly ashes triggers hydration process that in turn causes formation of cementitious compounds that are responsible for enhanced cementation of particles. The lime-fly ash mixtures exhibit low compressibility and high equilibrium void ratio values. On the other hand, longer duration of load increments allows considerable curing time for the pozzolanic reaction between lime and

* Corresponding author.
E-mail address: fnokonta@uj.ac.za (F. Okonta).

https://doi.org/10.1016/j.conbuildmat.2018.02.194
0950-0618/

Journal of Building Engineering 26 (2019) 100904

Contents lists available at ScienceDirect

Journal of Building Engineering

journal homepage: www.elsevier.com/locate/jobe

Role of fiber inclusion in adobe masonry construction

Innocent Kafodya[a,b,*], F. Okonta[a], Panos Kloukinas[c,d]

[a] Civil Engineering Science Department, University of Johannesburg, P.O Box 524, Auckland Park, 2006, South Africa
[b] Department of Civil Engineering, University of Malawi, The Polytechnic, Malawi
[c] Faculty of Engineering and Science, University of Greenwich, United Kingdom
[d] Department of Civil Engineering, University of Bristol, United Kingdom

ARTICLE INFO

Keywords:
Adobe bricks
Mortar
Masonry
Fiber reinforced soil
Sustainability

ABSTRACT

Adobe masonry construction constitutes a notable portion of the buildings in both urban and rural areas in less developed countries. Seismic performance of adobe buildings is poor, and low-cost retrofitting measures are required to enhance the resilience of such buildings during an earthquake. In this study, mechanical properties of fiber reinforced and unreinforced adobe masonry were investigated. Sisal fibers with length of 25 mm were used as reinforcing elements for mortar and adobe bricks at a fiber content of 0.75%. A series of laboratory tests were performed on masonry triplets, couplets and prisms to determine shear strength, tensile resistance and compressive strength, respectively. Uniaxial compression and diagonal compression shear tests were performed on wallets and wall panels, respectively to determine compressive strength and shear strength of the adobe masonry. Finite element linear elastic analysis was conducted using ANSYS Finite-Element code to evaluate the stress state of loaded wall panels. The structural design of adobe masonry walls was carried out according to BS5628 and Eurocode 6 standards, by utilising material properties acquired from the experiments. The results showed that fiber inclusion in the mortar caused an increase in tensile strength of 31%, friction coefficient of 22%, and prism compressive strength of 25% compared with unreinforced mortar. The reinforced wallets exhibited a twofold increase in compressive strength while reinforced wall panels indicated threefold increase in shear strength. The stress state in the reinforced and unreinforced wall panels was not a pure shear state and was better described by RILEM recommendations. The allowable vertical load resistance was found to be 40 kN/m and 100 kN/m for unreinforced and reinforced walls, respectively. The allowable lateral shear resistance was found to be 25 kN/m and 80 kN/m for unreinforced and reinforced walls, respectively. Reinforced masonry elements exhibited considerable ductility and unreinforced masonry elements showed brittle behaviour.

1. Introduction

Adobe is the oldest and widely used material for construction of dwelling houses. It is estimated that one third of the world's population and 50% of the population in the developing countries still live in the earthen buildings [1]. Earthen construction offers manifold benefits including cost effectiveness, lower embodied energy levels, high thermal mass and reduced use of non-renewable materials [2–4]. The interest in earthen construction in the developed countries has been driven by the demands for more sustainable form of built environment. In this regard, earthen materials have been the attractive alternative to conventional high energy demand construction materials [2]. Moreover, it is expected that the earthen structures in developing countries will continue to exist not only due to their economic benefits, but also because of cultural tradition and identity attached to them [5]. The application of adobe materials faces several constraints due to their brittle behaviour, low tensile strength and deterioration when exposed to moisture. However, the properties of adobe can be improved by mechanical compaction, chemical stabilisation with cement, lime and bitumen, and fiber inclusions such as straw [3,6]. Chemical stabilisation can significantly improve strength and water resistance of adobe. Typically, chemical binders are added at the contents between 4 and 10% of the soil dry weight [7,8]. On the other hand, the use of these additives significantly increases both material cost and environmental impact. Alternatively, natural fiber inclusions have been used in earthen construction to increase ductility, tensile strength, postcrack strength, erosion resistance, dimensional stability and reduce shrinkage cracks of the material [4].

The previous studies [9,10] focused on the solution to improve mechanical properties of adobe bricks with natural fibers and chemical

* Corresponding author.
E-mail address: ikafodya@poly.ac.mw (I. Kafodya).

https://doi.org/10.1016/j.jobe.2019.100904
Received 15 February 2019; Received in revised form 29 July 2019; Accepted 30 July 2019
Available online 30 July 2019

INTERNATIONAL JOURNAL OF GEOTECHNICAL ENGINEERING
https://doi.org/10.1080/19386362.2019.1611720

Cyclic and post-cyclic shear behaviours of natural fibre reinforced soil

Innocent Kafodya and Felix Okonta

Civil Engineering Science Department, University of Johannesburg, Johannesburg, South Africa

ABSTRACT

Soil behaviour under cyclic loading is a key component in assessing potential effects of earthquakes on infrastructure and the response of earth structures to dynamic loading. In this study, cyclic and post-cyclic shear behaviours of fibre reinforced and unreinforced soil were investigated. Series of undrained cyclic triaxial tests were performed to study effects of sisal fibres of 25 mm length and contents of 0.25%, 0.5% and 1% on the shear modulus, damping ratio, permanent strain, cumulative strain and liquefaction potential. The post- cyclic shear tests were conducted to study effects of fibre inclusion on the post cyclic energy absorbing capacity, toughness and static energy ratio. The results showed that fibre inclusions caused an increase in shear modulus to a limiting fibre content of 0.5% beyond which modulus reduced. The reduction was attributed to the loss of stiffness of soil composite due to high amount of voids. Fibre inclusions increased damping ratio due to enhanced resistance to deformation. Both permanent and cumulative strains reduced with fibre inclusions as a result of an increase in the resilience of soil composites to deformation. Both reinforced and unreinforced soil types exhibited high resistance to liquefaction. Increasing fibre content caused an increase in the post cyclic energy absorbing capacity, toughness and static energy ratio of the soil composite.

ARTICLE HISTORY
Received 3 March 2019
Accepted 22 April 2019

KEYWORDS
Fibre inclusion; cyclic loading; dynamic properties; post cyclic behaviour

Introduction

Soil reinforcement technique with randomly distributed fibres is used in various civil engineering applications like, retaining structures, slope stabilisation of embankments, sub-grade stabilisation, etc. The capability of fibre inclusions to improve geotechnical properties of soil has been extensively reported in the literature (Diambra et al. 2010; Ahmad, Bateni, and Azmi 2010; Das and Singh 2017; Diambra et al. 2013; Ibraim and Consoli 2018; Hejazi et al. 2012; Kafodya and Okonta 2018a; Kumar Patel and Singh 2017; Moghal et al. 2018; Tang et al. 2010; Kafodya and Okonta 2018b). Various types of randomly distributed elements, such as polymeric mesh elements, metallic fibres, synthetic fibres, discontinuous multi-oriented polypropylene elements and natural fibres have proven to be effective reinforcing elements of soil.

Many investigations related to the behaviour of fibre reinforced soil employed static loading conditions. The reports on the behaviour of fibre reinforced soil under cyclic loading are very limited in literature. Various methods, such as cyclic triaxial, resonant-column, torsional shear, bender elements and shake table are used to investigate dynamic properties of soil (Das and Ramana 2011). The dynamic characteristics of fibre reinforced soil are greatly influenced by fibre content, fibre length, loading repetition, confining pressure, loading frequency and shear strain amplitude (Li and Senetakis 2017; Sadeghi and Beigi 2014).

Shear modulus and damping ratio are the fundamental soil parameters in evaluating dynamic response of earth structures such as highway embankments and retaining walls. Some recent studies have attempted to investigate the dynamic properties and liquefaction behaviour of fibre reinforced soil using various methods. It was reported that fibre inclusions increase both shear modulus and damping ratio (Behzad Amir-Farya and Sherif Aggour 2015; Bozyigit et al. 2016). Shear modulus of the soil in low confining pressures (less than 100 kPa) is negligible and becomes considerable in high confining pressures (Shahnazari et al. 2009).

Shear modulus of fibre reinforced sand at very small strains reduces with an increase in fibre content and the trend is more pronounced at fibre contents greater than 0.5%. (Li and Senetakis 2017). Fibre inclusion tends to reduce the initial stiffness of soil composite at low strain level (Clariá and Vettorelo 2015). Shear modulus of clay sand decreases with increasing deviator stress ratio at high confining pressure and the rate of loss of shear modulus is much lower for fibre reinforced clay sand. In addition, an increase in shear modulus with loading repetition is more pronounced at higher deviator stress ratios (Sadeghi and Beigi 2014). Addition of basalt and glass fibres after freeze-thaw cycles increases damping ratio and shear modulus at constant confining pressure because of an increase in stiffness, but shear modulus decreases with increasing shear strain (Orakoglua et al. 2017). Fibre inclusions in sand increase liquefaction resistance and number of cyclic cycles to reach liquefaction (Mittal and Chauhan 2013; Ibraim et al. 2010; Karakan and Altun 2016; Maheshwari et al. 2012).

The aforementioned studies utilised synthetic fibres as reinforcing elements. These fibres are expensive and require a lot of energy in production. Natural fibres are more favourable than synthetic fibres due to their cost effectiveness and

CONTACT Innocent Kafodya ikafodya@poly.ac.mw Civil Engineering Science Department, University of Johannesburg, Johannesburg, South Africa

MethodsX 5 (2018) 848–856

Contents lists available at ScienceDirect

MethodsX

journal homepage: www.elsevier.com/locate/mex

Density control method for compression test of compacted lime-flyash stabilised fiber-soil mixtures

Innocent Kafodya, F Okonta*

Civil Engineering Science Department, University of Johannesburg, P.O Box 524, Auckland Park, 2006, South Africa

A B S T R A C T

The unconfined compressive strength test is the widely accepted protocol to investigate the strength properties of lime amended soil. As a quality control measure, specimens for unconfined compression test are prepared at a predetermined maximum dry density (MDD) using standard Proctor test. Replicating MDD in a small sized mould is difficult and subject to errors, which normally arise due to inconsistent compaction efforts. The conventional method for preparing specimens involves driving a core sampler into the compacted soil to extract the specimen. The approach proves to be laborious and is associated with high material usage, as such is not ideal for investigations of many variables. To address these challenges, an alternative protocol for specimen preparation at a controlled dry density was devised. In this study, a statistical analysis of the density values was used to validate the method. The regression analysis was employed to calibrate the compaction effort for a specified target density. The method offers manifold benefits such as;

- Improved quality of specimens.
- Reduced variability of UCS test data.
- Efficiency.
- Reduced material usage.

A R T I C L E I N F O

Method name: Standard test methods for laboratory compaction characteristics of soil using standard effort, West Conshohocken, PA, 2012, Standard test method for unconfined compressive strength of compacted soil-lime mixtures, West Conshohocken, PA, 200

Keywords: Dry density, Target density, Specimen, Compaction, Soil composite

Article history: Received 25 March 2018; Accepted 18 April 2018; Available online 21 April 2018

Abbreviations: MDD, maximum dry density; OMC, optimum moisture content; UCS, unconfined compressive strength; CV, coefficient of variation.

* Corresponding author.
E-mail address: fnokonta@uj.ac.za (F. Okonta).

https://doi.org/10.1016/j.mex.2018.04.010

International Journal of Geosynthetics and Ground Engineering (2019) 5:16
https://doi.org/10.1007/s40891-019-0169-7

ORIGINAL PAPER

Desiccation Characteristics and Desiccation-Induced Compressive Strength of Natural Fibre-Reinforced Soil

Innocent Kafodya[1] · F. Okonta[1]

Received: 11 April 2019 / Accepted: 24 June 2019

Abstract

In this study, desiccation characteristics of natural fibre-reinforced soil were investigated. The soil was mixed with sisal fibres (25 mm) at the fibre content of 0.5% and 1%. The effects of soil thickness on the desiccation characteristics were investigated using specimens with thickness of 6, 12 and 24 mm. Digital image analysis was used to study variation of crack morphology, width, surface crack area ratio, crack growth rate and shrinkage strain of the desiccated soil. The gravimetric measurements of moisture content were used to investigate rate of moisture loss and evolution of cracks with change in moisture. The effects of saturation and desaturation on the compressive strength of the soil were investigated by subjecting the compacted soil to wet and dry cycles. The results showed that crack morphology of the reinforced soil was characterised by small cell areas of irregular shapes, short and thin cracks and non-orthogonal crack intersections. Specimens with fibre content of 0.5% showed lower rate of moisture loss than unreinforced soil. This was attributed to the reduction of free moisture caused by fibre moisture absorption. Specimens with fibre content of 1% indicated higher rate of moisture loss than unreinforced soil due to an increase in the volume of water pathways. Crack width and surface crack area ratio showed reduction of 74% and 35%, respectively, with 1% fibre content. The crack growth rate and shrinkage strain significantly reduced with fibre inclusion. Increase in the soil thickness caused an increase in crack width and evaporation for both reinforced and unreinforced soil. Increasing number of wet and dry cycles up to 15 caused compressive strength degradation of 41% and 66% for compacted reinforced and unreinforced soil, respectively. Natural fibre inclusion can effectively be applied to control desiccation cracking of the soil which is beneficial in maintaining integrity of soil for various civil engineering applications.

Keywords Desiccation · Fibre reinforcement · Cracks · Moisture content

Introduction

Soil undergoes seasonal variations in water content at considerable depth due to seasonal changes in precipitation and evapotranspiration. Evaporation usually results in soil volumetric shrinkage that is accompanied by desiccation cracks. Desiccation cracks are more pronounced in clay-rich soils due to evolution of matric suction in the pore structure of the soils [1]. The presence of cracks significantly affects mechanical, hydrological, physicochemical and thermal properties of the soil [2–5]. The clay-rich soils are commonly used in the construction of buffers, mine tailings, dam liners and covers for waste repository. The desiccation cracks in these structures are the major factors that govern their hydraulic properties. For instance, cracking causes degradation of the containment function of the liner, which may lead to an increase in infiltration of surface water into the containment system or migration of the contained liquids into the surrounding soils and groundwater and may also lead to a decrease in the integrity and structural stability of the containment system. Water conductivity is drastically increased by cracking, leading to malfunction of the barrier systems [6]. Cracks may compromise water retention capacity of dams, leading to failures as reported by [7]. In other instances of exposed terrain, instability of natural slopes and vertical cuttings may occur when cracking causes groundwater recharge to be quicker than drawdown [8]. The bearing capacity of foundations is decreased with evolution of cracks [9]. The desiccation-induced cracks create zones of weakness in the soil mass with reduced mechanical properties and

✉ Innocent Kafodya
ikafodya@poly.ac.mw

[1] Civil Engineering Science Department, University of Johannesburg, P.O Box 524, Auckland Park 2006, South Africa

Published online: 01 July 2019

INTERNATIONAL JOURNAL OF GEOTECHNICAL ENGINEERING
https://doi.org/10.1080/19386362.2018.1542557

Effect of fibre surface coating on the mechanical properties of natural fibre-reinforced soil

Innocent Kafodya and Felix Okonta

Civil Engineering Science Department, University of Johannesburg, Johannesburg, South Africa

ABSTRACT

The application of natural fibres in soil reinforcement is cost-effective and environmentally friendly. However, natural fibres exhibit dimensional instability when exposed to moisture. Their hydrophilic characteristics affect mechanical performance and durability of natural fibre-reinforced composites. In this study, the effects of fibre surface coating on the mechanical properties of soil–fibre composite were investigated. Natural-based water repellent was coated onto sisal fibres to prevent water absorption. The single-fibre pull-out tests were conducted with varying soil matrix moisture contents and densities. Unconfined compression tests were performed on the soil composite containing 25 mm coated fibres at 0.75% fibre content. The results showed that interfacial shear strength (IFSS) of coated fibres was lower than uncoated fibres at the matrix optimum moisture content. This was attributed to the presence of thin film of moisture at fibre–matrix interface, which suppressed adhesion and mechanical interlock between fibre and soil matrix. Increasing matrix density led to high IFSS of both fibre types due to the enhanced interfacial frictional resistance. The composite with coated fibres exhibited higher rate of moisture loss due to the hydrophobic characteristics of fibres. Shear lag model was used to predict axial load transfer of fibres. The model prediction accuracy was dependent on the material properties, geometry and friction at fibre–matrix interface. Rosin can effectively be used to prevent water absorption of natural fibres and enhance long-term strength properties of natural fibre-reinforced soil.

ARTICLE HISTORY
Received 23 September 2018
Accepted 26 October 2018

KEYWORDS
Natural fibre; composite; interfacial shear strength; water repellent

Introduction

The soil reinforcement by high tensile strength fibres has become a widespread technique in earthwork construction. Fibre inclusions endow the soil with improved strength and ductility. The composite behaviour is governed by the content, nature (natural or synthetic), mechanical and geometrical properties of fibres. The improved engineering properties of fibre-reinforced soil have been reported by several investigators (Hejazi et al. 2012; Shukla, Sivakugan, and Das 2009; Rajeswari et al. 2017; Das and Singh 2017; Moghal et al. 2018; Kumar Patel and Singh 2017; Malidarreh et al. 2018). Investigations have shown that natural fibres improve compressive and shear strengths, bearing capacity and shrinkage of the soil (Dasaka and Sumesh 2011; Sarbaz, Ghiassian, and Akbar Heshmati 2014; Kafodya and Okonta 2018a). The sustainability and environmental friendliness of natural fibres have attracted wide applications of fibres in soil reinforcement of geosystems. However, natural fibres exhibit dimensional instability when exposed to moisture. Their hydrophilic characteristics undermine adhesion between fibres and soil matrix. The hygrothermal performance of natural fibre-reinforced composites is reduced with exposure to moisture (Pickering, Aruan Efendy, and Le 2016).

Investigations have shown that durability and mechanical properties of natural fibre composites are improved when fibres are coated with water repelling agents (Ahmad, Bateni, and Azmi 2010; Sarbaz, Ghiassian, and Akbar Heshmati 2014). The commonly used water repelling agents are bitumen and acrylic butadiene styrene. The aforementioned agents are expensive and energy intensive in production. Furthermore, bitumen is the toxic by-product of petroleum refinery. Its production is associated with emissions of hydrofluorocarbons that are environmentally unfriendly (Philibert et al. 2016). It is therefore imperative to find alternative water repelling agents that offer multifaceted economic and environmental benefits. The effective use of natural water repellent in soil–fibre reinforcement is a milestone towards achieving sustainable built environment. Meanwhile, investigations on the potential use of natural-based water repellents have received little attention.

Rosin shows high potential of water repellency and adhesion. It is a solid form of natural resin obtained from pine trees. The three types of rosins are gum, wood and tall oil. They are defined by the part of the pine tree from which they are obtained. About 90% of rosin composition is resin acid of similar molecular structure. The composition depends on the origin, type and geographical location of the tree. The abietic resin acid constitutes the highest percentage of the composition and provides rosin with hydrophobic properties (Wiyono, Tachibana, and Tinambunan 2006; Zheng et al. 2010; Wang et al. 2011; Kruge 2002; Jin et al. 2000). The objective of this study was to investigate the potential use of gum rosin in improving durability and mechanical properties of natural fibre-reinforced soil.

CONTACT Felix Okonta fnokonta@uj.ac.za Civil Engineering Science Department, University of Johannesburg, Johannesburg, South Africa